THESIS ON NATURAL AND EXACT SCIENCES B226

Development of CdTe Absorber Layer for Thin-Film Solar Cells

NICOLAE SPALATU

TUT
PRESS

TALLINN UNIVERSITY OF TECHNOLOGY
Faculty of Chemical and Materials Technology
Department of Materials Science
Laboratory of Thin Film Chemical Technologies

Dissertation was accepted for the defense of the degree of Doctor of Philosophy in Natural and Exact Sciences on 01.12.2016.

Supervisors: Dr. Jaan Hiie, Senior Research Scientist, Department of Materials Science, Tallinn University of Technology

Dr. Malle Krunks, Leading Research Scientist, Department of Materials Science, Tallinn University of Technology

Dr. Valdek Mikli, Senior Research Scientist, Department of Materials Science, Tallinn University of Technology

Opponents: Dr. Stephan Bücheler, Laboratory for Thin Films and Photovoltaics, Swiss Federal Laboratories for Materials Science and Technology (EMPA), Switzerland

Dr. Kaido Tammeveski, Chair of Colloid and Environmental Chemistry, Institute of Chemistry, University of Tartu

Defense of the thesis: February 03, 2017 at 13:00
Lecture hall: U06A-201
Tallinn University of Technology, Ehitajate tee 5, Tallinn

Declaration: Hereby I declare that this doctoral thesis, my original investigation and achievement, submitted for the doctoral degree at Tallinn University of Technology, has not been previously submitted for any academic degree.

Nicolae Spalatu

European Union
Regional Development Fund
Investing in your future

ISSN 1406-4723
ISBN 978-9949-83-068-8 (publication)
ISBN 978-9949-83-069-5 (PDF)

LOODUS- JA TÄPPISTEADUSED B226

CdTe absorberkile arendamine õhukesekilelistele päikesepatareidele

NICOLAE SPALATU

TTÜ
KIRJASTUS

TABLE OF CONTENTS

LIST OF PUBLICATIONS

The thesis is based on the following publications, which are referred to in the text by the Roman numerals **I–V**:

I. **N. Spalatu**, J. Hiie, V. Valdna, M. Caraman, N. Maticiuc, V. Mikli, T. Potlog, M. Krunks, V. Lughi, Properties of the $CdCl_2$ air-annealed CSS CdTe thin films, *Energy Procedia* **44** (2014) 85–95.

II. **N. Spalatu**, J. Hiie, V. Mikli, M. Krunks, V. Valdna, N. Maticiuc, T. Raadik, M. Caraman, Effect of $CdCl_2$ annealing treatment on structural and optoelectronic properties of close spaced sublimation CdTe/CdS thin film solar cells vs deposition conditions, *Thin Solid Films* **582** (2015) 128–133.

III. **N. Spalatu**, M. Krunks, J. Hiie, Structural and optoelectronic properties of $CdCl_2$ activated CdTe thin films modified by multiple thermal annealing, *Thin Solid Films* (2016) *in press,* http://dx.doi.org/10.1016/j.tsf.2016.09.042.

IV. N. Maticiuc, **N. Spalatu**, A. Katerski, J. Hiie, V. Mikli, M. Krunks, L. Dolgov, I. Sildos, Plasmonic modification of CdTe thin films by gold nanoparticles: Methods, difficulties and solutions, *Microelectronic Engineering* **126** (2014) 173–178.

V. **N. Spalatu**, J. Hiie, N. Maticiuc, M. Krunks, A. Katerski, V. Mikli, I. Sildos, Plasmonic effect of spray-deposited Au nanoparticles on the performance of CSS CdS/CdTe solar cells, *Applied Surface Science* **350** (2015) 69–73.

Copies of these articles are included in APPENDIX A.

AUTHOR´S CONTRIBUTION

The contribution by the author to the papers included in the thesis is as follows:

I. Deposition of CdTe thin films by CSS, post deposition $CdCl_2$ activation and thermal annealing of CdTe thin films, characterization of the film properties (XRD, photoluminescence, Raman spectroscopy, Van der Paw), analysis of the results, major role in writing.

II. Deposition of CdS and CdTe thin films by CSS, fabrication of CdTe/CdS thin film solar cells, post deposition $CdCl_2$ activation treatment of CdTe/CdS structures, characterization of CdTe properties in CdTe/CdS stack (XRD) characterization of CdTe/CdS thin film solar cells (I-V and EQE), analysis of the results, major role in writing.

III. Deposition of CdTe thin films by CSS, post deposition $CdCl_2$ activation, thermal annealing of CdTe films in H_2 at normal pressure, vacuum and closed quartz ampoules, characterization of the film properties (XRD, Van der Paw and photoluminescence), analysis of the results, major role in writing.

IV. Deposition of CdTe thin films by CSS, sputtering of Au nanoparticles onto CdTe thin films, characterization of the film properties (UV-vis spectroscopy, XRD) analysis of the results, minor role in writing.

V. Fabrication of plasmonic $Ni/Au_{NP}/CdTe/CdS/FTO$ thin film solar cells, characterization of electrical properties (I-V and EQE) of plasmonic $Ni/Au_{NP}/CdTe/CdS/FTO$ thin film solar cells, analysis of the results, major role in writing.

LIST OF ABBREVIATIONS

PV	Photovoltaic
c-Si	Crystalline silicon
a-Si	Amorphous silicon
CIS	$CuInS_2$
CIGS	$Cu(In, Ga)Se_2$
CPV	Concentrating photovoltaics
DSSC	Dye-sensitized solar cells
CdTe	Cadmium Telluride
CdS	Cadmium Sulfide
$CdCl_2$	Cadmium Chloride
TCO	Transparent Conductive Oxide
FTO	Fluorine doped Tin Oxide
ITO	Indium Tin Oxide
SnO_2	Tin oxide
CTO	Cd_2SnO_4
ZTO	Zn_2SnO_4
AZO	Aluminum doped zinc oxide
HRT	Highly resistive thin film
CSS	Close-Spaced Sublimation
VTD	Vapor Transport Deposition
MOCVD	Metal Organic Chemical Vapor Deposition
CBD	Chemical Bath Deposition
ED	Electrodeposition
HVE	High vacuum evaporation
SEM	Scanning Electron Microscopy
EDX	Energy Dispersive X-ray Spectroscopy
XRD	X-Ray Diffraction
PL	Photoluminescence
EQE	External Quantum Efficiency
ETAs	Extremely thin absorbers
SPR	Surface plasmon resonance
NPs	Nanoparticles
GBs	Grain boundaries
E_g	Optical bandgap
T_s	Substrate temperature
LT	Low substrate temperature
HT	High substrate temperature
FF	Fill Factor
J_{SC}	Short circuit current
V_{OC}	Open circuit voltage
η	Efficiency

INTRODUCTION

The development of cost-effective, high-performance solar cells is required to achieve grid parity with fossil fuels [1]. For decades, polycrystalline thin-film solar cells have been recognised as important sources of low-cost and environmentally friendly energy for the future [1, 2]. It has been argued that inexpensive, large-area deposition methods could be developed to yield high-efficiency devices and that monolithic integration methods could lower the cost of module fabrication [2]. Because it meets many of these goals, CdTe is today the most commercially successful thin-film photovoltaic (PV) material, with a major commercial impact on solar energy technology and an estimated market share of 5–6% [2, 3]. CdTe is a favourable material for PV applications because of its nearly ideal bandgap ($E_g = 1.5$ eV) and high optical absorption coefficient ($>10^5$/cm) [4], as recognised in the early 1980s when devices with efficiencies of ~10% were demonstrated [5, 6]. Three decades of research and development have resulted in the present record efficiency of 22.1% [7]. A breakthrough in the open-circuit voltage was reported in February, 2016, which increased the decades-old record of 800–900 mV to more than 1 V [1, 8]. The goal of all these efforts was to increase the efficiency, reliability, and lifetime of PV devices. However, despite these improvements, additional effort is needed in order to reach the theoretical limit of 30% [9]. Despite the high PV performance of CdTe solar cells, there are still several technology-related issues such as back-contact strategy, junction activation, and chloride treatment that require better understanding [2].

Irrespective of the CdTe film deposition method, $CdCl_2$ activation treatment in the presence of oxygen is a standard and vital step for the production of highly efficient CdTe solar cells [2, 4]. During the fabrication of a cell, this processing step is more important than back-contact fabrication because it has a significant impact on the surface composition and chemical nature of the interfaces. $CdCl_2$ treatment promotes grain growth by recrystallisation in the CdTe and CdS layers and passivates and reduces the density of the grain boundaries (GBs) [4, 10-14]. It is accepted that $CdCl_2$ treatment promotes p-type doping of CdTe via complex interactions between Cl and the native defects present in CdTe [4, 15-17]. However, such treatment causes segregation of $CdCl_2$ and $CdCl_2 \cdot 2CdO$ residual phases on the GBs and a high Cl concentration (over 10^{19} cm^{-3}) in the lattice [18-21]. High concentrations of residuals limit the density of charge carriers in p-type CdTe and cause hygroscopicity of the cells, both of which have a strong impact on cell performance [19, 22]. Thus, controlled thermal annealing in ambient conditions of chloride-activated CdTe films could be a way to remove residual phases, thus improving the optoelectronic properties of the CdTe films [22-24].

Developing an efficient device with a very thin CdTe absorber layer (≤1 μm thick) is important for the future growth of CdTe technology. Although a submicron-thick CdTe layer could be beneficial in terms of reducing the cost of materials and manufacturing, there are challenges related to reduced light absorption in thin absorber layers [2, 10, 25, 26]. Therefore, adoption of various light-trapping techniques is required. Employment of the plasmonic effect caused by metallic nanoparticles (NPs) has been found to be effective for enhancing light absorption in ultrathin semiconductor layers in thin-film solar cells [27-31].

In the current thesis, we systematically investigated the influence of different processing variables such as the substrate temperature for CdTe deposition, post-deposition $CdCl_2$ activation treatment, and subsequent multi-step thermal annealing on the structural and optoelectronic properties of close-spaced sublimated CdTe thin films and CdTe/CdS thin-film solar cells. In addition, we studied a novel approach for facilitating the plasmonic effect via incorporation of Au NPs into the CdTe absorber layer for increased light absorption and efficiency of the solar cell.

This thesis is composed of three main chapters. Following the Introduction, Chapter 1, “Literature overview,” provides a short review of PVs, followed by a general overview of CdTe/CdS thin-film solar cells. Further, the properties that make CdTe a favourable material for PVs, as well as the technical challenges associated with development of CdTe/CdS thin-film solar cells, are highlighted. Chapter 2 describes the experimental details of thin-film processing, as well as those of device fabrication. The techniques used to characterise the properties of thin films and solar cells are also introduced. Chapter 3 is divided into three sections and contains original experimental results and a discussion of those results. The first section reports the formation of CdTe/CdS solar cells whose properties are a function of the deposition conditions and post-deposition $CdCl_2$ activation treatment. The second section comprise systematic investigation of the influence of multi-step thermal annealing on the properties of $CdCl_2$-activated CdTe single layers. The third section is devoted to the plasmonic effect of Au NPs on the properties of the CdTe layers and on the performance of CdTe/CdS solar cells. The thesis concludes with a summary of the main goals achieved during the course of this study.

1. LITERATURE OVERVIEW

1.1. Photovoltaics

The development of sustainable energy sources remains essential in order to respond to increased demand caused by greater consumption and population growth [32, 33]. In addition to wind and hydropower, solar energy is one of the most important renewable energy sources [33]. Energy from the sun can be made available either by collecting the energy in the form of heat (solar thermal technology) or by directly converting the sunlight into electricity (PVs). PVs are one of the fastest growing renewable energy technologies, with an annual growth rate of 44%, and it is expected that PVs will play a major role in any future global electricity generation mix [34]. In 2014, the cumulative photovoltaic capacity increased by 40.1 GW, or 28%, and it reached at least 178 GW by the end of the year, which is sufficient to supply 1% of the world's current total electricity consumption of 18,400 TWh [34]. According to GlobalData's latest report, the global installed capacity of solar PVs will increase from 271.4 GW in 2016 at a compound annual growth rate of 13.1% to 756.1 GW in 2025 [35].

There is a wide range of PV cell technologies on the market today using different types of materials, and an even larger number will be available in the future [3, 32]. Crystalline silicon (c-Si) is the most commonly material used in the PV industry, and wafer-based c-Si PV cells and modules dominate the current market, comprising approximately 90% of the annual PV production [32, 33]. This is a mature technology that utilises the accumulated knowledge developed within the electronics industry, with well-developed mass production on a GW-scale. The record laboratory cell efficiencies are 25.6% and 20.8% for mono- and multi-crystalline silicon wafer-based technology, respectively [36, 37]. Although silicon technology is well developed, its potential for cost reduction is limited and the energy payback time is rather long. Thus, thin-film solar cells could be superior to silicon solar cells by lowering production costs and minimising material consumption. Thin-film solar cells comprise successive thin layers 1–4 μm thick deposited onto inexpensive substrates such as glass, polymers, or metals [33]. Thin-film cells require as much as 99% less material than crystalline solar cells while absorbing the same amount of sunlight. In addition, thin films can be used in flexible and lightweight structures, and thus they can be easily integrated into building components [building-integrated PVs (BIPVs)] [33]. Apart from numerous new application possibilities, this flexibility means production could be carried out using a roll-to-roll process, further reducing the production cost. The main thin-film materials commercially available are amorphous silicon (a-Si), cadmium telluride (CdTe), copper indium diselenide (CIS), and copper indium gallium diselenide (CIGS).

Amorphous silicon (a-Si) is the most attractive commercially available material because existing silicon solar-cell technology can be used for manufacturing. However, the known drawbacks of a-Si, i.e., poor absorption and degradation, are roadblocks for this technology [38]. Direct band gap semiconductor materials with high light absorption ability such as CIGS and CdTe are effective alternatives because of their rapidly increasing efficiencies and long-term stability. CdTe and CIGS PVs show world-record efficiencies of 22.1% and 22.3%, respectively, for small-area cells [7]. Although CIGS-based solar cells are the most efficient thin-film technologies, so far manufacturers have not been able to produce CIGS solar panels at prices competitive with CdTe solar panels. There is growing concern by some that the cost of fabricating CIGS products will make it difficult to compete with current grid prices [39]. There is a wide range of other PV cell technologies, such as concentrating PVs (CPVs), dye-sensitised solar cells, and organic solar cells, and novel and emerging solar-cell concepts, but these technologies and concepts are still being researched or they have not yet been widely commercialised [32, 33]. Figure 1.1 shows the highest efficiencies achieved to date with various materials.

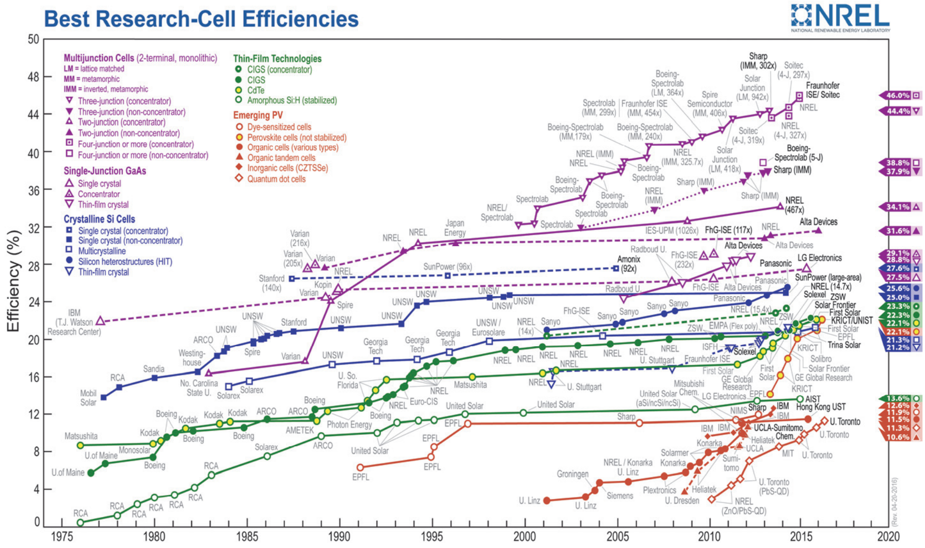

Fig. 1.1. Highest solar-cell efficiencies documented by the U.S. Department of Energy's National Renewable Energy Laboratory [7].

1.2. General overview of CdTe/CdS thin-film solar cells

1.2.1. History and milestones of CdTe solar cells

The development of CdTe solar cells was initially motivated by their potential for application in space-based communication satellites [40]. The first thin-film solar cell of the type n-CdTe/p-Cu_2Te, which had an efficiency of ~7%, was demonstrated by General Electric Research Laboratory in 1963 [41]. Difficulty in controlling the Cu_2Te formation process, poor device stability (caused by Cu diffusion), and lack of a transparent p-type conductor led to the quest for an alternative heterojunction partner for CdTe [40]. In 1972, Bonnet and Rabenhorst presented a paper at the 9th European Photovoltaic Specialists Conference describing the fabrication of a CdS/CdTe/Mo substrate structure using chemical vapour-deposited CdTe and vacuum-evaporated CdS films. The proposed structure had an efficiency of 5–6% [42]. Ten years later, Tyan et al. [5] presented a superstrate thin-film cell with more than 10% efficiency that was grown by close-spaced sublimation—the leading method of later high-efficiency devices. The realisation of a cell in a superstrate configuration was the first milestone of CdTe development. Intermixing between CdS and CdTe, which can easily happen during processing, was believed to be the reason for the superior performance of this configuration [40]. The most important milestone for thin-film CdTe cell performance, with a collateral benefit for processing tolerance, was the post-deposition air heat treatment of CdTe/CdS structures coated with $CdCl_2$ [4, 43]. During the 1990s, optimisation of the $CdCl_2$ treatment/contact/doping processes yielded an impressive cell efficiency of 15.8% [44]. In 2001, there was another important milestone when the National Renewable Energy Laboratory (NREL, USA) achieved 16.7% efficiency [45] as a result of high-temperature absorber film growth, the use of a highly transparent cadmium stannate (CTO) layer as the transparent conductive oxide (TCO), and successful implementation of zinc stannate (ZTO) as a high-resistivity transparent (HRT) layer [46] at the TCO/CdS interface. The most successful technologies for absorber preparation were close-spaced sublimation (CSS) [45] and vapour transport deposition (VTD) [47]. During the decade following these developments, the effects of post-deposition processes on device performance were better understood, and the VTD technique, which can form films on fast-moving substrates, was further optimised by First Solar, eventually becoming the most commercially successful approach [2, 4]. First Solar is a leading global provider of comprehensive photovoltaic (PV) solar energy solutions, with solar cells generating over 10 GW of energy installed worldwide [48]. This company holds the current records for the cell and module efficiency of CdTe PVs: 22.1% and 18.6%, respectively [7, 49].

1.2.2. Device structure

CdTe thin-film solar cells are multilayer structures consisting of semiconductor and metal layers. The primary p–n junction occurs between the p-type CdTe absorber and the n-type CdS layer. The electric field between the p- and n-type semiconductors allows separation of electron–hole pairs, which are generated when a photon is absorbed in the solar cell. The current is collected through electric contacts. One of the contacts needs to be transparent to allow sunlight to enter the solar cell. CdTe solar cells can be fabricated in superstrate or substrate configurations [2]. Devices with the superstrate configuration are processed by forming a transparent TCO/junction-partner/CdTe/back-contact stack on a transparent sheet, i.e., a superstrate, through which light enters the device (Fig. 1.2a) [2]. In the substrate configuration, the deposition sequence is reversed and the stack is formed on a substrate that does not have to be transparent (Fig. 1.2b) [2]. The highest-efficiency devices and commercialised modules are typically fabricated using the superstrate configuration.

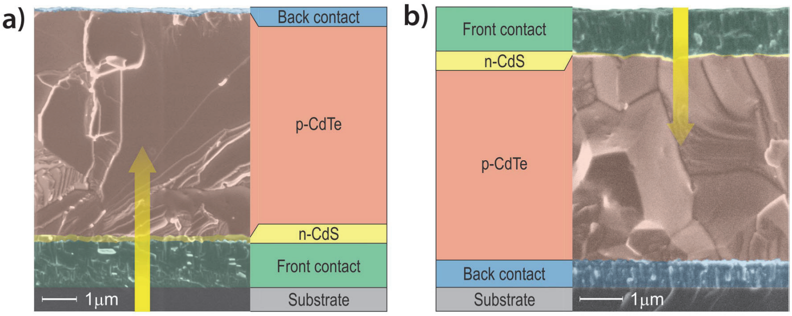

Fig. 1.2. Schematic of CdTe/CdS solar cells fabricated in (a) superstrate and (b) substrate configurations. The yellow arrows indicate the direction of illumination [50].

A crucial step in superstrate cell design is the choice of an appropriate substrate material. The substrate has to withstand high temperatures during subsequent processing steps and be transparent. Commonly used substrates are soda-lime glass and borosilicate glass, which have strain points at approximately 515 °C and 660 °C, respectively. For high efficiency, the junction is formed at temperatures close to 600 °C, limited by the strain point of the glass and the impurity diffusion from the glass into the CdTe absorber [2]. There is typically a diffusion barrier layer (a thin SiO_2 film) at the glass/TCO interface to control such diffusion [2]. The principle requirements for a TCO are that it must be optically highly transparent and highly conductive. A material whose optical transmission is higher than 80% and whose sheet resistance is 5–15 Ω/sq is considered suitable. Commonly used TCOs for PV applications are fluorine-doped SnO_2 (FTO) [51], tin-doped In_2O_3 (ITO) [52], aluminium-doped ZnO (AZO) [53], and Cd_2SnO_4 [54], all of which can be applied using different deposition techniques such as sputtering [53, 54], chemical vapour deposition [44], and spray deposition [55]. All high-efficiency CdTe cells utilise a highly resistive thin film (HRT) [46] as a buffer layer between the TCO and CdS layers. This layer reduces leakage current and improves CdS film quality. The most commonly used materials for this purpose are undoped tin oxide (SnO_2) [56], In_2O_3 [57], and zinc-doped tin oxide (ZTO) [53, 54].

Low-temperature growth processes (≤450 °C) enable the growth of CdTe on flexible substrates. The choice of flexible substrates is very limited because of the restrictions on the transparency of the substrate. The highest efficiencies achieved on flexible substrates were 16.2% on flexible Corning Willow glass [58] and 13.8% on transparent polyimide foil [59].

1.2.3. Relevant component layers and processing of CdTe solar cells

1.2.3.1. CdS layer and thin-film fabrication methods

High-efficiency CdTe solar cells generally use a CdS-based semiconductor as the n-type layer [54]. CdS crystallises in cubic zinc blende and/or hexagonal wurtzite structures [60], and it intrinsically grows as an n-type semiconductor [17]. For CdS thin films, there are widespread reports of E_g values that vary from 2.2 eV [61] to 2.6 eV [62] as a function of the deposition technique, deposition parameters, and post-deposition treatments [63]. The use of CdS as a buffer layer has advantages such as the reduced concentration of interface defect states at the p–n junction and proper energy band alignment with the CdTe layer [64]. Because CdS typically does not contribute photocurrent to the cell, its relatively narrow bandgap causes parasitic absorption at wavelengths lower than 500 nm; for this reason, its thickness needs to be reduced as much as possible [2]. However, a very thin CdS layer is more inclined to show pinhole formation, leading to shunting between the CdTe layer and the TCO. The use of an HRT layer on the TCO can prevent the formation of these shunts. The incorporation of oxygen into the CdS [54] film during deposition improves its durability when it is exposed to high CdTe deposition temperatures. The presence of oxygen reduces the vapour pressure and diffusivity, allowing ultrathin CdS films (<50 nm) to be fabricated [2]. The possible methods for depositing CdS onto a substrate include chemical bath deposition (CBD) [54, 65], sputtering [66], high-vacuum evaporation (HVE) [53, 67], CSS [54, 68], and metal organic chemical vapour deposition (MOCVD) [69].

1.2.3.2. CdTe absorber layer and thin-film fabrication methods

CdTe is a group II–VI compound semiconductor with a direct optical band gap of E_g = 1.49 eV and a high absorption coefficient (>5 × 10^5/cm), making it an ideal absorber-layer material for thin-film solar cells [4]. Figure 1.3 compares the theoretical efficiencies of solar cells and the optical absorption coefficients as a function of the band gap for CdTe and other materials commonly used in PV cells. The high CdTe absorption coefficient for photons with $E > E_g$ translates into 99% absorption of the absorbable AM1.5 photons within a 2-µm-thick film [4]. The theoretical efficiency limit of CdTe-based solar cells is approximately 30% [9].

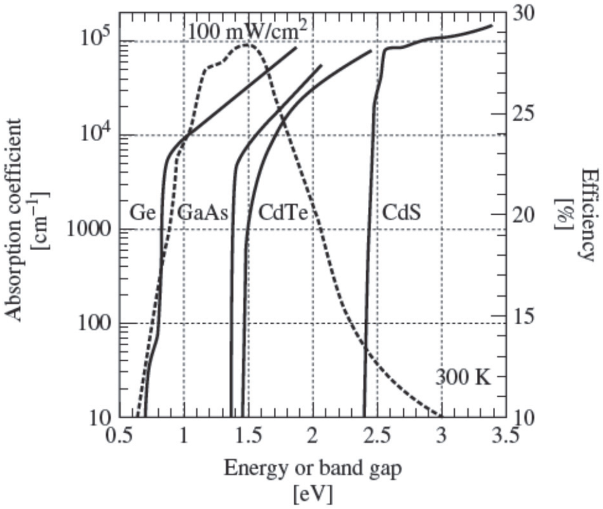

Fig. 1.3. Theoretical solar-cell efficiency (dotted line) for AM1.5 spectral irradiance as a function of the band gap and the absorption coefficient (solid line) as a function of energy for selected semiconducting photovoltaic materials [4].

CdTe is unique among the II–VI compounds in that it exhibits the highest average atomic number, the least negative formation enthalpy, the lowest melting temperature, the largest lattice parameter, and the highest ionicity [4]. The large negative formation enthalpy (ΔH_f = −22.4 kcal/mol) and the correspondingly low vapour pressure (p_{sat} = 10^{-5} at 400 °C) facilitate the synthesis of CdTe compounds. The phase diagram of CdTe [70] indicates a very narrow stability region (~10^{-6} at%) with perfect stoichiometry at temperatures below 500 °C (Fig. 1.4a). At temperatures higher than 500 °C, this region widens and becomes asymmetrical on the Cd-rich side up to 700 °C, becoming Te-rich at temperatures higher than 700 °C [4, 71]. The CdTe melting temperature, T_m = 1092 °C, is significantly higher than that of the individual elements, Cd (T_m = 321 °C) and Te (T_m = 450 °C) [4, 71]. Figure 1.4b presents the saturated vapour pressures for CdTe, Cd, Te, CdS, and $CdCl_2$ over the temperature range employed for the fabrication of the solar cells, i.e., from 100 to 600 °C. The high ionicity (72%) and strong chemical bonding (5.75 eV) of CdTe results in high chemical and thermal stability against electron/proton irradiation [4, 10].

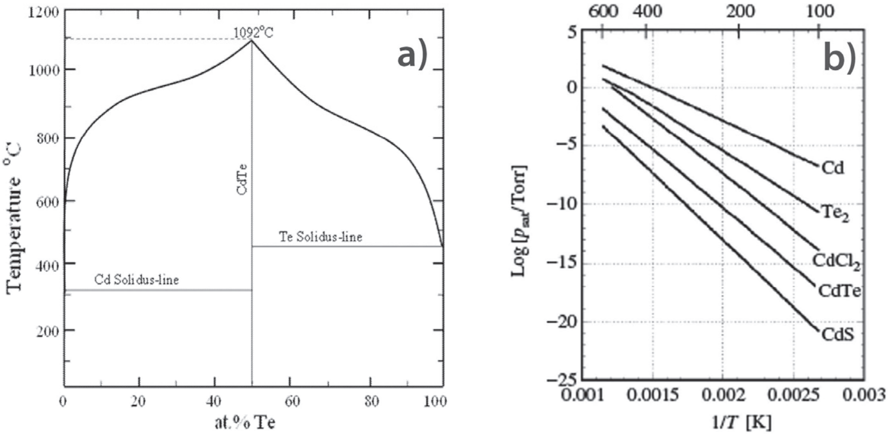

Fig. 1.4. (a) CdTe T – x phase diagram [87] and (b) vapour–solid p_{sat} versus 1/T diagram for CdTe, CdS, $CdCl_2$, Cd, and Te [54].

CdTe crystallises in a cubic zinc blende structure and allows both n- and p-type doping [17]. The defects controlling the electronic properties include native defects and defects caused by chemical impurities and their respective complexes. Native defects and impurity defects can occur substitutionally or interstitially. Cd vacancies (V_{Cd}) give rise to shallow acceptor states, whereas Cd substitution on a Te site (Cd_{Te}) gives rise to shallow donor states. Interstitial Cd (Cd_i) gives rise to relatively shallow donor states, whereas interstitial Te, Te_i, gives rise to deep donor states [4, 17, 40, 72]. Intrinsic p-type doping requires a Cd-poor preparation. The hole concentration is limited by the large defect transition energy of V_{Cd}^0 [40]. In CdTe solar cells, p-type CdTe is used and the desired acceptor doping is obtained using different post-deposition treatments, one of which is chloride activation. In this process, impurities such as $CdCl_2$ and oxygen are incorporated into the CdTe layer, where they may activate or passivate native defects [4, 73]. The effects that take place during chloride activation will be discussed in Section 1.2.3.3.

Using the simple phase diagram of CdTe and its congruent evaporation characteristics, high-rate deposition can be carried out using various techniques.

These techniques can be divided into high-temperature physical deposition methods (substrate temperature ≥500 °C), such as CSS [45] and VTD [47], and low-temperature deposition methods (substrate temperature ≤450 °C), such as MOCVD [69], sputtering [66], electrodeposition (ED) [74] and HVE [67]. The most widely used techniques for commercially manufacturing CdTe solar cells and modules are VTD and CSS. Figure 1.5 presents schematic views of these techniques, including nominal temperatures and pressure conditions, film thicknesses, and growth rates.

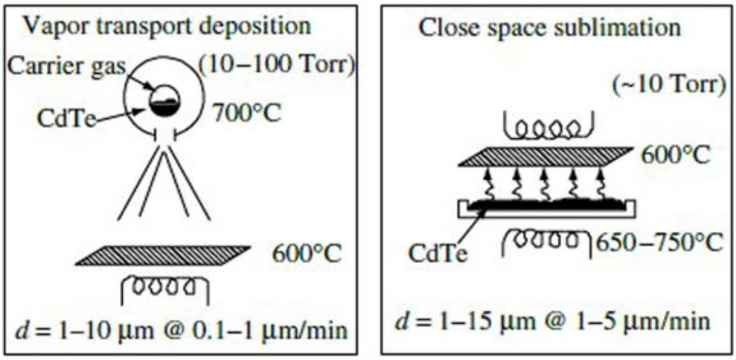

Fig. 1.5. Schematic representations of VTD and CSS CdTe deposition techniques. The rectangular cross section represents the substrate. The film thickness, d, and the growth rate are shown at the bottom of each panel [54].

Vapor transport deposition

VTD works by convective transfer of a vapour stream saturated with Cd and Te to the substrate, where supersaturation of the Cd and Te vapours results in condensation and a reaction to form CdTe [4, 47]. The CdTe source consists of a heated chamber containing solid CdTe. The carrier gas mixes with the Cd and Te vapours and is exhausted through a slit over or under the moving substrate at a distance of ~1 cm. The geometrical configuration of the source influences the uniformity and utilisation of the vapours in the carrier gas. The carrier-gas composition can be varied to include N_2, Ar, He, and O_2. The as-deposited VTD CdTe films exhibit nearly random orientation and grain sizes comparable to the film thickness [4]. VTD provides a very high deposition rate onto moving substrates and is currently the most successful technology used by First Solar for large-scale production of CdTe PV modules [47].

Close-spaced sublimation

The principle of CSS is very similar to that of VTD. The transport of species from the source to the substrate is controlled by diffusion. The distance between the source and substrate is 2–20 mm. The deposition rate can be in the micrometres per minute range. The CdTe source material (typical purity of 5N) is supported in a holder having the same area as the substrate. The source holder and substrate cover serve as susceptors for radiative heating and conduct heat to the CdTe source and the substrate, respectively [4, 40]. The ambient conditions for deposition can be varied to include nonreactive gases such as N_2, Ar, or He. A small partial pressure of O_2 appears to be crucial for obtaining good film density and good solar-cell junction quality [4]. The CSS process has been intensively investigated by groups at Kodak [5], USF [65, 75], NREL [45], and Antec [68, 76]. The CSS technique is commercially employed by Antec, Germany [76].

1.2.3.3. $CdCl_2$ treatment

Irrespective of the CdTe film deposition method, $CdCl_2$ treatment is an indispensable technique for producing efficient CdTe/CdS solar cells. As originally established, $CdCl_2$ treatment consists of immersing a CdTe/CdS/TCO/glass stack into $CdCl_2$–CH_3OH or $CdCl_2$–H_2O solutions [76-79]. When the stack is removed from the solution and dried, $CdCl_2$ forms on the surface of the CdTe layer. The subsequent activation treatment is performed in air at 380–450 °C, typically for 15–30 min [77-79]. For mass production, this process has been improved by using a $CdCl_2$ thin film deposited by vacuum evaporation [80] or CSS [76]. As alternative sources of Cl activators, several groups have applied different gases such as Freon® (HCF_2Cl) [81, 82] and HCl [11] and different salts such as $MnCl_2$ [79] and NaCl [83]. The activation heat treatment in different ambient gases (vacuum, inert gas, varying oxygen contents) was also investigated [84].

Structural effects and chemistry of the process

Irrespective of the employed method, $CdCl_2$ treatment has a strong influence on the structure of the CdTe and CdS layers and their interfaces. The treatment promotes grain growth and sintering by recrystallisation in the CdTe and CdS layers, and it passivates and reduces the density of GBs [10-14, 79, 81, 82, 84].

The recrystallisation of CdTe during $CdCl_2$ activation treatment depends on the initial grain size. The smaller the grain size, the more significant the grain growth [10-14]. CdTe films deposited by CSS at high substrate temperatures (≥500 °C) do not show any significant grain growth during the activation step [4, 12, 85], and it is likely that the treatment initiates densification of the layers by sintering. The deposition of CdTe films at high temperatures, $CdCl_2$ activation, and grain boundary diffusion are thought to be responsible for promoting interdiffusion at the CdTe/CdS interface and converting this interface into a $CdS_{1-y}Te_y/CdTe_{1-x}S_x$ junction [2, 4, 86, 88]. The values of x and y depend on the temperature: typical values are $x \approx 0.05$ and $y \approx 0.03$ [86, 87]. The alloy formation at the CdTe/CdS interface reduces the lattice mismatch at the junction from ~11 to ~9% and decreases the energy gap slightly on each side of the junction because of the optical bowing parameter induced by non-ideal mixing [2, 4, 86].

The mechanism of the $CdCl_2$ treatment is not yet fully understood. For the CdTe–$CdCl_2$ system, enhanced mobility of CdTe in the recrystallisation process can be expected for temperatures higher than the eutectic (~505 °C, Fig. 1.6). At these higher temperatures, melted solutions of CdTe in $CdCl_2$ with high concentrations of CdTe will form [88, 89].

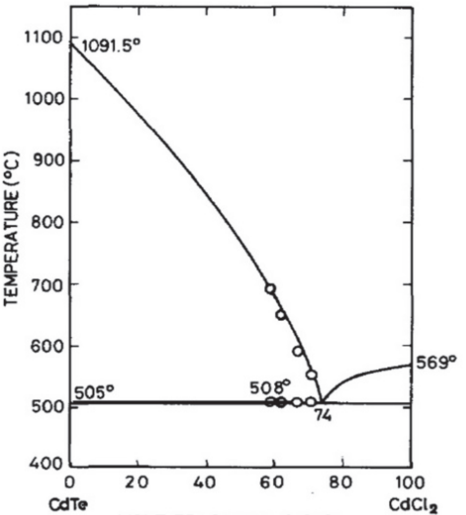

Fig. 1.6. Phase diagram of the CdTe–$CdCl_2$ system [89].

It is understood that solid $CdCl_2$ has little influence on the properties of the CdTe layers [88]. The direct reaction (Eq. 1.1) between CdTe and $CdCl_2$ upon formation of active Cd and $TeCl_2$ vapours is not thermodynamically favourable, although some authors have used this reaction to explain the recrystallisation activity of $CdCl_2$ [90].

$$\mathrm{CdCl_2(s) + CdTe(s) \leftrightarrow 2Cd(g) + TeCl_2(g)},\ \Delta G\ (400\ ^\circ\mathrm{C}) = 76.4\ \mathrm{kcal/mol} \tag{1.1}$$

Only strong oxidants such as oxygen and halogens can oxidise Te^{2-} ions and, by the formation of active $TeCl_2$ in the gas phase, promote intensive vapour-phase transport of CdTe. The reactions in a system containing CdTe, $CdCl_2$, and oxygen were described by McCandless et al. [88] as follows:

$$\mathrm{CdCl_2(s) + CdTe(s) + O_2(g) \leftrightarrow TeCl_2(g) + CdO(s)},\ \Delta G\ (400\ °\mathrm{C}) = -32.9\ \mathrm{kcal/mol} \quad (1.2)$$

$$\mathrm{CdTe(s) + TeCl_2(g) \leftrightarrow CdCl_2(g) + 2Te(s)},\ \Delta G\ (400\ °\mathrm{C}) = -14\ \mathrm{kcal/mol} \quad (1.3)$$

$$\mathrm{CdTe(s) + O_2(g) \leftrightarrow CdTeO_3(s)},\ \Delta G\ (500\ °\mathrm{C}) = -66.3\ \mathrm{kcal/mol} \quad (1.4)$$

According to the thermodynamically favoured reactions (1.2–1.4), volatile $TeCl_2$ species, free Te, and a solid CdO phase are produced. The formation of a gaseous $TeCl_2$ phase at the GBs provides for enhanced surface mobility of both Cd and Te atoms, which promotes CdTe grain growth [88].

For junction activation with Freon® gas [80, 81] during heat treatment at approximately 400 °C, CHF_2Cl decomposes and releases Cl gas, which acts as a catalyst for the chemical vapour-phase transport of CdTe according to the chain reaction:

$$\mathrm{CdTe(s) + 2Cl_2(g) \rightarrow CdCl_2(s) + TeCl_2(g) \rightarrow CdTe(s) + 2Cl_2(g)} \quad (1.5)$$

This process favours CdTe film recrystallisation and grain growth by vapour-phase chemical transport, enhances the film crystalline quality, and reorganises the CdS–CdTe interface [80, 81].

The aforementioned processes do not account for the formation of liquid flux, which is required in order to explain the sintering and densification of the CdTe grains, as previously demonstrated by the authors [80, 81, 88, 90]. According to differential thermal analyses, the melting point of the CdTe–$CdCl_2$–$CdTeO_3$ system is lower than the eutectic temperature of CdTe–$CdCl_2$, and the melting point of the CdTe–$CdCl_2$–$CdTeO_3$ system decreases as the molar portion of $CdTeO_3$ increases [91]. This observation justifies the application of liquid-phase recrystallisation and sintering rules to explain the processes going on during the $CdCl_2$:O_2 activation treatment step.

Electronic effects and doping

$CdCl_2$ treatment promotes p-type doping and increases the minority carrier lifetime. The ionised acceptor density is on the order of 10^{13}–10^{14} cm^{-3} [1, 51, 92], and the minority carrier lifetime increases from 50–100 ps to 1–15 ns [12, 40, 92, 93]. The limitations of p- and n-type doping via $CdCl_2$ treatment are believed to be caused by compensation effects in defect chemistry [1, 16, 17]. A

Cl atom is thought to substitute for a Te atom in CdTe and act as a shallow donor related to the formation of Cl_{Te}^{+}, with an energy level of $E_c = 0.014$ eV [17, 22, 94]. The Cl solubility on substitutional Te sites at 505 °C is approximately 10^{17} cm^{-3} [95]. With Cd vacancies, Cl forms defects, shallow acceptors or so-called A centres $[(V_{Cd}^{-2}Cl_{Te}^{+})^{-}]$ at $E_V = +0.12$ eV, and a neutral complex $(V_{Cd}^{2-}2Cl_{Te}^{+})$ [22, 94]. Cd vacancies are deep acceptors at $E_V = 0.47$ eV [96]. Castaldini et al. enumerated 12 defect trap levels for Cl dopants in CdTe and showed the role of A centres $[(V_{Cd}^{-2}Cl_{Te}^{+})^{-}]$ and mid-gap traps in the compensation process [94].

High concentrations of Cl (up to 10 mol% $CdCl_2$) are required for optimal recrystallisation and sintering in the $CdCl_2$ air treatment process [91]. The process results in segregation of $CdCl_2$ and $CdCl_2 \cdot 2CdO$ residual phases on the GBs [18-21] and high Cl concentrations in the CdTe lattice [22, 23], with a total concentration of more than 10^{19} cm^{-3} [20]. Terheggen et al. demonstrated by transmission electron microscopy the distribution of precipitates containing Cl, Cd, Te, and O at the CdTe/CdS interface [18]. Gessert et al. found that residuals are spatially discrete, located primarily along GBs, and likely comprise cadmium oxychloride [19]. They also demonstrated that the residuals penetrated deeply into the CdTe polycrystalline layer; ion-beam etching could not remove the residuals completely [19]. Presumably, high concentrations of residuals limit the density of charge carriers in p-type CdTe and cause hygroscopicity of the cells. They therefore have a strong impact on the cell performance [19, 22].

Controlled thermal annealing in relevant ambient of Cl-activated CdTe films could be a way to remove residuals, thus improving the optoelectronic properties of the CdTe films. Systematic studies of this were carried out by Valdna et al. [22, 23], who achieved high p-type conductivity in CdTe films without any acceptor dopant, but the concentration of Cl in the films was decreased by vacuum annealing. In the current investigation, the $CdCl_2$ treatment was carried out in closed evacuated quartz ampoules at 507 °C in the absence of oxygen. Although oxygen was not expected to form a shallow dopant, there are several reports on the doping effect of O_2 used as ambient during CdTe deposition [5, 40, 97]. By oxygen doping, the hole concentration can reach 10^{15} cm^{-3}, whereas without oxygen, it is one order of magnitude lower [40, 98]. So far, the best solar cell, which was made without intentional oxygen incorporation, showed an efficiency of 12.8% [99]. However, all high-efficiency CdTe solar cells (>15%) are fabricated in the presence of oxygen. Still, it is not clear which effect of oxygen in CdTe films is responsible for superior device performance [40].

1.2.3.4. Back contact

Back-contact formation is an important process step for fabricating high-efficiency devices. Generally, the formation of a low-resistance and stable electrical contact to the CdTe layer is challenging because of the formation of a Schottky barrier at the CdTe/metal interface, which is caused by the high electron affinity (χ = 4.5 eV) of the CdTe layer and Fermi-level pinning at the CdTe/metal interface [10, 14]. Most of the approaches used to obtain good contact to CdTe thin films rely on the introduction of a buffer layer with an electron affinity higher than that of the p-type CdTe and the formation of a heavily doped region at the back surface of CdTe. This heavily doped region either reduces the height of the barrier or moderates its width adjacent to the contact to promote tunnelling prior to back-contact formation [100, 101]. Chemical etching and the deposition of an additional Te layer on top of the CdTe layer are commonly used methods for producing a Te-rich p^+-doped layer, which effectively increases the conductivity, thus aiding the formation of tunnelling junctions with more reliable contact [102-104]. A Cu source layer is also deposited onto the clean surface, allowing Cu atoms to diffuse into the CdTe layer through moderate annealing [2, 4]. Cu source layers include Cu-doped graphite paste and low-resistivity compounds such as Cu_2Te [4] and Cu-doped ZnTe [105], which form low-resistance primary contacts with contact potential barriers below 0.3 eV [2, 4]. Traditionally, Cu is believed to be a p-type dopant in CdTe. After the doping step, high-efficiency devices are reported to have an ionised acceptor density in the $0.5–1 \times 10^{15}$/cm^3 range [50, 93]. Other buffer layers used include Sb_2Te_3 [106], As_2Te_3:Cu [107], and MoO_x [108]. After deposition of the buffer layer, a robust secondary contact is deposited on top of the CdTe layer in order to facilitate lateral current collection. The secondary contact in laboratory devices may be a single metal film such as Au, Ni, or Mo, which is usually deposited by vacuum evaporation or sputtering [2, 4].

1.3. Challenges associated with CdTe/CdS thin-film solar cells

The performance of CdTe/CdS solar cells strongly depends on the formation of the interface structure during thin-film deposition and any subsequent processing. In spite of significant tolerance to the deposition technique, there are some technology-related issues such as back-contact strategies and chloride activation treatment that require better understanding. The major issue associated with p-type CdTe is the difficulty in achieving low resistance and a stable electrical contact. This problem could be solved by incorporation of an optimal amount of Cu at the back contact. However, this requires delicate control as Cu deficiency can lead to non-ohmic behaviour, whereas excess Cu can affect the junction because of fast diffusion into the CdTe matrix. A full understanding of the role of Cu and other possible contact metals for back-contact chemistry and their behaviour within the device structure is required in order to optimise the device performance.

During the fabrication of solar cells, the $CdCl_2$ treatment step prevails over the back-contact formation because $CdCl_2$ treatment has a significant impact on the surface composition and the chemical nature of the interfaces, as well on the p-type conductivity in CdTe. The mechanism by which chloride treatment promotes structural and optoelectronic changes in CdTe and CdS is still ambiguous. Lack of a common understanding of the physicochemical processes behind this treatment step represents an impediment for further development of this promising device.

One critical issue in CdTe technology is reduction of the PV active layer thickness in order to lower production costs and reduce the use of Te. Devices with absorber thicknesses in the 0.8–1.15 μm range have been fabricated by low-temperature CSS [25] and sputtering [26] techniques, yielding efficiencies of 9.5 and 12.9%, respectively. However, there are two main challenges in processing cells with submicron-thick CdTe layers: increased recombination losses and reduced light-absorbing ability [2, 26]. In this sense, theoretical solutions such as electron back-reflectors [109] and plasmonic NPs [31] have been proposed for new CdTe solar-cell designs with extremely thin absorbers (ETAs).

1.3.1. Plasmonic absorption enhancement for CdTe solar cells with extremely thin absorbers

One of the promising solutions for enhancing the broadband light absorption of ETA solar cells is the use of the plasmonic effect via the incorporation of metal NPs [31]. When metallic NPs absorb light, the oscillating electromagnetic field of the light triggers polarisation of the conduction-band electrons on the surfaces of the NPs. The polarised electrons go through collective coherent oscillations with respect to the positive ions in the metallic lattice; these oscillations are called surface plasmon oscillations (Fig. 1.7a) [31, 110]. Because surface plasmon oscillation has the same frequency as the incident light, it is also known as surface plasmon resonance (SPR) [110]. Resonance between the oscillations of the surface electron plasma and the incident light results in a strong concentration of light energy and the electric field, enhancing light absorption and light scattering near metal NPs in a certain resonance spectral range [111, 112].

By placing metal NPs at the interface between two media, more light is scattered from the medium with the higher refractive index (Fig. 1.7b). Thus, metal NPs placed on top of the solar-cell absorber layer can provide more light scattering and harvesting inside the material [112]. Improved light absorption can also be realised through the incorporation of NPs within the active layer of the solar cell (Fig. 1.7c). Because the cross section of the plasmonic light absorption of the metal NPs is larger than its geometrical cross section, plasmon resonance in the metal could enhance light absorption in the semiconducting host within a certain spectral range [112].

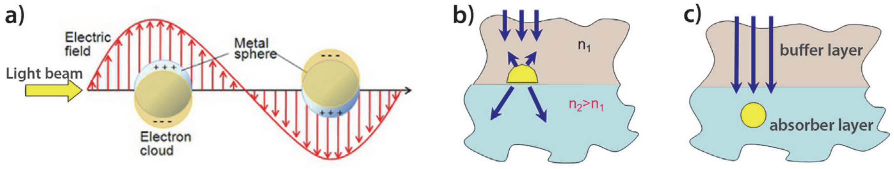

Fig. 1.7. (a) SPR of spherical metal NPs. (b) Light trapping in the medium with higher refractive index, where n_1 and n_2 are the refractive indices of the layers. (c) Enhancement of light trapping by plasmonic particles placed within the absorber layer.

Improved light absorption and photocurrent by the plasmonic effect of NPs have been demonstrated for thin-film Si solar cells [27], polymer cells [113], dye-sensitised cells [114], and ETA solar cells such as $CuInS_2$ [29, 30] and $Cu(In, Ga)Se_2$ [28]. Metal NPs have been made by various techniques, such as vacuum evaporation [115], spin coating [116], electrodeposition [117], and spray pyrolysis [29, 30]. However, no experimental results have yet been reported on the application of plasmonic NPs in CdTe solar cells.

Gu et al. theoretically demonstrated that combining periodic metal nanostructures on top of ultrathin CdTe layers can be an effective approach to enhancing broadband optical absorption by the CdTe absorber [31]. Among the various metals (Ag, Al, Au, Cu) and geometries investigated, i.e., nanodiscs (NDs) and nanospheres (NS), Al NDs tend to provide the maximum enhancement over the spectral absorption range of interest. The plasmon resonance wavelength of Al NDs leads to an optimal localised SPR spectrum that maximally matches the intrinsic CdTe absorption profile weighted with the solar spectrum [31].

Recently, Repan et al. theoretically showed for a CdTe/CdS solar cell the additional effect of metal NP placement with respect to the Te back contact [111]. The geometry used to simulate the effects of particle size, interparticle distance, and Te back contact on the plasmonic resonance is depicted in Fig. 1.8. Plasmon NPs were embedded or placed on top of the Te layer, into the CdTe material. To avoid spurious reflections from the simulation boundary, a perfectly matched layer boundary region was used.

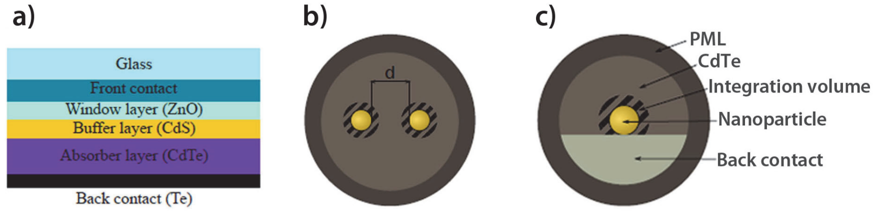

Fig. 1.8. (a) The considered solar-cell structure. (b) Simulation geometry of two NPs immersed in CdTe with a particle distance d. (c) Geometry used for simulations on the influence of CdTe–Te on Au NP effectiveness [34].

According to this theoretical study, the absorption in CdTe could be locally enhanced up to two-and-a-half times in the vicinity of noble metal NPs. Ag or Au NPs with diameters of 45–50 nm in particular provided theoretical enhancement of the light absorption in the 650–900 nm range, with a maximum at 815 nm. Interaction of plasmons induced in neighbouring NPs became significant only when the distance between them was quite small (≤50 nm), allowing for incorporation of the NPs into the CdTe material without strong broadening or redshifting of the plasmon resonance spectral band. These results suggest the technological feasibility of placing NPs in the CdTe layer close to the Te back contact to enhance the efficiencies of solar cells. This approach would significantly reduce the thickness of thin-film solar cells, thus decreasing demand for scarce semiconductor materials such as Te, the supply of which limits upscaling of CdTe solar cells.

1.4. Summary of the literature overview and aims of the study

The literature review can be summarised as follows:

1. CdTe is a group II–VI compound semiconductor that makes an excellent absorber for thin-film solar cells because of its nearly ideal direct band gap (E_g=1.5 eV at 300 K), high absorption coefficient (>5 × 10^5/cm), zinc blende or wurtzite structure in binary solids, and tuneable electrical properties. The theoretical limit to the efficiency of CdTe-based solar cells is approximately 30%.
2. Congruent evaporation characteristics enable high-rate deposition using various deposition techniques. The most widely used deposition techniques that have demonstrated viability for the commercial manufacture of CdTe solar cells and modules are VTD and CSS.
3. The performance of CdTe/CdS solar cells strongly depends on the formation of the interface structure during thin-film deposition and

any subsequent processing. Systematic investigation is necessary to understand the relationship between CSS deposition conditions and layer morphology and to identify the mechanisms leading to the different growth regimes and possible routes to controlling the film morphology and resulting efficiency.

4. $CdCl_2$ treatment is required for the fabrication of highly efficient CdTe/CdS solar cells. The treatment promotes grain growth by facilitating recrystallisation in CdTe and CdS layers and passivates and reduces the density of GBs. High concentrations of chloride (up to 10 mol% $CdCl_2$) are required for optimal recrystallisation and sintering in the $CdCl_2$ air treatment process. The process results in segregation of $CdCl_2$ and $CdCl_2 \cdot 2CdO$ residual phases on the GBs and high chlorine concentrations in the CdTe lattice, with a total concentration of more than 10^{19} cm^{-3}.
5. High concentrations of residuals limit the charge-carrier density in p-type CdTe and cause hygroscopicity of the cells, which strongly impacts cell performance. Controlled thermal annealing in relevant ambient of chloride-activated CdTe films could remove the residuals, thus improving the optoelectronic properties of the CdTe films.
6. CdTe technology is attractive in terms of its limited life-cycle greenhouse gas and heavy metal emissions, small carbon footprint, and short energy payback times. Limited Te availability limits the growth of this technology unless Te utilisation rates can be greatly enhanced along with device efficiencies.
7. Use of the plasmonic effect via the incorporation of metal NPs could boost the absorption of CdTe, making it possible to decrease the thickness of the PV active layer.

Based on the literature overview, this thesis has the following aims:

1. To design and develop a CSS system for the deposition of CdTe thin films and CdTe/CdS thin-film solar cells.
2. To investigate systematically the influence of different processing variables such as the substrate temperature for CdTe deposition, post-deposition $CdCl_2$ activation treatment, and subsequent multi-step thermal annealing on the structural and optoelectronic properties of CSS CdTe thin films and CdTe/CdS thin-film solar cells.
3. To describe the physicochemical processes responsible for the changes in the CdTe thin film and CdTe/CdS solar-cell properties with respect to different processing conditions
4. To study use of the plasmonic effect to increase light absorption and solar-cell efficiency via the incorporation of Au NPs into the CdTe absorber layer.

2. EXPERIMENTAL

2.1. Close-spaced sublimation system for thin-film deposition

A home-made CSS system was designed and built for this study. The main design requirement for the equipment was that it had to provide a high-purity deposition environment. A schematic diagram of the system is shown in Fig. 2.1a. The system consisted of two cylindrical graphite blocks stacked vertically on top of each other supported by sets of stainless steel cylindrical tubes and holders. A quartz tube was positioned within a cylindrical hole in one of the graphite blocks, which is referred to as the source graphite block. A substrate block was placed on top of the source block; a quartz crucible was used to hold the source material and to provide separation between the source and the substrate graphite blocks. Heating for both the source and substrate blocks was provided by tungsten coil heaters. Thermocouples were inserted inside the graphite blocks to control the temperature. The temperatures recorded for the substrate and source graphite blocks were assumed to be the actual temperatures of the substrate and the source material, respectively. The heaters were individually controlled. Two separate CSS chambers were set up for CdTe and CdS deposition, respectively. The deposition of the films was carried out using a specially designed vacuum system, also shown in Fig. 2.1b.

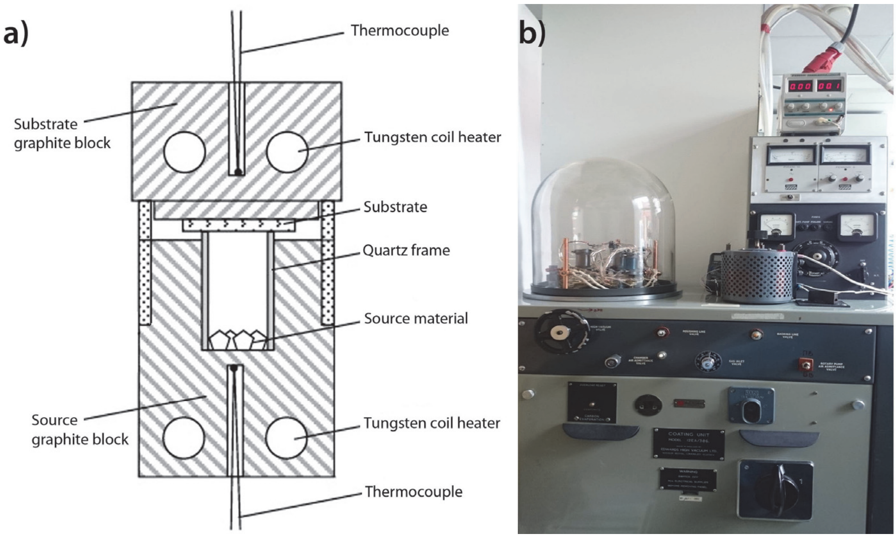

Fig. 2.1. (a) Schematic representation of CSS and (b) picture of vacuum systems.

2.2. Fabrication of CdTe thin films and CdTe/CdS solar cells

Glass/FTO substrate

FTO-coated soda-lime glass substrates (Sigma-Aldrich) were used for the fabrication of CSS CdTe/CdS solar cells in a superstrate configuration. The typical sheet resistance of the FTO layer was 13 Ω/sq, with a nominal film thickness of 200 nm. Prior to the deposition of the thin films, the 100 × 100 × 2 mm glass/FTO substrates were cleaved into smaller substrates with dimensions of 20 × 20 × 2 mm and cleaned. The cleaning procedure consisted of successively washing the substrates with water and soap, degreasing in a 10 g $K_2Cr_2O_7$ + 10 mL H_2O + 100 mL H_2SO_4 solution for 2–3 h at room temperature (RT), washing again in a series of ultrasonic baths containing deionised water, and final air drying.

CdS deposition

CdS thin films were deposited onto the FTO layer by CSS. The source was a powdered material with 5N (99.999%) purity (Alfa Aesar). The deposition time and source and substrate temperatures were kept constant for all CdS layers and were established at 10 min, 650 °C, and 400 °C, respectively. In a standard deposition cycle, the CdS thickness was approximately 150 nm.

CdTe deposition

The CSS CdTe absorber layers were deposited from CdTe source materials with 5N (99.999%) purity (Alfa Aesar). The source temperature and deposition time were kept constant at 610 °C and 5 min, respectively, whereas the substrate temperature was varied from 250 °C to 500 °C. The CdTe absorber layers were typically approximately 3–5 μm thick. A series of CdTe films were also directly grown onto chemically and thermally etched 20 × 20 × 1 mm roughened glass plates at substrate temperatures of 250 and 500 °C. Roughened glass plates with a root mean square roughness, Rq, of 2.66 nm (O. Kindler) were used to ensure better adhesion of the CdTe layers.

Post-deposition $CdCl_2$ treatment

The wet method was used for $CdCl_2$ treatment. A saturated solution was prepared by dissolving $CdCl_2$ powder (5N purity, supplied by Alfa Aesar) in methanol. The CdTe thin films and CdTe/CdS structures were soaked in the saturated solution for 1 h. After allowing the methanol to fully dry in ambient air, the samples were transferred to a furnace for activation heat treatment at 420 °C in air. The activation duration was set for 20 min. After cooling to RT, the activated samples were rinsed with deionised water and etched in a standard NP

(H_3PO_4:HNO_3:H_2O) solution to remove the $CdCl_2$ residue and to provide a suitable Te-rich surface. Samples were immersed in the solution for 30 s before being rinsed with de-ionised water and dried. The CdTe/glass samples were cleaved into smaller samples with dimensions of 5 × 5 mm and subjected to a series of thermal treatments under different conditions, which are described below.

Secondary thermal annealing of CdTe films in H_2 atmosphere

Thermal annealing of the CdTe-activated samples was carried out in a closed process tube in H_2 atmosphere. First, air in the process tube containing the samples was evacuated; the tube was then filled with 1 atm H_2 gas at room temperature, closed, and introduced into a cylindrical furnace. The annealing temperature was varied in the 250–570 °C range and the annealing time was fixed at 1 h. The furnace was slowly heated to the set temperature, allowing the residual precipitates to outdiffuse to the CdTe surface. The H_2 pressure in the process tube was maintained using a standard gas reduction system and was not influenced by the expansion of the gas at high annealing temperatures. The large diameter (55 mm) and volume (1500 mL) of the process tube ensured an excess of H_2 and gas convection flow so that the reaction products were transported to the colder part of the tube. After thermal annealing in H_2, the sample passed through two more treatments: vacuum and isothermal treatment.

Vacuum and isothermal annealing

Vacuum annealing of the samples was carried out in the same process tube described above at 470 °C for 1 h. Isothermal annealing was carried out with the CdTe samples in sealed-off evacuated ($\leq$1 Pa) quartz ampoules at 600 °C for 1 h. The ampoule volumes were typically approximately 10 cm^3. Prior to loading, the ampoules were etched in HF/HNO_3, followed by annealing at 1000 °C under dynamic vacuum.

Contacting

Different types of back contacts (Au, Ni, In, and Te) were formed by vacuum evaporation using source materials supplied by Sigma-Aldrich or Alfa Aesar. For the solar cells, Te/Au or Te/Ni back contacts with different geometries were deposited through an evaporation mica mask placed between the evaporation source and the sample. In and Au with dot contact geometries were used for measuring the resistivity of the CdTe single layers. Prior to the application of the metal contact, a thin layer of Te was deposited on top of the CdTe layer.

2.3. Incorporation of plasmonic Au nanoparticles into CdTe thin-film absorber

CdTe thin films with thicknesses of ~300 nm were deposited onto soda-lime glass substrates and coated with Au NPs using three different methods: spin coating, spray pyrolysis, and sputtering.

Au nanoparticles by spin coating

The spin coating of Au NPs was carried out using $HAuCl_4 \cdot 3H_2O$ ethanol solutions at concentrations of 0.05, 0.075, and 0.1 M at RT using two spin ramp rates: 600 rpm for 5 s and 1200 rpm for 20 s. After coating, the samples were dried in air at 85 °C for 40 min and air annealed on a hot plate at 380 °C for 1 h.

Au nanoparticles by spray pyrolysis

In the case of spray pyrolysis, the Au NPs were deposited using the same $HAuCl_4$ solution described above on preheated CdTe/glass substrates placed in a molten Sn bath. The substrate temperature was maintained at 360 °C with an accuracy of ±2 °C. The volume of the spray solution was varied from 2.5 mL to 15 mL, whereas the solution concentration of Au^{3+} and the flow rate were kept constant for all CdTe/glass samples: 2 mM and 1 mL/min, respectively. After coating, no drying or annealing was applied because the temperature was high enough to decompose the $AuCl_3$.

Au nanoparticles by sputtering

A thin film of Au was sputtered for 40–70 s onto a glass substrate, which was then air annealed at 500 °C for 30 min, causing coalescence of the nanoparticles into compact Au grains. The Au grains were then coated with a CdTe film via CSS.

2.4. Characterisation of thin films

Scanning electron microscopy

Surface and cross-sectional views of the samples were obtained using scanning electron microscopy (SEM) to evaluate the CdTe surface morphology and CdTe/CdS solar-cell structure. We used a Zeiss EVO-MA15 microscope and a Zeiss HR FESEM Ultra 55 system. Analysis of the SEM images was carried out by Dr. Valdek Mikli at Tallinn University of Technology.

Energy dispersive X-ray spectroscopy

Energy dispersive X-ray (EDX) spectroscopy was used to evaluate the elemental composition of the CdTe films. An Oxford Instruments PentaFet x3 spectrometer with an INCAEnergy EDS system and a Zeiss EVO-MA15 scanning electron microscope operated at an accelerating voltage of 7 kV were used in this analysis. Quantitative results were obtained with the help of a factory-defined standard using the PAP correction-a method for light elements. The EDS analyses were carried out by Dr. Valdek Mikli at Tallinn University of Technology.

X-ray diffraction

The phase composition and crystallographic properties were analysed by X-ray diffraction (XRD). XRD patterns were recorded at Tallinn University of Technology on a Rigaku Ultima IV system using monochromatic Cu Kα radiation (λ = 1.5406 Å, 40 kV at 40 mA) and equipped with a D/teX Ultra silicon line detector in the 2θ (Bragg–Brentano) regime using a 2θ step of 0.04°, a counting time of 2–10 s/step, and sample rotation. Crystal phases were identified using data issued by the Joint Committee on Powder Diffraction Standards (JCPDS). The crystallite sizes and lattice constants were calculated using Rigaku PDXL Version 1.4.0.3 software. The Debye–Scherrer formula was used to calculate the crystallite size (L).

$$B(2\theta) = \frac{K\lambda}{L cos\theta} \ , \qquad (2.1)$$

where B is the peak width, K is the Scherrer constant, λ is the wavelength of the X-ray radiation, and θ is one-half of the diffraction angle.

Photoluminescence and ultraviolet–visible spectroscopy

RT photoluminescence measurements were performed with a high-resolution micro-Raman spectrometer, Horiba Jobin Yvon HR800, equipped with a multichannel charge coupled device detection system in backscattering configuration. An incident Nd–YAG laser light with a wavelength of 532 nm (green laser) and a spot size 10 µm in diameter was used for excitation.

For steady-state photoluminescence (PL) measurements, the samples were mounted in a closed-cycle He cryostat and cooled to 8 K. A 441 nm He–Cd laser line with a maximum output of 80 mW was used for PL excitation. The spectra were recorded via a 400-mm focal length grating monochromator system and detected with an InGaAs detector.

The total optical transmittance and reflectance spectra of the CdTe films were measured in the 200–2500 nm wavelength range on a Jasco V-670 ultraviolet–

visible–near-infrared (UV–vis–NIR) spectrophotometer equipped with an integrating sphere.

Hall measurements

The resistivity, charge-carrier concentration, and mobility of the CdTe films were measured at RT using MMR's Variable Temperature Hall System and a Hall and van der Pauw Controller H-50. For Hall measurements, contacts were made through the CdTe layers by the evaporation of Au or In through a mask. The mica mask had openings for four-point contact van der Pauw geometry. The in-plane resistivity and hole densities were calculated for thicknesses of 2–3 μm, which were estimated from the SEM analysis. Each measurement was carried out ten times and the mean value was taken.

2.5. Characterisation of solar cells

Current–voltage characteristics and external quantum efficiency

For cell characterisation, we used the current–voltage characteristics (*J*–*V*) and the external quantum efficiency (EQE). The *J*–*V* curves were measured under a standard white light with an illumination intensity of 100 mW/cm^2 (AM1.5) using the four-point-probe technique on the AUTOLAB PGSTAT 30 and Oriel class A solar simulator 91159A at Tallinn University of Technology. The EQE was measured in the spectral region of 300–1000 nm using a computer-controlled SPM-2 monochromator (Carl Zeiss-Jena) and a 300 W Xe lamp as the excitation light source. The dispersed light from the Xe lamp incident on the solar cell as monochromatic light was optically chopped at 30 Hz.

3. RESULTS AND DISCUSSION

The following sections, 3.1–3.3, report the results of a systematic study of the structural, electrical, and optical properties of the CdTe thin films and CdTe/CdS solar cells as functions of CSS processing conditions, post-deposition thermal treatment, and the plasmonic effect of Au nanoparticles. Mechanisms of the physicochemical processes responsible for the changes in the properties of the CdTe thin films and CdTe/CdS solar cells are proposed. These results have been published in papers I–V.

3.1. Influence of substrate temperature and post-deposition $CdCl_2$ activation treatment

3.1.1. Effect of substrate temperature

CdTe thin films were deposited by CSS onto CdS/FTO/glass substrates, the experimental details of which were presented in Section 2.2. To investigate the influence of substrate temperature on the structural and morphological properties of the CdTe thin films, the temperature was varied from 250 to 500 °C while the source temperature and deposition time were kept constant at 610 °C and 3 min, respectively [II]. The changes in the structural and morphological properties of the films were studied by SEM and XRD.

The SEM investigation showed that the shape and size of the CdTe grains deposited onto the CdS/FTO/glass substrates greatly depended on the substrate temperature during deposition. Figure 3.1 shows the top- and cross-sectional-view SEM images of the CdTe/CdS/FTO/glass structures with CdTe deposited at substrate temperatures of 250–500 °C. The CdTe films deposited at 250 °C exhibit a highly porous structure with a wide grain-size distribution varying from approximately 0.1 µm to 1 µm. The grains have faceted shapes with sharp edges, and the surfaces form an ordered series of step terraces. By increasing the substrate temperature to 300–350 °C, the grain size increased to 1.5 µm and the size distribution was more homogeneous. Moreover, a change in the growth direction is observed at 300–350 °C, i.e., the films begin to form columnar-type structures normal to the CdS/FTO/glass substrate surfaces. This columnar-type growth was more pronounced in the films obtained at 350 °C, in which columns approximately 1–1.5 µm in diameter and either pyramidal or faceted in shape at the CdTe free surface extended through the layer (~4 µm). Further increasing the substrate temperature to 450–500 °C increased the grain size to 3–4 µm. These larger CdTe grains had irregular shapes and smooth crystal facets. In addition to increasing the grain size, the increased substrate temperature decreased the density of voids, resulting in films with a close-packed morphology.

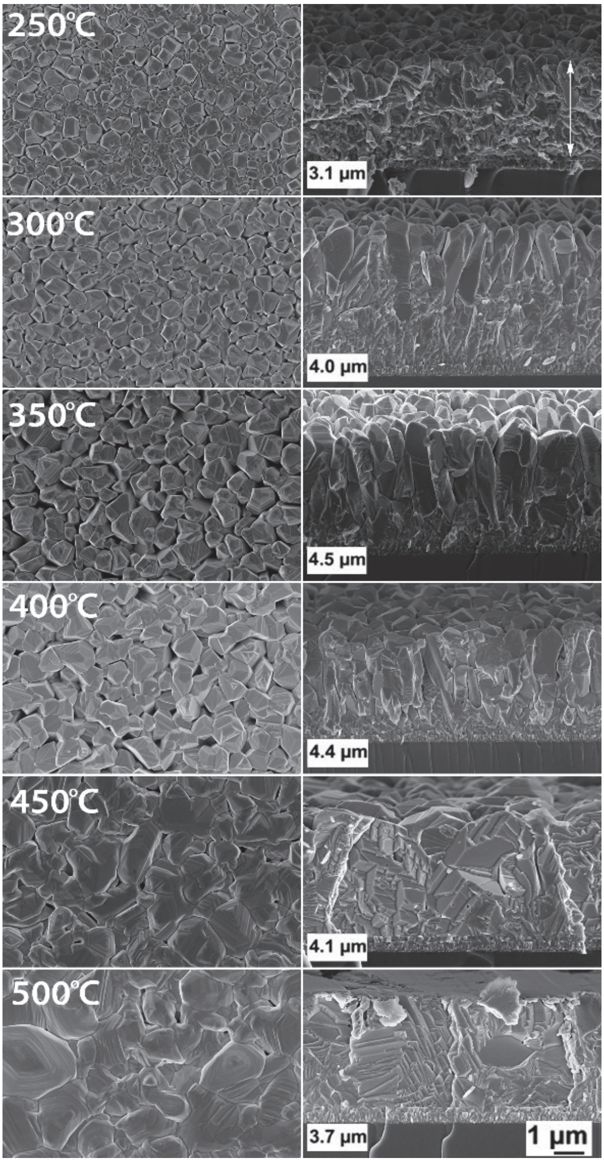

Fig. 3.1. SEM images (30,000× magnification) of CdTe/CdS/FTO/glass structures with CdTe deposited at substrate temperatures of 250–500 °C. Left: top view; right: cross-sectional view showing CdTe layer thickness [II].

Figure 3.2 displays the XRD patterns of CdTe/CdS/FTO/glass structures with CdTe deposited at substrate temperatures of 250–500 °C. The diffractograms show the main peaks from the (111), (220), (311), (400), (331), (422), and (551) planes of the cubic phase. At low substrate temperatures of 250–350 °C, strong orientation along the (111) direction is observed. With increasing substrate temperature, the preference for the (111) orientation decreased, as shown for the films deposited at 400 °C, and the intensities of the (220) and (311) peaks were as much as 40% of the (111) intensity (much higher than that of films deposited at 250–350 °C). Upon increasing the substrate temperature to 450 °C, the (111) preferred orientation was lost and the film exhibited a slight preference for the (220) orientation. At a substrate temperature of 500 °C, the orientation of the grains became more random.

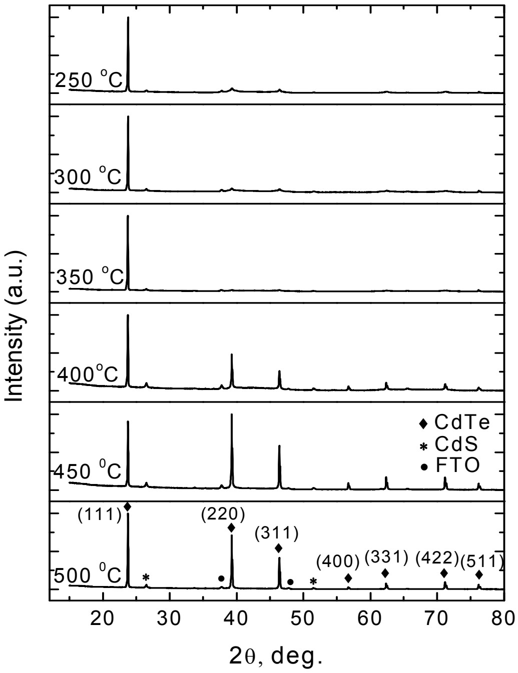

Fig. 3.2. XRD patterns of CdTe/CdS thin-film structures with CdTe deposited at substrate temperatures of 250–500 °C [II].

The differences in the grain size, shape, and orientation of the CdTe films can be explained by differences in the nucleation density and coalescence rates at the different substrate temperatures [118-120]. In the case of CSS, nucleation takes place via a vapour–solid-phase transition [119]. The atoms or molecules condense onto the surface of the substrate (called adatoms) and an initial set of nuclei is formed by deposition from the vapour phase. The adatoms, which are assumed to migrate across the surface by diffusion, may bind with other adatoms, undergo capture and be incorporated into an existing nucleus, or simply re-evaporate from the surface [118]. According to the thermodynamic theory of nucleation [118, 121], the critical radius, r_c, at which a spherical nucleus becomes stable enough to re-evaporate is given by the equation:

$$r_c = \frac{2\gamma V}{kTln(p/p_e)} \ , \qquad (3.1)$$

where γ is the surface energy, k is Boltzmann's constant, V is the volume of an adatom of deposited material, T is the temperature, p is the vapour pressure and p_e is the equilibrium vapour pressure. The equilibrium vapour pressure, p_e, is given by the Clausius–Clapeyron relation [121].

$$p_e = Aexp\left(\frac{-\Delta H_{vap}}{RT}\right), \qquad (3.2)$$

where ΔH_{vap} is the change in molar enthalpy for vapourisation, R is the universal gas constant, and A is a constant. It can be observed that the equilibrium vapour pressure increases exponentially with increasing temperature, leading to an exponential decrease in the supersaturation ration p/p_e. Thus, the critical radius and its dependence on the temperature and supersaturation ratio determine the nucleation density. Those nuclei that are stable enough to re-evaporation continue to grow by the addition of material from the vapour and by the surface diffusion of adatoms, thus forming islands [118, 119]. Further, the coalescence process, in which such islands come into contact with other islands and merge together, thus reducing the total surface area of the islands and their coverage of the substrate, is also determined by the substrate temperature [119]. Ostwald ripening and coalescence by growth are assumed to be the dominant coalescence processes in thin-film formation [119]. Following this theory, we can describe the growth mechanism of the CdTe films at different substrate temperatures.

At a low substrate temperature of 250 °C, adatom mobility and surface diffusion are low, and because of the supersaturation of the gas phase, the initial in-plane grain sizes are set by the saturation nucleation density, resulting in a wide distribution of grain sizes and hence a highly dispersed structure. The orientation of the grains is given by the orientation of the initial nuclei. For cubic CdTe, the densely populated (111) plane is the initial orientation.

At moderate substrate temperatures of 300–350 °C, adatom surface diffusion is significant, resulting in local epitaxial growth on individual grains. The grain coarsening occurs during the coalescence of small islands with large surface-to-volume ratios, whereas GBs become immobile in continuous layers [120]. A pronounced columnar structure develops, in which the columns are actually elongated grains. The faceted column tops increase the surface roughness, which increases with increasing thickness, giving rise to open column boundaries. The columns preserve the same (111) orientation of the initial nuclei.

At high substrate temperatures of 450–500 °C, adatoms are more mobile on the surface, leading to fewer nucleation sites. Therefore, complete coalescence will occur for relatively large islands because the rate of material transfer between islands is high. GB migration takes place not only during coalescence but throughout the film-thickening process. Orientation selection during the coalescence stage is more pronounced, and it is driven by a decrease in the total GB area, as well as by minimisation of the interfacial and surface energies [120]. Thus, large grains with low surface energies grow in both perpendicular and lateral directions, leading to the formation of a dense, continuous, and pore-free CdTe thin film with a random orientation.

The impact of substrate temperature on the microstructure of CdTe has been investigated by many groups [122-126]; however, only two studies, one by Luschitz et al. [125] and the other by Kosyak et al. [126], are comparable to our research in terms of the range of substrate temperatures used (200–550 °C) in CSS. Their investigations confirm our results as they show the same pattern of three different growth regimes as a function of the substrate temperature. However, the fact that these studies report some contradictory conclusions and one of them was not applied to solar cells motivated us to clarify the relation between substrate temperature, post-deposition treatment, and solar-cell performance.

3.1.2. Effect of post-deposition $CdCl_2$ activation treatment

Recrystallisation, grain growth, and sintering

Figure 3.3 shows the top and cross-sectional SEM views of $CdCl_2$-activated CdTe/CdS/FTO/glass structures with CdTe deposited at 250–500 °C. After the activation step, the surface of the CdTe film deposited at 250 °C consisted of rounded grains with penetrating boundaries and an average grain size of 2 μm. The film also exhibited a high inner porosity and a large number of voids. CdTe films deposited at 300 and 350 °C had relatively large grains (2–3 μm) with undetermined forms, traversing holes, and neck regions between the coalesced grains. Moreover, the cross-sectional images indicate that the grains lost their columnar structure. The surface layer was 1 μm thick with significant porosity. In the case of the CdTe films deposited at 450–500 °C, it appears that $CdCl_2$ activation did not influence the grain size of the CdTe films, but it did induce a sintering mechanism that decreased the number of intergranular pores.

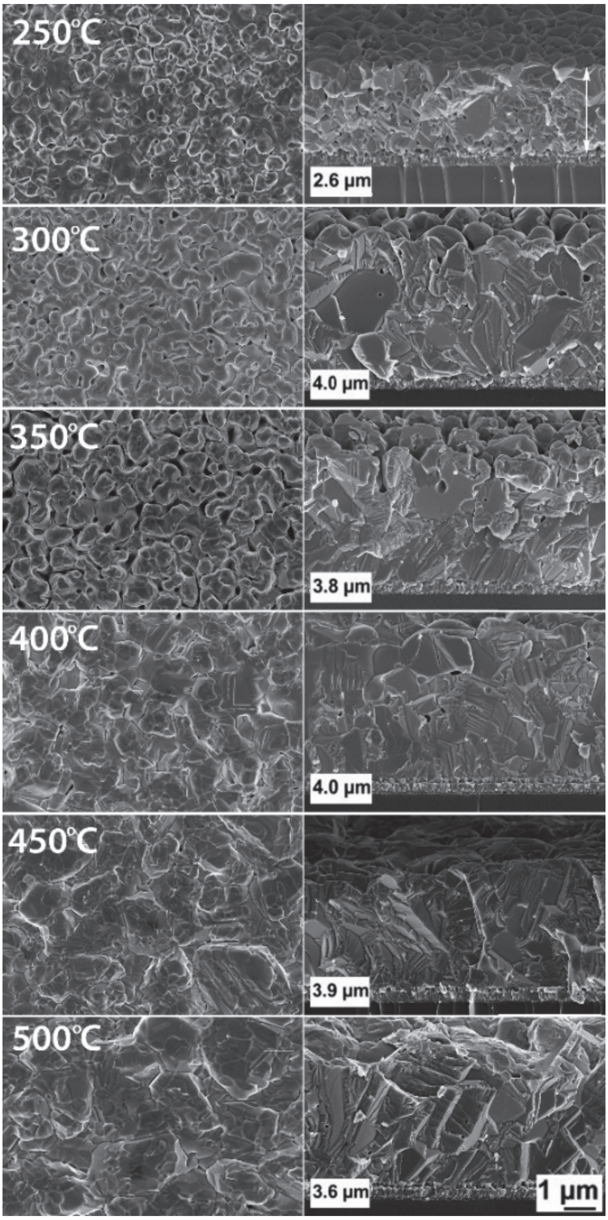

Fig. 3.3. SEM images (30,000× magnification) of CdTe/CdS/FTO/glass structures with CdTe deposited at substrate temperatures of 250–500 °C after $CdCl_2$ activation. Left: top view; right: cross-sectional view showing CdTe thickness [II].

Figure 3.4 shows the XRD patterns of $CdCl_2$-activated CdTe/CdS structures with CdTe deposited at 250–500 °C. As a result of $CdCl_2$ activation treatment, the preferential (111) orientation decreased for all deposition temperatures, in agreement with results reported in the literature [11-17]. For the films deposited at 250–300 °C, the intensity of the (111) peak was still higher than those of other peaks, but the (111) orientation was not as predominant as it was for the as-deposited CdTe films (Fig. 3.2) and the layers exhibited nearly random orientation. The preferential (111) orientation significantly decreased, however, for CdTe films deposited at 350–400 °C. In this case, the films exhibited a predominantly (220) orientation. $CdCl_2$-activated CdTe films formed at 450–500 °C exhibited random orientation.

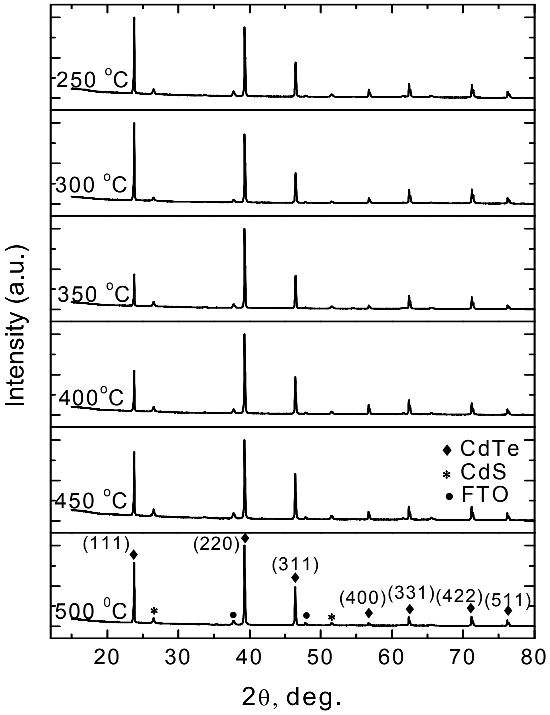

Fig. 3.4. XRD patterns of CdTe/CdS thin-film structures with CdTe deposited at substrate temperatures of 250–500 °C after $CdCl_2$ activation and NP etching [II].

The XRD patterns of the $CdCl_2$-activated CdTe/CdS structures show a set of peaks corresponding to the $CdCl_2$, $CdTeO_3$, CdO, and TeO_2 phases (Fig. 3.5). The appearance of such phases in the XRD patterns indicates oxidation on the surface of the CdTe layer during $CdCl_2$ activation. NP etching removed the oxidised products and residual $CdCl_2$ from the surfaces of the CdTe films (Fig. 3.4); however, the residual oxychlorides in the GBs could not be eliminated completely [18-20].

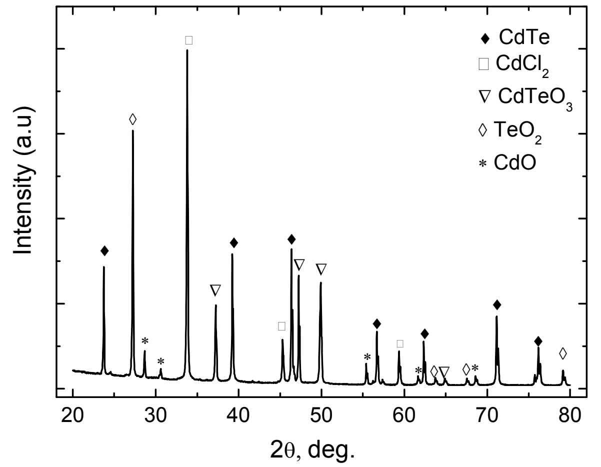

Fig. 3.5. XRD patterns of $CdCl_2$-activated CdTe/CdS structures without NP etching [I].

The crystallite sizes before and after $CdCl_2$ activation are listed in Table 3.1. The crystallite size increased from 13 nm to 94 nm when the substrate temperature was increased from 250 to 500 °C, in agreement with the SEM results (Fig. 3.1). As a result of $CdCl_2$ activation, the crystallite size of the CdTe films deposited at 250 °C increased considerably from 13 nm to 110 nm. This effect was less pronounced, however, in CdTe films deposited at 500 °C, in which the crystallite size increased only marginally from 94 nm to 110 nm during the same activation process.

Table 3.1. The average crystallite size (L) of CdTe layers deposited at 250–500 °C on CdS/FTO/glass substrates before and after $CdCl_2$ activation [II].

T_s, °C	L, nm as deposited	L, nm $CdCl_2$ activation
250	13	110
300	23	106
350	32	111
400	73	113
450	86	100
500	94	110

Based on the obtained results, we claim that $CdCl_2$ activation induces the formation of liquid flux and mass transport through the melted phase, promoting grain growth by recrystallisation and sintering in the CdTe films. Evidence for this is particularly provided by the extensive grain growth in the CdTe films deposited at low substrate temperatures. The formation of a liquid phase was facilitated by the formation of CdO, TeO_2, and $CdTeO_3$ oxide species (Fig. 3.5), which lowered the melting point of the CdTe–$CdCl_2$ eutectic to 380–400 °C [91]. The reactions in a system containing CdTe, $CdCl_2$, and oxygen were described by McCandless et al. [88] (Section 1.2.3.3). It is also important to consider the low diffusion coefficients of Cd and Te in the CdTe lattice ($D \approx 10^{-15}$ cm^2/s) [95] and the small partial pressure of CdTe at 420 °C [4], which does not promote mass transport through the vapour phase.

The liquid-phase recrystallisation of CdTe films during $CdCl_2$ activation treatment in air at 420 °C can be explained as follows. When the process quartz tube with CdTe samples coated with $CdCl_2$ is placed into the preheated furnace, it takes some time to reach the equilibrium composition of the flux solution and achieve uniform distribution of the liquid phase in the intergranular spaces. In the first step of the process, the intergranular capillaries are filled with the formed liquid phase of flux, which promotes grain growth by Ostwald ripening [119]. Because of the fast evaporation of $CdCl_2$, the volume of the flux decreases and the grains are compressed by the capillary contracting force created by surface tension on the liquid-phase meniscus between the contacting grains. Because annealing is carried out in open air at 420 °C, the volume of the liquid phase decreases because of the evaporation of $CdCl_2$, which leads to sintering of the grains and the creation of good contact between them. The degree and rate of liquid-phase sintering is inversely proportional to the dimensions of the initial CdTe particles. Thus, CdTe films deposited at low substrate temperatures have a highly dispersed structure with smaller grains (and thus respectively smaller crystallite sizes) and high surface energies. These grains are therefore more active for recrystallisation by mass transport through the $CdCl_2$ liquid flux. Because of the high solubility of CdS and CdTe in the $CdCl_2$ flux, the grain growth is accomplished by full recrystallisation, and the newly recrystallised lattice is randomly oriented. Similarly, CdTe films deposited at high substrate temperatures have large initial grain sizes (and thus respectively larger crystallite sizes) and low surface and interfacial energies. Therefore, little measurable grain growth occurs during $CdCl_2$ activation, suggesting that the recrystallisation occurs only on the surface/interface region of the initial CdTe grains. Under these conditions, the activation process induces a sintering mechanism, which decreases the number of intergranular pores. It has been widely found that CdTe films deposited by CSS at high substrate temperatures do not undergo strong recrystallization during the $CdCl_2$ activation process [12, 87, 125]. However, the number of structural defects is reduced, which affects the grain boundaries, resulting in a higher effective acceptor concentration [13, 106]. Thus, we succeeded in showing that $CdCl_2$ activation induces recrystallisation and grain growth as a function of the growth history of the film and the initial grain size.

Intermixing at the CdTe–CdS interface

To study the intermixing at the CdTe–CdS interface, the evolution of the CdTe lattice parameter was analysed before and after $CdCl_2$ activation for CdTe/CdS/FTO structures with CdTe deposited at substrate temperatures of 250–500 °C. The lattice parameter values are listed in Table 3.2. The lattice parameter of non-activated CdTe films systematically increased from 6.484 to 6.486 Å with increasing substrate temperature from 250 °C to 500 °C. Similar results were obtained by Rigana [127], where the phenomenon was explained by the development of internal stress in the film grains, and by McCandless [11] and Moutinho [12], where the phenomenon was explained by compressive strain due to the lattice mismatch between CdTe and CdS. In contrast to these previous explanations, we claim that this phenomenon is related to the highly defective structure of CdTe films grown at 250 °C. The small lattice parameter indicates the presence of vacancy-type defects, whose concentration decreases with increasing substrate temperature. Additionally, the increased lattice parameter at a substrate temperature of 500 °C indicates the absence of sulfur diffusion into CdTe in accordance with the low solid-state diffusion rate ($D \approx 10^{-15}$ cm^2/s) at this temperature [128].

As a result of $CdCl_2$ activation, the lattice parameter decreased for all CdTe films, in agreement with the results reported in [11, 12, 67, 86]. Romeo et al. explained this as being the result of relaxation of the compressive stress generated by the lattice and thermal mismatch between CdTe and the underlying substrate [67].

Table 3.2. Values of the lattice parameter (a_0) and the CdS weight fraction, x, in $CdTe_{1-x}S_x$ after $CdCl_2$ activation [II].

T_s, °C	a_0, Å as deposited	a_0, Å $CdCl_2$ activation	x in $CdTe_{1-x}S_x$
250	6.484	6.477	0.013
300	6.484	6.479	0.009
350	6.485	6.481	0.008
400	6.485	6.484	0.003
450	6.486	6.485	0.002
500	6.486	6.485	0.002

The decrease of the lattice parameter as a result of $CdCl_2$ activation has also been explained as being due to the formation of $CdTe_{1-x}S_x$ and $CdS_{1-y}Te_y$ alloys in the absorber layer, which occurs by interdiffusion [11, 12, 86, 88]. Figure 3.6 shows a broad and asymmetric XRD (511) peak with a tail, which is shifted toward a higher 2θ angle (lower *d*-spacing), indicative of alloy formation. The shift of the (511) peak position is more pronounced in the CdTe film deposited at 250 °C, and it corresponds to the decrease of the lattice parameter from 6.484 to 6.477 Å, indicating a significant degree of alloy formation. The high degree of alloy formation in the CdTe films with small grains and high GB densities was explained by McCandless et al. [4, 88] as being due to the "high partial pressure or concentration of $CdCl_2$, together with O_2, during $CdCl_2$ treatment." For structures with CdTe films deposited at 500 °C, the shift of the (511) peak with a decrease in the lattice parameter from 6.486 to 6.485 Å is insignificant, indicating a negligible degree of alloy formation. For the $CdTe_{1-x}S_x$ alloy, the weight fraction, x, was calculated using Vegard's law [129]; the values of x are included in Table 3.2. For the $CdCl_2$-activated structure with CdTe formed at 250 °C, the alloy formation indicates that $x = 0.013$, which is in agreement with results reported in [12]. Generally, it is reported that the formation of a $CdTe_{1-x}S_x$ alloy at the interface results in x not exceeding 0.06, which represents an equilibrium solubility limit for sulfur in CdTe, although a layer with a higher sulfur content might grow under non-equilibrium conditions [10, 86, 87].

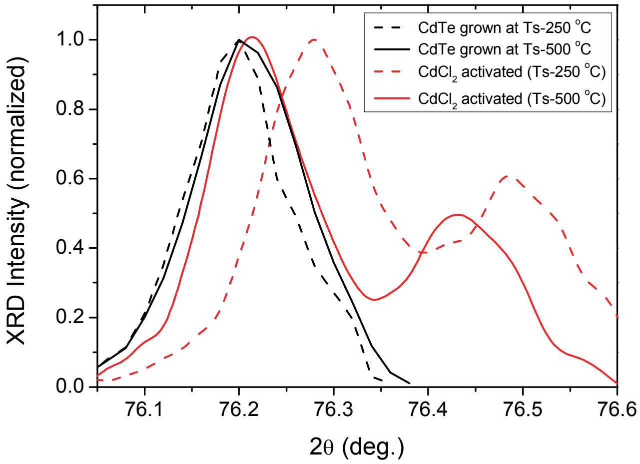

Fig. 3.6. High-resolution (511) XRD profiles of CdTe/CdS structures with CdTe deposited at 250 and 450 °C before and after $CdCl_2$ activation [II].

Based on the above results, we claim that the intermixing at the CdTe–CdS interface also takes place by liquid-phase recrystallisation, as described above, and not as a result of solid-state interdiffusion between the CdTe and CdS phases. In the case of solid-state interdiffusion, the amount of sulfur penetrating the bulk of CdTe from the grain boundary is dictated by the bulk diffusion coefficient of sulfur in CdTe, the value of which was estimated to be $D \approx 10^{-15}$ cm^2/s at 400 °C [128]. Considering such low diffusivity, the intermixing at the

CdTe–CdS interface can be explained by the mass transport of CdS and CdTe through the melted phase. Solid-phase diffusion in the bulk and at the GBs cannot explain the high concentration (approximately 10^{20} cm^{-3}) of sulfur, oxygen, and chlorine detected by secondary ion mass spectrometry at the CdTe–CdS interface [20]. In CdTe/CdS structures with highly dispersed CdTe grains deposited at 250 °C, the activation process caused heightened recrystallisation and grain growth. For the same structure, we observed a high degree of alloy formation at the interface. These effects were minimal in CdTe/CdS structures obtained at high temperatures of 450–500 °C. Thus, the smaller the initial grains of CdTe, the more intense the recrystallisation and grain growth by mass transport through the liquid phase and the greater the extent of intermixing at the CdTe–CdS interface. With significant intermixing, a region with a saturated concentration of flux components ($CdCl_2$, CdTe, and CdS) will abruptly form at the CdTe–CdS interface, which can affect the quality of the junction and hence the performance of the solar cell.

CdTe/CdS solar-cell performance

Figure 3.7 shows the current–voltage (*J–V*) characteristics measured under AM1.5 conditions for CdTe/CdS solar cells with CdTe obtained at substrate temperatures of 250–500 °C. The corresponding photovoltaic parameters are included in Table 3.3. All photovoltaic parameters, including the open-circuit voltage (V_{oc}), fill factor (FF), short-circuit current density (J_{sc}), and efficiency, systematically decreased as the substrate temperature decreased from 500 to 250 °C. The solar cell with the CdTe film deposited at 250 °C showed the lowest efficiency, only 2.3%. For this solar cell, the *J–V* curve exhibited a pronounced roll-over effect (photocurrent saturation at high forward bias). Such an anomaly in the *J–V* response of CdTe solar cells was well explained by Fahrenbruch [130] as resulting from the interaction of three effects: the low density of the electronically active p-type dopant, the similar densities of the compensating recombination centres, and the Schottky barrier between CdTe and the metal back contact. Because the structure obtained at 250 °C showed excessive recrystallisation and intermixing during $CdCl_2$ activation, the most evident roll-over in Fig. 3.7 would likely be due to a reduction in the acceptor density in CdTe. We assume that this reduced carrier density was generated by the self-compensation effect at high concentrations of chlorine incorporated into the CdTe lattice. When the CdTe absorber was obtained at 450 °C, the recrystallisation, intermixing, and chlorine incorporation took place in a more balanced manner, promoting an optimal acceptor density and the highest device performance (Table 3.3).

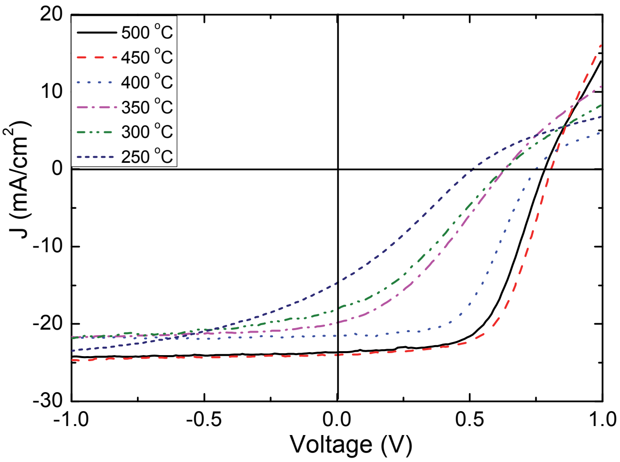

Fig. 3.7 Current–voltage characteristics of the CdTe/CdS solar cells with CdTe deposited at different substrate temperatures [II].

Table 3.3. Photovoltaic parameters of CdTe/CdS solar cells with CdTe deposited at different substrate temperatures [II].

T_s, °C	V_{oc}, mV	J_{sc}, mA/cm^2	FF, %	η, %
250	525	14.8	29.0	2.3
300	630	18.1	32.5	3.7
350	630	19.8	35.3	4.4
400	766	21.2	55.2	9
450	810	23.0	62.0	11.6
500	790	22.8	60.1	10.8

The above conclusions are supported by simultaneous changes in the short- and long-wavelength regions of the EQE (Fig. 3.8). The solar cell with the CdTe film deposited at 250 °C showed the highest EQE response in the short-wavelength region (400–500 nm) because of the thinning of CdS as a result of excessive intermixing, as previously indicated by XRD (Fig. 3.6). Although this enhancement is beneficial for window transmission, non-uniform CdS consumption may lead to the formation of parallel junctions between the absorber and the front contact, and hence to the reduction of solar-cell performance. In the long-wavelength region, the best EQE response was exhibited by the solar cell with a CdTe film obtained at 450 °C, implying better collection efficiency.

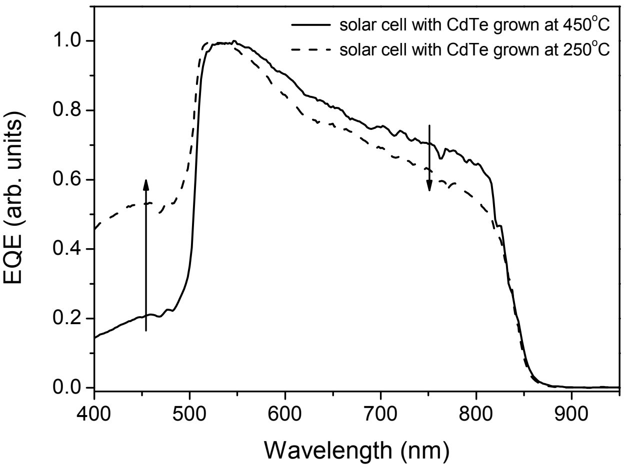

Fig. 3.8. EQE measurements of solar cells with CdTe films deposited at 250 and 450 °C [II].

To summarise, different structural and morphological properties of CdTe films obtained at distinctive regions of temperature (250–500 °C) are explained in terms of nucleation and growth theory. We claim that the subsequent $CdCl_2$ activation promotes the formation of melted flux, which induces recrystallisation, grain growth, and intermixing in the CdTe/CdS structures via mass transport through the liquid phase. The extent of recrystallisation and intermixing increased with decreasing substrate temperature from 450 to 250 °C, whereas the solar-cell efficiency decreased from 11.6 to 2.3%, respectively. Such a systematic reduction of the solar-cell efficiency was the key question that directed us to the investigation of single CdTe layers.

3.2. Properties of CdTe single layers modified by multi-step thermal annealing in various ambient conditions

3.2.1. Approach of multi-step thermal annealing

$CdCl_2$ activation treatment is complicated by the high vapour pressure of $CdCl_2$ and the presence of oxygen. The process results in the segregation of $CdCl_2$ and $CdCl_2 \cdot 2CdO$ residual phases on the GBs [18-21] and in incorporation of high chlorine concentrations into the CdTe lattice [22, 23]. As we have shown, grain growth takes place by mass transport through the liquid flux. The equilibrium between the liquid flux and solid CdTe determines the rate of chlorine doping according to the distribution coefficient (k_d) between the liquid and solid phases at the processing temperature (Eq. 3.3) [131].

$$k_d = \frac{C_S}{C_L} \quad , \qquad (3.3)$$

where $C_S \approx 10^{19}$ cm^{-3} [20] and $C_L \approx 10^{22}$ cm^{-3} are the chlorine concentrations in the solid and liquid flux, respectively. Such a high value of $k_d \approx 10^{-3}$ indicates the incorporation of high chlorine concentrations in the lattice of growing CdTe, which is assured by the limitless supply of chlorine in the liquid flux.

A high concentration of incorporated chlorine, as well as residuals from GBs, strongly limit the density of charge carriers in p-type CdTe by self-compensation and cause hygroscopicity of the solar cell. One solution for gettering these residual impurities from CdTe films and hence improving their optoelectronic properties is to apply controlled thermal annealing in relevant ambient conditions. In paper [V], we showed that thermal annealing in the presence of hydrogen can be a convenient and appropriate method for controlling the oxygen content, which tends to retain excess $CdCl_2$ on the GBs as $2CdO{\cdot}CdCl_2$. We assumed that the reaction with hydrogen removes oxygen by water evaporation. Excess Cd and free $CdCl_2$ can be removed by evaporation at higher temperatures, especially in vacuum. The thermodynamically favoured reaction between hydrogen and solid CdO [132] is given as:

$$\mathrm{H_{2(g)} + CdO_{(s)} \rightarrow H_2O + Cd_{(s,l)}},\ \Delta G\ (250\ ^{\mathrm{o}}\mathrm{C}) = -2.6 \text{ and at } 570\ ^{o}C - 6.5 \text{ kcal/mol} \qquad (3.4)$$

The reaction between hydrogen and solid $CdCl_2$ is not thermodynamically favoured [132], shown as follows:

$$\mathrm{H_{2(g)} + CdCl_{2(s,l)} \leftarrow 2HCl + Cd_{(s,l)}},\ \Delta G\ (250\ ^{\mathrm{o}}\mathrm{C}) = 27.4 \text{ and at } 570\ ^{\mathrm{o}}\mathrm{C}\ 14.4 \text{ kcal/mol} \qquad (3.5)$$

Thus, by subsequent thermal annealing, we can control the residuals in polycrystalline CdTe thin films. By optimisation of the chlorine concentration in the lattice, we can approach the ideal electroneutrality condition, given as $[(V_{Cd}Cl_{Te})^{-}] = p^{+}$, implying high p-type conductivity in CdTe [22]. Valdna et al. showed low-resistance p-type conductivity in CdTe films, which was achieved with no acceptor dopant. However, the concentration of chlorine in the films was decreased by vacuum annealing and heat treatment under Te vapour pressure [22, 23]. These arguments substantiate the systematic investigation of changes in the structural and optoelectronic properties of $CdCl_2$-doped CdTe films induced by subsequent multi-step thermal annealing in H_2, vacuum, and closed isothermal conditions.

Two sets of CdTe films were used for these treatments. The first set was deposited at a substrate temperature of 250 °C and the second set was deposited at 500 °C. For reference, the CdTe films deposited at 250 °C were labelled as

LT, whereas the ones deposited at 500 °C were labelled as HT. A detailed description of the annealing process was presented in Section 2.2.

3.2.2. Structural properties

Similar to the XRD patterns of CdTe deposited onto CdS (Fig. 3.2), untreated LT CdTe films had a strong (111) preferred orientation, whereas the HT films exhibited a random orientation. However, after the $CdCl_2$ activation and treatment processes, all the films exhibited random orientation. The values of the lattice parameter and the average crystallite size after each treatment step are shown in Table 3.4.

Table 3.4. Values of average crystallite size (L) and lattice parameter (a_0) for LT and HT CdTe films after all treatment steps [III].

Sample	Treatment conditions	T_a[a], °C	L, nm	a_0, Å
LT CdTe	as deposited	-	85	6.484
	$CdCl_2$	-	134	6.477
	H_2	250-500 570	144-148 99	6.480 6.471
	Vacuum	250-500 570	120-130 90	6.481-6.482 6.474
	Isothermal[c]	250-500 570	110-120 95	6.472 6.468
HT CdTe	as deposited	-	144	6.486
	$CdCl_2$	-	150	6.484
	H_2	250-500 570	153-159 144	6.485 6.485
	Vacuum[b]	250-500 570	139-149 138	6.486-6.487 6.485
	Isothermal[c]	250-500 570	120-137 95	6.486-6.487 6.484

[a] *Hydrogen annealing temperatures 250-570 °C, 1 h.*
[b] *Vacuum annealing at 470 °C, 1 h of CdTe films which passed H_2 annealing step.*
[c] *Isothermal anneal at 600 °C, 1 h of CdTe films which passed H_2 and vacuum annealing steps.*

The crystallite size of the LT CdTe films increased dramatically from 85 nm to 134 nm as a result of $CdCl_2$ activation. For the HT films, this effect was less pronounced because the crystallite size increased only from 140 nm to 150 nm. These changes in crystallite size after $CdCl_2$ activation are in good agreement with our observations of the CdTe/CdS structures and confirm once again our statement regarding the formation of a liquid phase that induces recrystallisation, grain growth, and sintering (Fig. 3.9).

Subsequent H_2 annealing at 250 °C slightly increased the crystallite size of both the LT and HT CdTe films from 134 nm to 144 nm and from 150 nm to 153 nm, respectively. A gradual increase in the temperature of H_2 annealing from 250 to 500 °C assured an additional increase in the crystallite size of both films (Table 3.4). An additional interesting effect was observed for films annealed in H_2 at 250 °C. The surfaces of both the LT and HT films were covered by needle-shaped particles (Fig. 3.9c). Based on EDX analysis (not shown), these particles showed a significantly higher concentration of Te as compared to the remaining film surface.

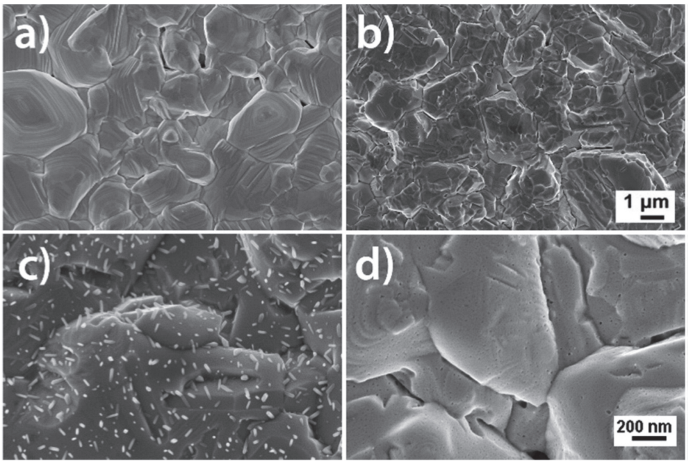

Fig. 3.9. SEM top-view images of the CdTe surface: (a) after CdTe deposition, (b) after $CdCl_2$ activation, and after H_2 thermal annealing at (c) 250 °C and (d) 300 °C [III].

We assumed that during H_2 annealing, a uniform Te film (which is usually formed on the CdTe surface and also at the GBs after NP etching) would start to agglomerate on the surface in the form of needle-shaped particles. Due to the H_2 contra pressure and low partial vapor pressure of Te at 250 ^oC the needle-shaped particles are stable and apparently located on the extended defects (like GB and dislocation loops). This experimental fact also indicates to the out diffusion of Te which is formed in result of reaction between TeO_2 and H_2 at 250 ^oC, $\Delta G \approx -42$ kcal/mol [132]. At an increased temperature gradient (300 °C), these Te needles evaporated from the CdTe surface, leaving behind a dimpled surface. The appearance of these dimples, which had diameters of ~20 nm, might have been due to the solubility of CdTe in the Te solid phase. At higher H_2 treatment temperatures (350–500 °C), the surface of the CdTe layer remained clean, as it did for H_2 treatment at 300 °C (Fig. 3.9d). This Te from the surface and the GBs of CdTe, as well as CdO and TeO_2 residuals (Fig. 3.5), actively reacted with H_2 already at 250 °C, contributing to the growth of additional crystallites (Table 3.4). As the temperature of H_2 annealing increased from 500 to 570 °C, the crystallite size significantly decreased, indicating intensive sublimation of CdTe. This was confirmed by the decrease in CdTe thickness from 2 µm to 1 µm.

The evolution of the lattice parameter values for both the LT and HT films after treatment are reflected in the displacement of the main (111) XRD peak (Fig. 3.10).

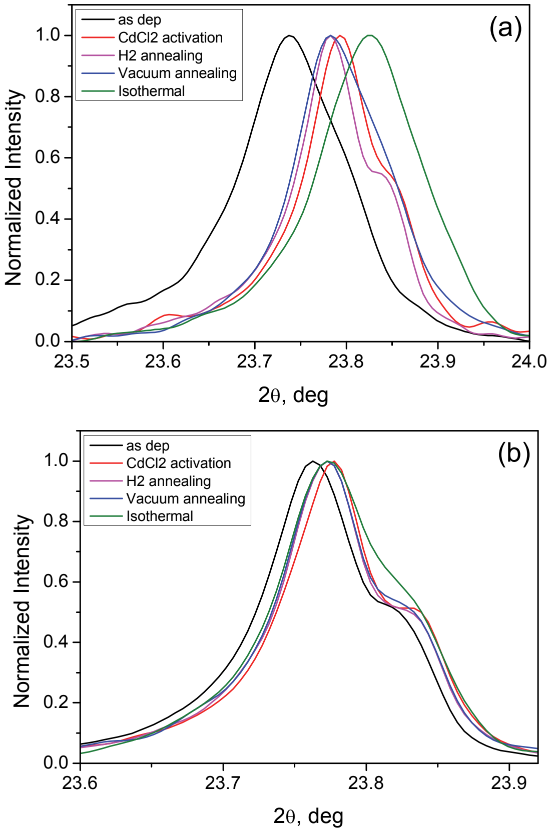

Fig. 3.10. Displacement of the (111) peak vs. thermal annealing conditions for (a) LT and (b) HT CdTe thin films [III].

After $CdCl_2$ activation, high-resolution analysis demonstrated a shift of the (111) peak toward higher 2θ values. This shift was more pronounced in the LT CdTe films (Fig. 3.10a) and corresponded to the decrease in the lattice parameter from 6.484 to 6.477 Å (Table 3.4). For the HT films, the shift of the (111) peak was less significant, with a corresponding decrease in the lattice parameter from

6.486 to 6.485 Å. A similar effect was observed for the (511) peak in the CdTe/CdS activated structures (Fig. 3.6) and is explained by the formation of a $CdTe_{1-x}S_x$ alloy at the CdTe–CdS interface. Considering the incorporation of $CdCl_2$ into the CdTe lattice, we explain the shift of the (111) peak shown in Fig. 3.10 by the presence of chlorine on Te sites, the formation of Cd vacancies, and probably the incorporation of oxygen on Te sites. The atomic sizes of chlorine (102 pm) and oxygen (66 pm) are smaller than the atomic size of Te (138 pm) [133], and thus together with Cd vacancies, they cause a contraction of the CdTe sub-lattices and hence a decrease of the lattice parameter (Table 3.4). On the other hand, the slight displacement of the (111) peak toward a lower 2θ region is accompanied by lattice relaxation as a result of the removal of oxygen and $CdCl_2$ impurities by H_2 and vacuum annealing. It should be mentioned that subsequent thermal annealing in vacuum at 470 °C showed the same trend as in the H_2 annealing in terms of the changes of lattice parameter.

The last treatment of the multi-step approach was the subsequent isothermal annealing in ampoules at 600 °C. For LT films that passed H_2 and vacuum annealing, this isothermal step ensured a strong shift of the (111) peak toward higher 2θ values (Fig. 3.10a), corresponding to a considerable decrease in the lattice parameter (Table 3.4). As compared to H_2 and vacuum annealing, the higher solubility of $CdCl_2$ in CdTe at 600 °C resulted in a stronger decrease of the lattice parameter for the LT films. At the same time, a significant decrease of crystallite size was observed for both the LT and HT films. Because of the high temperature used (600 °C) and the large volume of the ampoule (~10 cm^3) as compared to the small volume of the CdTe film (5 × 5 × 0.2 mm), a remarkable amount of CdTe and $CdCl_2$ may sublimate into the gas phase as a function of the decrease of crystallite size. Moreover, homogeneous chlorine doping through the volume of the layer is assured by the thermodynamic equilibrium between the solid and vapour phases.

3.2.3. Optoelectronic properties

The deposited LT and HT films were characterised as having high dark resistivity, indicating that intrinsic defects electrically compensate, resulting in a semi-insulating CdTe material. Table 3.5 shows the resistivity values for both the LT and HT CdTe films after all thermal annealing steps. After $CdCl_2$ activation, the p-type resistivity of both samples decreased significantly. The LT CdTe film had a dark resistivity of 10^7 Ω·cm, which was approximately ten times higher than the resistivity of the HT film (7×10^5 Ω·cm). The photoconductivity of the LT film was poor, with a dark-to-light resistance ratio of $K_F = 12.5$, whereas the HT film exhibited prominent photoconductivity, with a high dark-to-light resistance ratio of $K_F = 70$ (Table 3.5).

Table 3.5. Resistivity values vs. annealing conditions for LT and HT CdTe films [III].

Sample	Treatments	T_a[a], °C	R_D, Ω/□	R_L, Ω/□	K_F	ρ_D, Ω·cm
LT CdTe	$CdCl_2$	-	5×10^{10}	4×10^{9}	12.5	10^{7}
	H_2	250	8×10^{11}	10^{11}	8	1.6×10^{8}
		300-500	$(5-8)\times10^{11}$	$(1-1.8)\times10^{10}$	$35\leq K_F\leq50$	$(1-1.6)\times10^{8}$
		570	10^{12}	2.8×10^{11}	3.6	2×10^{8}
	Isothermal[b]	H250	1.5×10^{8}	1×10^{8}	1.5	3×10^{4}
		H300	1.5×10^{8}	1.3×10^{8}	1.15	3×10^{4}
		H350	8×10^{7}	7.5×10^{7}	1.05	1.6×10^{4}
		H400	2.2×10^{7}	2.1×10^{7}	1.04	4.4×10^{4}
		H450	7×10^{6}	6.9×10^{6}	1.01	1.4×10^{3}
		H500	5×10^{6}	5×10^{6}	1	10^{3}
		H570	5×10^{8}	4.8×10^{8}	1.04	10^{5}
HT CdTe	$CdCl_2$	-	3.5×10^{9}	5×10^{7}	70	7×10^{5}
	H_2	250	10^{10}	1.5×10^{8}	66	2×10^{6}
		300-350	4×10^{9}	3×10^{7}	130	8×10^{5}
		400-500	$(7-9)\times10^{10}$	$(1-2)\times10^{9}$	$35\leq K_F\leq90$	$(1.4-1.8)\times10^{7}$
		570	2.5×10^{11}	1.2×10^{9}	208	5×10^{7}
	Isothermal[b]	H250	5×10^{7}	7×10^{6}	7.1	10^{4}
		H300	1.3×10^{7}	6×10^{6}	2.16	$2.6.\times10^{3}$
		H350	1.6×10^{7}	4×10^{6}	4	3.2×10^{3}
		H400	4×10^{7}	1×10^{7}	4	8×10^{3}
		H450	2.5×10^{7}	4.5×10^{6}	5.5	5×10^{3}
		H500	1.3×10^{7}	1.1×10^{7}	1.18	2.6×10^{3}
		H570	5×10^{7}	2.5×10^{6}	20	10^{4}

[a] *Hydrogen annealing temperatures 250-570 °C, 1h. R_D and R_L - resistance under dark and light conditions; K_F is dark to light resistance ratio; ρ is resistivity.*

[b] *Isothermal annealing at 600 °C for 1 h of CdTe films which passed H_2 and vacuum annealing steps.*

The high resistivity and poor photoconductivity of the LT film suggest that $CdCl_2$ activation left too high a concentration of chlorine in the CdTe film, which promoted an increase in the concentration of neutral complex defects ($V_{Cd}{}^{2-}2Cl_{Te}{}^{+}$). As a result, the p-type resistivity increased and the photoconductivity decreased. In the HT film, the chloride concentration seemed to be more balanced with the concentration of native defects (V_{Cd}). Because of the lower amount of chloride incorporated in the HT films, the concentration of shallow acceptor centres [$(V_{Cd}{}^{2-}Cl_{Te}{}^{+})^{-}$] increased and the p-type properties and photoconductivity improved.

In order to confirm these statements, we measured the photoluminescence spectra at 9 K of both the LT and HT CdTe films before and after $CdCl_2$ activation (Figs. 3.11a and b). The PL spectrum of the as-deposited LT CdTe film exhibited a very weak and broad emission in comparison to the as-deposited HT CdTe film, which revealed a very intense emission band around the 1.478 eV spectral region. It also exhibited a weak emission near the band gap region (1.598 eV). The weak and broad emission of the as-deposited LT film can be explained by the high concentration of defects and the density of the GBs, which provided an effective channel for non-radiative recombination [134] (Fig. 3.11a). In the as-deposited HT film, the weak emission around the 1.59 eV spectral region (Fig. 3.11b) is related to the ground-state acceptor-bound exciton decay (A^0X) [135]. This acceptor-bound exciton feature prevailed in the PL spectrum observed for the range of as-deposited CdTe films, which were usually p-type [135, 136]. Usually, the presence of excitons is an indication of low defect concentration and high crystalline quality.

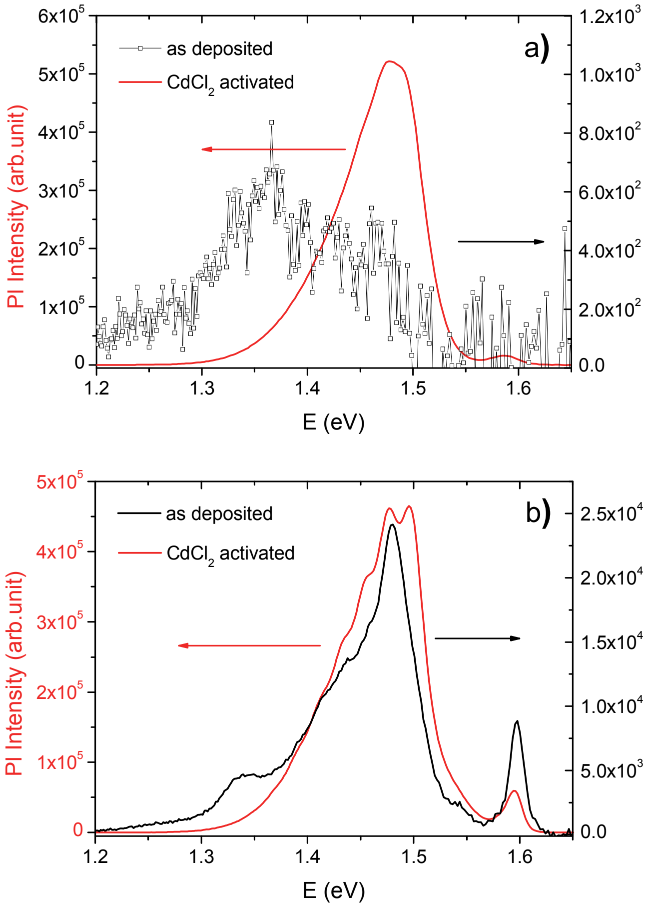

Fig. 3.11. Photoluminescence spectra of CdTe films: (a) LT CdTe and (b) HT CdTe before and after $CdCl_2$ activation.

For the as-deposited HT film, the broad emission band at approximately 1.478 eV (Fig. 3.11b, black band) is known as the Y-band. It has been observed in single crystals and epitaxial and polycrystalline films of CdTe by many authors [137-140]. This emission band is characterised by some rather unusual features for a deep-level emission band having a weak phonon coupling and a relatively broad zero-phonon line [135]. Different recombination mechanisms have been proposed to explain this emission. Dean et al. [137] and Seto et al. [138] showed that this luminescence feature was due to the recombination of excitons bound to extended dislocations. Leipner et al. [139] showed by cathodoluminescence studies that the emission at 1.478 eV is caused by point defects that are probably vacancies. In our study, the latter mechanism seems to be more probable because in as-deposited CdTe films, Cd vacancies represent the main native defects.

After $CdCl_2$ activation, the intensity of the 1.478 eV PL band increased significantly in both the LT and HT CdTe films (Figs. 3.11a and b, red bands), with the PL intensity of the LT CdTe film higher than that of the HT one. Moreover, the spectrum of the HT CdTe-activated film exhibited a very prominent phonon structure. There was also an emission near the band gap region (~1.59 eV), which is represented in both the LT and HT films. The feature at 1.59 eV is related to the recombination of excitons localised at the chlorine A centre $[(V_{Cd}^{2-}Cl_{Te}^{+})^{-}]$ and/or excitons bound at a different acceptor complexes consisting of a Cd vacancy and two Cl donors $(V_{Cd}^{2-}2Cl_{Te}^{+})$ [135, 141]. The spectral profile of the broad 1.478 eV PL band suggests the presence of more than one transition. According to Hofmann [140], there may be at least three independent emission bands in this spectral region. One band, located at 1.45 eV and exhibiting phonon replicas, arises from donor–acceptor recombinations between a shallow Cl donor and a Cu_{Cd} acceptor. Usually this band is detected in CdTe doped with Cu and Cl. The second band has a zero-phonon line at 1.478 eV, which is believed to be due to a donor–acceptor emission between a Cl_{Te}^{+} donor and an A centre $[(V_{Cd}^{2-}Cl_{Te}^{+})^{-}]$. There is also a third band, which is of unknown origin and has a strong line at 1.475 eV. These three bands, which have almost the same energies, are totally mixed in many crystals and have, therefore, caused considerable confusion [140, 142]. In this study, considering that the main dopant is chlorine, the 1.478 PL emission band is most probably related to the donor–acceptor recombination between the Cl_{Te}^{+} donor and the $[(V_{Cd}^{2-}Cl_{Te}^{+})^{-}]$ shallow acceptor. In this emission band could also be involved different chlorine neutral complex defects, such as $(V_{Cd}^{2-}2Cl_{Te}^{+})$ or $(Te_{i}^{2-}2Cl_{Te}^{+})$, which usually form in chlorine-doped CdTe [22, 94]. Valdna [22, 23] observed a strong correlation between the intensity of the 1.4 PL band and the concentration of these defects in chlorine-doped CdTe films. He showed that a high chlorine concentration increases the intensity of the 1.4 PL band and decreases the p-type conductivity of CdTe layers due to the formation chlorine-based neutral complexes. Our results support the conclusions arrived at in [22, 23]. Thus, in the LT CdTe-activated film, the broad and very intense 1.478 eV

PL band with no noticeable phonon replicas and very weak exciton emission indicates that the activation step left too high a chlorine concentration in the CdTe lattice. As the chlorine concentration increased, the concentration of the Cl_{Te}^{+} donors compensated the shallow acceptor; as a result, the p-type conductivity of the LT CdTe film decreased. Similarly, in the HT-activated film, the presence of a prominent phonon replica structure and excitons resulted in better crystallinity and a lower concentration of neutral complex defects, yielding better p-type conductivity. Thus, the PL results of the LT and HT films before and after $CdCl_2$ activation are in good accordance with the changes in the electrical properties from the same processing steps.

We next investigated the changes in the optoelectronic properties induced by subsequent multi-step thermal annealing in H_2, vacuum, and isothermal conditions. Subsequent thermal annealing in H_2 at 250 °C increased the dark resistivity of both the LT and HT CdTe films by nearly one order of magnitude, from 10^7 to 10^8 $\Omega\cdot$cm and from 7×10^5 to 2×10^6 $\Omega\cdot$cm for LT and HT, respectively. At the same time, the value of K_F remained practically unchanged (Table 3.5). The abrupt increase in resistivity of both the LT and HT films can be explained by the increased activity of H_2 at 250 °C, which provided excess Cd from CdO, decreasing the concentration of Cd vacancies (V_{Cd}), thereby increasing the resistivity of CdTe. Further increasing the H_2 annealing temperature from 300 to 500 °C did not change the dark resistivity of LT CdTe; nevertheless, the film exhibited relatively high photoconductivity, suggesting the partial removal of $CdCl_2$ and excess Cd and the stability of the acceptor–donor concentration ratio in H_2 atmosphere. Considering the higher concentration of residual components on the GBs in LT CdTe, more time is needed for their outdiffusion. The ration of the donor–acceptor defect concentration in LT CdTe was also determined by the constant ratio of the Cd and Te partial pressures in H_2 atmosphere. In comparison to LT films, different features were found to be characteristic for HT films for a distinct H_2 annealing temperature range. At annealing temperatures between 300 and 350 °C, the resistivity of the HT films sharply decreased by nearly half an order of magnitude, from 2×10^6 to 8×10^5 $\Omega\cdot$cm, accompanied by increasing photoconductivity (Table 3.5). In this case, the evaporation of excess Cd occurred over a shorter period of time because of the lower concentration of residual components on the GBs. In this region of temperatures, characteristics similar to those of the initial activated films were revealed. A further increase in the H_2 annealing temperature from 400 to 500 °C increased the resistivity of the HT samples by nearly one order of magnitude, from 8×10^5 to 10^7 $\Omega\cdot$cm, thus showing the same photoconductivity as the activated films (Table 3.5). At the same time, the resistivity was approximately one order of magnitude lower than that of the LT films, indicating a lower concentration of dopant impurities in HT CdTe. With H_2 annealing at 570 °C, the resistivity of both the LT and HT CdTe films increased considerably, suggesting that this was the critical temperature at which gettering and sublimation occurred, so actively that excessively removing both active components from the lattice and the main material. On the other hand, at such high temperatures, this process might be accompanied by deeper redistribution of the dopant throughout the layers.

The thermal annealing in vacuum at 470 °C showed the same trends as those seen for the H_2 annealing step in terms of the changes of electrical properties in both the LT and HT films (Table 3.5). As a result of final isothermal annealing at 600 °C, the dark resistivity sharply decreased by approximately four orders of magnitude for the LT CdTe films (from 10^7 to 10^3 $\Omega\cdot$cm) and by three orders of magnitude for the HT CdTe films (from 2×10^6 to 10^3 $\Omega\cdot$cm). A hole density of $\sim10^{15}$ cm^{-3} was achieved for both the LT and HT films as a result of subsequent thermal annealing in H_2 at 500 °C, vacuum annealing at 470 °C, and isothermal annealing at 600 °C. The H_2 pre-annealing temperature of 500 °C and the subsequent vacuum and isothermal annealing seem to be the optimal conditions to achieve the highest p-type conductivity in CdTe films.

The electrical properties correlated well with the PL measurements. Thus, subsequent H_2 and vacuum annealing decreased the intensity of the 1.478 eV PL band in both the HT and LT films (Figs. 3.12a, b), which can be attributed to the outdiffusion of residual oxides and excess of chlorine. After these processing steps, the presence of at least two emission bands with peaks at 1.478 and 1.43 eV were clearly distinguished. The energetic distance between these two bands was approximately 50 meV, indicating that there were two different recombination centres. The delimitation of these two bands was more prominent in the LT CdTe film. The prevalence of one or the other emission band was determined by the H_2 thermal annealing temperature. Thus, in both films, the 1.478 eV emission band prevailed at low H_2 annealing temperatures (250–300 °C), whereas at high H_2 annealing temperatures (400–500 °C), the 1.43 eV band predominated. The spectrum of the HT CdTe film preserved the phonon replica structure and emission in the excitonic spectral region. The prevalence of the 1.478 eV emission band at low H_2 annealing temperatures could be related to the presence of a high concentration of chlorine neutral complexes. The high concentration of neutral complexes was assured by the high concentration of chlorine in the CdTe lattice. At high H_2 annealing temperatures, the concentration of these defects decreased due to the outdiffusion of chlorine. As a result, the concentration of shallow acceptors $[(V_{Cd}Cl_{Te})^-]$ increased and determined the emission at 1.43 eV. This assumption is supported by the absence of this emission in the as-deposited films and by the improvement in the electrical properties as a result of isothermal annealing. After isothermal annealing, the spectra of both LT and HT films still consisted of two bands, but the distance between them was smaller and the slightly apparent shift was not real anymore. In addition, the PL bands looked more symmetrical. The symmetrical profile, together with the disappearance of the phonon replica structure and excitonic emission, indicates that the overall defect concentration increased. Because the electrical properties of the films improved as a result of this processing step, we assume that this improvement was determined by the increase in the overall concentration of shallow acceptor defects $[(V_{Cd}Cl_{Te})^{-}]$, which are responsible for p-type conductivity in CdTe films.

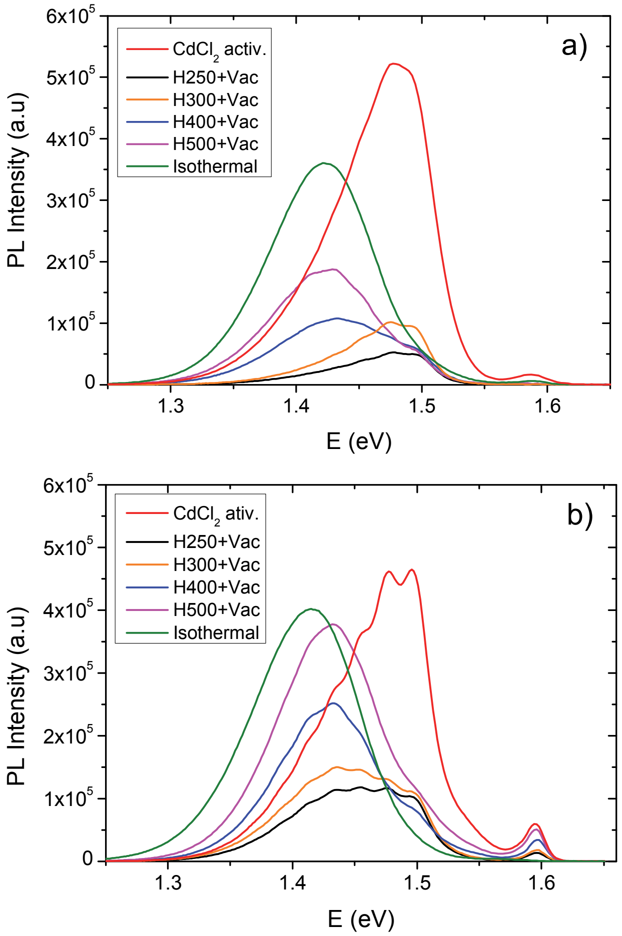

Fig. 3.12. Photoluminescence spectra of CdTe thin films vs. thermal annealing conditions: (a) LT CdTe and (b) HT CdTe.

To summarise, the influence of multi-step thermal annealing in H_2, vacuum, and closed isothermal conditions on the properties of $CdCl_2$-activated CdTe single layers deposited at substrate temperatures of 250 °C and 500 °C was systematically investigated in terms of the formation of p-type conductivity. The $CdCl_2$-activated CdTe films had high resistivities and high dark-to-light resistance ratios. Subsequent H_2 and vacuum thermal annealing increased the resistivity and photoconductivity of the films. The dark resistivity sharply decreased by approximately four orders of magnitude as a result of isothermal annealing at 600 °C, and a hole density of $\sim 10^{15}$ cm^{-3} was achieved. A shift of the main (111) peak indicated processes taking place inside the CdTe lattice. The changes in the electrical properties correlate well with defect features in the photoluminescence spectra. By controlling the thermal annealing conditions, substantial improvement in the CdTe optoelectronic properties was achieved.

3.3. Plasmonic modification of CdTe thin films and CdTe/CdS solar cells by Au nanoparticles

As discussed in Section 1.3, one of the critical issues in CdTe technology is reducing the PV active layer thickness in order to lower production costs and reduce the need for Te. Theoretically, employment of the plasmonic effect using metallic nanoparticles has been found to be effective for enhancing light absorption in ultrathin CdTe layers in thin-film solar cells. Considering these approaches, we studied the plasmonic effect of Au nanoparticles (NPs) on the properties of CdTe absorber layer [IV] and on the performance of CdTe/CdS solar cells [V]. The Au NPs were incorporated into CdTe absorber layer by spray pyrolysis, spin coating and sputtering methods (Section 2.3).

3.3.1. Spin coating of Au solution onto CdTe layer

Spin coating of an $HAuCl_4$ solution onto CdTe layers and subsequent annealing in air at 380 °C resulted in Au NPs and wires binding the NPs in a web and covering the surface of the CdTe layer (Fig. 3.13). We assumed that these wires represented residual cadmium oxychloride ($2CdO \cdot CdCl_2$) created during the air annealing process [143] as an intermediate product of the $HAuCl_4$ reaction with CdTe [144]. From the SEM images, the mean size and spacing of the Au NPs were estimated to be 100 nm and 300 nm, respectively.

The SPR valley at 577 nm in the transmittance spectrum of the CdTe–Au layer (Fig. 3.14a) confirms the plasmonic absorption resonance of the incorporated Au NPs. However, this effect did not lead to a noticeable enhancement in the absorption over the entire wavelength range (Fig. 3.14b). Moreover, the reflectance and transmittance spectra showed the disappearance of the CdTe absorption edge in the 800 nm region (Fig. 3.14a), indicating the removal of the CdTe film during the spin-coating process.

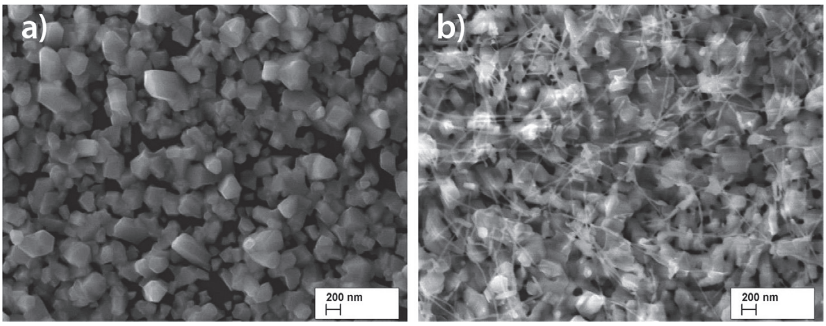

Fig. 3.13. SEM surface view of CdTe film: (a) as-deposited and (b) with Au NPs obtained by spin coating [IV].

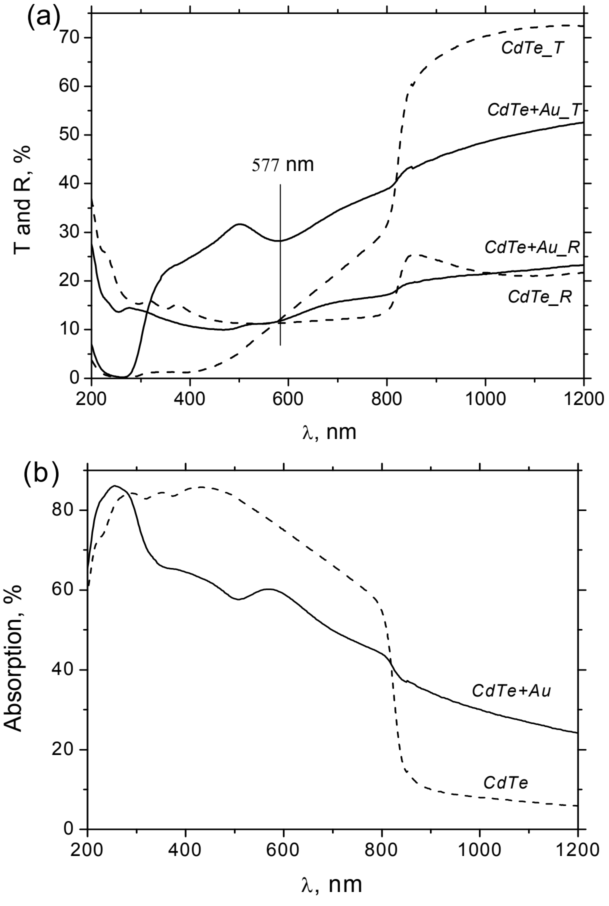

Fig. 3.14. (a) Transmittance and reflectance (b) absorbance spectra of the as-deposited CdTe films (CdTe) and CdTe with Au NPs obtained by spin coating (CdTe + Au) [IV].

To understand the disappearance of the CdTe band edge (Fig. 3.14), we analysed the reactions that could take place in the air annealing of the CdTe layer with a spin-coated $HAuCl_4$ solution: oxidation of CdTe to $CdTeO_3$ ($CdO\cdot TeO_2$) (Eq. 3.6), decomposition of $HAuCl_4$ (Eq. 3.7, 3.8), and formation of $CdCl_2$ and Te_2 (Eq. 3.9). These reactions may form a viscous phase of CdTe + $CdTeO_3$ + $CdCl_2$ flux [91, 143], which has a low melting temperature (<400 °C).

$$1.5O_2(g) + CdTe(s) \rightarrow CdTeO_3(s) \tag{3.6}$$

$$CdTeO_3(s) + 2CdTe(s) \rightarrow 3CdO(s) + 1.5Te_2(g) \tag{3.6a}$$

$$2HAuCl_4(s) \rightarrow 2HCl(g) + 2AuCl_3(s) \tag{3.7}$$

$$2AuCl_3(s) \rightarrow 2Au(s) + 3Cl_2(g) \tag{3.8}$$

$$2HCl(g) + 2Cl_2(g) + 3CdTe(s) \rightarrow 3CdCl_2(s) + H_2Te(g) + Te_2(g) \tag{3.9}$$

We carried out some calculations to evaluate the impact of the $CdCl_2$-containing flux on the CdTe film after coating it with the $HAuCl_4\cdot 3H_2O$ solution. Au NPs with diameters and spacings of 50 nm (minimal values for a 2% absorption enhancement [111]) covered 0.4 cm^2 of a 1 cm^2 CdTe film surface. Based on the mass of Au, the amount of Au in the $HAuCl_4$ solution was calculated to be 1.32×10^{-5} mol. Because each mole of $HAuCl_4$ yields two moles of $CdCl_2$, a 1 cm^2 CdTe film will contain 2.65×10^{-5} mol of $CdCl_2$. Therefore, the mass ratio of $CdCl_2$ (created by $HAuCl_4$) to CdTe is at least 25. Considering the solubility of CdTe in the $CdCl_2$ flux (~25%) [145], it is highly likely that the CdTe film will disappear. Therefore, although RT spin coating of Au NPs from a $HAuCl_4$ solution on CdTe layers is a very simple technique, it should be discarded because of the substantial removal of CdTe by reactions with the chloride flux during the annealing process.

3.3.2. Spray pyrolysis of Au solution on the CdTe layer

Spraying $HAuCl_4$ solutions of various amounts (from 2.5 mL to 15 mL) generated distributions of Au NPs with different spacings and sizes (Fig. 3.15). As compared to the RT spin coating of large drops of an Au-containing solution, spray-coated $HAuCl_4$ interacts differently with the CdTe absorber because of the relatively high temperature of the substrate (360 °C). At this temperature, the reaction products quickly evaporate, leaving a CdTe surface free of the oxychloride residuals that can damage the CdTe absorber, as in the case of the spin-coating method.

For better understanding of the microscopic images of sprayed Au on CdTe and on reference glass are presented in Fig. 3.15 b. At the lowest quantity of the $HAuCl_4$ solution, Au NPs with a mean size of 30 nm were formed, while increasing the amount of the solution led these crystallites to coagulate into grains with the size from 80 nm to 100 nm (Fig. 3.15 b). The size of these Au-containing grains corresponds to the optimal theoretical diameter of 90 nm and spacing of 202 nm, which should result in a 50% increase in absorption and a 36% increase in the efficiency of a CdTe solar cell [31].

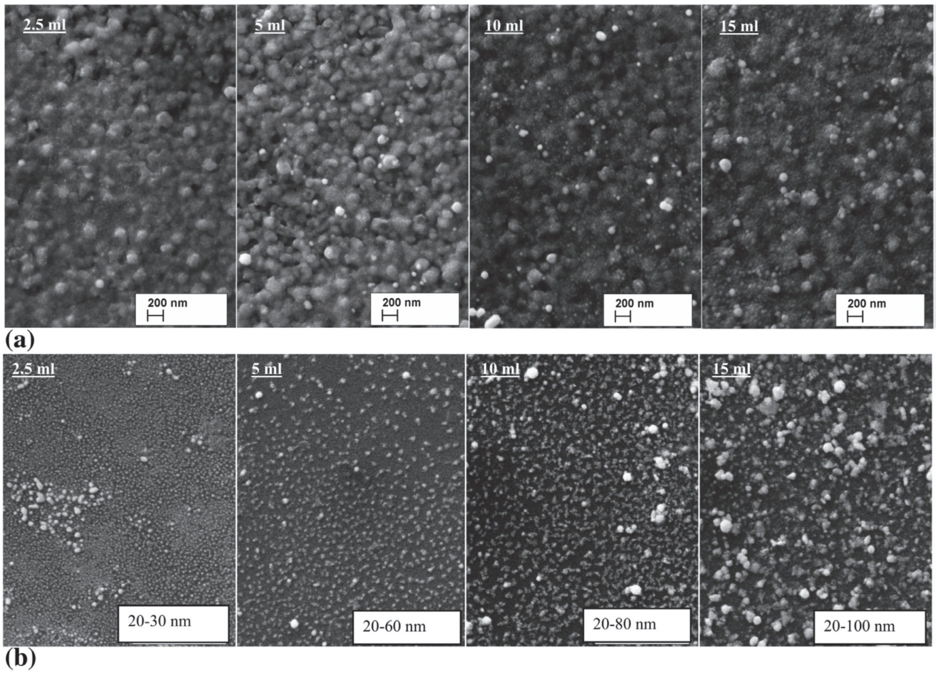

Fig. 3.15. SEM images of Au particles obtained by spray pyrolysis on (a) CdTe thin films and on (b) corresponding reference glass (estimated size of Au-containing grains is included) with 2.5, 5, 10, and 15 mL of $HAuCl_4$ solution [IV].

The absorption of the CdTe layer was enhanced over the 400–1000 nm wavelength range when Au NPs were sprayed on top of the CdTe layer (Fig. 3.16b). The plasmonic effect was observed for the CdTe–Au samples sprayed with 10 and 15 mL of $HAuCl_4$ solution (Fig. 3.16a). For these amounts of $HAuCl_4$ solution, the XRD patterns recorded greater intensities of (021) and (300) AuCd peaks at 29.7° and 38.2° (Fig. 3.17). The SPR peak located at 570 nm (Fig. 3.16a) redshifted slightly because of the decreased separation of the NPs [146] and the increased agglomeration of Au crystallites with the 15 mL Au solution. In addition, the 570 nm peak became broader as the particle diameter increased to 100 nm upon increasing the amount of sprayed $HAuCl_4$ from 10 to 15 mL (Fig. 3.16b). This broadening is attributed to the enhanced radiation damping by large particles, as described by Hu [147].

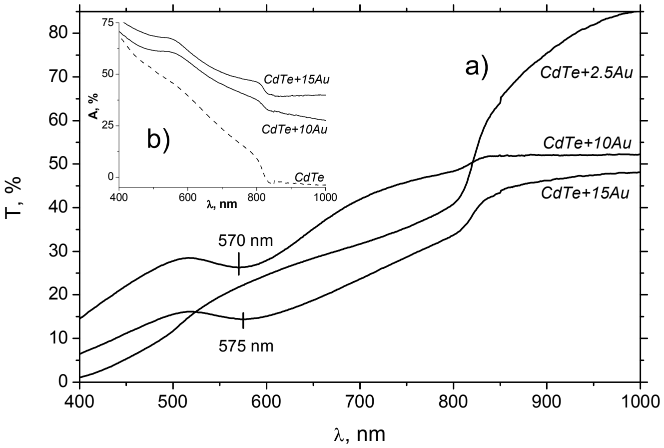

Fig. 3.16. (a) Total transmittance and (b) absorption spectra of CdTe films sprayed with 2.5, 10, and 15 mL of $HAuCl_4$ solution [IV].

The appearance of the (200) CdTe peak at 30.76° for 10 and 15 mL of $HAuCl_4{\cdot}3H_2O$ solution (Fig. 3.17) shows that higher quantities of Au increase the amount of chloride flux, which actively promotes the recrystallisation of CdTe. It is interesting that the Au NPs obtained by spray pyrolysis on the CdTe surface actually consisted of an Au–Cd (JCPDS no. 01-072-8534) [148] intermetallic phase (Fig. 3.17). We attribute this to the fact that the substrate temperature (360 °C) was higher than the eutectic temperature of the Au–Cd system (310 °C) [149].

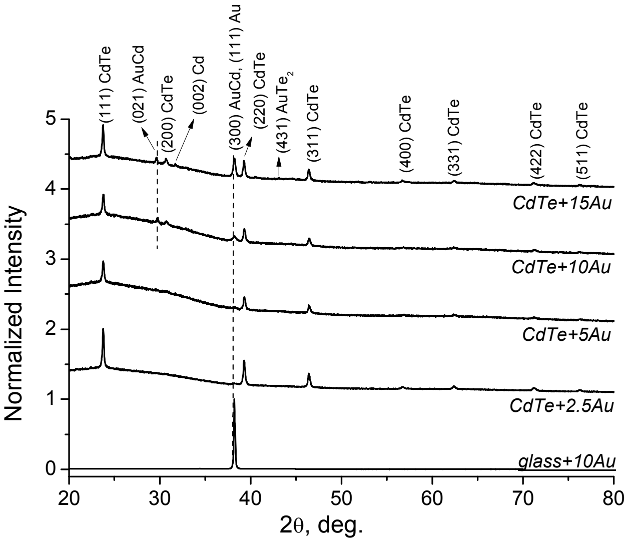

Fig. 3.17. XRD patterns of reference glass and CdTe films spray coated with different amounts of Au solution [IV].

Increasing the amount of sprayed $HAuCl_4$ solution did not affect the size of these AuCd crystallites (~30 nm); rather, it contributed to the agglomeration of the Au NPs into larger grains (Fig. 3.15). The appearance of an $AuTe_2$ peak (JCPDS no. 03-065-2443) [148] in the XRD pattern of the CdTe + 15 mL Au layer might be linked to the presence of metallic Te (Figs. 1a, 4). These phases indicate that excess $HAuCl_4$ was present on the CdTe surface. Therefore, 10 mL of $HAuCl_4 \cdot 3H_2O$ solution is sufficient to spray onto the CdTe surface to obtain the plasmonic effect.

3.3.3. Sputtered and annealed Au between glass surface and CdTe layer

The surface morphology of sputtered and annealed Au NPs on the glass substrates shows a very uniform distribution of isolated particles with a mean diameter of 40 nm (Fig. 3.18a). These NPs agglomerated as large particles, with diameters varying from 1 to 3 µm (Fig. 3.18b). In addition, the agglomeration of Au NPs was confirmed by the colour transition of the glass–Au samples from reddish to purple after annealing in air due to the plasmonic coupling between particles [190]. The size distribution and spacing of the Au particles were not strongly influenced by the duration of sputtering (Figs. 3.18b and c).

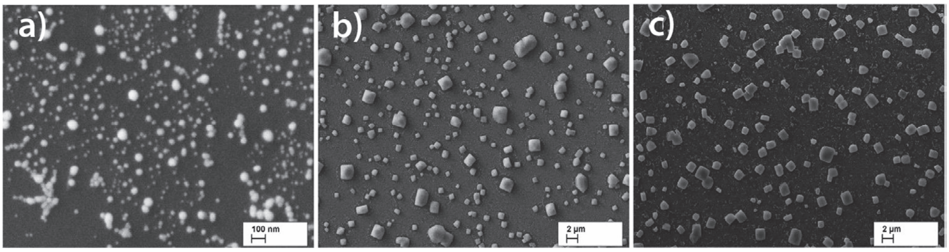

Fig. 3.18. SEM surface views of glass following Au sputtering for (a, b) 40 s and (c) 70 s after air annealing [IV].

The transmittance spectra of the glass–Au–CdTe samples (Fig. 3.19) exhibited surface plasmon features at 592 nm and 570 nm for the Au/glass samples sputtered under CdTe for 40 s and 70 s, respectively. Fig. 3.19 suggests that 40 s of Au sputtering is sufficient to facilitate an efficient plasmon effect for the CdTe absorber. However, the 570 nm SPR peak, which corresponds to the 70 s Au sputtering, is closer to the theoretical SPR of Au particles. The shift of the SPR peak for CdTe samples with spin-coated and sprayed Au on top could be related to the dependence of the SPR peak position on the dielectric constant of the surrounding environment [150]. An intermetallic $Au_{0.3}Te_{0.7}$ phase (Fig. 3.20), which has a high concentration of charge carriers, may form a shell for plasmon Au NPs and slightly shift the peak position.

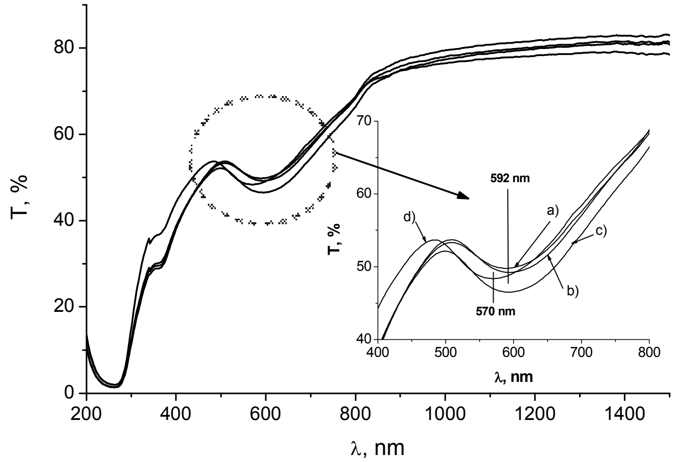

Fig. 3.19. Transmittance spectra of sputtered and air-annealed Au on glass and CSS deposition of CdTe. Duration of sputtering: (a) 40, (b) 50, (c) 60, and (d) 70 s [IV].

The appearance of the $Au_{0.3}Te_{0.7}$ (JCPDS no. 01-074-5406) [148] phase (Fig. 3.20) can be explained by its thermodynamic stability [149, 151], the dissociation of CdTe, and the high volatility of Cd, resulting in excess metallic Te. The radiative heat transport in the CSS CdTe deposition process could locally increase the substrate temperature above 300 °C for fractions of seconds, allowing for a reaction between Au and Te, producing $Au_{0.3}Te_{0.7}$. Although the sputtering method generated pure Au particles, the subsequent deposition of the CdTe absorber resulted in the formation of additional phases around the Au NPs that contributed to the shift of the SPR peak.

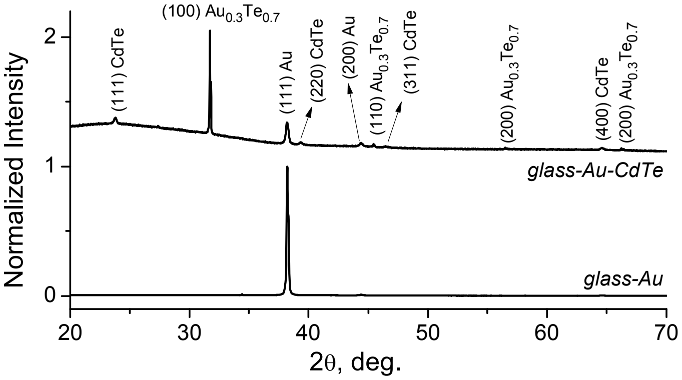

Fig. 3.20. XRD pattern of Au sputtered for 70 s, annealed on glass, and coated with CdTe film [IV].

To summarise, we tried to incorporate Au NPs into the CdTe layer to obtain the plasmonic effect in order to increase the absorption in the CdTe absorber. Au NPs were deposited onto the CdTe films by three different methods: spin coating, spray pyrolysis, and sputtering. Each method resulted in different plasmonic effects for the CdTe layers. Spin coating of the $HAuCl_4$ solution and air annealing generated oxychloride residuals and substantially removed the CdTe layer. For this reason, the spin-coating method should be discarded.

Both spray coating and sputtering methods formed Au-containing NPs with diameters of 30–40 nm. Increasing the amount of $HAuCl_4$ or increasing the Au sputtering time did not increase the size of the Au NPs; rather, these increases tended to agglomerate the Au particles into grains with diameters of ~90 nm and 1–3 µm for the spray and sputtering methods, respectively. Spray pyrolysis formed Au NPs on the CdTe surface with sizes close to the size suggested by the results of theoretical studies, but the sputtering technique provided purer Au NPs. However, with both techniques, interactions between CdTe and Au at high temperatures resulted in the formation of intermetallic compounds such as AuCd, $AuTe_2$, or $Au_{0.3}Te_{0.7}$. The formation of these intermetallic phases, which likely depended on the deposition parameters such as substrate temperature or how the substrate temperature was maintained, is an important characteristic of the CdTe layers. Because of the chemical interaction between Au and CdTe, high-temperature processes for forming Au NPs should be avoided.

3.3.4. Plasmonic effect of spray-deposited Au nanoparticles on the performance of CSS CdS/CdTe solar cells

Spray pyrolysis seemed to be a more suitable method for incorporating Au nanoparticle because it promoted the formation of Au NPs on the CdTe surface with sizes close to that suggested by the theoretical studies. Therefore, we decided to demonstrate the technological feasibility of placing chemically sprayed Au NPs between the CdTe absorber and the Te/Ni back contact to enhance the efficiency of CdS/CdTe solar cells [V].

Figure 3.21 shows the SEM cross-sectional images of Ni/Te/Au NP/CdTe/CdS/FTO/glass plasmonic structures. As seen after $CdCl_2$ heat treatment and etching of the CdTe/CdS structure, the surface of the CdTe film remained smooth without residuals (Fig. 3.21a), whereas in the case of the $HAuCl_4$-sprayed films, the CdTe surface was coated with a tightly adhering thin layer (Figs. 3.21b, c). This surface layer was composed of aggregated grains approximately 200 nm in size, and EDX analysis of the surface layer showed a significantly higher concentration of Cl in the aggregated grains as compared to the rest of the surface (Table 3.6 and Fig. 3.21c). However, at the maximum amount of $HAuCl_4$ solution (15 mL), this surface layer became porous, substantially reducing the area of the back contact with CdTe.

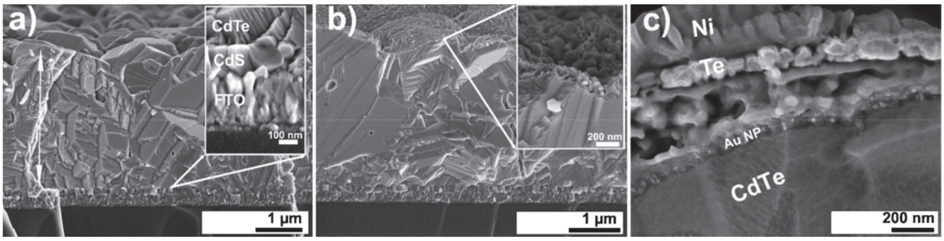

Fig. 3.21. Cross-sectional images of (a) CdTe/CdS/FTO/glass reference sample, (b)after spray coating of 10 mL and (c) 15 mL of $HAuCl_4$ solution and back-contact Te/Ni [V].

The EDX analysis of the Au-sprayed CdTe surface indicated a 1:1 ratio of Cd and Te in the reference structure and increased contamination of the surface by oxides and chlorides with increasing amounts of Au solution from 2.5 to 15 mL (Table 3.6). These observations are in good agreement with the XRD data (Fig. 3.17), which indicated that the Au-containing grains consisted of Au and intermetallic compounds of AuCd and $AuTe_2$, as well as residuals of non-volatilised flux decomposition such as CdO, TeO_2, and $CdCl_2$.

Table 3.6. Elemental composition of CdTe/CdS structures sprayed with different amounts of Au solution [V].

Sample	Scanned area	Elements, at. %				
		Cd	Te	Cl	Au	O
Reference	300x300 µm	50.46	49.48	-	-	-
AuNP-2.5 ml	300x300 µm	41.12	38.35	1.78	0.83	17.92
AuNP-5 ml	300x300 µm	31.55	31.00	4.84	1.70	30.92
AuNP-7.5 ml	300x300 µm	29.91	29.86	5.17	2.00	33.06
AuNP-10 ml	300x300 µm	27.27	26.77	8.22	2.48	35.25
AuNP-10 ml	area 1 on Fig. 3.21c	60.94	-	39.06	-	-
AuNP-15 ml	300x300 µm	22.69	22.79	9.59	3.17	41.76

In order to show the effect of Au NPs spray deposited onto the CdTe surface and CdTe/CdS solar-cell performance, including the effect of NP size and solution concentration, we investigated the plasmonic effect for the CdTe–Au layers from their spectral responses. Figure 3.22 shows that when these CdTe–Au layers were used in a CdS/CdTe solar cell, the EQE was primarily enhanced in the region of 600–840 nm because of the gain in optical absorbance induced by the SPR. A condition for this effect to occur is a scattering medium with a low refractive index. The refractive index of Au is 1.5–0.2 [152], whereas that of CdTe is 3–2.6 [153] and that of Te is 4.8. When larger volumes of the Au-containing solution (up to 15 mL) were sprayed onto the CdTe, a further relative increase in the EQE was evident because of the previously mentioned broadening of the 570 nm plasmonic resonance peak.

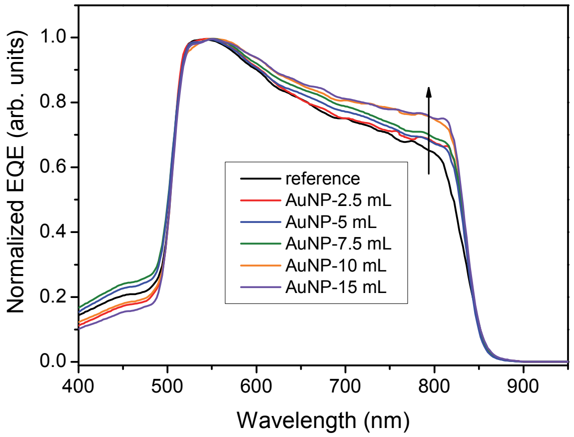

Fig. 3.22 Normalised EQE curves of CdTe/CdS solar cells sprayed with different amounts of Au solution [V].

The highest EQE was that of the CdS/CdTe structure with 10 mL of sprayed solution. At this amount of solution, an optimal balance between the size and distribution of the Au NPs and the additionally formed aggregate grains (Fig. 3.21) caused a wide absorption band and a corresponding EQE gain due to the overlapping plasmon resonances [112]. The EQE spectra looked similar for both the 10 mL and 15 mL of Au solution, indicating that the higher amount of $HAuCl_4$ formed larger conglomerates with no change in the interparticle distance.

The representative photovoltaic *J–V* characteristics and parameters of the CdS/CdTe solar cells with and without Au NPs (Fig. 3.23 and Table 3.7) indicate a variation in the photovoltaic parameters of the plasmonic CdTe/CdS solar cell using different amounts of sprayed Au solution.

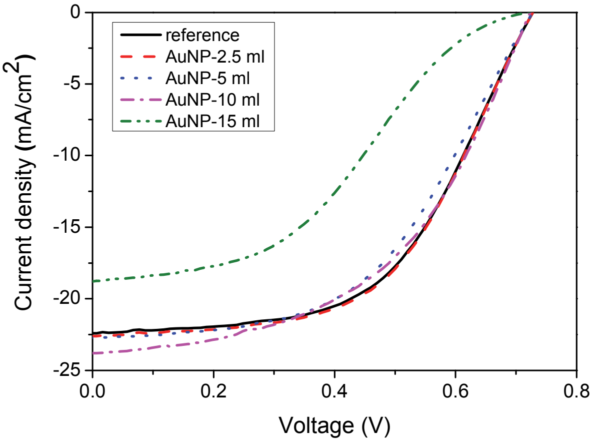

Fig. 3.23. J–V characteristics of CdTe/CdS solar cells with and without (reference) sprayed Au NPs [V].

Table 3.7. Photovoltaic parameters of CdTe/CdS plasmonic solar cells [V].

Sample	V_{oc}, mV	J_{sc}, mA/cm^2	FF, %	η, %
Reference	740	22.4	50	8.3
AuNP-2.5ml	740	22.5	50	8.3
AuNP-5ml	740	22.7	49	8.3
AuNP-7.5ml	740	23.8	49	8.6
AuNP-10ml	740	24	50	8.9
AuNP-15ml	720	18.5	39	5.2

The conversion efficiency gradually improved from 8.3% to 9% and the J_{sc} value increased from 22.4 to 24 mA/cm^2. The highest conversion efficiency was reached for the CdS/CdTe solar cell with 10 mL of $HAuCl_4$ solution. The same sample showed better absorption and EQE gain (Fig. 3.22) because of the optimal balance between the size (80 nm) and distribution of the Au NPs. When the amount of $HAuCl_4$ solution was higher than the optimal 10 mL, both the J_{sc} and FF values decreased because of the porous surface layer, which substantially reduced the area of the back contact with CdTe (Fig. 3.21c). These results, together with EQE improvement, suggest that the enhanced conversion efficiency of plasmonic CdTe/CdS solar cells was generated by fundamental optical engineering via the incorporated Au NPs. The charge transfer at the back-contact region (Ni/Te/Au/CdTe) could be improved as compared to the reference back contact (Ni/Te/CdTe), but the presence of resonant absorption peaks in the red/infrared region (Fig. 3.16) presented clear evidence of the contribution by the plasmon effect.

To summarise, the chemical spray pyrolysis of a $HAuCl_4$ ethanol solution was shown to be a feasible and flexible method for depositing Au NPs 30–100 nm in size onto the CdTe surface. Also, the CdTe–Au layers were implemented in a CdS/CdTe solar cell. The EQE of the solar cell was enhanced in the 600–840 nm range, with the highest EQE achieved by the CdS/CdTe structure with 10 mL of the sprayed solution. The same amount of Au-containing solution sprayed onto the CdTe increased the J_{sc} value and efficiency of the plasmonic CdS/CdTe solar cell from 22.4 to 24 mA/cm^2 and from 8.3% to 9%, respectively. This is attributed to the suitable size of Au NPs, which resulted in large absorption and a corresponding EQE enhancement because of the overlapping plasmon resonances. The 15 mL sprayed solution generated a porous CdTe surface layer and degraded the photovoltaic parameters of the CdS/CdTe solar cell. Although this is a very promising design structure, additional studies should be performed to better understand the influence of Au NP parameters on the final characteristics of CdS/CdTe solar cells and improve their efficiency.

CONCLUSIONS

A systematic study of changes in the properties of CdTe thin films and CdTe/CdS solar cells induced by post-deposition thermal treatments and the plasmonic effect of Au nanoparticles in solar cells was carried out in order to understand the physicochemical mechanisms of the processes which is essential for optimization of high-efficiency solar cells. The results are as follows:

1. The structural and morphological properties of CdTe layers deposited onto CdS/FTO/glass substrates strongly depended on the substrate temperature. Different sizes and shapes of CdTe grains were obtained at distinctive regions of substrate temperature (250–500 °C) and were explained in terms of nucleation and growth theory.
2. As a result of $CdCl_2$ activation the extent of recrystallization and intermixing decreases with increase of the substrate temperature from 250 to 450 ºC, whereas the solar cell efficiency is improved from 2.3 to 11.6%, respectively.
3. It is claimed that the $CdCl_2$ activation process induced formation of a liquid flux and mass transport through the melted phase, promoting grain growth and intermixing at the CdTe/CdS interface by recrystallisation and sintering.
4. Grain growth was accomplished by the incorporation of flux components into the growing CdTe lattice in saturation concentrations according to the distribution coefficient between the liquid and solid phases at the processing temperature.
5. The doping density depended on the time, temperature, and initial grain size of the CdTe films, being higher for initially fine-grained material.
6. Changes in the optoelectronic properties of $CdCl_2$-activated CdTe films in the multi-step thermal annealing processes were explained with the removal of chlorine from the CdTe lattice by H_2 and vacuum annealing and with the homogeneous distribution of chlorine doping through the layer by isothermal treatment.
7. By controlling the thermal annealing conditions, substantial improvement in the CdTe optoelectronic properties was achieved.
8. For the first time, we experimentally demonstrated that the deposition of Au NPs on top of the CdTe absorber material increased the absorption ability, short-circuit current density, and conversion efficiency of the CdTe/CdS solar cells.
9. The EQE of the solar cell with the implemented Au NPs was enhanced in the range of 600–840 nm. The J_{sc} and efficiency of the

plasmonic CdS/CdTe solar cell increased from 22.4 to 24 mA/cm^2 and from 8.3 to 9%, respectively.

As a result of the present work, the effects of $CdCl_2$ activation treatment on the properties of CSS CdTe thin films and CdTe/CdS solar cells, which are still considered controversial, have received an unambiguous physicochemical explanation.

ACKNOWLEDGEMENTS

I would like to thank Dr. Tamara Potlog from Moldova State University for connecting me with Estonia in 2011 and for opening the opportunity to study at Tallinn University of Technology. I express my sincerest gratitude to my supervisors Dr. Jaan Hiie, Dr. Malle Krunks and Dr. Valdek Mikli for their unconditional support, guidance and understanding over the years of studies. Special thanks go to my first supervisor. Jaan, thank you for everything: your patience, knowledge, kindness, sense of humour, countless late discussions and that magic phrase: “Главное — не перестараться!!”.

I am thankful to Dr. Vello Valdna for valuable discussions and technical support, to Dr. Arvo Mere for technical supervision, to Dr. Natalia Maticiuc for excellent teamwork and many fruitful discussions, to Dr. Taavi Raadik for support with Raman and photoluminescence measurements, to Prof. Jüri Krustok for useful discussions, to Dr. Atanas Katerski and Dr. Ilona Oja Acik for their support and useful collaboration. Thanks to all my friendly colleagues for inspiring discussions and pleasant working atmosphere.

I wish to thank Prof. Andres Öpik, the Head of the doctoral studies curriculum "Chemical and materials technology", Faculty of Chemical and Materials Technology in Tallinn University of Technology for providing the opportunity to participate in the PhD studies at the faculty and in the graduate school; Prof. Enn Mellikov and Marit Kauk-Kuusik, Heads of the Department of Materials Science, for the opportunity to use high-end research equipment within the Department.

The work was financially supported by European Union through 7th FP project FLEXSOLCELL (GA-2008-230861); Estonian Ministry of Education and Research (IUT19-4, SF0140092s08); Estonian Science Foundation (ETF9142, ETF9081); European Union through the European Regional Development Fund: Project TK114 (Centre of Excellence “Mesosystems: Theory and Applications”, TK114, 3.2.0101.11-0029), AR12118 (“Efficient plasmonic absorbers for solar cells”, 3.2.1101.12-0023) and TK141 (“Advanced materials and high-technology devices for sustainable energetics, sensorics and nanoelectronics”, 1.01.2016-1.03.2023); FMTDK graduate school “Functional materials and technologies” receiving funding from the European Social Fund under Project 1.2.0401.09-0079 in Estonia, Internationalization Program DoRa5 and ASTRA “TUT Institutional Development Programme for 2016-2022” graduate school „Functional materials and technologies" (2014-2020.4.01.16-0032).

I would like to express my warmest gratitude to my family for their encouragement and generous support.

ABSTRACT

Photovoltaic (PV) technology based on CdTe thin films offers an effective option for the production of solar electricity owing to lower production costs and increased efficiency of as much as 22%. The current market share of CdTe PV technology is approximately 5% of the current worldwide annual PV production. Despite the relatively high efficiency of laboratory solar cells, there are still several technology-related issues such as junction activation and Te availability that need to be addressed. Systematic research on the processing steps, as well as application of new innovative concepts, is essential to solving the persistent challenges in CdTe technology.

The aim of the thesis was to study systematically the impact of post-deposition thermal treatments and the plasmonic effect of Au nanoparticles on the properties of CdTe thin films and CdTe/CdS solar cells and to understand the underlying physicochemistry, which is essential for optimisation of high-efficiency solar cells.

The thesis is based on five publications, and it is composed of three chapters. Following the Introduction, Chapter 1, “Literature overview,” provides a short review of the history of photovoltaics, followed by a general overview of CdTe/CdS thin-film solar cells. Further, the properties that make CdTe a favourable material for photovoltaics, as well as the technological challenges associated with the development of CdTe/CdS thin-film solar cells, are highlighted. Chapter 2 describes the experimental details of thin-film processing, as well as those of device fabrication. The techniques used to characterise the properties of thin films and solar cells are also introduced. Chapter 3 is divided into three sections and contains original experimental results and a discussion of those results. The first section reports the formation of CdTe/CdS solar cells as a function of the deposition conditions and post-deposition $CdCl_2$ activation treatment. The second section comprise systematic investigation of the influence of multi-step thermal annealing on the properties of $CdCl_2$-activated CdTe single layers. The third section is devoted to the plasmonic effect of Au NPs on the properties of the CdTe layers and on the performance of CdTe/CdS solar cells.

CdTe thin films and CdTe/CdS solar cells were prepared by close-spaced sublimation, followed by wet $CdCl_2$ treatment and thermal annealing in air at 420 °C. Additionally, multi-step thermal annealing in hydrogen, vacuum, and closed quartz ampoules was carried out for CdTe single layers. As a different approach, plasmon nanoparticles were incorporated into CdTe thin films by spin coating, sputtering, and spray pyrolysis. Scanning electron microscopy, energy dispersive X-ray spectroscopy, X-ray diffraction analysis, photoluminescence, ultraviolet–visible spectroscopy, and the Hall effect were applied to study the

materials, whereas, current–voltage and external quantum efficiency measurements (EQE) were used for cell characterisation.

The structural and morphological properties of CdTe layers deposited on CdS/FTO/glass substrates strongly depended on the substrate temperature and $CdCl_2$ activation process. CdTe grains of different sizes and shapes were obtained at distinctive regions of substrate temperature (250–500 °C) and were explained in terms of nucleation and growth theory. The subsequent $CdCl_2$ activation promoted recrystallisation and resulted in equally large CdTe crystallites, independent of the substrate temperature. Moreover, this activation step implied formation of a $CdTe_{1-x}S_x$ alloy at the CdTe/CdS interface. The intermixing intensified with decreasing substrate temperature and reduced the CdS thickness. Although a higher short-wavelength quantum efficiency was obtained, non-uniform CdS consumption led to the formation of parallel junctions between the absorber and the front contact, reducing the performance of the CdTe/CdS solar cells. So far, a conversion efficiency of 11.6% was obtained for solar cells with CdTe deposited at high substrate temperatures of 400–500 °C. Systematic lowering of the solar-cell efficiency from higher to lower substrate temperatures was the key question that guided our initial investigation of CdTe single layers.

The influence of multi-step thermal annealing in H_2, vacuum, and closed isothermal conditions on the properties of $CdCl_2$-activated CdTe single layers deposited at substrate temperatures of 250 °C and 500 °C was systematically investigated to follow the formation of p-type conductivity. The $CdCl_2$-activated CdTe films had high resistivity and a high dark-to-light resistance ratio. Subsequent H_2 and vacuum thermal annealing increased the resistivity and photoconductivity of the films. The dark resistivity sharply decreased by approximately four orders of magnitude as a result of isothermal annealing at 600 °C, and a hole density of $\sim 10^{15}$ cm^{-3} was achieved. A shift of the main (111) peak indicated processes taking place inside the CdTe lattice. The changes in the electrical properties correlated well with the defect features the in the photoluminescence spectra.

The incorporation of Au nanoparticles (NPs) into the CdTe layer was studied in order to increase the absorption in the CdTe layer via the plasmonic resonance effect. Spray deposition formed Au NPs on the CdTe surface whose sizes were close to that suggested by theoretical studies, but sputtering provided purer NPs. Interactions between CdTe and Au in the range of annealing temperatures used in this study resulted in the formation of intermetallic compounds, such as AuCd, $AuTe_2$, or $Au_{0.3}Te_{0.7}$, which were characteristic of both techniques and were detrimental to the fabricated solar devices. The EQE of the solar cell with Au NPs was enhanced in the 600–840 nm range. The J_{sc} value and efficiency of a plasmonic CdS/CdTe solar cell increased from 22.4 to 24 mA/cm^2 and from 8.3 to 9%, respectively.

Based on these findings, it is claimed that $CdCl_2$ activation process induced formation of a liquid flux and mass transport through the melted phase, promoting grain growth and intermixing at the CdTe/CdS interface by recrystallisation and sintering. The grain growth was accomplished by incorporation of flux components into the growing CdTe lattice in saturation concentrations according to the distribution coefficient between liquid and solid phases at the processing temperature. The doping density depended on the time, temperature, and initial grain size of the CdTe films; it was higher for initially fine-grained material. Changes in the optoelectronic properties of $CdCl_2$-activated CdTe films as a result of the thermal annealing processes were connected with the removal of chlorine from the CdTe lattice by H_2 and vacuum annealing and with the homogeneous distribution of chlorine doping through the layer by isothermal treatment.

The novelty of the current study lies in the application of liquid-phase recrystallisation and sintering theory to explain the physicochemical processes involved in the post-deposition thermal treatment of CdTe films and solar cells. For the first time, we have a complete picture of the evolution of the electrical, structural, and optical properties of CdTe as a result of the CdTe–$CdCl_2$:O_2 activation process. By controlling the thermal annealing conditions, substantial improvement of the CdTe optoelectronic properties was achieved. For the first time, we have experimentally demonstrated that the deposition of Au NPs on top of the CdTe absorber material increases the absorption ability, short-circuit current density, and conversion efficiency of CdTe/CdS solar cells.

KOKKUVÕTE

CdTe õhukestel kiledel baseeruv foto-volt (PV) tehnoloogia on üks efektiivsetest võimalustest päikeseelektri tootmiseks tänu madalatele tootmiskuludele ja patarei kõrgele kasutegurile - kuni 22 %. Praegune CdTe PV turuosa moodustab ligikaudu 5 % aastasest PV maailmatoodangust. Vaatamata laboratoorsete elementide kõrgele efektiivsusele on mitmeid tehnoloogiaga seotud küsimusi nagu siirde aktiveerimine ja telluuri kättesaadavus. Nii töötlemisetappide käigus toimuvate protsesside süstemaatiline uurimistöö kui ka uute innovaatiliste kontseptsioonide rakendamine on olulised lahendamaks CdTe tehnoloogia jooksvaid probleeme.

Käesolev süstemaatiline töö on pühendatud CdTe õhukeste kilede ja CdTe/CdS päikesepatareide omaduste kujunemise uurimisele sadestusjärgsete termiliste käsitluste ning Au nanoosakeste plasmon-mõju toimel, eesmärgiga tundma õppida toimuvate protsesside füüsikalis-keemilisi mehhanisme, mis on olulised kõrge efektiivsusega päikesepatareide tootmise optimeerimisel.

Antud uurimus baseerub viiel publikatsioonil ja on jaotatud kolmeks peatükiks. Sissejuhatusele järgnev esimene peatükk koosneb kirjandusülevaatest, mis algab fotovolt-tehnika ja CdTe/CdS päikesepatareide üldise lühiülevaatega. Järgnevalt kirjeldatakse CdTe kui soodsa fotovolt-materjali omadusi, samuti CdTe/CdS päikesepatareide arenguga seotud tehnoloogilisi võimalusi. Teises peatükis kirjeldatakse detailselt õhukeste kilede käsitlemiseks ja päikesepatareide valmistamiseks töös kasutatud eksperimentaalseid meetodeid ja seadmeid ning tuuakse välja keemilis-füüsikaliste omaduste määramise meetodid. Kolmas peatükk on jaotatud kolmeks alapeatükiks ja sisaldab originaalseid eksperimentaalseid tulemusi ning arutelu. Esimene alapeatükk kirjeldab CdTe/CdS päikesepatareide omaduste muutuseid sõltuvalt sadestamise tingimustest ja sadestusjärgsest $CdCl_2$ aktivatsioonkäsitlusest. Teises alapeatükis jätkub mitmeastmelise termilise lõõmutuse mõju süstemaatiline uurimine $CdCl_2$ aktiveeritud CdTe kilede omadustele. Kolmas alapeatükk on pühendatud Au nanoosakestest tingitud plasmonmõjule nii CdTe kilede omadustele kui ka CdTe/CdS päikesepatareide jõudlusele.

CdTe õhukesed kiled ja CdTe/CdS päikesepatareid valmistati lähidistants-sublimatsiooni meetodil, millele järgnes märg $CdCl_2$ käsitlus ja termiline lõõmutamine õhus temperatuuril 420 ^{o}C. Kirjeldatud käsitlusega CdTe kiled lõõmutati mitmeastmeliselt vesinikus, vaakumis ja suletud kvartsampullides. Plasmonmõju jälgimiseks inkorporeeriti spin-katmise, katoodpihustamise ja pihustus-pürolüüsi meetoditel töötlemata CdTe õhukestesse kiledesse Au nanoosakesed. CdTe õhukesi kilesid ja CdTe/CdS päikesepatareisid uuriti skaneeriva elektronmikroskoopia, röntgenmikroanalüüsi, röntgendifraktsiooni, fototoluminestsentsi, UV-Vis spektroskoopia ja Hall'i efekti meetoditel.

Valmistatud CdTe/CdS päikesepatareidel mõõdeti volt-amper sõltuvus ning väline kvantefektiivsus.

CdS/FTO/klaas alustele sadestatud CdTe kilede struktuursed ja morfoloogilised omadused sõltusid oluliselt aluse temperatuurist ning $CdCl_2$ aktivatsiooni protsessist. Aluse erinevatel temperatuuridel (250-500 °C) sadestatud CdTe terade suuruse ja kuju erinevusi selgitati idutsentrite moodustumise ning kasvu teooriatega. Järgnev $CdCl_2$ aktivatsioon põhjustas kile rekristallisatsiooni ja sõltumata aluse temperatuurist moodustusid suured ning ligikaudu võrdse läbimõõduga CdTe kristallid. Selles aktivatsiooni staadiumis tekkis CdTe/CdS piirpinnale $CdTe_{1-x}S_x$ sulam. Faaside segunemine oli intensiivsem madalatel aluspinnatemperatuuridel sadestatud CdTe kiledel, mistõttu vähenes CdS kile paksus. Vaatamata sellele, et lühilaineline kvantefektiivsus suurenes, põhjustas CdS kile paksuse ebaühtlane vähenemine paralleelsiirete moodustumist absorberi ja akna kontaktpindade vahel ning vähendas CdTe/CdS päikesepatarei jõudlust. Töös uuritud kilede parim konversiooniefektiivsus 11,6 % saavutati CdTe sadestusaluse kõrgetel temperatuuridel 400-500 °C. Päikesepatarei efektiivsuse langus sadestusaluse temperatuuri alanemisega kujunes antud töö võtmeküsimuseks suunates uurimused CdTe/CdS struktuuridelt CdTe kiledele.

Edasi uuriti süsteemselt klaasplaadile sadestatud ja $CdCl_2$ aktiveeritud CdTe kilede p-juhtivuse kujunemist järjestikuste vesinik- ja vaakumlõõmutuste ning suletud isotermiliste lõõmutuste toimel nii madalal 250 °C kui ka kõrgel temperatuuril 500 °C. $CdCl_2$ aktiveeritud CdTe kiledel oli suur takistus ja kõrge pime-valgus takistuse suhe. Nende kilede järjestikune termiline lõõmutamine vesinikus ja vaakumis suurendas takistust ning fotojuhtivust. Kilede isotermilisel lõõmutamisel kvartsampullides 600 °C juures vähenes pimetakistus järsult nelja suurusjärgu võrra. P-tüüpi laengukandjate tiheduseks saadi $\sim 10^{15}$ cm^{-3}. Röntgendifraktsiooni analüüsist saadud (111) põhipiigi nihkumine viitas CdTe kristallvõres toimuvatele muutustele. Elektrilised omadused korreleerusid hästi muutustega fotoluminestsents-spektrites, mis viitab tunnustatud teooriatele, et töötluste käigus võredefektide tihedus väheneb.

Kolmandas alapeatükis uuriti kulla nanoosakeste inkorporeerimise võimalusi CdTe kihti, et plasmoonilise resonantsefekti kaudu suurendada valguse absorbtsiooni õhukeses kiles. Vastavalt teoreetiliselt arvutatud mõõtudele tekitati pihustuspürolüüsi meetodil CdTe pinnale Au nanoosakesed. Samas tagas katoodpihustamise meetod puhtamad Au osakesed. Mõlema meetodi puhul oli osakeste kuju ja suuruse reguleerimiseks vajalikud kõrged temperatuurid, mille juures tekkivad intermetalsed ühendid AuCd, $AuTe_2$ ja $Au_{0.3}Te_{0.7}$, mis on kahjulikud päikesepatarei toimele. Au nanoosakestega plasmoonilise CdS/CdTe päikesepatarei väline kvantefektiivsus tõusis piirkonnas 600-840 nm, lühisvool J_{sc} ja efektiivsus suurenesid vastavalt 22,4 kuni 24 mA/cm^2 ja 8.3 % kuni 9 %.

Saadud tulemuste alusel väidame, et $CdCl_2$ aktivatsioonil õhu käes tekkis sula fluss, mis kiirendas tera kasvu rekristallisatsiooni ja paakumise kaudu ning faaside segunemist CdTe/CdS siirdel. Tera kasvuga kaasnes flussi komponentide inkorporeerumine kasvavasse CdTe kile kristallvõresse, mis toimus protsessi temperatuurile vastavas küllastuslikus kontsentratsioonis vedel-tahke vahelise tasakaalulise jaotuskoefitsiendi järgi. Legeerumise aste sõltus protsessi ajast, temperatuurist ja CdTe lähtetera suurusest, olles suurem peeneteralisemal lähtematerjalil. $CdCl_2$ aktiveeritud CdTe kilede optoelektroonsete omaduste muutumine termilisel lõõmutamisel oli seotud kloriidi eemaldumisega CdTe kristallvõrest nii H_2- kui ka vaakumlõõmutusel ja kloori homogeense jaotumisega läbi kile isotermilisel käsitlusel.

Käesoleva uurimistöö uudsus seisneb vedelfaasilise rekristallisatsiooni ja paakumise teooria rakendamisel CdTe kilede ja päikesepatareide sadestusjärgsel termilisel käsitlusel kulgevate füüsikalis-keemiliste protsesside selgitamiseks. Esmakordselt on loodud tervikpilt CdTe elektriliste, struktuursete ja optiliste omaduste kujunemise kohta $CdTe\text{-}CdCl_2{:}O_2$ protsessi käigus. Termilise lõõmutamise tingimuste kontrollimisega saavutati CdTe optoelektroonsete omaduste oluline paranemine. Esmakordselt demonstreerisime eksperimentaalselt et Au nanoosakeste sadestamisel CdTe absorbermaterjali peale suureneb CdTe/CdS päikesepatareides absorbtsioonivõime, lühisvool ja konversiooni efektiivsus.

REFERENCES

1. K. Lynn, T. Ablekim, S. Swain, Solar cells based on cadmium telluride with an open-circuit voltage greater than 1V, *SPIE Newsroom: Optics and photonics technical articles* (2016).
2. B.M. Başol, B. McCandless, Brief review of cadmium telluride-based photovoltaic technologies, *Journal of Photonics for Energy* **4** (2014) 040996-1.
3. Frauenhofer ISE Photovoltaics Report 2014, http://www.ise.fraunhofer.de/de/ downloads/pdffiles/aktuelles/photovoltaics-report-in-englischer-sprache.pdf, retrieved on 16.3.2015.
4. B.E. McCandless, J.R. Sites, Cadmium telluride solar cells, in Handbook of Photovoltaic Science and Engineering, A. Luque and S. Hegedus, Eds., West Sussex, England: John Wiley & Sons Ltd.; 2003, 617-662.
5. Y. Tyan, E. A. Perez-Albuerne, Efficient thin film CdS/CdTe solar cells. In: Proceedings 16th IEEE PVSC: 1982 Sept. 27-30, New York, USA.
6. B.M. Basol, High efficiency electroplated heterojunction solar cell, *J. Appl. Phys.* **55** (1984) 601-603.
7. M.A. Green, K. Emery, Y. Hishikawa, W. Warta, and E.D. Dunlop, Solar cell efficiency tables (version 47), *Prog. Photovolt. Res. Appl.* **24** (2016) 3-11.
8. J.M. Burst, J.N. Duenow, D.S. Albin, E.Colegrove, M.O. Reese, J.A. Aguiar, C.-S. Jiang, M.K. Patel, M.M. Al-Jassim, D. Kuciauskas, S. Swain, T. Ablekim, K.G. Lynn & W.K. Metzger, CdTe Solar Cells with Open-Circuit Voltage Breaking the 1 V Barrier, *Nat. Energy* **1** (2016) 16015.
9. J.J. Loferski, Theoretical Considerations Governing the Choice of the Optimum Semiconductor for Photovoltaic Solar Energy Conversion, *J. Appl. Phys.* **27** (1956) 777-784.
10. S.G. Kumar and K.S.R. Koteswara Rao, Physics and chemistry of CdTe/CdS thin film heterojunction photovoltaic devices: fundamental and critical aspects, *Energy Environ. Sci.* **7** (2014) 45-102.
11. B.E. McCandless, I. Youm, R.W. Birkmire, Optimization of Vapor Post Deposition Processing for Evaporated CdS/CdTe Solar Cells, *Prog. Photovoltaics* **7** (1999) 21-30.
12. H.R. Moutinho, R.G. Dhere, M.M. Al-Jassim, D.H. Levi, L.L. Kazmerski, Investigation of induced recrystallization and stress in close-spaced sublimated and radio-frequency magnetron sputtered CdTe thin films, *J. Vac. Sci. Technol.* **17** (1999) 1793-1798.
13. M. Terheggen, H. Heinrich, G. Kostorz, D. Baetzner, A. Romeo and A.N. Tiwari, Analysis of Bulk and Interface Phenomena in CdTe/CdS Thin-Film Solar Cells, *Interface Sci.* **12** (2004) 259-266.
14. K. Durose, P.R. Edwards and D.P. Halliday, Materials aspects of CdTe/CdS solar cells, *J. Cryst. Growth* **197** (1999) 733-742.

15. U. Jahn, T. Okamoto, A. Yamada and M. Konagai, Doping and intermixing in CdS/CdTe solar cells fabricated under different conditions, *J. Appl. Phys.* **90** (2001) 2553-2558.
16. Y. Marfaing, Fundamental studies on compensation mechanisms in II–VI compounds, *J. Cryst. Growth* **161** (1996) 205-213.
17. U.V. Desnica, Doping limits in II-VI compounds-challenges, problems and solutions, *Prog. Cryst. Growth and Charact.* **36** (1998) 291-357.
18. M. Terheggen, H. Heinrich, G. Kostorz, A. Romeo, D. Baetzner, A.N. Tiwari, A. Bosio, N. Romeo, Structural and chemical interface characterization of CdTe solar cells by transmission electron microscopy, *Thin Solid Films* **431-432** (2003) 262-266.
19. T.A. Gessert, M.J. Romero, C.L. Perkins, S.E. Asher, R. Matson, H. Moutinho, D. Rose, Microscopic analysis of residuals on polycrystalline CdTe following wet $CdCl_2$ treatment, *Mat. Res. Soc. Symp. Proc.* **668** (2001) H1.10.1-6.
20. K. Durose, M.A. Cousins, D.S. Boyle, J. Beier, D. Bonnet, Grain boundaries and impurities in CdTe/CdS solar cells, *Thin Solid Films* **403-404** (2002) 396-404.
21. S.P. Harvey, G. Teeter, H. Moutinho, M.M. Al-Jassim, Direct Evidence of Enhanced Chlorine Segregation at Grain Boundaries in Polycrystalline CdTe Thin Films via Three-Dimensional TOF SIMS Imaging, *Prog. Photovoltaics* **23** (2015) 838-846.
22. V. Valdna, p-type doping of CdTe, *Solid State Phenom.* **67-68** (1999) 309-314.
23. V. Valdna, J. Hiie and A. Gavrilov, Defects in Chlorine-doped CdTe Films, *Solid State Phenomena* **80-81** (2001) 155-162.
24. N. Spalatu, M. Krunks, J. Hiie, Structural and optoelectronic properties of $CdCl_2$ activated CdTe thin films modified by multiple thermal annealing, *Thin Solid Films* (2016) in Press.
25. V. Krishnakumar, A. Barati, H.J. Schimper, A. Klein, W. Jaegermann, A possible way to reduce absorber thickness in thin film CdTe solar cells, *Thin Solid Films* **535** (2013) 233-236.
26. N.R. Paudel, K.A. Wieland, and A.D. Compaan, Ultrathin CdS/CdTe solar cells by sputtering, *Sol. Energy Mater. Sol. Cells* **105** (2012) 109-112.
27. V.E. Ferry, M.A. Verschuuren, H.B.T. Li, E. Verhagen, R.J. Walters, R.E.I. Schropp, H.A. Atwater, A. Polman, Light trapping in ultrathin plasmonic solar cells, *Opt. Express* **18** (2010) A237-A245.
28. G. Yin, A. Steigert, P. Andrae, M. Goebelt, M. Latzel, P. Manley, I. Lauermann, S. Christiansen, M. Schmid, Integration of plasmonic Ag nanoparticles as a back reflector in ultra-thin Cu(In,Ga)Se_2 solar cells, *Applied Surface Science* **355** (2015) 800-804.
29. E. Kärber, A. Katerski, I.O. Acik, V. Mikli, A. Mere, I. Sildos, M. Krunks, Low-cost plasmonic solar cells prepared by chemical spray pyrolysis, *Beilstein J. Nanotechnol.* **5** (2014) 2398-2402.

30. A. Katerski, E. Kärber, I.O. Acik, L. Dolgov, A. Mere, I. Sildos, V. Mikli, M. Krunks, Modification of light absorption in thin $CuInS_2$ films by sprayed Au nanoparticles, *Nanoscale Research Letters* **9** (2014) 494.
31. Q. Gu, Plasmonic metallic nanostructures for efficient absorption enhancement in ultrathin CdTe-based photovoltaic cells *J. Phys. D Appl. Phys.* **43** (2010) 465101 1-5.
32. F. Blaabjerg and D.M. Ionel, Renewable Energy Devices and Systems-State-of-the-Art Technology, Research and Development, Challenges and Future Trends, *Electric Power Components and Systems*, **43** (2015) 1319-1328.
33. International Renewable Energy Agency (IRENA), Renewable Energy Technologies: Cost Analysis of Solar Photovoltaics, 1 (2012) 1-45, available at: www.irena.org/Publications.
34. EPIA, Global market outlook for photovoltaics 2014-2018, http://www.epia.org/fileadmin/user_upload/Publications/EPIA_Global_Market, Outlook_for_Photovoltaics_2014-2018_-_Medium_Res.pdf, retrieved on 16.3.2015.
35. GlobalData, Solar Photovoltaic (PV) Market, Update 2016 - Global Market Size, Market Share, Average Price, Regulations and Key Country Analysis to 2025, http://energy.globaldata.com.
36. K. Masuko, M. Shigematsu, T. Hashiguchi, D. Fujishima, M. Kai, N. Yoshimura, T. Yamaguchi, Y. Ichihashi, T. Mishima, N. Matsubara, T. Yamanishi, T. Takahama, M. Taguchi, E. Maruyama, and S. Okamoto, Achievement of More Than 25% Conversion Efficiency with Crystalline Silicon Heterojunction Solar Cell, *IEEE J. Photovoltaics* **4** (2014) 1433-1435.
37. D.D. Smith, P. Cousins, S. Westberg, R. De Jesus-Tabajonda, G. Aniero, and Y.-C. Shen, Toward the practical limits of silicon solar cells, *IEEE J. Photovoltaics* **6** (2014) 1465-1469.
38. C. Radue, E.E. van Dyk, A comparison of degradation in three amorphous silicon PV module technologies, *Solar Energy Materials & Solar Cells* **94** (2010) 617-622.
39. M. Powalla, B. Dimmler, Scaling up issues of CIGS solar cells, *Thin Solid Films* **361-362** (2000) 540-546.
40. R. Scheer, H.W. Schock, Chalcogenide Photovoltaics: Physics, Technologies, and Thin Film Devices. Weinheim, Germany: Wiley-VCH, 2011.
41. D.A. Cusano, CdTe solar cells and photovoltaic heterojunctions in II–VI compounds, *Solid State Electron.* **6** (1963) 217.
42. D. Bonnet, H. Rabenhorst, New results on the development of a thin-film p-CdTe-n-CdS heterojunction solar cell. In: Proceedings of the 9th IEEE Photovoltaic Specialist Conference: 1972, Silver Springs, USA.
43. P. Meyers, C. Liu, T. Frey, Heterojunction p-i-n photovoltaic cell, U.S. Patent 4710589 (1987).

44. J. Britt and C. Ferekides, Thin film CdS/CdTe solar cell with 15.8% efficiency, *J. Appl. Phys.* **62** (1993) 2851-2852.
45. X. Wu, R.G. Dhere, D.S. Albin, T.A. Gessert, C. DeHart, J.C. Keane, A. Duda, T.J. Coutts, S. Asher, D.H. Levi, H.R. Moutinho, Y. Yan, T. Moriarty, S. Johnston, K. Emery, and P. Sheldon, 16.5% efficient CdS/CdTe polycrystalline thin film solar cell. In: Proceedings of the 17th European PVSEC: 2001, October Munich, Germany.
46. J.F. Jordan, Photovoltaic cell and method, U.S. Patent 5261968 (1993).
47. D. Rose, R. Powell, U. Jayamaha, M. Maltby, D. Giolando, A. McMaster, K. Kormanyos, G. Faykosh, J. Klopping, G. Dorer, R&D of CdTe-absorber photovoltaic cells, modules and manufacturing equipment: plan and progress to 100 MW/yr. In: Proceedings of the 28th IEEE PVSC: 2000, Sept. 15-22; New York, USA.
48. First Solar press release: First Solar marks new milestone with 10 gigawatts of installed PV capacity, http://investor.firstsolar.com/releasedetail.cfm?ReleaseID= 891800, 2015, retrieved on 17.03.15.
49. First Solar press release: First Solar Achieves world record 18.6 % thin film module convesion efficiency, http://investor.firstsolar.com/releasedetail.cfm?ReleaseID=917926, 2015, retrieved on 15.06.15.
50. L. Kranz, C. Gretener, J. Perrenoud, R. Schmitt, F. Pianezzi, F. Mattina, P. Blösch, E. Cheah, A. Chirilă, C.M. Fella, H. Hagendorfer, T. Jäger, S. Nishiwaki, A.R. Uhl, S. Buecheler and A.N. Tiwari, Doping of polycrystalline CdTe for high-efficiency solar cells on flexible metal foil, *Nature communications* **4** (2013) 1-7.
51. N.R. Paudel, Y. Yan, Fabrication and characterization of high-efficiency CdTe-based thin-film solar cells on commercial SnO_2:F-coated soda-lime glass substrates, *Thin Solid Films* **549** (2013) 74.
52. T. Liu, X. Zhang, J. Zhang, W. Wang, L. Feng, L. Wu, W. Li, G. Zeng, and B. Li, Interface study of ITO/ZnO and ITO/SnO_2 complex transparent conductive layers and their effect on CdTe solar cells, *Int. J. Photoenergy* **2013** (2013) 765938 1-8.
53. J. Perrenoud, L. Kranz, S. Buecheler, F. Pianezzi, A.N. Tiwari, The use of aluminium doped ZnO as transparent conductive oxide for CdS/CdTe solar cells, *Thin Solid Films* **519** (2011) 7444-7448.
54. X. Wu, High-efficiency polycrystalline CdTe thin-film solar cells, *Solar Energy* **77** (2004) 803-814.
55. A. Crossay, S. Buecheler, L. Kranz, J. Perrenoud, C.M. Fella, Y.E. Romanyuk, A.N. Tiwari, Spray-deposited Al-doped ZnO transparent contacts for CdTe solar cells, *Sol. Energy Mater. Sol. Cells* **101** (2012) 283.
56. D.H. Rose, F.S. Hasoon, R.G. Dhere, D.S. Albin, R.M. Ribelin, X.S. Li, Y. Mahathongdy, T.A. Gessert, P. Sheldon, Fabrication procedures and

process sensitivities for CdS/CdTe solar cells, *Prog. Photovolt.: Res. Appl.* **7** (1999) 331.

57. T. Takamoto, T. Agui, H. Kurita, M. Ohmori, Improved junction formation procedure for low temperature deposited CdS/CdTe solar cells, *Sol. Energy Mater. Sol. Cells* **49** (1997) 219.
58. T.M. Barnes, W.L. Rance, J.M. Burst, M.O. Reese, D.M. Meysing, C.A. Wolden, H. Mahabaduge, J. Li, J.D. Beach, T.A. Gessert, S.M. Garner, P. Cimo, W.K. Metzger, High-efficiency flexible CdTe superstrate devices. In: Proceedings of the 40th IEEE Photovolt. Specialists Conf.: 2014 June 8-13; Denver, Colorado.
59. Empa press release: Effizienz-Weltrekord für CdTe-Solarzellen dank farbloser Polyimidfolie, http://www.empa.ch/plugin/template/empa/*/108486, 2011, retrieved on 17.3.2015.
60. S. Adachi, Properties of group-IV, III-V and II-VI semiconductors, Chichester: John Wiley & Sons, Ltd; 2005.
61. S.A. Al Kuhaimi, Influence of preparation technique on the structural, optical and electrical properties of polycrystalline CdS films, *Vacuum* **51** (1998) 349-355.
62. P.J. George, A. Sanchez, P.K. Nair, M.T.S Nair, Doping of chemically deposited intrinsic CdS thin films to n type by thermal diffusion of indium *Appl. Phys. Lett.* **66** (1995) 3624-3626.
63. M.B. Ortuno-Lopez, M. Sotelo-Lerma, A. Mendoza-Galvan, R. Ramirez-Bon, Optical band gap tuning and study of strain in CdS thin films, *Vacuum* **76** (2004) 181-184.
64. J. Fritsche, D. Kraft, A. Thissen, T. Mayer, A. Klein, andW. Jaegermann, Band energy diagram of CdTe thin film solar cells, *Thin Solid Films* **403-404** (2002) 252.
65. T.L. Chu, S.S. Chu, C. Ferekides, C.Q. Wu, J. Britt, C. Wang, 13.4% efficient thin-film CdS/CdTe solar cells, *J. Appl. Phys.* **70** (1991) 7608.
66. A. Gupta, A.D. Compaan, All-sputtered 14% CdS/CdTe thin-film solar cell with ZnO:Al transparent conducting oxide, *Appl. Phys. Lett.* **85** (2004) 684.
67. A. Romeo, D.L. Bätzner, H. Zogg, A.N. Tiwari, Recrystallization in CdTe/CdS, *Thin Solid Films* **361-362** (2000) 420-425.
68. D. Bonnet, Manufacturing of CSS CdTe solar cells, *Thin Solid Films* **361** (2000) 547.
69. S.J.C. Irvine, V. Barrioz, D. Lamb, E.W. Jones, R.L. Rowlands-Jones, MOCVD of thin film photovoltaic solar cells - Next-generation production technology, *J. Cryst. Growth* **310** (2008) 5198.
70. M.R. Lorenz, Phase equilibria in the system Cd-Te, *J. Phys. Chem. Solids* **23** (1962) 939-947.
71. M. Aven, J. Prener, Physics and Chemistry of II-VI Compounds, New York: John Wiley and Sons, Ltd; 1967, 211-212.

72. M. Burgelman, Cadmium telluride thin films solar cells: characterization, fabrication and modelling. J. Poortmans, V. Arkhipov, editors. Thin film solar cells fabrication, characterization and applications, Chichester: John Wiley & Sons Ltd.; 2006, 277-314.
73. B. Basol, Processing high efficiency CdTe solar cells, *Int. J. Solar Energy* **12** (1992) 25-35.
74. B.M. Basol, Electrodeposited CdTe and HgCdTe solar cells, *Solar Cells* **23** (1988) 69.
75. C.S. Ferekides, D. Marinskiy, V. Viswanathan, B. Tetali, V. Palekis, P. Selvaraj, D.L. Morel, High efficiency CSS CdTe solar cells, *Thin Solid Films* **361-362** (2000) 520-526.
76. D. Bonnet, H. Richter, K. Jaeger, The CTS thin film solar module-closer to production. In: Proceedings of the 13th European Photovoltaic Solar Energy Conference: 1995 Oct 23-27; Bedford, England.
77. B.E. McCandles, L. Moulton, R. Birkmire, Recrystallisation and sulphur diffusion in $CdCl_2$-treated CdTe/CdS thin films, *Prog. Photovolt. Res. Appl.* **5** (1997) 249-260.
78. D.K. Koll, A.H. Taha, D.M. Giolando, Photochemical ''Self-healing'' pyrrole based treatment of CdS/CdTe photovoltaics, *Solar Energy Materials & Solar Cells* **95** (2011) 1716-1719.
79. T. Potlog, L. Ghimpu, P. Gashin, A. Pudov, T. Nagle, J. Sites, Influence of annealing in different chlorides on the photovoltaic parameters of CdS/CdTe solar cells, *Sol. Energy Mater. Sol. Cells* **80** (2003) 327-334.
80. N. Romeo, A. Bosio, V. Canevari, A new method to prepare efficient CdTe/CdS thin film solar cells. In: Proceedings of the 11th European Photovoltaic Solar Energy Conf.: 1992 Oct 12-16; Montreux, Switzerland.
81. A. Romeo, S. Buecheler, M. Giarola, M. Mariotto, A.N. Tiwari, N. Romeo, A. Bosio and S. Mazzamuto, Study of CSS- and HVE-CdTe by different recrystallization processes, *Thin Solid Films* **517** (2009) 2132-2135.
82. S. Mazzamuto, L. Vaillant, A. Bosio, N. Romeo, N. Armani, G. Salviati, A study of the CdTe treatment with a Freon gas such as CHF_2Cl, *Thin Solid Films* **516** (2008) 7079-7083.
83. Marc Köntges, Beleuchtungsabhängiger Ladungstransport durch tiefe kompensierende Störstellen in CdTe und Cu(In,Ga)Se_2-Solarzellen, PhD thesis, University of Oldenburg / IFSH (2002) (in German).
84. K. Nakamura, T. Fujihara, T. Toyama, H. Okamoto, Influence of $CdCl_2$ treatment on the structural and electrical properties of highly efficient 2-μm thick CdS/CdTe thin film solar cells, *Jpn. J. Appl. Phys.* **41** (2002) 4474-4480.
85. M.A. Cousins, K. Durose, Grain structure of CdTe in CSS-deposited CdTe/CdS solar cells, *Thin Solid Films* **361-362** (2000) 253-257.
86. B.E. McCandless, M.G. Engelmann, R.W. Birkmire, Interdiffusion of CdS/CdTe thin films: Modeling x-ray diffraction line profiles, *Journal of Applied Physics* **89** (2001) 988-994.

87. K. Ohata, J. Saraie, T. Tanaka, Phase diagram of the CdS-CdTe peudobinary system, *Jpn. J. Appl. Phys.* **12** (1973) 1198-1204.
88. B.E. McCandless, Thermochemical and Kinetic Aspects of Cadmium Telluride Solar Cell Processing, *Mat. Res. Soc. Symp. Proc.* **668** (2001) H1.6.1-H1.6.12.
89. J. Saraie, M. Kitagawa, M. Ishida, T. Tanaka, Liquid phase epitaxial growth of CdTe in the CdTe-$CdCl_2$ system, *Journal of Crystal Growth* **43** (1978) 13-16.
90. N. Romeo, A. Bosio, V. Canevari, A. Podestà, Recent progress on CdTe/CdS thin film solar cells, *Solar Energy* **77** (2004) 795-801.
91. J. Hiie, CdTe:$CdCl_2$:O_2 annealing process, *Thin Solid Films* **431-432** (2003) 90-93.
92. A. Kanevce, D.H. Levi, D. Kuciauskas, The role of drift, diffusion, and recombination in TRPL of CdTe solar cells determined through numerical simulation, *Prog. Photovolt: Res. Appl.* **22** (2014) 1138-1146.
93. M. Gloeckler, I. Sankin, Z. Zhao, CdTe solar cells at the threshold to 20% efficiency, *IEEE Journal of Photovoltaics* **3** (2013) 1389-1393.
94. A. Castaldini, A. Cavallini, B. Fraboni, P. Fernandez, J. Piqueras, Deep energy levels in CdTe and CdZnTe, *J. Appl. Phys.* **83** (1998) 2121-2126.
95. D Shaw, E Watson, The diffusion of chlorine in CdTe, *J. Phys. C: Solid State Phys.***17** (1984) 4945-4950.
96. B.K Meyer, D.M Hofmann, Anion and cation vacancies in CdTe, *Applied Physics Materials Science & Processing* **61** (1995) 213-215.
97. P. Nollet, M. Burgelman, S. Degrave, J. Beie, Importance of air ambient during $CdCl_2$ treatment of thin film CdTe solar cells studied through temperature dependent admittance spectroscopy. In: Proceedings of the 29th IEEE Photovoltaic Specialist Conference: 2002 May 19-24; New Orleans, Louisiana, USA.
98. Y.S. Tyan, Topics on thin film CdS/CdTe solar cells, *Solar Cells* **23** (1988) 19-29.
99. D.H. Rose, D.S. Albin, R.J. Matson, A.B. Swartzlander, X.S. Li, R.G. Dhere, S. Asher, F.S. Hasoon, P. Sheldon, Effects of oxygen during close-spaced sublimation of CdTe solar cells, *Mat. Res. Soc. Symp. Proc.* **426** (1996) 337.
100. D. S. Albin, S. H. Demtsu and T. J. McMahon, Film thickness and chemical processing effects on the stability of cadmium telluride solar cells, *Thin Solid Films* **515** (2006) 2659-2668.
101. H. Uda, S. Ikegami, H. Sonomura, Annealing effect of Cu_2Te Au contact to evaporated CdTe film on photovoltaic properties of CdS/CdTe solar cell, *Sol. Energy Mater. Sol. Cells* **50** (1998) 141-146.
102. A. Niemegeers, M. Burgelman, Effects of the Au/CdTe back contact on IV and CV characteristics of Au/CdTe/CdS/TCO solar cells, *J. Appl. Phys.* **81** (1997) 2881-2886.

103. X. Li, D.W. Niles, F.S. Hasoon, R.J. Matson, P. Sheldon, Effect of nitric-phosphoric acid etches on material properties and back-contact formation of CdTe-based solar cells, *J. Vac. Sci. Technol.* **17** (1999) 805-809.

104. B.H. Hamadani, J. Roller, P. Kounavis, N.B. Zhitenev, D.J. Gundlach, Modulated photocurrent spectroscopy of CdTe/CdS solar cells—equivalent circuit analysis, *Solar Energy Materials & Solar Cells* **116** (2013) 126-134.

105. B. Späth, J. Fritsche, F. Säuberlich, A. Klein, and W. Jaegermann, Studies of sputtered ZnTe films as interlayer for the CdTe thin film solar cell, *Thin Solid Films* **480-481** (2005) 204-207.

106. D.L. Bätzner, A. Romeo, M. Terheggen, M. Döbeli, H. Zogg, A.N. Tiwari, Stability aspects in CdTe/CdS solar cells, *Thin Solid Films* **451-452** (2004) 536.

107. N. Romeo, A. Bosio, S. Mazzamuto, A. Romeo, L. Vaillant-Roca, High efficiency CdTe/CdS thin film solar cells with a novel back contact. In: Proceedings of the 22nd Europ. Photovolt. Solar Energy Conf.: 2007 Sep 3-7; Milan, Italy.

108. H. Lin, W. Xia, H.N. Wu, C. Tang, CdS/CdTe solar cells with MoO_x as back contact buffers, *Appl. Phys. Lett.* **97** (2010) 123504.

109. K.J. Hsiao, J.R. Sites, Electron reflector to enhance photovoltaic efficiency: application to thin film CdTe solar cells, *Prog. Photovolt.: Res. Appl.* **20** (2012) 486-489.

110. H. Atwater, A. Polman, Plasmonics for improved photovoltaic devices. *Nat. Mater.* **9** (2010) 205-213.

111. T. Repän, S. Pikker, L. Dolgov, A. Loot, J. Hiie, M. Krunks, I. Sildos, Increased Efficiency inside the CdTe Solar Cell Absorber Caused by Plasmonic Metal Nanoparticles, *Energy Procedia* **44** (2014) 229-233.

112. T. Repän, L. Dolgov, A. Katerski, I. Oja Acik, E. Kärber, A. Mere, V. Mikli, M. Krunks, I. Sildos, $CuInS_2$ solar cell absorber plasmonically modified by gold nanoparticles, *Appl. Phys.* **117** (2014) 455-458.

113. J. Yang, J. You, C.-C. Chen, W.-C. Hsu, H.-R. Tan, X.W. Zhang, Z. Hong, Y. Yang, Plasmonic Polymer Tandem Solar Cell, *ACS Nano* **5** (2011) 6210-6217.

114. M.D. Brown, T. Suteewong, R.S.S Kumar, V. D'Innocenzo, A. Petrozza, M.M. Lee, U. Wiesner, H.J. Snaith, Plasmonic Dye-Sensitized Solar Cells Using Core−Shell Metal−Insulator Nanoparticles, *Nano Lett.* **11** (2011) 438-445.

115. A. Schaub, P. Slepička, I. Kašparkova, P. Malinsky, A. Mackova, V. Švorčik, Gold nanolayer and nanocluster coating induced by heat treatment and evaporation technique, *Nanoscale Res. Lett*. **8** (2013) 249.

116. I.O. Acik, L. Dolgov, M. Krunks, A. Mere, V. Mikli, S. Pikker, A. Loot, I. Sildos, Surface plasmon resonance caused by gold nanoparticles formed on sprayed TiO2 films, *Thin Solid Films* **533** (2014) 144-147.

117. M.S. El-Deab, T. Sotomura, T. Ohsaka, Oxygen reduction at Au nanoparticles electrodeposited on different carbon substrates, *Electrochim Acta* **52** (2006) 1792-1798.
118. J.D. Major, K. Durose, Early stage growth mechanisms of CdTe thin films deposited by close space sublimation for solar cells, *Solar Energy Materials & Solar Cells* **95** (2011) 3165-3170.
119. L. Eckertova, Physics of Thin Films, New York: Plenum Publishing Corporation; 1986, 96-142.
120. I. Petrova, P.B. Barna, L. Hultman, J.E. Greene, Microstructural evolution during film growth, *J. Vac. Sci. Technol.* **215** (2003) S117-S128.
121. M. Ohring, The Materials Science of Thin Films, London: Academic Press Ltd.; 1992, 195-247.
122. J.H. Lee, Y.-K. Park, K.-J. Yang, Effects of the Growth Temperature on the Properties of CdTe Thin Films for Solar Cell Applications, *Jpn. J. Appl. Phys.* **40** (2001) 6741.
123. S.N. Alamri, The growth of CdTe thin film by close space sublimation system, *Phys. Status Solidi* **200** (2003) 352-360.
124. V.D. Falcão, W.A. Pinheiro, C.L. Ferreira, L.R. de Oliveira Cruz, Influence of Deposition Parameters on the Properties of CdTe Films Deposited by Close Spaced Sublimation, *Mater. Res.* **9** (2006) 29-32.
125. J. Luschitz, B. Siepchen, J. Schaffner, K. Lakus-Wollny, G. Haindl, A. Klein, W. Jaegermann, CdTe thin film solar cells: interrelation of nucleation, structure and performance, *Thin Solid Films* **517** (2009) 2125.
126. V. Kosyak, A. Opanasyuk, P.M. Bukivskij, Yu.P. Gnatenko, Study of the structural and photoluminescence properties of CdTe polycrystalline films deposited by close spaced vacuum sublimation, *J. Cryst. Growth* **312** (2010) 1726.
127. M.B. Rigana, N. Madhusudhana Rao, S. Kaleemulla, M. Shobana, N. Sai Krishna, M. Kuppan, Effect of substrate temperature on structural and optical properties of nanocrystalline CdTe thin films deposited by electron beam evaporation, *J. Nano-Electron. Phys.* **5** (2013) 03019.
128. R.C. Rodríguez, P.B. Perez, D.P. Delgado, F.C. Briones, J.L. Peña, S diffusion at the CdTe/CdS interface grown by rf magnetron sputtering, *Materials Letters* **37** (1998) 281-284.
129. H. P. Klug, L. E. Alexander, X-Ray Diffraction Procedures for Polycrystalline and Amorphous Materials, New York: Wiley Ltd.; 1974, 562.
130. T.J. McMahon, A.L. Fahrenbruch, Insights into the nonideal behavior of CdS/CdTe solar cells. In: Conference Record of the 28th IEEE Photovoltaic Specialists Conference: 2000 Sep 15-22; Anchorage, USA.
131. R. Harjula, Theory of ion exchange. I.D. Wilson, E.R. Adlard, M. Cooke, C.F. Poole, editors. Encyclopedia of separation science, London: Academic Press 1st edition; 2000, 1651-1661.

132. Database of HSC Chemistry Ver. 6.0., Outoukumpu Research Oy, Pori, Finland.
133. B. Cordero, V. Gómez, A.E. Platero-Prats, M. Revés, J. Echeverría, E. Cremades, F. Barragán, S. Alvarez, Covalent Radii Revisited, *Dalton Trans.* (2008) 2832-2838.
134. V.V. Tetyorkin, A.V. Sukach, S.V. Stariy, V.A. Boiko, Photoluminescence studies of CdTe polycrystalline films, *J. Semicond. Phys. Quantum Electron. Optoelectron.* **15** (2012) 340.
135. D.P. Halliday, M.D.G. Potter, J.T. Mullins, A.W. Brinkman, Photoluminescence study of a bulk vapour grown CdTe crystal, *Journal of Crystal Growth* **220** (2000) 30-38.
136. T. Taguchi, C. Onodera, Shallow acceptor bound-excitons in CdTe Epitaxial layers on (100) GaAs, *Mat. Sci. Forum* **65** (1990) 235-240.
137. P.J. Dean, Photoluminescence as a diagnostic of semiconductors, *Prog. Crystal Growth Characterization Mater.* **5** (1982) 89-174.
138. S. Seto, A. Tanaka, Y. Masa, M. Kawashima, Chlorine-related photoluminescence lines in high-resistivity Cl-doped CdTe, *Journal of Crystal Growth* **117** (1992) 271-275.
139. H.S. Leipner, J. Schreiber, H. Uniewski, S. Hilderbrant, Dislocation luminescence in cadmium telluride, *Scanning Microscopy* **12** (1998) 149-160.
140. D.M. Hofmann, P. Omling, H.G. Grimmeiss, B.K. Meyer, K.W. Benz, D. Sinerius, Identification of the chlorine A center in CdTe, *Phys. Rev. B.* **45** (1992) 6247-6250.
141. H.Y. Shin, C.Y. Sun, Photoluminescence spectra of Cl-doped CdTe crystals, *Journal of Crystal Growth* **186** (1998) 354-361.
142. J. Krustok, V. Valdna, Deep center luminescence in p-type CdTe, *J. Appl. Phys.* **80** (1996) 1757-1762.
143. J. Hiie, V. Valdna, A. Taklaja, Modeling of Flux Composition for Thermal $CdCl_2$:O_2 Annealing of Polycrystalline CdTe, *Mat. Res. Soc. Symp. Proc.* **763** (2003) 1-6.
144. P. Ramamurthy, E.A. Secco, The CdO–$CdCl_2$ reaction studied by thermal analysis and X-ray diffraction: X-ray diffractogram and infrared spectrum of $CdCl_2$•2CdO, *Can. J. Chem.* **47** (1969) 1045-1050.
145. V.N. Tomashik, V.I. Gritziff, Phase Diagrams of II–VI Semiconductor Compounds, Kiev: Naukova Dumka, 1982 (in Russian).
146. J.B. Lassiter, J. Aizpurua, L.I. Hernandez, D.W. Brandl, I. Romero, S. Lal, J.H. Hafner, P. Nordlander, N.J. Halas, Close encounters between two nanoshells, *Nano Lett.* **8** (2008) 1212-1218.
147. M. Hu, J. Chen, Z.-Y. Li, L. Au, G.V. Hartland, X. Li, M. Marquez, Y. Xia, Gold nanostructures: engineering their plasmonic properties for biomedical applications, *Chem. Soc. Rev.* **35** (2006) 1084-1094.
148. International Centre for Diffraction Data (ICDD), PDF-2 Release, 2008.

149. H. Okamoto, T.B. Massalski, Bull. Alloy Phase Diagrams 7 (52-53) (1986) 172-173.
150. U. Kreibig, M. Vollmer, Optical Properties of Metal Clusters, Springer, Berlin, 1995.
151. J. Wang, X.G. Lu, B. Sundman, X. Su, Thermodynamic reassessment of the Au–Te system, *J. Alloys Compd.* **407** (2006) 106-111.
152. A.D. Rakic, A.B. Djurisic, J.M. Elazar, M.L. Majewski, Optical properties of metallic films for vertical-cavity optoelectronic devices, *Appl. Opt.* **37** (1998) 5271-5283.
153. P. Hlidek, J. Bok, J. Franc, R. Grill, Refractive index of CdTe: spectral and temperature dependence, *J. Appl. Phys.* **90** (2001) 1672-1674.

APPENDIX A

PAPER I

N. Spalatu, J. Hiie, V. Valdna, M. Caraman, N. Maticiuc, V. Mikli, T. Potlog, M. Krunks, V. Lughi, Properties of the $CdCl_2$ air-annealed CSS CdTe thin films, Energy Procedia 44 (2014) 85-95.

Available online at www.sciencedirect.com

ScienceDirect

Energy Procedia 44 (2014) 85 – 95

Energy Procedia

E-MRS Spring Meeting 2013 Symposium D - Advanced Inorganic Materials and Structures for Photovoltaics, 27-31 May 2013, Strasbourg, France

Properties of the $CdCl_2$ air-annealed CSS CdTe thin films

Nicolae Spalatu[a]*,Jaan Hiie[b], Vello Valdna[b],Mihail Caraman[a], Natalia Maticiuc[b],
ValdekMikli[b], Tamara Potlog[a], Malle Krunks[b],Vanni Lughi[c]

[a]*Physics Department, Moldova State University, A. Mateevici str. 60, Chisinau MD 2009, Republic of Moldova*
[b]*Department of Materials Science, Tallinn University of Technology, Ehitajate tee 5, Tallinn 19086, Estonia*
[c]*Department of Industrial Engineering and Information Technology, University of Trieste, via Valerio 6a, Trieste,34127, Italy*

Abstract

Thin 7-9 μm CdTe films have been deposited on soda lime glass by close-spaced sublimation (CSS). By controlling the CSS temperature-time profile of source and substrate the pinhole-free CdTe films with a good adhesion on roughened glass were prepared. The classical solution-based $CdCl_2$ was applied to enhance the film crystallinity and optoelectronic properties of the CdTe layers. The layers were characterized by X-ray diffraction, Raman and Photoluminescence spectroscopy, scanning microscopy (SEM), energy dispersive X-ray microanalysis and Van der Paw method. $CdCl_2$ heat treatment is a key step in CdTe device processing. Howeverthe process leaves a significant amount of chlorine-rich residue on the CdTe surface that decreases performance of the solar cell.Annealing of the $CdCl_2$-treated polycrystalline CdTeimproves the optoelectronic properties and thus enhances the performance of CdTe/CdS solar cells. A correlation between the structural and optoelctronic properties of CdTe layers and annealing conditions in nitrogen atmosphere at 250, 400 and 450°C for 60 min of the $CdCl_2$treated layers has been found.

Selection and peer-review under responsibility of The European Materials Research Society (E-MRS)

*Keywords:*CdTe;thin films; $CdCl_2$ treatment; N_2 annealing;structural properties; optoelectronic properties; solar cell efficiency.

---

* Corresponding author. Tel.: +372-620-3366; fax: +372-620-2020.
*E-mail address:*nickspalatu@gmail.com

1876-6102
Selection and peer-review under responsibility of The European Materials Research Society (E-MRS)
doi:10.1016/j.egypro.2013.12.013

1. Introduction

At the present time the development of high-performance and low-cost solar cells for production of nonconventional energy sources based on the photovoltaic effect is an urgent scientific and technological problem [1].The CdTe polycrystalline films as an absorber layers are one of the most promising candidates for thin film solar cells due to its direct optical bandgap with energy of about E_g=1.5 eV and high absorption coefficient $>5\cdot10^5$/cm[2,3,4]. Therefore, more than 90% of the incident light is absorbed in a few micrometers of the material. In this case, it is possible to fabricate a complete photovoltaic device using only thin film technology.Record conversion efficiency of 17.3% was recently reported by First Solar for polycrystalline CdTe thin-film solar cell modules[5]. However, the theoretical estimations of possible photovoltaic solar energy conversion into electricity for CdTe are of about 29 % [6].

Because of its low sublimation temperature, CdTe polycrystalline films can be prepared by several techniques, such as thermal evaporation, electro deposition, sputtering, molecular beam deposition, hot-wall vacuum evaporation, close-spaced sublimation (CSS), etc. [1,7].The CSS technique is one of the various techniques that have produced encouraging results [1,7,8,9].During CdTe solar-cell fabrication, after deposition of the absorber layer of CdTe, a standard $CdCl_2$ heat treatment must be carried out in order to improve the cell performance [10,11]. The $CdCl_2$ heat treatment has been proved to be a key process step in the fabrication of highlyefficient CdTe cells.It was reported to be able to enhance CdTe grain growth, to reduce the defect density in the films, to promote the interdiffusion at the CdTe/CdS junction interface, to passivate grain boundaries, and thereby to improve solar-cell efficiency [12–15]. Unfortunately, the effect of grain boundaries and other structural defects on the device properties is not fully understood and the fundamental properties of the CdTe films are not well known [13,14]. $CdCl_2$ treatment also dopes CdTe with chlorine. Systematic studies should be carried out to understand the mechanism of $CdCl_2$ treatment on efficiency increase as well as the effect on the CdTe surface modification and micro-structural and electronic properties. The $CdCl_2$ heat treatment, which is usually carried out in the air atmosphere, is a process whichleaves a significant amount of chlorine-rich residue and enhances oxidation of the film surface. It was reported that the residual oxide phases and excess substitutional chlorine in CdTe layer increases the series resistance of the cell and decreases the hole concentration, and as a result, decreases the efficiency of solar cell [12-16].

The main objective of the work is to study structural, photoluminescence and electrical properties of the $CdCl_2$ doped CdTe polycrystalline films deposited by CSS in order to understand the nature and chemical composition of $CdCl_2$ heat-treatment products and interaction mechanism with solid CdTe. Also, the influence of annealing under nitrogen atmosphere upon the defect composition and resistivity of the doped with chlorine CdTe thin films.

2. Experimental details

CdTe films with a thickness of 5-7μm were prepared by CSS of 6N purity CdTe powder onto the roughened, degreased in K2Cr2O7 + 10-ml H2O + 100-ml H2SO4solution, at room temperature, rinsed in double-distilled water,driedand thermally etched 2×2 cm^2 glass substrates. Source material was heated in the graphite boat by a tungstencoils connected to the main power supply through temperature controller with K-type thermocouple. The substrate was fixed at a distance of 7mm from the source material, which also was heated by a similar system, while the(type K) thermocouple was placed above the substrate. The source temperature was kept at 610^{o}C, while substrate temperatures of 450^{o}C and 500^{o}C were applied for deposition of corresponding samples. The pressure during deposition was below $2\cdot10^6$Torr. The deposition time of each film was 5 min, after which the source and substrate heaters were switched off. The chamber was opened after the temperature fell below 50^{o}C.

After the deposition of CdTe layers,the samples were soaked in a saturated $CdCl_2$ solutions for 3-4 hours, followed by a 30 min heat treatment in air at 400±5^{o}C and etched in NP (H_3PO_4:HNO_3:H2O) to remove the oxide residues. Heat treatments of the samples were carried out in a two-zone tube furnace. The $CdCl_2$treated layers were annealed in nitrogen atmosphere at 250, 400 and 450^{o}C for 60 min.

The structure of the films was studied by XRD usinga Rigaku X-ray diffractometer with Cu $K\alpha_1$/40kV/40mA radiation source (λ=1.54056 Å) and their microstructure waschecked with scanning electron microscope (SEM). The X-ray diffraction (XRD) analysis was performed using Rigaku software PDXL.Photoluminescence and Raman measurements were performed at room temperature with high resolution micro-Raman spectrometer

Horiba JobinYvon HR800, equipped with multichannel CCD detection system in backscattering configuration. The incident Nd-YAG laser light with λ=532 nm and spot size of 10 μm in diameter, was used for excitation.The resistivity measurements were performed by Van der Paw method using indium electrodes.

3. Experimental results and discussions

In Fig.1.for all as deposited samples, the XRD spectra showed a strong preferentially (111) texture orientation together with the low intensity peaks, which correspond to the diffraction from the (220), (311), (400), (331), (422), and (551) planes of the cubic phase, respectively. The as-deposited CdTe at substrate temperature of 450°C exhibits a strong (111) preferred orientation, however the intensities of the (220), (311),..,(511) peaks are slightly lower than the intensity of the (111) peak. With increase in the substrate temperature the preference for the (111) orientation is decreased, as is shown for as-deposited layer grown at 500°C, but the intensities of the (220) and (311) are up to 40% of the (111) intensity (higher as compared with sample grown at 450°C). This suggests that at higher substrate temperatures is ensured better growth of a dense structure, thus the films grow both in a perpendicular, as well as in lateral directions.

In both cases, at moderate and higher substrate temperature, after $CdCl_2$ treatment, air annealing at 400°C and NP(H_3PO_4:HNO_3:H2O) etching (Fig.1. b) the loss in thepreferentially (111) texture orientation is slightly enhanced, while the intensities of the (220) and (311) peaks are increased significantly. This observation is in good accordance with some reports about decrease of the (111) peaks after the $CdCl_2$ treatment and air annealing, which depends on the annealing temperature and the amount of $CdCl_2$[17,18]. This may be an indication of change in stoichiometry and a certain degree of randomization in the film texture with annealing depending on the character of the substrates used. It is known that the crystallographic rearrangements are related to the stress in the films and to application of annealing at 400°C and on the $CdCl_2$ sintering flux. The creation of new grains as a result of a disintegration of some large grains is due to the relaxation of the excessive strains in the lattice. The coalescence of small grains into bigger ones is caused by the $CdCl_2$annealing process [24]. In order to study the stress in CdTe films, the XRD measurements were analysedusing Rigaku software PDXL. The (111) peak positions for both as deposited films and the films annealed at 400°C are at $2\theta = 23.73°$ and 23.74°,respectively corresponding to lattice parameter values of 6.49 Å and 6.48Å, therefore the as-deposited layers have a slightly higher lattice constant compared to the recrystallized layers. A.Romeo, A.N. Tiwariet al. suggestedthat this effect is due to the fact ofthe relaxation of the compressive stress which is generatedby the lattice and thermal mismatch between the CdTe andthe underlying substrate[18, 21].

One main observation in Fig. 1.is that when coated and soaked with a $CdCl_2$ layer,the CdTe film showed a set of peaks corresponding to different phases of $CdCl_2$, $CdCl_2{\cdot}H_2O$, $CdTeO_3$, $Cd_2(OH)_3Cl$, however after $CdCl_2$ heat treatment in air at 400°C and etching , the CdTe film showed a much stronger oxidation, as can be seen by the comparative XRD intensity shown in Fig. 1(d, e).The main oxidesformed were $CdTeO_3$,TeO_2, CdOand Te_2O_5. The dominant oxides were $CdTeO_3$ and TeO_2. The changes of the peak intensities and the emergence of these phases agrees well with those observed in other published works[19,20,18]. From the analysis of XRD spectra we can see that for both substrate temperatures, after coating and soaking with $CdCl_2$, the films were not oxidized, or the amount of oxides formed was not large enough to be detected by using XRD scattering technique.After $CdCl_2$heat treatment in air at 400°C, the diffraction patternindicates the presence of much more intensive oxide peaks. Supposedly oxides may be formed around and above a temperature of 400°C at the CdTe surface.

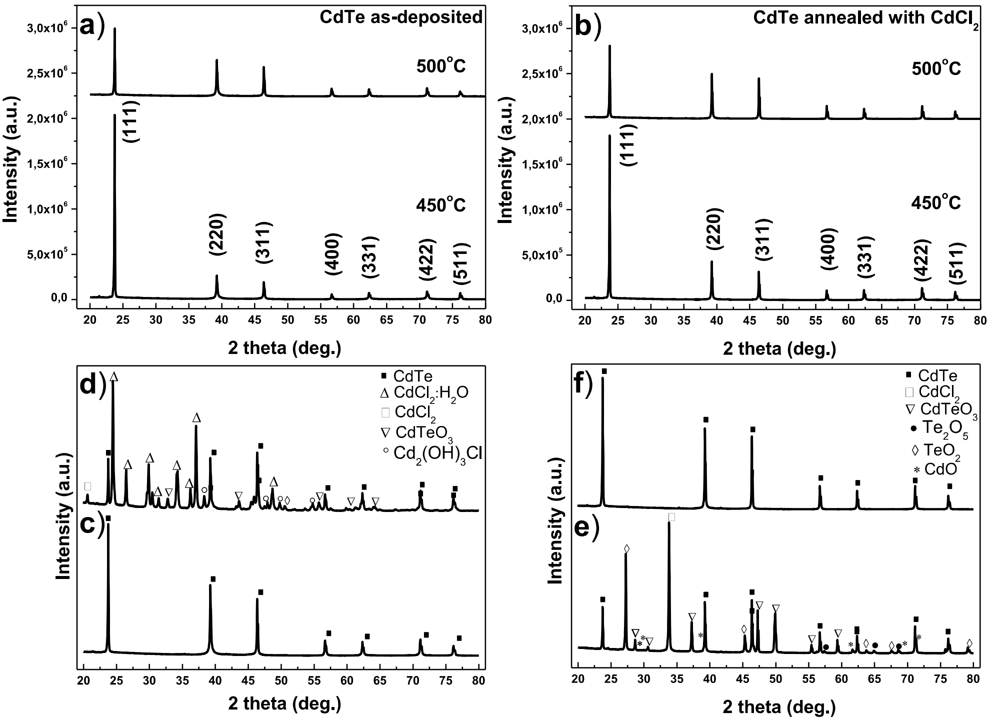

Fig. 1 (a) and (b) X-ray diffraction of CdTe films obtained at two different substrate temperatures, before and after annealing in presence of $CdCl_2$; (d) Detailed X-ray diffraction peaks of the CdTe film after soaking in $CdCl_2$ solution; (e) and (f) After $CdCl_2$ heat treatment in air at 400°C and etching in NP ($HNO_3 + H_3PO_4 + H_2O$) solution.

The surface morphology of the as-deposited, heat-treated and $CdCl_2$-treated samples is shown in Fig. 2. SEM investigation of two kinds of CdTe samples deposited at a substrate temperature of 450 and 500°C (a, c) shows that the films have a columnar-like structure with clear growth texture, without cracks or pinholes, implying the quality of the films. The cross-sectional images for both kinds of growing at 450 and 500°C after $CdCl_2$ heat treatment are shown in fig. 2 (b, d). The diameter of columnar-like cristallites strongly depends on the growth condition (substrate temperature -T_s, evaporator temperature -T_e, $\Delta T = T_e - T_s$). Grain size of grow samples depends on grain size of the substrate inversely proportional. The columnar-like structure was most pronounced in the films obtained at the growth conditions near the thermodynamic equilibrium (Ts=500°C, ΔT=100°C). In this case, the film has practically a monoblok structure along the layer thickness, and the grain size is about of 4-5 µm. After the $CdCl_2$ heat treatment (b,d), the overall surface morphology of the CdTe films did not change significantly, however some definite trend in terms of the changes in the shape and size of the CdTe grains were observed. The $CdCl_2$ treatment as a process with formation of a liquid flux, re-crystallizes the CdTe layers in such a way that some of the small grains coalesce into bigger toghether while some of the bigger grains divide into smaller ones and reorient themselves, which gives an entirely different microstructure. Smaller grains are more active and have higher solubility in the melted flux contributing to stronger mass transport. The process is characteristic for the sintering in the presence of liquid phase. The SEM images support the XRD results.

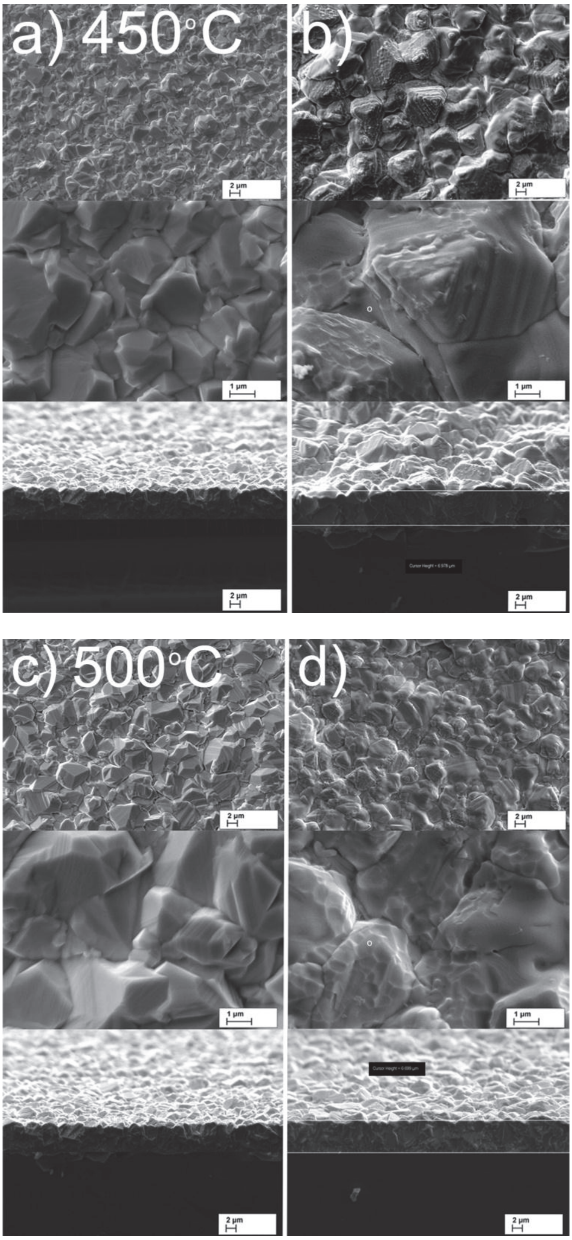

Fig. 2 (a, c) SEM surface morphology and cross-sectional microstructure of CdTe films deposited at a temperatures of 450 and 500°C respectively, without a $CdCl_2$ heat treatment; (b,d) SEM surface morphology and cross-sectional microstructure of CdTe films, after $CdCl_2$ heat treatment and eaching.

Effects of the heat treatment steps on the morphology of CdTe film also were investigated by the more sensitive Raman scattering. Fig. 3 (a) and (b) show the surface Raman scatterings of CdTe layers (1) as-deposited on the heated substrate at 450 and 500°C, (2) treated with $CdCl_2$, (3) treated with $CdCl_2$ and annealed in air at 400°C for 30 min and (4) eched in NP(HNO_3 + H_3PO_4 + H_2O)solution respectively. The as-deposited films at a both substrate temperatures of 400 and 500°C have a relatively stronger peaks at 125, 141 and 167 cm^{-1}which according to some authors [O. R. Ochoa et. al.],correspond to the scatering of Te, Te/CdTe and CdTe LO (Longitudinal optical mode) respectively. LO and TO Raman peaks of bulk CdTe are found at 169 and 141 cm^{-1} [28]. The Te detected by the sensitive Raman scattering exists as precipitates in CdTe, which were formed by aggregation of the Te_2 molecules during the CdTe film deposition. Te precipitates exist as nanocrystallites in a random distribution in CdTeand they have at least two orders of magnitude larger scattering cross-section compared to that of CdTe[16,22,27]. So the high Raman intensity of Te compared to that of CdTe shown in Fig. 3 does not mean a comparable material content for Te and CdTe in the films.

Raman scattering of the $CdCl_2$ treated CdTe films (curves 2 and 3) showed a stronger $CdCl_2$ Raman peaks at 220 and 231 cm^{-1} together with slightly lower intensity peaks of Te and CdTe, implying that the layers were dip-coated with a $CdCl_2$ saturated solution.

After $CdCl_2$ heat treatment and etching (curves 4), the intensity of the TeRaman peak at 125 slightly increased, higher as compared to the as-deposited layer, however the LOCdTe Raman peak positions and linewidths show no definite trend in terms of the $CdCl_2$heat treatment.Increases in the intensity of the mode observed for Te at 125 cm^{-1} suggests that NP etch creates Te excess on the CdTe surface and therefore is detected by Raman.

The effect of the $CdCl_2$ annealing process on the structural properties of CdTe films is to promote re-cristallization, which is obviousthe results of XRD and SEM of the sample; as a result the morphology of theCdTe is strongly affected. Moreover, the results of XRD show that the crystallization and morphology of the CdTe is strongly affected not only by the $CdCl_2$ treatment, but also by the condensation temperature on the substrate.

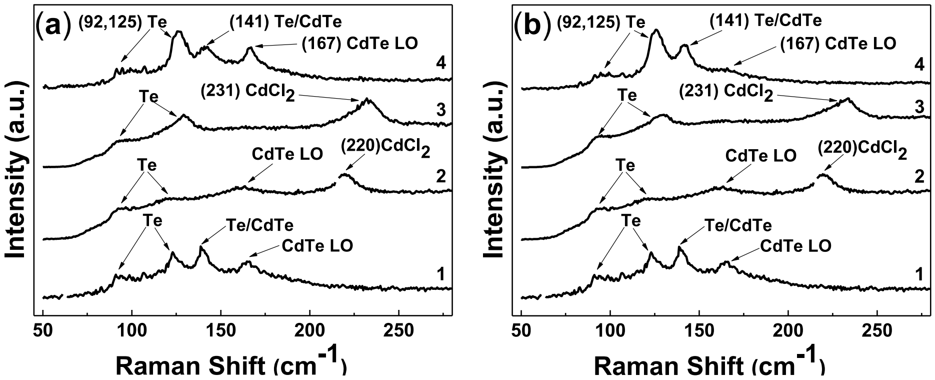

Fig. 3 (a) and (b) Raman spectra of the CdTe films recorded at room temperature for the samples obtained at the substrate temperatures of 450 and 500°C: (1) as-deposited on the heated substrate at 450 and 500°C, (2) treated with $CdCl_2$, (3) treated with $CdCl_2$ and annealed in air at 400°C for 30 min and (4) eched in NP(HNO_3 + H_3PO_4 + H_2O) solution respectively.

One of the most important effects is that the presence of the $CdCl_2$ treatment as a process with formation of liquid flux and to hire the rules of liquid phase recrystallization, dopes CdTe with chlorine, but leaves a significant amount of chlorine-rich residue and enhances the film surface oxidation[13-15]. It is known that the low resistance p-type conductivity in CdTe can be attributed to the low concentration of chlorine (10^{16}- 10^{18} at/cm^3) in the CdTe lattice [12,29]. The NP(HNO_3:H_3PO_4:H_2O)solutionremoves flux residue and chlorine from the surface. It is clear,that not before full removal of the residues the concentrations of the chlorine in the telluride lattice can bedecreased and regulated. Even in the case of NP(HNO_3:H_3PO_4:H_2O)solution etch removes all detectable traces of chlorine from the surface, solution etch will not be able to remove the traces from the grain-boundaries[12].Excess substitutional chlorine increases photoconductivity and decreases *p*-type conductivity of CdTe [13]. Vacuum annealing removes flux residue and decreases the chlorine concentration, implying the changes in the optoelectronic properties[13,14]. Taking into account these and based on the experiments presented above, the following steps have been focused on the investigation of changes in the optoelectronic properties as a result of annealing in nitrogen atmosphere. Figure 4 shows the photoluminescence spectra of $CdCl_2$ doped CdTe films, annealed at different temperatures under nitrogen atmosphere. The doping information, thermal treatments and resistivity of samples are summarized in table 1. The sheet resistance at room temperature for the as-grown sample is ~10^{11} ohm per sq. while it has been decreased to ~10^8 ohm per sq. in the $CdCl_2$-treated samples. In general, as-deposited CdTe films fabricated by various techniques have high electrical resistivity ($10^7$to 10^9 Ω·cm). Table 1 shows resistivity value versus annealing at different temperatures under nitrogen atmosphere of samples after recrystallization. The optimal annealing temperature at our preparative conditions, where the resistivity has the smallest value, is around 450°C. As can be seen from fig. 4 a) and table 1, after $CdCl_2$ heat treatment, the samples have an intense 1.5 eV PL band, whereas the resisitivity and dark to light resistance ratio K_F have quite high values. This can be explained by the fact that $CdCl_2$ heat treatment leaves too high chlorine concentration in CdTe lattice, which generates a high concentration of the isoelectronic complexes $V_{Cd}2Cl_{Te}$andTe_i2ClTe[13]. As a result, the resistivity of CdTe increases but not yet photoconductivity is formed. Thus, the higher is the *p*-type resistivity of the film the stronger is the intensity of the 1.5 eV PL band.

Table 1: Thermal treatment and resistivity values of CdTe samples*

Sample No.	$T_{substrate}$	d (μm)	Dopant	$CdCl_2$ thermal treatment T_rx t_r (°C x h)	Annealed in Nitrogen atm. T_a x t_a (°C x h)	R_{dark} Ω/□	R_{light} Ω/□	ρ_{dark} (Ω*cm)	K_F
S1	450	7	CdCl2	400 x 0,5	--	$2*10^8$	$2*10^7$	$1.4*10^5$	10
					250 x 1	$5*10^8$	$4*10^7$	$3.5*10^5$	12.5
					400 x 1	$7*10^7$	$1.5*10^7$	$4.9*10^4$	4.6
					450 x 1	$7*10^7$	$2*10^7$	$7*10^4$	3.5
S2	500	7	CdCl2	400 x 0,5	--	$2.5*10^8$	$3*10^7$	$1.7*10^5$	8
					250 x 1	$7*10^8$	$6*10^7$	$4.9*10^5$	11.6
					400 x 1	$3*10^7$	$1*10^7$	$2.1*10^4$	3
					450 x 1	$2*10^7$	$1*10^7$	$1.4*10^4$	2

* d is thickness of CdTe films, μm; T_r and t_r are recrystallization temperature and time respectively; $T_a$and t_a are temperature and time of annealing in nitrogen atmosphere; R_{dark} is dark resistance;$R_{light}$is light resistance; K_F is dark to light resistance ratio; ρ is resistivity.

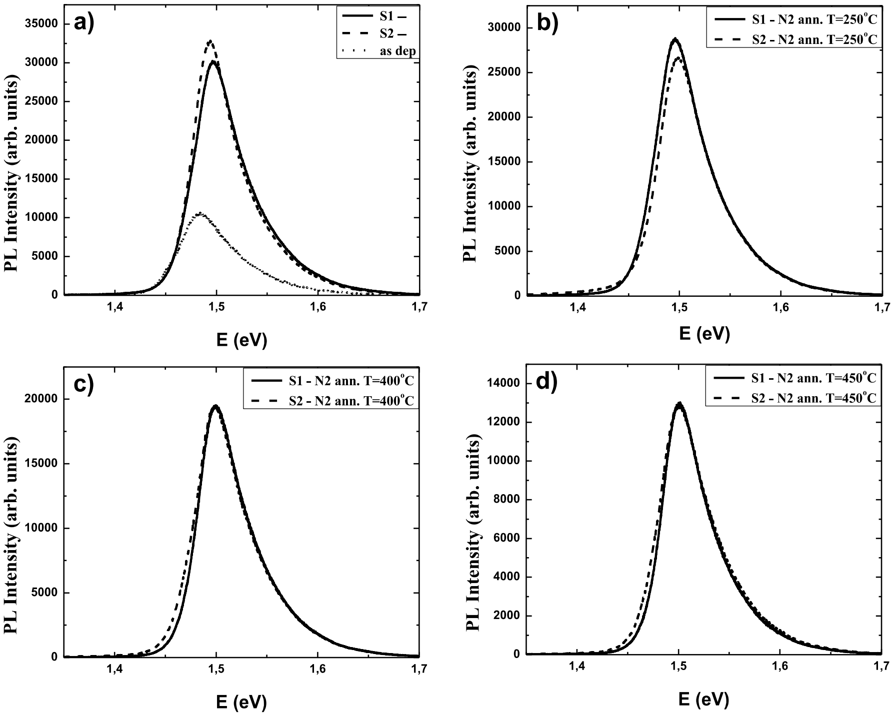

Fig. 4 Photoluminiscence spectra of $CdCl_2$ doped CdTe films recorded at room temperature for samples obtained at two different substrate temperatures Ts, and annealed at different temperatures under nitrogen atmosphere.

At small chlorine concentrations mainly complexes $V_{Cd}Cl_{Te}$and Te_iCl_{Te} are formed in CdTe and these complexes are shallow acceptors in CdTe and cause high *p*-type conductivity of CdTe at 300 K [13]. Figure 4 b) shows the photoluminescence spectra of chlorine doped CdTe thin films and annealed under nitrogen atmosphere at temperature of 250°C. It can be observed, that the annealing in nitrogen atmosphere at 250°C slightly decreases the intensity of the 1.5 eV PL band and resistivity of films implying that the process of outdiffusion of chlorine has been started. Further annealing under nitrogen atmosphere at higher temperatures of 400 and 450°C show definite trend in terms of the decreasing of 1.5 eV PL band and resistivity values, that one can attribute to more intensive process of outdiffusion of chlorine and generation of more cadmium vacancies due to a higher partial vapor pressure and mobility of cadmium [14]. As a results decreases the concentration of chlorine-based neutral complexes and increases the concentration of A-centers. The main defects which form the 1.5 eV PL band here are substitutional chlorine Cl_{Te}^{+} (donor) and complex $V_{Cd}Cl_{Te}^{-}$(acceptor). If chlorine concentration is decreased first decreases the concentration of Cl_{Te}, and as a result, the intensity of the 1.5 eV PL band and resistivity of films. Cl_{Te}seems to be a main hole trap in doped with chlorine *p*-type CdTe. One order of magnitude conductivity may be correspond to the corresponding increase in the concentration of charge carriers.

4. Conclusions

The effect of the $CdCl_2$immersion and heating on the structural properties of polycrystalline CdTe films is to promote re-crystallization, which is obvious by the results of XRD and SEM of the samples; as a result the morphology of the CdTe is strongly affected. The crystallization and morphology of the CdTe polycrystalline thin films are strongly affected not only by the $CdCl_2$ treatment but also by the condensation temperature on the substrate.

The experimental results presented by Raman and XRD, showed that the presence of $CdCl_2$ enhanced the film surface oxidation during the annealing process in the air atmosphere. Also, Raman scattering show that Te exists as precipitates in CdTe, and $CdCl_2$ heat treatment enhanced these precipitates in the films.

$CdCl_2$ heat treatment as a process with formation of a liquid flux and to hire the rules of liquid phase recrystallization, which betters the structure and increases conductivity, dopes CdTe with chlorine, but leaves too high chlorine concentration in CdTe. Excess substitutional chlorine increases the resistivity of films and the intensity of the 1.5 eV PL band of $CdCl_2$ doped films.

Annealing in nitrogen atmosphere removes flux residue and decreases the chlorine concentration, also decreases the resistivity of films and the intensity of the 1.5 eV PL band of $CdCl_2$ doped films. One order of magnitude conductivity may be correspond to the corresponding increase in the concentration of charge carriers and we believe it will promote to increase of CdTe solar cell efficiency. The experimental results reported in this study should help understand the mechanism of the key fabrication step, specifically the $CdCl_2$treatment, on the efficiency increase for a CdTe solar cell.

Acknowledgments

This work was supported by the target financing projects SF0140099s08 and SF0140092s08, by the European Union through the 7th FP project FLEXSOLCELL (GA-2008-230861), by the European Regional Development Fund (Centre of Excellence "Mesosystems: Theory and Applications", TK114), by Estonian Science Foundation Grant ETF9142 and by Estonian Ministry of Education and Research through the program AR10128 .

References

[1] Poortmans J, Arkhipov V. Thin Film Solar Cells: Fabrication, Characterization and Application, John Wiley & Sons, Chichester, (2006); 471.

[2] Horodyský P, Hlídek P. Free-exciton absorption in bulk CdTe: temperature dependence.*PhysStatus Solidi (b)*(2006);243:494.

[3]Fonthal G, Tirado-Mejía L, Marín-Hurtado JI, Ariza-Calderón H, Mendoza-Alvarez JG. Temperature dependence of the band gap energy of crystalline CdTe.*J. Phys. Chem. Solids* (2000);61: 579.

[4] EnloeWS, Parker JC.An electroreflectance study of CdTe.*J. Appl. Phys.* (1987);61:2005.

[5] U.S Department of Energy, Energy Efficiency & Renewable Energy 2010 Solar Technologies Market Report, Colden, CO http://www.nrel.gov/docs/fy12osti/51847.pdf(2011).

[6] Birkmire RW, Eser E.Polycrystalline thin film solar cells: Present Status and Future Potential. *Annu. Rev. Mater. Sci*. (1997);27:625.

[7] Abbas Shah N, Ali A, Ali Z, Maqsood A, AqiliAKS.Properties of Te-rich cadmium telluride thin films fabricated by closedspace sublimation technique. *J. Crystal Growth* (2005);284:477.

[8] Luschitz J, Siepchen B, Schaffner J, Lakus-Wollny K, Haindl G, Klein A, Jaegermann W.CdTe thin film solar cells: Interrelation of nucleation, structure, and performance. *Thin Solid Films* (2009);517:2125.

[9] Lee JH, Lim DG, Yi JS. *Sol. Energy Mat. Sol. Cells* (2003);75:235.

[10] McCandless BE, Hegedus SS, Birkmire RW, Cunningham D. Correlation of surface phases with electrical behavior in thin-film CdTedevices. *Thin Solid Films* (2003); 431:249.

[11] Wu X.High-efficiency polycrystalline CdTe thin-film solar cells.*Sol. Energy*(2004); 77:803.

[12] Hiie J.CdTe:CdCl :O annealing process.*Thin Solid Films* (2003);431-432:90-93.

[13] Valdna V. p-Type Doping of CdTe. *Solid State Phenomena*(1999);67-68:309-314.

[14] Valdna V, Hiie J, Gavrilov A. Defects in Chlorine-Doped CdTe Thin Films. *Solid State Phenomena*(2001); 80-81:155-162.

[15] Hiie J, Valdna V. Proceedings of the 17th European Photovoltaic Solar Energy Conference, 22–26 October, Munich, Germany, WIP, (2001); 1240.

[16] Bai Z, Yang J and Wang D.Thin film CdTe solar cells with an absorber layer thickness in micro- and sub-micrometer scale. *Appl. Phys. Lett.*(2011); 99:143502.

[17] RomeoA et al., Proc. 2nd World Conf. Exhibition Photovoltaic Solar Energy Conv., Vienna, Austria, July 1997.

[18] Romeo A, Batzner DL, Zogg H, Tiwari AN. Recrystallization in CdTe/CdS. *Thin Solid Films* (2000);361-362:420-425.

[20] Moutinho HR, Al-Jassim MM, Levi DH, Dippo PC, Kazmerski LL. Effects of $CdCl_2$ treatment on the recrystallization and electro-optical properties of CdTe thin films.*J. Vac. Sci.Technnol.*(1998); 16:1251-1257.

[19] Zelaya-Angel O, Picos-Vega A, Ramirez-Bon R, Espinoza-BeltranFJ.Thermophysical properties of materials and devices. *Vacuum* (1999); 52:99.

[21] Moutinho HR et al. Alternative procedure for the fabrication of close-spaced sublimated CdTe solar cells. *J. Vac. Sci. Technol*. (2000); A 18:1599-1603.

[22] Rodriguez ME, Zelaya-Angel O, Perez Bueno JJ, Jimenez-Sandoval S, Tirado L.Influence of Te inclusions and precipitates on the crystalline and thermal properties of CdTe single crystals. *J. Cryst.Growth* (2000); 213:259-266.

[23] Moutinho HR, Al-Jasim MM, Abufoltuh FA, Levi DH, Dippo PC, Dhere RG, Kazmerski LL. Studies of recrystallization of CdTe thin films after $CdCl_2$ treatment. IEEE 26th Photovoltaic Specialists Conference, 1997.

[24] Infante H, Gordillo G. Effect of the $CdCl_2$ Treatment on the Morphology and Structural Properties of CdTe Thin Films Deposited by the CSS Method. *Surf. Rev. Lett.* (2002); 9:1681.

[25] Shin SH, Bajaj J, Moudy LA and Cheung DT. Characterization of Te precipitates in CdTe crystals. *Appl.Phys. Lett*. (1983);43:68-70.

[26] Olego DJ, Raccah PR, Faurie JP.Compositional dependence of the Raman frequencies and line shapes of $Cd_{1-x}Zn_xTe$ determined with films grown by molecular-beam epitaxy. *Phys.Rev.*(1986);B 33(6):3819-3822.

[27] Ochoa OR, Witkowski III EJ, Colajacomo C.Raman characterization of CdTenanocrystallites embedded in a

glass matrix. *Journal of Materials Science Letters*(1997);16:613-616.

[28] Rowe JM, Nicklow RM, Price DL, Zanio K.Lattice dynamics of cadmium telluride.*Phys. Rev.*(1974);B 10(2):671-675.

[29] Shaw D, Watson E. The diffusion of chlorine in CdTe.*J.Phys.C: Solid State Phys.* (1984);17:4945.

PAPER II

N. Spalatu, J. Hiie, V. Mikli, M. Krunks, V. Valdna, N. Maticiuc, T. Raadik, M. Caraman, Effect of $CdCl_2$ annealing treatment on structural and optoelectronic properties of close spaced sublimation CdTe/CdS thin film solar cells vs deposition conditions, Thin Solid Films 582 (2015) 128-133.

Thin Solid Films 582 (2015) 128–133

Contents lists available at ScienceDirect

Thin Solid Films

journal homepage: www.elsevier.com/locate/tsf

Effect of $CdCl_2$ annealing treatment on structural and optoelectronic properties of close spaced sublimation CdTe/CdS thin film solar cells vs deposition conditions

N. Spalatu [a,*], J. Hiie [a], V. Mikli [a], M. Krunks [a], V. Valdna [a], N. Maticiuc [a], T. Raadik [a], M. Caraman [b]

[a] Department of Materials Science, Tallinn University of Technology, Ehitajate tee 5, 19086 Tallinn, Estonia
[b] Physics Department, Moldova State University, A. Mateevici str. 60, Chisinau MD 2009, Republic of Moldova

ARTICLE INFO

Available online 28 November 2014

Keywords:
Cadmium telluride
Thin films
Cadmium chloride treatment structural properties
Optoelectronic properties
Solar cells efficiency

ABSTRACT

CdTe/CdS thin films were deposited by close-spaced vacuum sublimation at substrate temperatures 250–500 °C. The effect of substrate temperature in conjunction with $CdCl_2$ heat treatment on the properties of CdTe/CdS thin films and devices is reported. X-ray diffraction measurements of structural properties of the films were carried out to study their phase composition and texture. Surface morphology, grain size and growth mechanism of the films were determined by the scanning electron microscopy. The photoluminescence measurements allowed us to establish the correlation between the point and extended defect structure on the one hand and the growth conditions on the other. The CdTe/CdS solar cells fabricated at high substrate temperature, exhibited improved electrical characteristics compared to cells fabricated at low substrate temperature, yielding a high efficiency.

1. Introduction

Polycrystalline thin-film CdTe has shown considerable promise for terrestrial photovoltaic applications due to its near-optimum bandgap, high absorption coeffcient and relative ease of film formation. Thin-film CdTe/CdS cells with effciencies greater than 10% have been demonstrated using CdTe deposited by a variety of techniques over a wide range of deposition temperatures [1–3]. Record conversion efficiency of 17.3% was recently reported by First Solar for polycrystalline CdTe thin-film solar cell modules [4]. However, the theoretical estimations of possible photovoltaic solar energy conversion into electricity for CdTe are of about 29% [5]. Because of its low sublimation temperature, CdTe polycrystalline films can be prepared by several techniques [6–9]. The closed-space sublimation technique (CSS) is one of the various techniques that have produced encouraging results. During CdTe solar-cell fabrication, after deposition of the absorber layer of CdTe, a standard $CdCl_2$ heat treatment must be carried out in order to improve the cell performance [10,11]. The $CdCl_2$ heat treatment has been proved to be a key process step in the fabrication of highly efficient CdTe cells. It was reported to be able to enhance CdTe grain growth, to reduce the defect density in the films, to promote the interdiffusion at the CdTe/CdS junction interface to passivate grain boundaries, and thereby to improve solar-cell efficiency [12–14]. Unfortunately, the effect of grain boundaries and other structural defects on the device properties is not fully understood and the fundamental properties of the CdTe films are not well known. Systematic studies should be carried out to understand the mechanism of $CdCl_2$ treatment on efficiency increase as well as the effect on the CdTe surface modification and micro-structural and electronic properties.

The main objective of the work is to study the effect of CSS deposition conditions on structural and optoelectronic properties of CdS/CdTe thin films and solar cells.

2. Experimental details

The devices were fabricated in a superstrate configuration by CSS on Corning 7059 glass coated with a 200 nm thick fluorine doped tin oxide layer (FTO). Films of CdS, 150–180 nm thick, were deposited at 400 °C from high-purity CdS powder. CdTe films with a thickness of 3–5 μm were deposited onto CdS layers from 99.999% purity CdTe powder. Source material was heated in the graphite boat by a tungsten coils connected to the main power supply through temperature controller with K-type thermocouple. The substrate was fixed at a distance of 7 mm from the source material, which also was heated by a similar system, while the type K thermocouple was placed above the substrate. The source temperature was kept at 610 °C, while substrate temperatures varied from 250 to 500 °C. The residual pressure during deposition was below 2×10^{-4} Pa. The deposition time of each film was 5 min, after which the source and substrate heaters were switched off. The chamber was opened after the temperature fell below 30 °C.

After deposition the CdTe/CdS/FTO/glass samples were soaked in a saturated $CdCl_2$ methanol solution (2.15 g/100 mL methanol), followed by a 30 min heat treatment in air at 420 °C in a two-zone tube furnace.

---

[*] Corresponding author: Tel.: +372 6203366; fax: +372 6202020.
E-mail address: nickspalatu@gmail.com (N. Spalatu).

http://dx.doi.org/10.1016/j.tsf.2014.11.066
0040-6090/

The heat treated samples were rinsed in deionized water and etched in standard NP (H3PO4:HNO3:H2O) solution to remove the $CdCl_2$ and oxide residues. To finish the cells, the Te/Au bi-layer back contact was deposited by thermal evaporation. Anhydrous, 99.99% $CdCl_2$ was supplied from Alfa Aesar.

The structure of the films was studied with Rigaku Ultima IV diffractometer (Cu Kα radiation, $\lambda = 1.5406$ Å, 40 kV at 40 mA; silicon strip detector D/teX Ultra, Rigaku, Japan) in the Bragg–Brentano (θ–2θ) geometry and their morphology was checked by a scanning electron microscope (SEM) Zeiss EVO-MA15 at a 10 kV operating voltage. The crystallite size and lattice parameters were calculated using the PDXL Version 1.4.0.3 software on the Rigaku system. Solar cells were characterized by current–voltage (*I*–*V*) and quantum efficiency (QE) measurements under simulated standard test conditions. *I*–*V* curves were measured at room temperature with illumination of 100 mW/cm^2 using the Oriel class A solar simulator 91159A. The quantum efficiency of the solar cells was measured in the range of 300–1000 nm on a Newport Oriel kit that uses 300 W Xe-lamp, high-resolution monochromator (Cornerstone 260), a digital dual-channel lock-in detector (Merlin), and a calibrated silicon reference detector. The Xe-lamp is a light source to simulate the conventional AM1.5 spectrum for testing of solar cells. The dispersed light from the Xe lamp, incident on the solar cell as monochromatic light was optically chopped at 30 Hz.

3. Results and discussion

3.1. SEM and X-ray diffraction studies

SEM investigation of the CdTe films deposited on CdS/FTO/glass at the different growth conditions shows that the shape and size of grains of the polycrystalline films greatly depend on the substrate temperature during deposition. The grain size was found to increase with the substrate temperature. The cross-sectional images of the CdTe films deposited on CdS/FTO/glass at the different growth conditions, before and after $CdCl_2$ heat treatment are shown in Fig. 1. It can be observed from Fig. 1(a) that the films deposited at the lowest substrate temperatures $T_s \leq 300$ °C exhibit a faceted and highly dispersed structure with average grain size about $d \leq 0.8$ μm. The orientation of crystallites is uniaxial. The increase of the substrate temperature, leads to an increase in grain size up to d ~ 2 μm at $T_s = 350$ °C and consequently a decrease in porosity. Further increase of the substrate temperature $T_s \geq 400$ °C, results in an increase in grain size up to 4 μm. Besides increasing the grain size, the increase in the substrate temperature decreases the density of voids and films had a close-packed morphology. Moreover, as can be clearly seen from SEM images the change of the thin film growth mechanism occurred at 300 and 350 °C. In this case, the films have a columnar-like structure with a clear growth texture. The columnar-like structure was most pronounced in the film obtained at 350 °C. The diameter of the columns strongly depends on the growth conditions (substrate temperature—T_s, evaporator temperature—T_e, $\Delta T = T_e - T_s$). These changes observed in growth mechanism might be induced by particular specific thermodynamic parameters during the CSS deposition and nucleation processes [15,16]. The films obtained at the growth conditions close to the thermodynamic equilibrium ($T_s = 450 - 500$ °C) have practically a monoblock structure along the layers thickness, without porosity or voids, indicating high packing density of the films. It should be mentioned that these results (SEM) are in good correlation with published results obtained at comparable temperature regimes by Luschitz et al. [17] as well as Kosyak et al. [18]. Thus, for CSS CdTe films prepared at different substrate temperatures, Luschitz et al. found three different growth regimes where in the first regime (up to 320 °C) the grains grow as columnar extended grains, in the second regime (above 370 °C) the grains are considerably larger and have lost the columnar morphology, and in the high temperature growth regime the grains seem to be rather compact and dense, implying film quality. The same author highlights that the films formed at the transition regime (340 °C) seem to expose very promising film morphology. Kosyak et al. got SEM images which show a highly dispersed structure for films obtained at $T_s \leq 200$ °C and columnar-type growing for $T_s \geq 350$ °C. It is reasonable to say that an

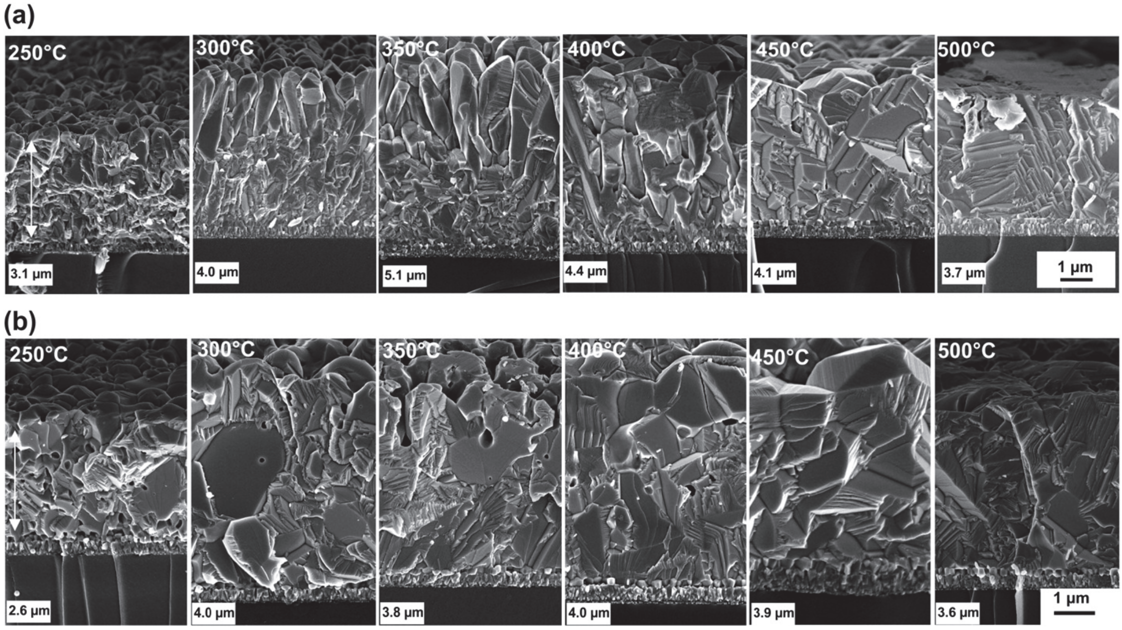

Fig. 1. SEM surface morphology and cross-sectional microstructure of CdTe/CdS thin films deposited at different substrate temperatures, (a) before and (b) after $CdCl_2$ heat treatment.

overview of the results that were achieved by both author as well our results describe the same pattern of three different growth regimes in which the changes in structure and morphology to electrical properties of solar cells have been produced from the different films. It should be noted that the formed structure and growth regimes depend also on the CdTe deposition, configuration and geometrical parameters of CSS system; therefore this might to be an important aspect which can explain the difference between the results.

After $CdCl_2$ treatment, the film surface consisted of rounded grains with penetrating boundaries. A subsequent $CdCl_2$ heat treatment further increased the grain size, resulting in planar surface morphology and lateral grain size of ~5 μm, suggesting dramatic reduction of the grain boundary density. The cross-sectional images of the $CdCl_2$ treated film deposited at 250 °C (Fig. 1(b)) show that the film has high inner porosity and density of voids, with large grain size (larger as compared to the film deposited at 250 °C). Furthermore, the cross-sectional images of the films grown at 300 and 350 °C and treated in $CdCl_2$ changed dramatically (Fig. 1, b). Thus, the columnar-like structure disappears for films deposited at 300–350 °C after $CdCl_2$ treatment; nevertheless a 1 μm thick surface layer has large porosity. A subsequent $CdCl_2$ heat treatment of the films grown at substrate temperature $T_s \geq 400$ °C promoted formation of a block structure with extra-large grain size without pores and voids, implying good crystalline quality of the films.

X-ray diffraction patterns (XRD) of the CdTe films deposited at the different growth conditions, before and after $CdCl_2$ heat treatment, are presented in Fig. 2 (a, b). X-ray diffractograms show the peaks from (111), (220), (311), (400), (331), (422), and (551) planes of the cubic phase. It is observed that the films obtained at the substrate temperatures 250, 300 and 350 °C exhibits a strong (111) preferred orientation of the crystallites along (111) plane parallel to the substrate. With an increase in the substrate temperature the preference for the (111) orientation is decreased, as is shown for films deposited at 400 °C, as the intensities of the (220) and (311) peaks are up to 40% of the (111) intensity (much higher as compared with films grown at low temperatures).

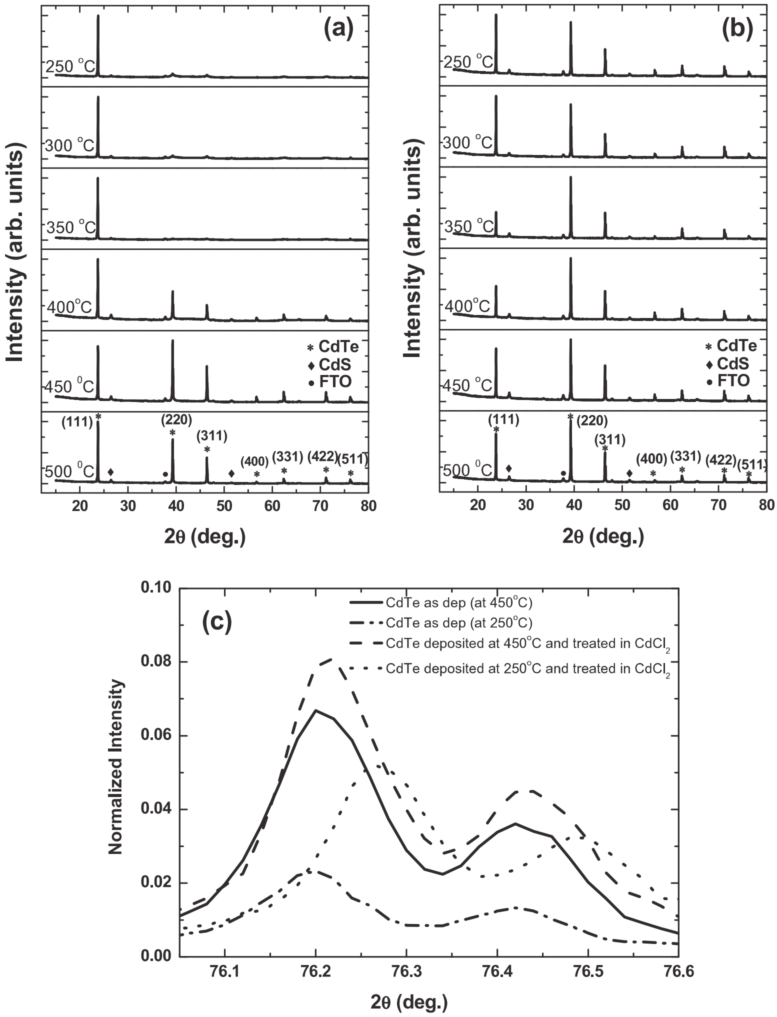

Fig. 2. XRD patterns of CdTe/CdS thin films deposited at the different substrate temperatures T_s, (a)—before and (b)—after $CdCl_2$ heat treatment. (c). High resolution (511) XRD profiles of CdTe/CdS thin films deposited at substrate temperatures 250 and 450 °C, before and after $CdCl_2$ heat treatment.

Furthermore, the intensities of (220) and (311) peaks strongly increase when the substrate temperature increases ($T_s > 400$ °C). This suggests that higher substrate temperature ensured better growth of a dense structure; thus the films grow both in a perpendicular, as well as in lateral directions. In both cases, at lower and higher substrate temperatures, after $CdCl_2$ treatment, air annealing at 420 °C and NP etching solution (Fig. 2, b) the preferential (111) orientation is decreased as the intensities of the (220) and (311) peaks are increased significantly. This observation is in good accordance with results reported in [19,20] about the decrease of the (111) peaks after the $CdCl_2$ treatment and air annealing, which depends on the annealing temperature and the amount of $CdCl_2$. After $CdCl_2$ heat treatment of the samples grown at 250 and 300 °C the intensities of the (220) and (311) peaks are slightly lower than the intensity of the (111) peak. However, for the $CdCl_2$ treated films grown at $T_s > 350$ °C, the intensity of the (111) peak is lower than that of the (220) peak, implying that the films are not (111) textured and has a predominance of the (220) orientation. These variations of the intensity of Bragg peaks suggest that $CdCl_2$ heat treatment, as a process with formation of liquid flux and to hire the rules of liquid phase recystallization, change dramaticly atomic arrangement and hence a certain degree of randomization in the CdTe film texture. The $CdCl_2$ treatment recrystallizes the CdTe layers in such a way that some of the small grains coalesce into bigger ones while some of the bigger grains divide into smaller ones and reorient themselves, which gives an entirely different microstructure [21]. The film deposited at the lowest substrate temperature exhibits a highly dispersed structure with smaller grains which are more active and have higher solubility in the melted flux, contributing to stronger mass transport. The process is characteristic for the sintering in the presence of liquid phase [22]. We consider that the structural changes in the $CdCl_2$ heat treatment process are very complex and we assume that this includes all the main steps of recrystallization, grain growth and sintering. The prevalence of one or another step depends on the proportion between solid and liquid flux phases. Due to high solubility of CdS and CdTe in $CdCl_2$ flux, in the first step of the process the main mechanism of grain growth is accomplished by recrystallization. Considering that annealing is carried out in air, due to evaporation of $CdCl_2$ the volume of liquid phase decreases which leads to the sintering of the grains and creation of good contact between them.

It is known that the crystallographic rearrangements are related to the stress in the films and to application of air annealing at 420 °C in the $CdCl_2$ sintering flux [23,24]. In order to study the stress and intermixing in CdTe films, the XRD measurements were analyzed by Rigaku software PDXL. Changes in the crystallite size and lattice parameter before and after $CdCl_2$ treatment are listed in Table 1. As given in Table 1, the lattice parameter of the CdTe films increased from 6.482 to 6.486 Å when the substrate temperature of the films increased from 250 °C to 500 °C. The increase in the lattice constant with the increase of substrate temperature may be due to development of internal stress in the film grains wihich triggers the prolongation [25]. Also, we got an increase in crystallite size from 131 to 936 Å for the change in the substrate temperature from 250 to 500 °C, which was calculated by using XRD diffractograms and Scherrer's formula. After $CdCl_2$ treatment the crystallite size increases considerably and has a similar value for all samples. It can be seen from Table 1, that the as deposited films grown at different substrate temperatures have a high in-plane lattice constant compared to the recrystallized films. Thus, the lattice parameter of as-deposited films decreses from 6.486 to 6.481 Å for the $CdCl_2$ treated films. A.Romeo, A.N. Tiwari et al., suggested that this effect is due to the fact of the relaxation of the compressive stress which is generated by the lattice and thermal mismatch between the CdTe and the underlying substrate [26]. The lattice parameter may also decrease due to the formation of $CdTe_{1-x}S_x$ and $CdS_{1-y}Te_y$ alloys in the absorber layer which occurs by interdiffusion between CdS and CdTe during $CdCl_2$ treatment in air [13,27]. The progressive diffusion, which creates a distribution of lattice parameters within the film, can be easily detected with X-ray diffraction line-profile analysis. The analysis of the data presented in Fig. 2(c) proved the changes in the XRD profiles of the CdTe (511) peak for $CdCl_2$ treated films. Therefore, the $CdCl_2$ tratment produced a broad asymmetric peak with a tail extending towards higher angle (lower *d*-spacing), indicative of significant alloying with CdS. Alloy formation is more pronunced in films deposited at low substrate temperature having small grains and high grain-boundary density. In such films, a high partial pressure or concentration of $CdCl_2$ together with O_2 during $CdCl_2$ treatment will result in considerable alloy formation. For samples, deposited at high temperature and having large grains, the absorber layer exhibits a narrow CdTe (511) XRD profile, indicating a negligible degree of alloy formation. The SEM images support the XRD results.

Table 1
Structural parameters of CdTe/CdS thin films, before and after $CdCl_2$ treatment.

T_s	Cryst. size, (Å) /as deposited films	Cryst. size, (Å) /after $CdCl_2$ treatment	a_0, (Å) /as deposited films	a_0, (Å) /after $CdCl_2$ treatment
250	131	1103	6.483	6.481
300	225	1061	6.484	6.481
350	319	1117	6.485	6.481
400	729	1134	6.485	6.484
450	857	995	6.486	6.485
500	936	1100	6.486	6.485

3.2. Photoluminescence

Photoluminescence spectra (PL) are always used to explore defects and traps. But the density of trap states depends critically on the deposition parameters and hence on the substrate temperature [28]. Changes in phase, band gap and density of traps will be reflected on the photoluminescence spectra. In Fig. 3 the room temperature PL spectra of the CdTe/CdS samples obtained at different substrate temperatures, before and after $CdCl_2$ treatment, are shown. For all as deposited samples PL emission band is peaked at 1.49 eV. Moreover, the amplitude of the PL intensities strongly depends on the growth conditions. As it can be seen from Fig. 3, the most intense band corresponds to the films obtained at high temperatures 450 and 500 °C. Therefore, CdTe/CdS films obtained at such growth condition have high crystallinity and reaveled in more perfect structure. This result is in good accordance with the data presented above by SEM and XRD. The PL intensity decreased with the smallest grain size in the film. Therfore, the dislocation density for these films is larger than in the case of films grown at high temperature. In addition, PL emission in a polycrystalline system may be significantly influenced by grain boundaries (GBs). One effect of GBs is that the PL bands are broadened by the variety of recombination

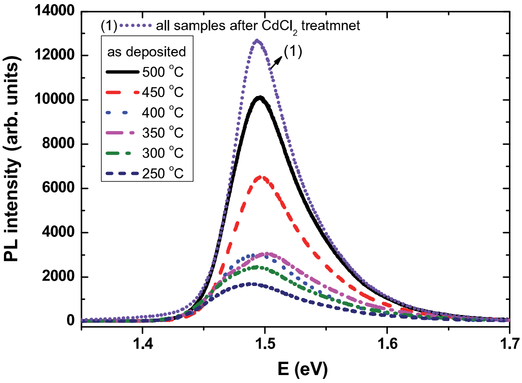

Fig. 3. The room temperature photoluminescence spectra of the CdTe/CdS thin films obtained which were grown at the different substrate temperatures.

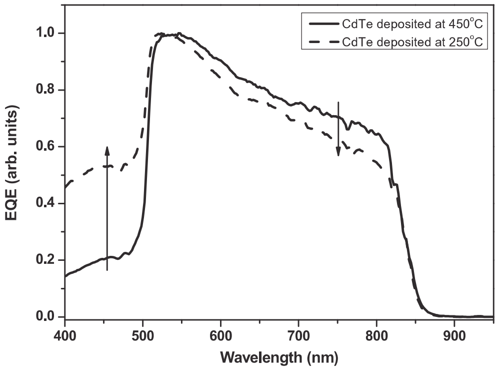

Fig. 4. QE measurements of solar cells for CdTe films deposited at substrate temperatures 250 and 450 °C.

centers that can exist in a polycrystalline film [29]. At low substrate temperature GBs can provide an effective chanel for non-radiative recombination. After $CdCl_2$ treatment the relative PL intensity increases considerably reaching a similar value for all samples (Fig. 3, curve 1). It has been shown that the increase of the PL intesity is strongly affected by $CdCl_2$ annealing which leaves too high chlorine oncentration in CdTe lattice and generates a high concentration of the isoelectronic complexes $V_{Cd}2Cl_{Te}$ and Te_i2ClTe. The main defects which form the 1.49 eV PL band here are substitutional chlorine Cl_{Te}^{+} (donor) and complex $V_{Cd}Cl_{Te}^{-}$ (acceptor) [30–32]. It was observed that after $CdCl_2$ heat treatment the PL spectra for the films grown at smallest temperatures exhibit high intensities (much higher as compared to the as deposited). This result is in a good accordance with the data presented by SEM and XRD where for the films deposited at the lowest temperature having submicrometer initial crystallite size, significant recrystallization mechanism occurs during the $CdCl_2$ treatment. Thus, the highly dispersed structure with high surface energy is more active for recrystallization by mass transport trough $CdCl_2$ liquid flux. The process is characteristic for the sintering in the presence of liquid phase. For the samples grown at high temperature a small difference between the PL intensities before and after $CdCl_2$ treatment occurred. Also, according to the data presented above by X-ray pattern for the films which have a large initial grain size and perfect structure, the recrystallization process occurs through the diffusion mechanism. Thus, for the films obtained at such growth condition the chlorine concentration is much lower than in the films grown at smallest temperature, implying the optoelectronic properties and hence the performance of the devices.

3.3. Quantum efficiency measurements and device results

Quantum efficiency measurements (Fig. 4) showed enhanced response in the blue wavelength region for the cells grown at lowest substrate temperature indicating excessive consumption of CdS during the $CdCl_2$ annealing process. Such CdS consumption during $CdCl_2$ annealing process is commonly observed due to CdS–CdTe intermixing [33–35]. XRD measurements confirm that excessive consumption of CdS observed by EQ for cells grown at lowest substrate temperature and treated in $CdCl_2$ originates from enhanced CdS–CdTe intermixing. The degree of alloying is indicated by simultaneous changes in short wavelength response (due to the change in CdS thickness) and the long wavelength response (due to the formation of lower band gap intermixed CdS_xTe_{1-x}). Excessive intermixing can result in direct connections between the absorber and front electrical contact as FTO, giving rise to inferior junction properties, which reduce open-circuit voltage (V_{OC}) and fill factor (FF) [36]. The device results for the structures obtained at different growth conditions are listed in Table 2. It was observed that the photovoltaic properties of the solar cells strongly depend on the growth condition, intermixing and pinholes. The primary influence of the high substrate temperature in combination with $CdCl_2$ treatment is on the good crystalline quality of both CdTe/CdS on the junction ensuring better photovoltaic parameters and hence the highest efficiency of 11.6%. At this temperature, an ideal balance is obtained between defect annealing and interdiffusion. The CdTe solar cell, which was grown at smallest temperature, exhibited the worst cell performance with an efficiency of only 2.3%, and the poor performance is attributed to the presence of pinholes and excessive intermixing which increased in the $CdCl_2$ treated case (Fig. 5).

Table 2
Device results.

T_s	V_{oc} (mV)	J_{sc} (mA/cm^2)	FF (%)	Eff (%)
250	525	14.8	29.0	2.3
300	630	18.1	32.5	3.7
350	630	19.8	35.3	4.4
400	766	21.2	55.2	9
450	810	23.0	62.0	11.6
500	790	22.8	60.1	10.8

V_{oc}—open-circuit voltage.
J_{sc}—short-circuit current density.
FF—fill factor.
Eff—efficiency.

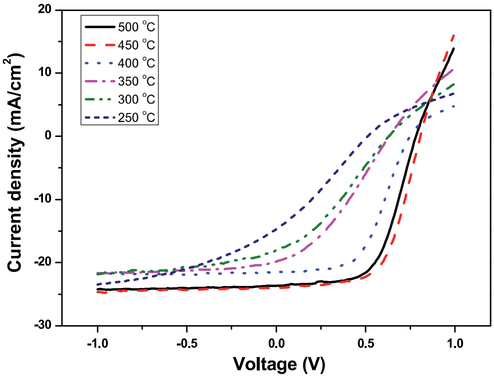

Fig. 5. Current–voltage characteristics of the CdTe/CdS solar cells deposited at different substrate temperatures.

4. Conclusions

In this work we studied the effect of deposition temperature in conjunction with $CdCl_2$ treatment on structural and optoelectronic properties of CSS CdTe/CdS thin film solar cells. It was shown that an increase of the substrate temperature from 250 to 500 °C leads to the changing of the film growth mechanism. Structural, morphological and PL spectra characterization of the CdTe/CdS structures after $CdCl_2$ treatment has highlighted progressive recrystallization, grain growth and interdiffusion. Interdiffusion between CdS and CdTe occurs during the $CdCl_2$ heat treatment, which was more pronounced for the structures obtained at low substrates temperature, yielded in low efficiency cells. The CdTe solar cells deposited at high substrate temperature showed extremely high crystalline quality CdTe/CdS heterojunction and highest efficiency.

Acknowledgments

This study was supported by the European Social Fund's Doctoral Studies under project 1.2.0401-0079 in Estonia, by the European

Union through the 7th FP project FLEXSOLCELL (GA-2008-230861), by the European Regional Development Fund (Centre of Excellence “Mesosystems: Theory and Applications”, TK114), by Estonian Science Foundation Grant ETF9142 and by Estonian Ministry of Education and Research through the program AR12118 and Target Financing project IUT 19-4.

References

[1] T.L. Chu, S.S. Chu, High efficiency thin film CdS/CdTe solar cells, Int. J. Sol. Energy 12 (1992) 121.
[2] T.L. Chu, S.S. Chu, Recent progress in thin film cadmium telluride solar cells, Prog. Photovolt. Res. Appl. 1 (1993) 31.
[3] D. Bonnet, The CdTe thin film solar cell—an overview, Int. J. Sol. Energy 12 (1992) 1.
[4] U. S Department of Energy, Energy Efficiency & Renewable Energy, 2010 Solar Technologies Market Report, Colden, CO, http://www.nrel.gov/docs/fy12osti/51847.pdf2011.
[5] R.W. Birkmire, E. Eser, Polycrystalline thin film solar cells: present status and future potential, Annu. Rev. Mater. Sci. 27 (1997) 625.
[6] W. Huber, A. Lopez-Otero, The electrical properties of CdTe films grown by hot wall epitaxy, Thin Solid Films 58 (1979) 21.
[7] N. Abbas Shah, A. Ali, Z. Ali, A. Maqsood, A.K.S. A. K.S., Properties of Te-rich cadmium telluride thin films fabricated by closed space sublimation technique, J. Cryst. Growth 284 (2005) 477.
[8] N. Nakayama, H. Matsumoto, A. Nakano, S. Ikegami, H. Uda, T. Yamashita, Ceramic thin film CdTe solar cell, J. Appl. Phys. 19 (1980) 703.
[9] J.H. Lee, D.G. Lim, J.S. Yi, Electrical and optical properties of CdTe films prepared by vacuum evaporation with close spacing between source and substrate, Sol. Energy Mater. Sol. Cells 75 (2003) 235.
[10] B.E. McCandless, S.S. Hegedus, R.W. Birkmire, D. Cunningham, Correlation of surface phases with electrical behavior in thin-film CdTe devices, Thin Solid Films 431–432 (2003) 249.
[11] X. Wu, High-efficiency polycrystalline CdTe thin-film solar cells, Sol. Energy 77 (2004) 803.
[12] R.W. Birkmire, B.E. McCandless, S.S. Hegedus, Effects of processing on CdTe/CdS materials and devices, Int. J. Sol. Energy 12 (1992) 145.
[13] B.E. McCandless, R.W. Birkmire, Optimization of vapor post-deposition processing for evaporated CdS/CdTe solar cells, Prog. Photovolt. Res. Appl. 7 (1999) 21.
[14] R.W. Birkmire, B.E. McCandless, W.N. Shafarman, CdTe/CdS solar cells with transparent contacts, Sol. Cells 23 (1988) 115.
[15] J.D. Major, K. Durose, Early stage growth mechanisms of CdTe thin films deposited by close space sublimation for solar cells, Sol. Energy Mater. Sol. Cells 95 (2011) 3165.
[16] J. Luschitz, K. Lakus-Wollny, A. Klein, W. Jaegermann, Growth regimes of CdTe deposited by close-spaced sublimation for application in thin film solar cells, Thin Solid Films 515 (2007) 5814.
[17] J. Luschitz, B. Siepchen, J. Schaffner, K. Lakus-Wollny, G. Haindl, A. Klein, W. Jaegermann, CdTe thin film solar cells: interrelation of nucleation, structure and performance, Thin Solid Films 517 (2009) 2125.
[18] V. Kosyak, A. Opanasyuk, P.M. Bukivskij, Yu.P. Gnatenko, Study of the structural and photoluminescence properties of CdTe polycrystalline films deposited by close-spaced vacuum sublimation, J. Cryst. Growth 312 (2010) 1726.
[19] A. Salavei, I. Rimmaudo, F. Piccinelli, A. Romeo, Influence of CdTe thickness on structural and electrical properties of CdTe/CdS solar cells, Thin Solid Films 535 (15) (2013) 257.
[20] H.R. Moutinho, M.M. Al-Jassim, D.H. Levi, P.C. Dippo, L.L. Kazmerski, Effects of CdCl2 treatment on the recrystallization and electro-optical properties of CdTe thin films, J. Vac. Sci. Technol. 16 (1998) 1251.
[21] H. Infante, G. Gordillo, Effect of the $CdCl_2$ treatment on the morphology and structural properties of CdTe thin films deposited by the CSS method, Surf. Rev. Lett. 9 (2002) 1681.
[22] J. Hiie, CdTe:$CdCl_2$:O_2 annealing process, Thin Solid Films 431–432 (2003) 90.
[23] Brian E. McMacandless, J.R. Stes, Cadmium telluride solar cells, in: A. Luque, S. Hegedus (Eds.), Handbook of Photovoltaic Science and Engineering, John Wiley & Sons, 2003, p. 618.
[24] A. Romeo, S. Buecheler, M. Giarola, G. Mariotto, A.N. Tiwari, N. Romeo, A. Bosio, S. Mazzamuto, Study of CSS- and HVE-CdTe by different recrystallization processes, Thin Solid Films 517 (2009) 2132.
[25] M.B. Rigana, N. Madhusudhana Rao, S. Kaleemulla, M. Shobana, N. Sai Krishna, M. Kuppan, Effect of substrate temperature on structural and optical properties of nanocrystalline CdTe thin films deposited by electron beam evaporation, J. Nano-Electron. Phys. 5 (3) (2013) 03019.
[26] A. Romeo, D.L. Batzner, H. Zogg, A.N. Tiwari, Recrystallization in CdTe/CdS, Thin Solid Films 361-362 (2000) 420.
[27] M. Herndon, A. Gupta, V. Kaydanov, R. Collins, Evidence for grain-boundary-assisted diffusion of sulfur in polycrystalline CdS/CdTe heterojunctions, Appl. Phys. Lett. 75 (1999) 3503.
[28] D. Bhattacharyya, S. Chaudhuri, A.K. Pal, Electrical conduction at low temperatures in polycrystalline CdTe and ZnTe films, Mater. Chem. Phys. 40 (1995) 44.
[29] V.V. Tetyorkin, A.V. Sukach, S.V. Stariy, V.A. Boiko, Photoluminescence studies of CdTe polycrystalline films, J. Semicond. Phys. Quantum Electron. Optoelectron. 15 (4) (2012) 340.
[30] V. Valdna, p-Type doping of CdTe, Solid State Phenom. 67–68 (1999) 309.
[31] V. Valdna, J. Hiie, A. Gavrilov, Defects in chlorine-doped CdTe thin films, Solid State Phenom. 80–81 (2001) 155.
[32] N. Spalatu, J. Hiie, V. Valdna, M. Caramana, N. Maticiuc, V. Mikli, T. Potlog, M. Krunks, V. Lughi, Properties of the $CdCl_2$ air-annealed CSS CdTe thin films, Energy Procedia 44 (2014) 85.
[33] L. Kranz, J. Perrenoud, F. Pianezzi, C. Gretener, P. Rossbach, S. Buecheler, A.N. Tiwari, Effect of sodium on recrystallization and photovoltaic properties of CdTe solar cells, Sol. Energy Mater. Sol. Cells 105 (2012) 213.
[34] B.E. McCandless, R.W. Birkmire, Analysis of post deposition processing for CdTe/CdS thin film solar cells, Sol. Cells 31 (1991) 527.
[35] M. Terheggen, H. Heinrich, G. Kostorz, D. Baetzner, A. Romeo, A.N. Tiwari, Analysis of bulk and interface phenomena in CdTe/CdS thin-film solar cells, Interface Sci. 12 (2004) 259.
[36] K.W. Böer, CdS enhances V_{OC} and FF in CdS/CdTe and CdS/CuInSe$_2$ solar cells, J. Appl. Phys. 107 (2010) 023701.

PAPER III

N. Spalatu, M. Krunks, J. Hiie, Structural and optoelectronic properties of $CdCl_2$ activated CdTe thin films modified by multiple thermal annealing, Thin Solid Films (2016) *in press,* http://dx.doi.org/10.1016/j.tsf.2016.09.042.

ARTICLE IN PRESS
TSF-35507; No of Pages 6
Thin Solid Films xxx (2016) xxx–xxx

Contents lists available at ScienceDirect

Thin Solid Films

journal homepage: www.elsevier.com/locate/tsf

Structural and optoelectronic properties of $CdCl_2$ activated CdTe thin films modified by multiple thermal annealing

N. Spalatu *, M. Krunks, J. Hiie

Department of Materials Science, Tallinn University of Technology, Ehitajate tee 5, 19086 Tallinn, Estonia

ARTICLE INFO

Article history:
Received 6 May 2016
Received in revised form 21 September 2016
Accepted 21 September 2016
Available online xxxx

Keywords:
Cadmium telluride
Thin films
Cadmium chloride activation
Thermal annealing
Structural properties, optoelectronic properties

ABSTRACT

Traditional $CdCl_2$ thermal treatment of CdTe/CdS heterostructure results in grain growth, sintering and incorporation of Cl into CdTe lattice, substantially improving performance of the cells. The process is complicated by high vapor pressure of $CdCl_2$ and presence of oxygen. Considering volatility of $CdCl_2$ and presence of residual oxidation products we provide systematic investigation results on the influence of subsequent multiple annealing in hydrogen (H_2), vacuum and closed isothermal conditions on the properties of $CdCl_2$ activated CdTe films (thickness 2 μm) deposited by close spaced sublimation at low (250 °C) and high (500 °C) substrate temperature onto roughened glass. Structural and optoelectronic properties of thermal annealed films were compared. High resolution X-ray analysis demonstrates the shift of the main (111) peak in accordance with mobility of $CdCl_2$ impurity between ambient and CdTe crystal in good correlation with optoelectronic properties. $CdCl_2$ activated CdTe films have high resistivity and high dark to light resistance ratio. Subsequent hydrogen and vacuum thermal annealing increases the resistivity and photoconductivity of the films. The dark resistivity has been sharply decreased by about four orders of magnitude in result of isothermal annealing at 600 °C. By controlling the thermal annealing conditions, substantial improvement of CdTe optoelectronic properties has been achieved.

1. Introduction

Cadmium telluride (CdTe) has been regarded as one of the most promising absorber materials for cost-effective thin-film photovoltaic devices and thus continues to attract attention and research endeavors for decades [1–2]. After nearly 20 years of the rather stagnant progress, remarkable improvements in the efficiency of CdTe-based solar cells were achieved recently, reaching 22.1% [3]. A breakthrough in the open-circuit voltage (V_{oc}) was finally reported earlier this year, from the decades-old records of 800–900 mV to over 1 V [4]. All of these efforts aimed to increase the efficiency, reliability and life time of this device, and there is still a large space for improvements before reaching the theoretical limits (30%) [5]. Despite the high photovoltaic performance of these solar cells, there are still several aspects such as technology related issues, back contact strategy, and/or junction activation that require more optimization and better understanding [6].

Irrespective of CdTe film deposition method, $CdCl_2$ activation is standard and vital step in CdTe device processing that promotes recrystallization and sintering of both CdS and CdTe layers substantially improving the optoelectronic properties of the solar cell [7–11]. However, during this process some residual $CdCl_2$ may segregate and after washing the water-insoluble oxychlorides can stick to the CdTe surface [12]. M. Terheggen et al. have demonstrated for the first time a direct imaging of Cl diffusion along CdTe grain boundaries and spatial distribution of Cl, Cd, Te and O at the CdTe/CdS interface [13]. T.A. Gessert et al. also found that residuals are spatially discrete, located primarily along grain boundaries, and are likely of cadmium oxychloride. Results also show that the residuals may penetrate deep into the CdTe such that typical ion-beam etching procedures do not produce complete residual removal [14]. The chloride in the lattice together with residual phases of $CdO\cdot CdCl_2$ and the solid solution of CdTe in $CdCl_2$ on grain boundaries limit the concentration of holes in CdTe and cause hygroscopicity of the cells, having a strong impact upon the PV performance [14,15]. As a solution for gettering of residual impurities from CdTe films is applied a controlled thermal annealing after the $CdCl_2$:O_2 activation step. Valdna et al. have shown low resistance p-type conductivity in CdTe films, achieved without any acceptor dopant, but the concentration of chlorine in the films was decreased by the help of vacuum annealing and heat treatment under tellurium vapor pressure [16,17]. Considering all these approaches, controlled thermal annealing in relevant ambient of the CdTe:$CdCl_2$:O_2 material is shown as a possible way for removal of the residues so-called gettering, which can improve the optoelectronic properties of the CdTe films. In our previous studies [18,19] we described results of systematic investigations of changes in morphology, structural and optoelectronic properties of close spaced sublimated (CSS) CdTe

---

* Corresponding author.
E-mail address: nickspalatu@gmail.com (N. Spalatu).

http://dx.doi.org/10.1016/j.tsf.2016.09.042
0040-6090/© 2016 Elsevier B.V. All rights reserved.

Please cite this article as: N. Spalatu, et al., Structural and optoelectronic properties of CdCl2 activated CdTe thin films modified by multiple thermal annealing, Thin Solid Films (2016), http://dx.doi.org/10.1016/j.tsf.2016.09.042

thin films and CdTe/CdS structures resulting from different deposition conditions and $CdCl_2$ activation process. Here we report a systematic investigation of the influence of subsequent multiple annealing in H_2, vacuum and closed isothermal conditions on the properties of $CdCl_2$:O_2 heat treated CdTe thin films. In addition, we discuss the mechanism responsible for the changes in structural and optoelectronic properties of CdTe thin films.

2. Experimental details

CdTe films with a thickness of ~2 μm were prepared by CSS of 5 N (99.999%, Alfa Aesar) purity of CdTe source materials onto 2 × 2 × 0.1 cm roughened glass at substrate temperatures of 250 and 500 °C (to simplify the text description, we named the low and high deposition temperatures of CdTe films as LT and HT CdTe). Roughened glass substrates with root mean square $R_q = 2.66$ nm (supplied from O. Kindler company) were used in order to ensure better adhesion of CdTe. After deposition the CdTe/glass samples were soaked in a saturated $CdCl_2$ methanol solution (2.15 g/100 ml methanol), followed by a 30 min heat treatment in air at 420 °C in a two-zone tube furnace. The heat treated samples were then rinsed in deionized water and etched in standard NP (H_3PO_4:HNO_3:H_2O) solution to remove the $CdCl_2$ and oxide residues. Anhydrous, 99.99% $CdCl_2$ was supplied from Alfa Aesar. The $CdCl_2$ activation process was the last stage of preparation for the so-called initial samples. In the next step $CdCl_2$ activated CdTe samples were cleaved into smaller pieces (5 × 5 mm) and then annealed in hydrogen ambient under different conditions. For this stage, vacuumed process tube with samples was filled with 1 atm hydrogen gas at room temperature then closed and introduced into a cylindrical furnace. Annealing temperature varied in the range of 250 to 570 °C while annealing time was fixed at 1 h. The furnace was slowly heated up to the set temperature allowing the residual precipitates to out-diffuse to the CdTe surface. The hydrogen pressure in the process tube was maintained by a standard gas reduction system and was not influenced by expansion of gas at high temperatures of annealing. Large diameter (55 mm) and volume (1500 cm^3) of the process tube ensured an excess of H_2 and the gas convection flow so that the reaction products were transported to the colder part of the tube. After annealing in H_2 the sample passed through two more treatments: vacuum and isothermal treatment. Vacuum annealing of the samples were carried out in the same process tube at 470 °C for 1 h. Isothermal annealing was carried out with the CdTe samples in sealed off, evacuated (at a pressure ≤ 1 Pa.) quartz ampoules at 600 °C for 1 h. Ampoule volumes were typically about 10 cm^3 and prior to loading were etched in HF/HNO_3 followed by annealing at 1000 °C under dynamic vacuum.

The structure of the films was studied with Rigaku Ultima IV diffractometer (Cu Kα radiation, $\lambda = 1.5406$ Å, 40 kV at 40 mA; silicon strip detector D/teX Ultra, Rigaku, Japan) in the Bragg–Brentano (θ–2θ) geometry and their morphology was checked by a scanning electron microscope (SEM) Zeiss EVO-MA15 at a 10 kV operating voltage. The crystallite size and lattice parameters were calculated using the PDXL Version 1.4.0.3 software on the Rigaku system. The resistivity measurements were performed by Van der Pauw method using indium electrodes. Current-voltage (I-V) characteristics of CdTe/In showed linear behavior indicating that the contacts were ohmic. Light resistance was measured using a 75 W glow lamp. Conductivity type of samples was checked up by measuring the polarity of thermovoltage.

3. Results and discussion

Starting from the beginning we have come up with a hypothesis that by changing the temperature and environment of the thermal annealing process one can remove the residues and decrease concentration of $CdCl_2$ active components and improve the optoelectronic properties of CdTe thin films. Generally, incorporation of $CdCl_2$ into CdTe crystalline lattice is given by the reaction [20,21]:

$$nCdTe + CdCl_2 \rightarrow Cd_{n+1}Te_n2Cl_{Te}V_{Cd} \quad (1)$$

Showing that one $CdCl_2$ molecule can generate one V_{Cd} per every pair of incorporated Cl_{Te}. In result of dissociation of the $(V_{Cd}2Cl_{Te})^{\times}$ neutral defect, the created shallow acceptor defect $(V_{Cd}Cl_{Te})^{-}$ compensates the Cl_{Te}^{+} shallow donor (Eq. (2)), so that the $CdCl_2$ doped CdTe thin film represents a compensated and highly resistive p-type semiconductor [20,21]:

$$(V_{Cd}2Cl_{Te})^{\times} \rightarrow (V_{Cd}Cl_{Te})^{-} + Cl_{Te}{}^{+} \quad (2)$$

$CdCl_2$ activation step, carried out in air, is a complex process which involves multiple reactions between the CdTe, $CdCl_2$ and O_2 in the polycrystalline CdTe layers [22]:

$$CdTe_{(s)} + CdCl_{2(s)} + O_{2(g)} \rightarrow CdO_{(s)} + TeCl_{2(g)} \quad (3)$$

$$TeCl_2 + CdTe \rightarrow CdCl_2 + Te$$

$$CdO + CdCl_2 \rightarrow 2CdO \cdot CdCl_2$$

$$CdTe + O_2 \rightarrow CdTeO_3$$

In result of these reactions the formed glassy mixture of CdTe-$CdCl_2$-$CdTeO_3$-Te (flux) has low melting point, promoting intensive recrystallization, grain growth and sintering of highly doped CdTe [23]. High doping is based on the equilibrium between liquid flux and solid CdTe. Presence of residual oxides and $CdCl_2$ components in CdTe lattice and on grain boundaries (GB) have an important impact on the electrical behavior of CdTe [14,15]. In this sense, thermal annealing in the presence of hydrogen can be a convenient and appropriate method to control the oxygen content which tend to retain an excess $CdCl_2$ on the GB as $2CdO \cdot CdCl_2$. It is assumed that reaction with hydrogen could result in removal of oxygen by water evaporation together with formation of Cd excess and free $CdCl_2$ which can be removed by evaporation at higher temperatures, especially in vacuum. The thermodynamically favored reaction between hydrogen and solid CdO is [24]:

$$H_{2(g)} + CdO_{(s)} \rightarrow H_2O + Cd_{(s,l)}, \Delta G\ (250\,^{\circ}C) = -2.6 \text{ and at } 570\,^{\circ}C - 6.5\ \text{kcal/mol} \quad (4)$$

The reaction between hydrogen and solid $CdCl_2$ is not thermodynamically favored [24]:

$$H_{2(g)} + CdCl_{2(s,l)} \rightarrow 2HCl + Cd_{(s,l)}, \Delta G\ (250\,^{\circ}C) = 27.4 \text{ and at } 570\,^{\circ}C\ 14.4\ \text{kcal/mol} \quad (5)$$

Thus, by subsequent thermal annealing we expect to get advantage for controlling of residuals in polycrystalline CdTe thin films. By optimization of chlorine concentration in lattice, we can approach to the ideal electro neutrality condition as $[(V_{Cd}Cl_{Te})^{-}] = p^{+}$, implying high p-type conductivity in CdTe [17]. These arguments substantiate systematic investigation of changes in structural and optoelectronic properties $CdCl_2$ doped CdTe films induced by subsequent multiple annealing in H_2, vacuum and closed isothermal conditions.

3.1. Structural properties

Structural properties of CdTe thin films were analyzed on the basis of X-ray diffraction measurements (XRD). All CdTe films on glass, before and after any of the treatments exhibits a strong (111) preferred orientation. The lattice parameter and the average crystallite size were calculated using PDXL-software and are tabulated in Table 1. Debye-Scherrer formula was used for calculating the crystallite size. As can be seen the

Please cite this article as: N. Spalatu, et al., Structural and optoelectronic properties of CdCl2 activated CdTe thin films modified by multiple thermal annealing, Thin Solid Films (2016), http://dx.doi.org/10.1016/j.tsf.2016.09.042

Table 1
Values of average crystallite size and lattice parameter for LT and HT CdTe thin films after all treatments steps.

Sample	Treatment conditions	T_a[a] (°C)	Crystallite size (nm)	Lattice constant (Å)
LT CdTe	As deposited	–	85	6.484
	$CdCl_2$	–	134	6.477
	H_2	250–500	144–148	6.480
		570	99	6.471
	Vacuum	250–500	120–130	6.481–6.482
		570	90	6.474
	Isothermal[b]	250-500	110-120	6.472
		570	95	6.468
HT CdTe	As deposited	–	144	6.486
	$CdCl_2$	–	150	6.484
	H_2	250–500	153–159	6.485
		570	144	6.485
	Vacuum	250–500	139–149	6.486–6.487
		570	138	6.485
	Isothermal[b]	250-500	120-137	6.486-6.487
		570	95	6.484

[a] Hydrogen annealing temperature 250–570 °C, 1 h. T_a is annealing temperature for each treatment step.

[b] Isothermal annealing at 600 °C for 1 h of CdTe films which passed H_2 and vacuum annealing steps.

crystallite size of LT CdTe samples increases dramatically in the $CdCl_2$ activation process (from 85 nm to 134 nm). This effect is less pronounced, however, in HT CdTe films for which the crystallite size increases only marginally (from 140 nm to 150 nm) during $CdCl_2$ treatment. Thus, crystallite growth of CdTe after $CdCl_2$ activation depends on the initial crystallite size of CdTe; the smaller the crystallite size, the more significant is the crystallite growth. We consider that the mechanism by which $CdCl_2$ treatment at 420 °C in air promotes structural changes in CdTe is most likely by formation of liquid flux and liquid phase assisted recrystallization of CdTe. Evidence for this is provided by extensive crystallite growth in LT CdTe films in the $CdCl_2$ activation process. It is also important to consider the low diffusivity of Cl in CdTe at 420 °C (with bulk and boundary diffusion coefficients: $D_B \sim 10^{-13}$ cm^2/s and $D_{GB} \sim 10^{-8}$ cm^2/s, respectively) [22,25]. The incorporation of chlorine into CdTe lattice substantially differs for liquid phase recrystallization and simple indiffussion of chlorine in CdTe. Thus, LT CdTe exhibiting a highly dispersed structure with smaller grains and high grain boundary density is more active for recrystallization by mass transport trough $CdCl_2$ liquid flux and due to high solubility of CdTe in $CdCl_2$ flux, the grain growth is accomplished by full recrystallization and full saturation of crystallite volume by $CdCl_2$. In parallel, for HT CdTe film with a densely packed larger grain size (respectively large crystallite size) the recrystallization occurs only on the surface region of the CdTe grains, implying insignificant grain growth. Thereby, it can be assumed that in such films the grains will be inhomogeneously doped by slow indiffussion, resulting in low concentration of $CdCl_2$ compared to LT CdTe. It is widely accepted that CdTe films deposited by CSS at high substrate temperature do not undergo strong recrystallization during $CdCl_2$, but reduce the structural defects and affect the grain boundary, resulting in higher effective acceptor concentration [22,26,27]. It has been shown that the larger CdTe grains exhibit enhanced carrier depletion along GB indicating to p-type compensation due to Cl segregation, a donor impurity in CdTe [28]. We note that the amount of Cl incorporated in the CdTe material is dependent on the nature of the deposited layers, and prehistory of these layers will be reflected in the next annealing steps.

Subsequent thermal annealing in H_2 slightly increases the crystallite size of both LT and HT CdTe films (from 134 nm to 144 nm and from 150 nm to 153 nm respectively). Moreover, a slow but gradual increase in the crystallite size of both samples was assured by the gradual increase of the temperature of H_2 annealing from 250 to 500 °C. In addition, other quite interesting effect was observed for samples annealed in H_2 at 250 °C where the CdTe surface is covered by needle-shaped particles (SEM Fig. 1c). The energy dispersive X-ray analysis (not shown) of these particles showed a significantly higher concentration of Te compared to the large surface. We assume that during H_2 annealing a uniform Te film (which is usually formed on the CdTe surface and also at grain boundaries after NP etching) starts to agglomerate on the surface in the form of needle-shaped particles. Due to stationary atmosphere of H_2 ambient and due to the low gradient of temperature between 250 °C and the cold end of process tube, agglomerates of Te leave the CdTe surface but sublimate back on the extended defects (like GB and dislocation loops). The extended defects in CdTe surface can act as nucleation centers needed for the growth of Te needles. At increased gradient of temperature (300 °C) these Te needles manage to evaporate from CdTe surface, leaving behind a surface with dimples. Appearance of these dimples with ~20 nm diameter might be due to high solubility of CdTe in the solid phase of Te. At higher temperatures of H_2 treatment (350–500 °C) the surface of CdTe layer remains clean as for 300 °C. The increased concentration of Te on the CdTe surface and also at GB

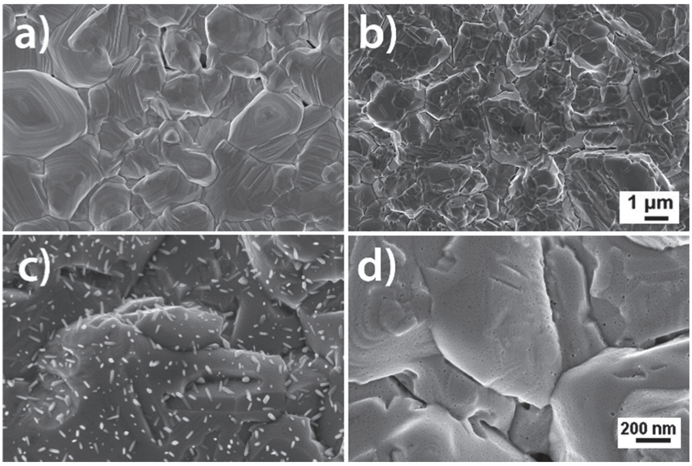

Fig. 1. SEM top view pictures of CdTe surface: after CdTe deposition (a), after $CdCl_2$:O_2 activation (b), after H_2 thermal annealing at 250 °C (c) and 300 °C (d).

Please cite this article as: N. Spalatu, et al., Structural and optoelectronic properties of CdCl2 activated CdTe thin films modified by multiple thermal annealing, Thin Solid Films (2016), http://dx.doi.org/10.1016/j.tsf.2016.09.042

together with presence of high concentration of residual components like CdO, TeO_2, will actively react with hydrogen contributing to additional growth of crystallites. Supplementary crystallite growth demonstrates that the reaction between hydrogen and residual components already begins intensively at 250 °C. Starting from 500 °C the crystallite size slightly decreases and further increase in annealing temperature to 570 °C result in significant decreasing of crystallites, indicating the intensive sublimation of CdTe. The film thicknesses after this annealing step ranged between 0.8 and 1 μm.

All changes in the lattice parameter for both LT and HT CdTe films after all treatments are reflected in the narrow-angle XRD patterns of the main (111) peak profiles (Fig. 2a, b) Thus, after $CdCl_2$ activation high resolution XRD analysis demonstrates the shift of the main (111) peak toward high 2-theta values. Considering the incorporation of $CdCl_2$ into CdTe lattice, this shift can be explained by the creation of chlorine on tellurium site and cadmium vacancies (according to the reaction (1)) and probably incorporation of oxygen on tellurium site. The atomic size of chlorine (102 pm) and oxygen (66 pm) are smaller than of tellurium size (138 pm) [29] and together with Cd vacancies they cause the contraction of both CdTe sub-lattices and hence decreasing the lattice parameter (Table 1). On the other hand, slight displacement of the (111) peak toward lower 2-theta region with decreased lattice constant are accompanied by the lattice relaxation in result of removal of oxygen and $CdCl_2$ impurities by H_2 and subsequent vacuum annealing. Further isothermal annealing in ampoules at 600 °C of the LT CdTe samples which passed through H_2 and vacuum treatment ensures strong shift of the (111) peak toward higher 2-theta values, accompanied by considerable decrease in the lattice constant (Fig. 2a). Additionally, the isothermal annealing in ampoules at 600 °C result in significant decrease of crystallite size in both LT and HT CdTe films (Table 1). Large volume of ampule ($V \sim 10$ cm^3) in comparison with small size and mass of the samples (size: 5 × 5 × 1 mm) and high temperature 600 °C provides sublimation of remarkable part of the CdTe and $CdCl_2$ into gas phase, implying significant decrease of crystallite size and homogeneous chlorine doping trough the volume of the layer due to thermodynamic equilibrium between solid and vapor phases. It should be emphasized that the solubility of $CdCl_2$ in CdTe substantially increases at higher temperatures resulting in further decrease of lattice constant which is more pronounced for LT CdTe.

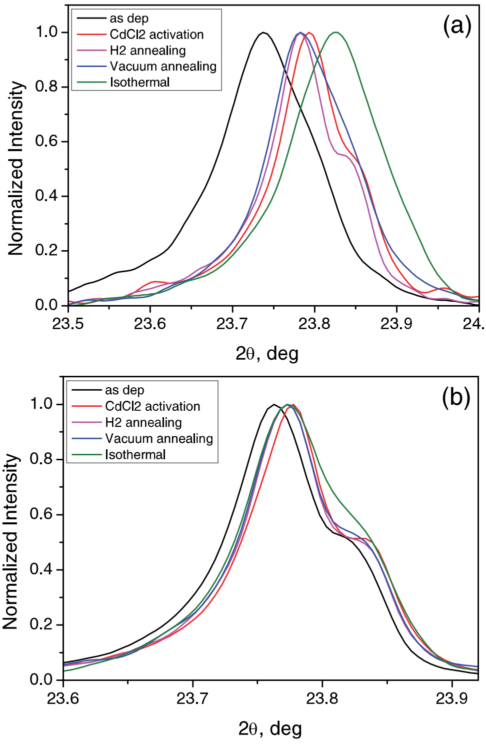

Fig. 2. Displacement of the (111) peak vs thermal annealing conditions for LT (a) and HT (b) CdTe thin films.

3.2. Optoelectronic properties

As deposited films are characterized by high dark resistivity indicating that intrinsic defects electrically compensate CdTe resulting in semi-insulating material. Table 2 show resistivity values for both LT and HT CdTe thin films after all thermal annealing steps. As can be seen, after $CdCl_2$ activation process the p-type resistivity of both samples decreases significantly. Thus, the dark resistivity of LT CdTe sample is equal to 10^7 $\Omega \cdot cm$, and higher by about an order of magnitude compared to HT sample whose resistivity is equal to 7×10^5 $\Omega \cdot cm$. It should be noted that the photoconductivity of $CdCl_2$ activated LT CdTe sample is poor, with dark to light resistance ratio $K_F = 12.5$. However, HT CdTe activated sample exhibited prominent photoconductivity, with high dark to light resistance ratio $K_F = 70$. The high resistivity and poor photoconductivity of LT CdTe samples confirms our supposition that $CdCl_2$ treatment leaves too high chloride concentration in these films. At high chloride concentrations the concentration of incorporated complex defects $V_{Cd}2Cl_{Te}$ increases. As a result, the p-type resistivity increases and dumping the photoconductivity. In parallel, in HT CdTe activated samples the chloride concentration seems to be more balanced with the concentration of native defects (V_{Cd}). Thus, it could be assumed that due to a lower amount of incorporated chloride in these films, the concentration chloride-based complexes ($V_{Cd}^{2-}2Cl_{Te}^{+}$) drops and increases the concentration of shallow acceptors or so called A-centers $(V_{Cd}^{2-}Cl_{Te}^{+})^{-}$ that increases both p-type and photo conductivities. So, the changes in electrical and structural properties in both $CdCl_2$ activated LT and HT CdTe films are in good correlation.

Subsequent thermal annealing in H_2 at 250 °C increased the dark resistivity of both CdTe films by nearly an order of magnitude (from 10^7 to 10^8 $\Omega \cdot cm$ and from 7×10^5 to 2×10^6 $\Omega \cdot cm$ for LT and HT respectively), however K_F remaining practically unchangeable (Table 2). The abrupt increase in resistivity of the films can be explained by increased activity of H_2 at 250 °C which provide excess of cadmium from CdO, promoting to decrease in the concentration of cadmium vacancies (V_{Cd}), thereby increasing surface resistivity of CdTe. Further increase in the H_2 annealing temperature from 300 to 500 °C does not change the dark resistivity of LT CdTe, nevertheless the films exhibited relatively high photoconductivity, suggesting partial removal of $CdCl_2$ and Cd excess and stability of acceptor-donor concentration ratio in H_2 atmosphere. Considering the higher concentration of residual components on the grain boundaries in LT CdTe, more time is needed for their out diffusion. The ratio of donor –acceptor defect concentration in LT CdTe is also determined by the constant ratio of Cd and Te partial pressures in hydrogen atmosphere. Instead, in the analyses of the HT CdTe films, different features were found to be characteristic for distinct H_2 annealing temperature range. Thus, at annealing temperatures between 300 and 350 °C, the sheet resistance of HT samples sharply decreased by nearly half order of magnitude (from 2×10^6 to 8×10^5 $\Omega \cdot cm$) accompanied by increasing in the photoconductivity. In this case, the evaporation of excess Cd takes place in a shorter time due to the lower concentration of residual components on the grain boundaries and in this region of temperatures the similar characteristics of the material like initial activated samples have been revealed. Further increase in the annealing temperature from 400 to 500 °C increases the resistivity of HT samples by nearly one order of magnitude (from 8×10^5 to 10^7 $\Omega \cdot cm$), maintaining the

Please cite this article as: N. Spalatu, et al., Structural and optoelectronic properties of CdCl2 activated CdTe thin films modified by multiple thermal annealing, Thin Solid Films (2016), http://dx.doi.org/10.1016/j.tsf.2016.09.042

Table 2
Resistivity values vs thermal annealing conditions for both LT and HT CdTe samples.

Sample	Treatment conditions	T_a[a] (°C)	R_D (Ω/□)	R_L (Ω/□)	K_F	ρ_D (Ω·cm)
LT CdTe	$CdCl_2$	–	5×10^{10}	4×10^{9}	12.5	10^{7}
	H_2	250	8×10^{11}	10^{11}	8	1.6×10^{8}
		300–500	$(5–8) \times 10^{11}$	$(1–1.8) \times 10^{10}$	$35 \leq K_F \leq 50$	$(1–1.6) \times 10^{8}$
		570	10^{12}	2.8×10^{11}	3.6	2×10^{8}
	Isothermal[b]	H250	1.5×10^{8}	1×10^{8}	1.5	3×10^{4}
		H300	1.5×10^{8}	1.3×10^{8}	1.15	3×10^{4}
		H350	8×10^{7}	7.5×10^{7}	1.05	1.6×10^{4}
		H400	2.2×10^{7}	2.1×10^{7}	1.04	4.4×10^{4}
		H450	7×10^{6}	6.9×10^{6}	1.01	1.4×10^{3}
		H500	5×10^{6}	5×10^{6}	1	10^{3}
		H570	5×10^{8}	4.8×10^{8}	1.04	10^{5}
HT CdTe	$CdCl_2$	–	3.5×10^{9}	5×10^{7}	70	7×10^{5}
	H_2	250	10^{10}	1.5×10^{8}	66	2×10^{6}
		300–350	4×10^{9}	3×10^{7}	130	8×10^{5}
		400–500	$(7–9) \times 10^{10}$	$(1–2) \times 10^{9}$	$35 \leq K_F \leq 90$	$(1.4–1.8) \times 10^{7}$
		570	2.5×10^{11}	1.2×10^{9}	208	5×10^{7}
	Isothermal[b]	H250	5×10^{7}	7×10^{6}	7.1	10^{4}
		H300	1.3×10^{7}	6×10^{6}	2.16	$2.6. \times 10^{3}$
		H350	1.6×10^{7}	4×10^{6}	4	3.2×10^{3}
		H400	4×10^{7}	1×10^{7}	4	8×10^{3}
		H450	2.5×10^{7}	4.5×10^{6}	5.5	5×10^{3}
		H500	1.3×10^{7}	1.1×10^{7}	1.18	2.6×10^{3}
		H570	5×10^{7}	2.5×10^{6}	20	10^{4}

[a] Hydrogen annealing temperature 250–570 °C, 1 h. T_a is annealing temperature for each treatment step; R_D and R_L - resistance under dark and light conditions; K_F is dark to light resistance ratio; ρ is resistivity.

[b] Isothermal annealing at 600 °C for 1 h of CdTe films which passed H_2 and vacuum annealing steps.

photoconductivity in the same limits of activated samples. At the same time the resistivity is lower by about an order of magnitude compared to LT samples indicating to the lower concentration of dopant impurities in HT CdTe. At high temperature of 570 °C the resistivity of both CdTe films increases considerably, suggesting that this is the critical temperature at which the gettering and sublimation occur so actively that excessively removes both active components from the lattice and the main material. On the other hand, at such high temperature this process might be accompanied by deeper redistribution of the dopant trough the full thickness of layers. The prehistory of the treatments and features of the obtained structures will be strongly reflected on the final isothermal annealing step. Thereby, the dark resistivity has been sharply decreased by about four orders of magnitude for LT CdTe films (from 10^7 to 10^3 Ω·cm) and by three orders of magnitude for HT CdTe (from 2×10^6 to 10^3 Ω·cm) in result of isothermal annealing at 600 °C. The H_2 pre-annealing temperature 500 °C seems to be the optimal temperature which gives in the final isothermal annealing step the smallest values of the resistivity and dark to light resistance ratio. It is expected that thermal annealing in hydrogen, vacuum and closed isothermal conditions will provide CdTe layers with suitable properties for high efficiency CdTe/CdS thin films solar cells.

4. Conclusions

In this work, we systematically investigated results on the influence of subsequent multiple annealing in hydrogen, vacuum and closed isothermal conditions on the properties of $CdCl_2$ activated CSS CdTe films. Changes in structural and optoelectronic properties of CdTe films in the thermal annealing process are connected with chlorine incorporation in CdTe lattice in the $CdCl_2$ activation process, with removal of oxygen and $CdCl_2$ impurities by H_2 and vacuum annealing and with homogeneous chlorine doping by isothermal treatment. Structural characterization of the LT CdTe thin films has highlighted progressive recrystallization and grain growth in the $CdCl_2$ activation process. HT CdTe films do not undergo significant recrystallization and grain growth upon $CdCl_2$ activation step. High resolution XRD analysis demonstrates the shift of the main (111) peak in accordance with mobility of $CdCl_2$ impurity between ambient and CdTe crystal indicating to processes taking place inside the crystalline lattice of CdTe. $CdCl_2$ activated CdTe films have high resistivity and high dark to light resistance ratio. Subsequent hydrogen and vacuum thermal annealing increases the resistivity and photoconductivity of the films. The dark resistivity has been sharply decreased by about four orders of magnitude in result of isothermal annealing at 600 °C. By controlling the thermal annealing conditions, substantial improvement of CdTe optoelectronic properties has been achieved. The gained knowledge about influence of annealing conditions on the properties of CdTe films will facilitate further investigations on CdTe/CdS heterostructures for elaboration of high efficiency solar cells.

Acknowledgements

This work was financially supported by the Estonian Ministry of Education and Research [IUT19-4], by the European Regional Development Fund project: TK141 Centre of Excellence “Advanced materials and high-technology devices for sustainable energetics, sensorics and nanoelectronics” (1.01.2015–1.03.2023), by Estonian Science Foundation Grant [ETF9142] and European Union through the 7th FP project FLEXSOLCELL (GA-2008-230861).

References

[1] F.V. Wald, Applications of CdTe—a review, Rev. Phys. Appl. 12 (1977) 277–290.

[2] D. Bonnet, The CdTe thin film solar cell-an overview, Int. J. Sol. Energy 12 (1992) 1.

[3] http://www.nrel.gov/ncpv/images/efficiency_chart.jpg.

[4] J.M. Burst, J.N. Duenow, D.S. Albin, E. Colegrove, M.O. Reese, J.A. Aguiar, C.S. Jiang, M.K. Patel, M.M. Al-Jassim, D. Kuciauskas, S. Swain, T. Ablekim, K.G. Lynn, W.K. Metzger, CdTe solar cells with open-circuit voltage breaking the 1 V barrier, Nat. Energy 1 (2016) 16015.

[5] R.W. Birkmire, E. Eser, Polycrystalline thin film solar cells: present status and future potential, Annu. Rev. Mater. Sci. 27 (1997) 625.

[6] S.G. Kumar, K.S.R.K. Rao, Physics and chemistry of CdTe/CdS thin film heterojunction photovoltaic devices: fundamental and critical aspects, Energy Environ. Sci. 7 (2014) 45–102.

[7] A. Bosio, N. Romeo, S. Mazzamuto, V. Canevari, Polycrystalline CdTe thin films for photovoltaic applications, Prog. Cryst. Growth Charact. Mater. 52 (2006) 247–279.

[8] I.V. Fisher, K.D. Dobson, J. Nair, E. Bezalel, G. Hodes, D. Cahen, Factors affecting the stability of CdTe/CdS solar cells deduced from stress tests at elevated temperature, Adv. Funct. Mater. 13 (2003) 289–299.

[9] M. Terheggen, H. Heinrich, G. Kostorz, D. Baetzner, A. Romeo, A.N. Tiwari, Analysis of bulk and interface phenomena in CdTe/CdS thin-film solar cells, Interface Sci. 12 (2004) 259–266.

Please cite this article as: N. Spalatu, et al., Structural and optoelectronic properties of CdCl2 activated CdTe thin films modified by multiple thermal annealing, Thin Solid Films (2016), http://dx.doi.org/10.1016/j.tsf.2016.09.042

[10] K. Durose, P.R. Edwards, D.P. Halliday, Materials aspects of CdTe/CdS solar cells, J. Cryst. Growth 197 (1999) 733–742.
[11] B.E. McCandless, K.D. Dobson, Processing options for CdTe thin film solar cells, Sol. Energy 77 (2004) 839–856.
[12] D.W. Niles, D. Waters, D. Rose, Chemical reactivity of $CdCl_2$ wet-deposited on CdTe films studied by X-ray photoelectron spectroscopy, Appl. Surf. Sci. 136 (1998) 221–229.
[13] M. Terheggen, H. Heinrich, G. Kostorz, A. Romeo, D. Baetzner, A.N. Tiwari, A. Bosio, N. Romeo, Structural and chemical interface characterization of CdTe solar cells by transmission electron microscopy, Thin Solid Films (2003) 262–266.
[14] T.A. Gessert, M.J. Romero, C.L. Perkins, S.E. Asher, R. Matson, H. Moutinho, D. Rose, Microscopic analysis of residuals on polycrystalline CdTe following wet $CdCl_2$ treatment, Mat. Res. Soc. Symp. Proc. 668 (2001) H1.10.1–H1.10.6.
[15] M. Terheggen, H. Heinrich, G. Kostorz, D. Baetzner, A. Romeo, A.N. Tiwari, Analysis of bulk and interface phenomena in CdTe/CdS thin-film solar cells, Interface Science 12 (2004) 259–266.
[16] V. Valdna, p-type doping of CdTe, Solid State Phenom. 67-68 (1999) 309–314.
[17] V. Valdna, J. Hiie, A. Gavrilov, Defects in chlorine-doped CdTe thin films, Solid State Phenom. 80-81 (2001) 155–162.
[18] N. Spalatu, J. Hiie, V. Valdna, M. Caraman, N. Maticiuc, V. Mikli, T. Potlog, M. Krunks, V. Lughi, Properties of the $CdCl_2$ air-annealed CSS CdTe thin films, Energy Procedia 44 (2014) 85–95.
[19] N. Spalatu, J. Hiie, V. Valdna, M. Caramana, N. Maticiuc, V. Mikli, T. Potlog, M. Krunks, V. Lughi, Properties of the $CdCl_2$ air-annealed CSS CdTe thin films, Energy Procedia 44 (2014) 85–95.
[20] Y. Marfaing, Impurity doping and compensation mechanisms in CdTe, Thin Solid Films 387 (2001) 123–128.
[21] O.A. Matveev, A.I. Terent'ev, Basic principles of post growth annealing of CdTe:Cl ingot to obtain semi-insulating crystals, Semiconductors 34 (2000) 1264–1269.
[22] B.E. McCandless, in: R. Noufi, R.W. Birkmire, D. Lincot, H.W. Schock (Eds.),II–VI Compound Semiconductor Photovoltaic Materials, San Francisco, USA, April 16–20, 2001, Mater. Res. Soc. Symp. Proc., 668, 2001, p. H1.6.1.
[23] J. Hiie, CdTe:CdCl2:O2 annealing process, Thin Solid Films 431–432 (2003) 90.
[24] Database of HSC Chemistry Ver. 6.0., Outoukumpu Research Oy, Pori, Finland.
[25] D. Shaw, E. Watson, The diffusion of chlorine in CdTe, J. Phys. C: Solid State Phys. 17 (1984) 4945–4950.
[26] M.A. Cousins, K. Durose, Grain structure of CdTe in CSS-deposited CdTe/CdS solar cells, Thin Solid Films 361–362 (2000) 253–257.
[27] A. Romeo, M. Terheggen, D.A. Ras, D.L. Batzner, F.J. Haug, M. Kalin, D. Rudmann, A.N. Tiwari, Progr., Development of thin-film Cu(In, Ga)Se_2 and CdTe solar cells, Prog. Photovolt: Res. Appl 12 (2004) 93–111.
[28] M. Tuteja, P. Koirala, V. Palekis, S. MacLaren, C.S. Ferekides, R.W. Collins, A.A. Rockett, J. Phys. Chem. C 120 (2016) 7020–7024.
[29] B. Cordero, V. Gómez, A.E. Platero-Prats, M. Revés, J. Echeverría, E. Cremades, F. Barragán, S. Alvarez, Covalent Radii Revisited, Dalton Trans. (2008) 2832–2838.

Please cite this article as: N. Spalatu, et al., Structural and optoelectronic properties of CdCl2 activated CdTe thin films modified by multiple thermal annealing, Thin Solid Films (2016), http://dx.doi.org/10.1016/j.tsf.2016.09.042

PAPER IV

N. Maticiuc, **N. Spalatu**, A. Katerski, J. Hiie, V. Mikli, M. Krunks, L. Dolgov, I. Sildos, Plasmonic modification of CdTe thin films by gold nanoparticles: Methods, difficulties and solutions, Microelectronic Engineering 126 (2014) 173–178.

Microelectronic Engineering 126 (2014) 173–178

Contents lists available at ScienceDirect

Microelectronic Engineering

journal homepage: www.elsevier.com/locate/mee

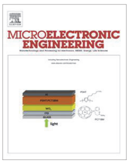

Plasmonic modification of CdTe thin films by gold nanoparticles: Methods, difficulties and solutions

N. Maticiuc [a,*], N. Spalatu [a], A. Katerski [a], J. Hiie [a], V. Mikli [b], M. Krunks [a], L. Dolgov [c], I. Sildos [c]

[a] Institute of Materials Science, Tallinn University of Technology, Tallinn, Ehitajate tee 5, 19086, Estonia
[b] Centre for Materials Research, Tallinn University of Technology, Tallinn, Ehitajate tee 5, 19086, Estonia
[c] Institute of Physics, University of Tartu, Tartu, Riia 142, 51014, Estonia

ARTICLE INFO

Article history:
Received 21 October 2013
Received in revised form 4 July 2014
Accepted 18 July 2014
Available online 29 July 2014

Keywords:
CdTe
Au nanoparticles
Plasmonic effect
Spin coating
Spray pyrolysis
Sputtering

ABSTRACT

Despite numerous theoretical studies on CdTe absorbers with embedded metal nanoparticles (NPs), no technological reports are found. We present an experimental study of 300-nm-thick CdTe absorber layers deposited by close spaced sublimation with incorporated gold NPs to obtain the effect of surface plasmon resonance (SPR). Gold NPs were formed from a $HAuCl_4 \cdot 3H_2O$ solution in ethanol and deposited by spin coating or spray pyrolysis on the top of CdTe film. As alternative, sputtering followed by air annealing of gold thin layer was applied to form Au NPs between the glass substrate and the CdTe layer. The properties of these structures were studied by UV–VIS spectroscopy, scanning electron microscopy, energy dispersive spectroscopy, and X-ray diffraction.

The SPR effect was observed in the wavelength region of 570–590 nm for CdTe layers, with Au NPs measuring 30–40 nm in size. At the increased amount of sprayed $HAuCl_4 \cdot 3H_2O$ solution the nanoparticles were agglomerated into grains and the SPR peak shifted to longer wavelengths. In the case of spin coating the $HAuCl_4$ solution decomposes on the CdTe surface and by chemical reaction contributed to the substantial removal of the CdTe. Sputtering and spray pyrolysis methods did not change the bulk CdTe layer and introduced the plasmonically enhanced absorption, but led to the formation of additional intermetallic phases, such as AuCd, $Au_{0.3}Te_{0.7}$ or $AuTe_2$. The $Au_{0.3}Te_{0.7}$ phase is supposed to play the role of a shell for Au NPs shifting the 592 nm SPR peak to lower wavelengths. Chemical processes responsible for these effects are discussed.

1. Introduction

In recent years, thin film photovoltaics (PV) have attracted the attention of scientific society due to simplicity of manufacturing, yearly increased efficiency and ease of mounting on different surfaces. Thin film solar cell technology is increasing in capacity and market share and now accounts for approximately 20% of the PV market. CdTe solar cells represent approximately half of this market, with the rest being divided between thin film silicon and $Cu(In,Ga)Se_2$ [1]. One limitation still faced by all thin film solar cell technologies is the low light absorption near the band gap edge [2]. This low light absorption is also an issue for CdTe solar cells, which recently increased in efficiency to 20.4% [3]. It is critical to structure the CdTe solar cell such that light can be trapped inside the active layer by increased absorbance. A relatively new method of achieving light trapping in thin film absorber is the application of metallic nanoparticles that have surface plasmon resonance (SPR). Proper engineering of these structures enables light to be concentrated and 'folded' into a thin semiconductor layer, thereby increasing its absorption [2]. This approach would reduce significantly the thickness of thin film solar cells, decreasing demand for scarce semiconductor material as Te, the supply of which limits the scale-up of CdTe solar cells [4].

Combining periodic metal nanostructures on top of ultrathin CdTe layer was theoretically demonstrated to be an effective approach to enhance broadband optical absorption by the CdTe absorber [5]. Among various metals (Ag, Al, Au, Cu) and geometries under investigation (nanodisc (ND), nanosphere (NS)), Al NDs tend to provide the maximum enhancement over the spectral absorption range of interest. The plasmon resonance wavelength of Al ND leads to an optimal localized surface plasmon resonance (SPR) spectrum that maximally matches the intrinsic CdTe absorption profile weighted with the solar spectrum [5].

The optimal parameters of metal nanoparticles (NPs) to enhance the absorption of CdTe absorber were studied theoretically

---

[*] Corresponding author. Tel.: +372 620 3366; fax: +372 620 2020.
E-mail address: nataliamaticiuc@yahoo.com (N. Maticiuc).

http://dx.doi.org/10.1016/j.mee.2014.07.016

[2,5] but yet to our knowledge no experimental data confirmed these results. Moreover, little information is available about suitable technology for the incorporation of metal NPs into CdTe absorber layer. Experience from the technology of Si solar cells with incorporated NPs highlights various methods for the inclusion of NPs in thin film absorbers: sputtering on a one-dimensional sinusoidal grating with a certain period and amplitude [6]; using arrays [7]; evaporation, in which a very thin metal layer is deposited by vacuum evaporation and then annealed so that the metal islands coalesce into metal particles [8]; chemical solution deposition, where the device surface is exposed to a solution containing colloidal NPs and then blown dry [9]; imprint lithography, in which a sol–gel mask is defined by soft lithography using a rubber stamp, followed by metal evaporation and lift-off [10].

This study presents experimental results for a CdTe absorber with incorporated Au NPs. The SPR peaks of gold nanostructures can be tuned from the visible to the near infrared region by controlling their shape and periodicity [11]. The inert nature of gold and the instability of gold oxides at low temperature [12] make gold nanostructures well suited for various applications [11] including CdTe solar cells. One of the first techniques [13] used to prepare gold NPs is the reduction of $HAuCl_4$ by citrate in water (Turkevich method) [14]. Our experiments were performed using the same $HAuCl_4 \cdot 3H_2O$ reagent solution as a precursor for Au NPs. The Au NPs were incorporated into CdTe layers by spray pyrolysis, spin coating and sputtering methods, and the results from these methods were compared.

2. Materials and methods

CdTe thin films with a thickness of ~300 nm were prepared by close spaced sublimation (CSS) onto cleaned soda-lime glass substrates by taking 6N pure CdTe powder (Alfa Aesar) as the source material. The deposition was carried out at a pressure below $2 \cdot 10^{-6}$ Torr with the source to substrate distance of 0.7 cm. The films were deposited at the source temperature of 550 °C and at the substrate temperature of 300 °C, controlling the temperature through a K-type thermocouple. The deposition lasted for ~1 min, after which the chamber was slowly cooled down to 50 °C.

The Au NPs on the CdTe films were formed by three methods: spin coating, spray pyrolysis and sputtering. The spin coating was carried out with $HAuCl_4 \cdot 3H_2O$ ethanol solution at concentrations: 0.05 M, 0.075 M and 0.1 M at room temperature (RT) in two spin ramp rates: 600 rpm for 5 s and 1200 rpm for 20 s. After coating, samples were dried in air at ~85 °C for 40 min and air annealed on a hot plate at 380 °C for 1 h.

In the case of spray pyrolysis the Au NPs were deposited from the same $HAuCl_4$ solution on preheated CdTe/glass substrates placed onto a molten Sn bath. The substrate temperature was maintained at 360 °C with an accuracy of ±2 °C. The volume of the spray solution varied from 2.5 ml to 15 ml, while the solution concentration of Au^{3+} and the flow rate were kept constant for all CdTe/glass samples: 2 mM and 1 ml/min, respectively. After the coating no drying or annealing was applied for sprayed samples due to enough high temperature for decomposition of $AuCl_3$.

In a different approach, a thin film of Au was sputtered for 40–70 s on glass substrate, which was then air annealed at 500 °C for 30 min to coalesce into compact Au grains. The grains were coated with a CSS CdTe film.

All the CdTe-Au layers were characterized by X-ray diffraction (XRD), optical transmission and reflection spectra, scanning electron microscopy (SEM) and energy-dispersive X-ray spectroscopy (EDX). XRD measurements were collected with a Rigaku Ultima IV diffractometer with Cu Kα radiation in the Bragg–Brentano (θ–2θ) geometry. The crystallite size and lattice parameters were calculated using the PDXL Version 1.4.0.3 software on the Rigaku system. The optical total transmittance and reflectance spectra of the films were measured in the wavelength range of 200–2500 nm on a Jasco V-670 UV–VIS–NIR spectrophotometer equipped with an integrating sphere. A high resolution SEM apparatus (Zeiss EVO-MA15) was used at a 10 kV operating voltage, while the elemental composition was analyzed by EDX with the Röntec EDX XFlash 3001 detector and the Oxford Instruments INCA Energy system.

3. Results and discussion

3.1. Spin coated Au solution on CdTe layer

Spin coating of $HAuCl_4$ on CdTe layers and subsequent annealing in air at 380 °C resulted in Au NPs and wires binding the NPs as a web and covering the surface of CdTe layer (Fig. 1). We assume that these wires represent the residual cadmium oxychloride ($2CdO \cdot CdCl_2$) created in the air annealing process [15] as an intermediate product of the $HAuCl_4$ reaction with CdTe [16]. From SEM images, the mean size and spacing of Au NPs were estimated as on the order of 100 nm and 300 nm, respectively.

The SPR valley at 577 nm in the transmittance spectrum of the CdTe–Au layer (Fig. 2a) confirms the plasmonic absorption resonance of incorporated Au NPs. However, this effect did not lead to a noticeable enhancement in the absorption over the entire wavelength range (Fig. 2b). Moreover, reflectance and transmittance spectra show the disappearance of the CdTe absorption edge in the 800 nm region (Fig. 2a) indicating the removal of the CdTe film in the spin coating process.

To understand the disappearance of the CdTe band edge (Fig. 2), we analyzed the reactions that may take place in the air annealing process of the CdTe layer with spin coated $HAuCl_4$ solution: oxidation of CdTe to $CdTeO_3$ ($CdO \cdot TeO_2$) (1), decomposition of $HAuCl_4$ (2, 3), and formation of $CdCl_2$ and Te_2 (4). These reactions may form the viscous phase of $CdTe + CdTeO_3 + CdCl_2$ flux [15,17], which has a low melting temperature (<400 °C).

$$0.5O_2(g) + CdTe(s) \rightarrow CdTeO_3(s) \tag{1}$$

$$CdTeO_3(s) + 2CdTe(s) \rightarrow 3CdO(s) + 1.5Te_2(g) \tag{1a}$$

$$2HAuCl_4(s) \rightarrow 2HCl(g) + 2AuCl_3(s) \tag{2}$$

$$2AuCl_3(s) \rightarrow 2Au(s) + 3Cl_2(g) \tag{3}$$

$$2HCl(g) + 2Cl_2(g) + 3CdTe(s) \rightarrow 3CdCl_2(s) + H_2Te(g) + Te_2(g) \tag{4}$$

We carried out some calculations to evaluate the impact of the $CdCl_2$-containing flux on the CdTe film after coating with the $HAuCl_4 \cdot 3H_2O$ solution. Au NPs with both a diameter and spacing of 50 nm (minimal values for a 2% absorption enhancement [18]) cover 0.4 of a 1 cm^2 CdTe film surface. Based on the mass of gold, the amount of gold in the $HAuCl_4$ solution was calculated as $1.32 \cdot 10^{-5}$ mol. As each mole of $HAuCl_4$ yields two moles of $CdCl_2$, a 1 cm^2 CdTe film will contain $2.65 \cdot 10^{-5}$ mol of $CdCl_2$. Therefore, the mass ratio of $CdCl_2$ (created by $HAuCl_4$) to CdTe is at least 25. Considering the solubility of CdTe in the $CdCl_2$ flux (~25%) [19], it is highly likely that the CdTe film will disappear. Therefore, though the RT spin coating of Au NPs from $HAuCl_4$ solution on CdTe layers is a very simple technique, it should be discarded due to the substantial removal of CdTe by the reactions with chloride flux in the annealing process.

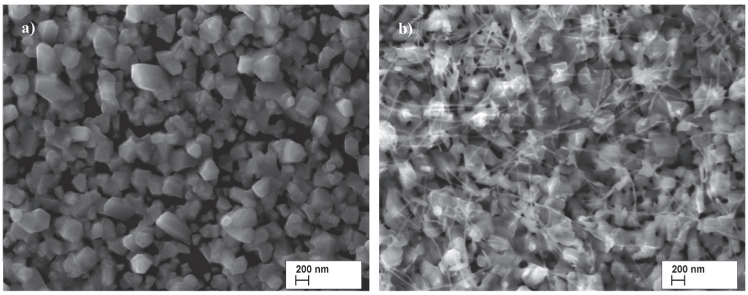

Fig. 1. SEM surface view of CdTe film: as deposited (a) and with Au NPs obtained by spin coating (b).

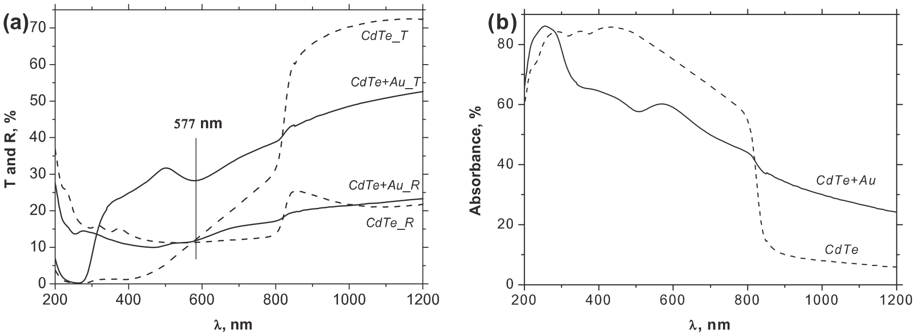

Fig. 2. Transmittance, reflectance (a) and absorbance (b) spectra of as deposited CdTe films (CdTe) and CdTe with Au NPs obtained by spin coating (CdTe + Au).

3.2. Spray pyrolysis of Au solution on the CdTe layer

Compared to RT spin coating of large drops of Au-containing solution, during the spray coating the $HAuCl_4$ interacts differently with the CdTe absorber due to the relatively high temperature of the substrate (360 °C). At this temperature the reaction products quickly evaporate, leaving a CdTe surface free of the oxychloride residuals which can damage the CdTe absorber as in the case of spin coating method.

Spraying the $HAuCl_4$ solution in various amounts (from 2.5 ml to 15 ml) generated distributions of Au NPs with different spacing and size (Fig. 3a). For better understanding of the microscopic images of sprayed Au on CdTe and on reference glass are presented in Fig. 3b. At the lowest quantity of the $HAuCl_4$ solution, Au NPs with a mean size of 30 nm were formed (determined from XRD data by Sherrer's formula), while increasing the amount of the solution led these crystallites to coagulate into grains with the size from 80 nm to 100 nm (Fig. 3b). The size of these Au-containing grains corresponds to the optimal theoretical diameter of 90 nm and spacing of 202 nm, which should result in a 50% increase in absorption and a 36% increase in the efficiency of a CdTe solar cell [5].

The absorption of the CdTe layer was enhanced over the 400–1000 nm wavelength range when Au NPs are sprayed on top of the CdTe layer (Fig. 4b). The plasmonic effect was observed for the CdTe-Au samples sprayed with 10 and 15 ml of $HAuCl_4$ solution (Fig. 4a). For these amounts of $HAuCl_4$ solution the XRD patterns recorded greater intensity of (021) and (300) AuCd peaks at 29.7 and 38.2 degrees (Fig. 5). The SPR peak located at 570 nm (Fig. 4a) shifts slightly to the red due to the decreased separation of NPs [20] and the increased size of agglomerated Au crystallites at 15 ml Au solution. In addition, the 570 nm peak becomes broader as the particle diameter increases to 100 nm with increasing the amount of sprayed $HAuCl_4$ from 10 to 15 ml (Fig. 3b). This broadening is attributed to the enhanced radiation damping by large particles as described by Hu et al. [11].

Appearance of the (200) CdTe peak at 30.76 deg for 10 and 15 ml of $HAuCl_4{\cdot}3H_2O$ solution (Fig. 5) show that higher quantity of Au increases the amount of chloride flux which actively promotes recrystallization of CdTe. It is interesting that the Au NPs obtained by spray pyrolysis on CdTe surface actually consist of an Au–Cd (JCPDS 01-072-8534) [22] inter-metallic phase (Fig. 5). We attribute this to fact that the substrate temperature (360 °C) is higher than the eutectic temperature of the Au–Cd system (310 °C) [21]. Increasing the amount of sprayed $HAuCl_4$ solution does not affect the size of these AuCd crystallites (~30 nm), rather contributing to the agglomeration of these Au NPs into larger grains (Fig. 3). The appearance of the peak of $AuTe_2$ (JCPDS 03-065-2443) [22] in the XRD pattern of the CdTe + 15Au layer might be linked with the presence of metallic Te (1a, 4). These phases indicate that an excess of $HAuCl_4$ is present on the CdTe surface. Therefore, 10 ml of $HAuCl_4{\cdot}3H_2O$ solution is sufficient to spray on the CdTe surface to obtain the plasmonic effect.

3.3. Sputtered and annealed Au between glass surface and the CdTe layer

The surface morphology of sputtered and annealed Au NPs on glass substrate illustrates a quite uniform distribution of isolated particles with a mean diameter of 40 nm (Fig. 6a). These NPs agglomerate as large particles with diameters varying from 1 to 3 μm (Fig. 6b). In addition, the agglomeration of gold NPs was con-

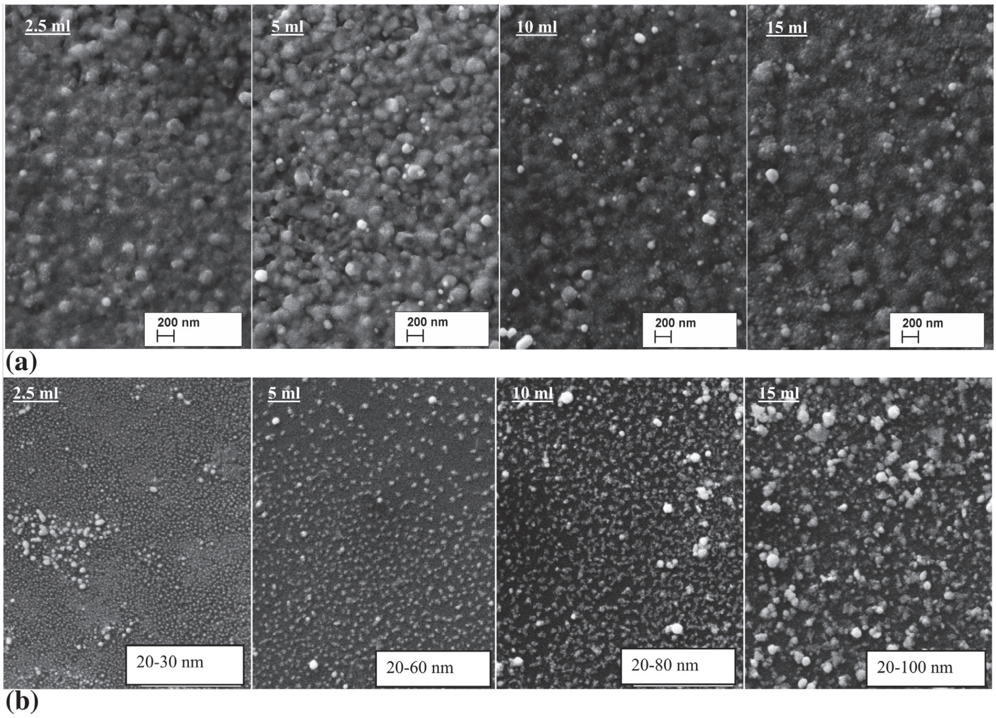

Fig. 3. SEM images of Au particles obtained by spray pyrolysis on CdTe thin films (a) and on corresponding reference glass (estimated size of Au-containing grains is included) (b) at different amounts of $HAuCl_4$: 2.5 ml, 5 ml, 10 ml and 15 ml.

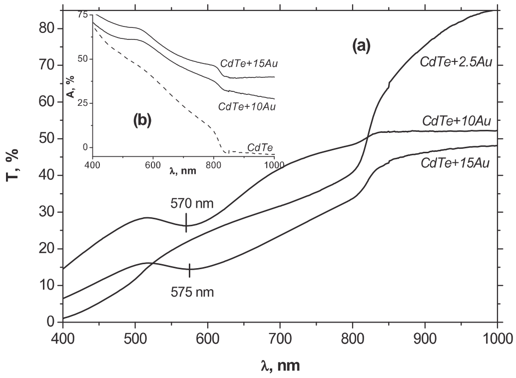

Fig. 4. Total transmittance (a) and absorption (b) spectra of CdTe films sprayed with different amounts of Au solution: 2.5 ml, 10 ml and 15 ml.

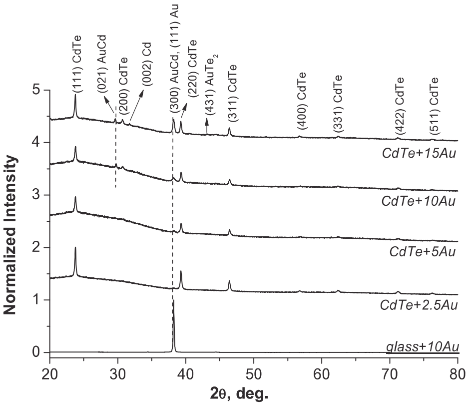

Fig. 5. XRD pattern of reference glass and CdTe films spray-coated with different amounts of Au solution.

firmed by the color transition of glass–Au samples from reddish to purple after annealing in air. This is due to the plasmonic coupling between particles [11]. The size distribution and spacing of Au particles are not strongly influenced by the duration of sputtering (Fig. 6b and c).

The transmittance spectra of glass–Au–CdTe samples (Fig. 7) exhibit surface plasmon features at 592 nm and 570 nm for the Au/glass samples sputtered under CdTe for 40 s and 70 s, respectively. Fig. 7 suggests that 40 s of Au sputtering is sufficient for CdTe absorber with an efficient plasmon effect. However, the 570 nm SPR peak which corresponds to the 70 s Au sputtering is closer to the theoretical SPR of Au particles. The shift of the SPR peak compared to CdTe samples with spin coated and sprayed Au on top could be related to the dependence of the SPR peak position on the dielectric constant of the surrounding environment [23]. The inter-metallic $Au_{0.3}Te_{0.7}$ phase (Fig. 8), which has a high concentration of charge carriers, may form a shell for plasmon Au NPs and slightly shift the peak position.

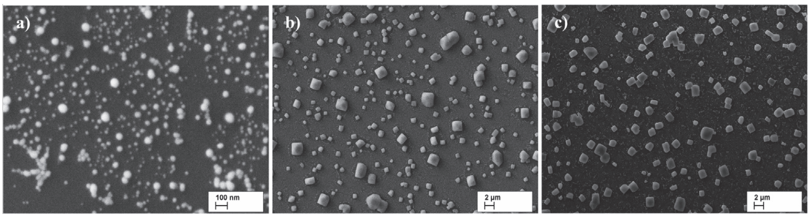

Fig. 6. SEM surface views of glass following Au sputtering for 40 s (a and b) and 70 s (c) after air annealing.

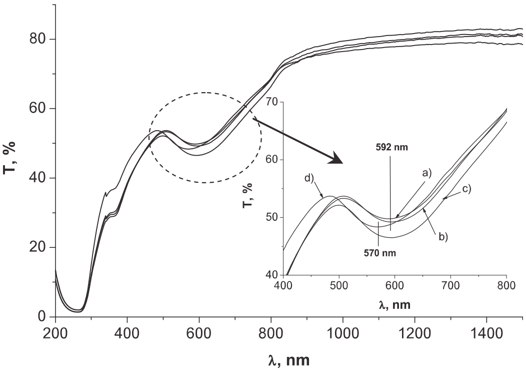

Fig. 7. Transmittance spectra of sputtered and air-annealed Au on glass and CSS deposition of CdTe. Duration of sputtering: 40 s (a), 50 s (b), 60 s (c) and 70 s (d).

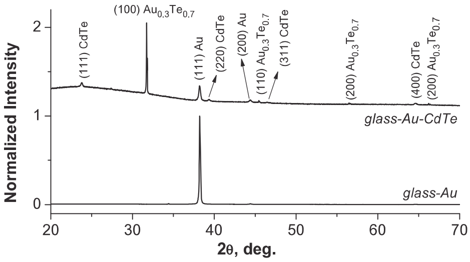

Fig. 8. XRD pattern of Au sputtered for 70 s and annealed on glass and coated with CdTe film.

The appearance of the $Au_{0.3}Te_{0.7}$ (JCPDS 01-074-5406) [22] phase (Fig. 8) can be explained by its thermodynamic stability [21,24], the dissociation of CdTe and the high volatility of Cd, resulting in excess of metallic Te. The radiative heat transport in the CSS process of CdTe deposition could locally increase the substrate temperature above 300 °C for fractions of seconds, allowing for the reaction between Au and Te to produce $Au_{0.3}Te_{0.7}$. Although the sputtering method generates pure Au particles, the following deposition of CdTe absorber results in formation of additional phases around the Au NPs which contribute to the shift of the SPR peak.

4. Conclusions

In this work we tried to incorporate gold NPs into CdTe layer to obtain the plasmonic effect that would increase the absorption in the CdTe absorber. Au NPs were deposited on the CdTe films by three different methods: spin coating, spray pyrolysis and sputtering. Each method resulted in different plasmonic effects for CdTe layers. Spin coating of $HAuCl_4$ solution and air annealing generate oxychloride residuals and substantially remove the CdTe layer. For this reason, the spin coating method should be discarded.

Both spray and sputtering methods formed Au-containing NPs with diameters of 30–40 nm. Neither increases in the amount of $HAuCl_4$ nor in the sputtering time of gold increase the size of Au NPs but rather tend to agglomerate these particles into grains with diameters of ~90 nm and 1–3 µm for the spray and sputtering methods, respectively. To summarize, the spray pyrolysis forms on CdTe surface Au NPs close to the size suggested by the theoretical studies, but sputtering technique provide more pure NPs. However, interactions between CdTe and Au at high temperature resulting in the formation of inter-metallic compounds, such as AuCd, $AuTe_2$ or $Au_{0.3}Te_{0.7}$, are characteristic of both techniques. The formation of these inter-metallic phases, which likely depend on deposition parameters, such as substrate temperature or how this temperature is maintained, is an important peculiarity for CdTe layers. Due to the chemical interaction between gold and CdTe, the high temperature processes for formation of Au NPs should be avoided.

So, additional studies should be performed to better understand the process of formation of Au-containing NPs and other compounds on CdTe layers; this will allow to control the plasmonic effect and to improve the absorber properties.

Acknowledgements

This study was supported by European Regional Development Fund (“Efficient plasmonic absorbers for solar cells” (3.2.1101.12-0023) and TK114 “Mesosystems: Theory and Applications” (3.2.0101.11-0029)), by European Social Fund’s Doctoral Studies and Internationalization Program Dora, by European Union through 7th FP project FLEXSOLCELL (GA-2008-230861), by Estonian Science Foundation Grant ETF9142 and by Estonian Ministry of Education and Research (SF0140092s08, IUT19-4).

References

[1] M. Edoff, Ambio 41 (2012) 112–118.
[2] H.A. Atwater, A. Polman, Nat. Mater. 9 (2010) 205–213.
[3] First Solar Sets 20.4% Record for CdTe Solar Cell Efficiency, <http://investor.firstsolar.com/releasedetail.cfm?ReleaseID=828273> (Accessed 25 February 2014).
[4] A. Feltrin, A. Freundlich, Renew. Energy 33 (2008) 180–185.
[5] Q. Gu, J. Phys. D Appl. Phys. 43 (2010) (465101.1-5).
[6] F.-J. Haug, T. Söderström, O. Cubero, V. Terrazzoni-Daudrix, C. Ballif, J. Appl. Phys. 104 (2008) (064509.1-7).
[7] C. Hägglund, M. Zäch, G. Petersson, B. Kasemo, Appl. Phys. Lett. 92 (2008) (053110.1-3).
[8] S. Pillai, K.R. Catchpole, T. Trupke, G. Zhang, J. Zhao, M.A. Green, Appl. Phys. Lett. 88 (2006) (161102.1-3).
[9] D. Derkacs, S.H. Lim, P. Matheu, W. Mar, E.T. Yu, Appl. Phys. Lett. 89 (2006) (093103.1-3).

[10] V.E. Ferry, M.A. Verschuuren, M.C. van Lare, R.E.I. Schropp, H.A. Atwater, A. Polman, Nano Lett. 11 (2011) 4239–4245.
[11] M. Hu, J. Chen, Z.-Y. Li, L. Au, G.V. Hartland, X. Li, M. Marquez, Y. Xia, Chem. Soc. Rev. 35 (2006) 1084–1094.
[12] M.A. Montero, M.R. Gennero de Chiavlo, A.C. Chiavlo, J. Mater. Chem. 19 (2009) 3276–3280.
[13] M.-C. Daniel, D. Astruc, Chem. Rev. 104 (2004) 293–346.
[14] J. Turkevich, P.C. Stevenson, J. Hillier, Discuss. Faraday Soc. 11 (1951) 55–75.
[15] J. Hiie, V. Valdna, A. Taklaja, Mater. Res. Soc. Symp. 763 (2003) B8.22.1–B8.22.6.
[16] P. Ramamurthy, E.A. Secco, Can. J. Chem. 47 (1969) 1045–1050.
[17] J. Hiie, Thin Solid Films 431–432 (2003) 90–93.
[18] T. Repän, S. Pikker, L. Dolgov, A. Loot, J. Hiie, M. Krunks, I. Sildos, Energy Procedia 44 (2014) 229–233.
[19] V.N. Tomashik, V.I. Gritziff, Phase Diagrams of II–VI Semiconductor Compounds, Naukova Dumka, Kiev, 1982 (in Russian).
[20] J.B. Lassiter, J. Aizpurua, L.I. Hernandez, D.W. Brandl, I. Romero, S. Lal, J.H. Hafner, P. Nordlander, N.J. Halas, Nano Lett. 8 (2008) 1212–1218.
[21] H. Okamoto, T.B. Massalski, Bull. Alloy Phase Diagrams 7 (52–53) (1986) 172–173.
[22] International Centre for Diffraction Data (ICDD), PDF-2 Release, 2008.
[23] U. Kreibig, M. Vollmer, Optical Properties of Metal Clusters, Springer, Berlin, 1995.
[24] J. Wang, X. Gang Lu, B. Sundman, X. Su, J. Alloys Compd. 407 (2006) 106–111.

PAPER V

N. Spalatu, J. Hiie, N. Maticiuc, M. Krunks, A. Katerski, V. Mikli, I. Sildos, Plasmonic effect of spray-deposited Au nanoparticles on the performance of CSS CdS/CdTe solar cells, Applied Surface Science 350 (2015) 69-73.

Applied Surface Science 350 (2015) 69–73

Contents lists available at ScienceDirect

Applied Surface Science

journal homepage: www.elsevier.com/locate/apsusc

Plasmonic effect of spray-deposited Au nanoparticles on the performance of CSS CdS/CdTe solar cells

N. Spalatu[a], J. Hiie[a], N. Maticiuc[a], M. Krunks[a], A. Katerski[a], V. Mikli[a], I. Sildos[b]

[a] Department of Materials Science, Tallinn University of Technology, Tallinn, Ehitajate tee 5, Tallinn 19086, Estonia
[b] Institute of Physics, University of Tartu, Riia 142, Tartu 51014, Estonia

ARTICLE INFO

Article history:
Received 30 November 2014
Received in revised form 15 March 2015
Accepted 9 April 2015
Available online 18 April 2015

Keywords:
CdS/CdTe solar cell
Au nanoparticles
Spray pyrolysis
Plasmonic effect

ABSTRACT

In order to improve the light trapping in CdTe thin-film solar cells, a coupling with plasmonic nanostructures is believed to increase the absorption as a result of the enhanced electric field and forward-scattering upon excitation of the surface plasmon resonance (SPR). The simulation studies suggest a technological feasibility of placing metallic nanoparticles on CdTe before back contacting. We have applied the chemical spray pyrolysis of different amounts of $HAuCl_4$ ethanol solution to incorporate Au nanoparticles into CdTe and used this layer in CdS/CdTe solar cells. CdTe films show the SPR effect and an enhanced light absorption in the visible range of spectrum, whereas the CdS/CdTe solar cell have an improved conversion efficiency due to the presence of Au nanoparticles. The processes responsible for these advancements are discussed.

1. Introduction

Thin-film solar cells show a great promise for the next generation of solar power conversion due to their cheap processing, good flexibility, light weights and ease of integration. Moreover, significantly reduced cell thickness of 1–2 μm for thin-film cells makes them more easily meet the requirement that minority carrier diffusion length should be several times the base thickness to have all the photo-carriers collected [1,2]. Polycrystalline thin-film CdTe has shown considerable promise for terrestrial photovoltaic applications due to its near-optimum bandgap, high absorption coeffcient and relative ease of film formation. However, the low light absorption at nearbandgap range and the limited availability of tellurium (Te) element on the earth have become two major concerns for further developments of CdTe photovoltaics towards future terawatt-scale electricity generation [2,3]. It is critical to structure the CdTe solar cell such that light can be trapped inside the active layer by increased absorbance. Recently, metallic nanoparticles have been suggested to be effective solutions for broadband light absorption enhancement for ultrathin semiconductor layers in thin-film solar cells. Metal nanoparticles provide absorption enhancement in solar cells by two mechanisms: (i) light trapping and optical path length enhancement via scattering of incoming light, and (ii) local absorption enhancement by strong local fields caused by plasmon resonance of the particle [4,5]. Combining periodic metal nanostructures on top of ultrathin CdTe layer was theoretically demonstrated to be an effective approach to enhance broadband optical absorption by the CdTe absorber. The optimal parameters of metal nanoparticles (NPs) to enhance the absorption of CdTe absorber were studied theoretically [2,6] but yet to our knowledge no experimental data confirmed these results. Moreover, little information is available about suitable technology for the incorporation of metal NPs into CdTe absorber layer. There are several methods reported for fabricating Au NP films from presynthesized colloidal Au NPs (with or without ligands), such as sol gel, in situ preparation, immersion, atomic layer deposition (ALD), plasma assisted physical vapour deposition (PAPVD), etc. [7–9]. There are also reports on direct formation of Au NPs on a glass substrate using ultrasonic spray pyrolysis techniques [10,11].

In our previous studies we simulated one of the easiest ways to embed nanoparticles into the absorber layer closer to the back contact [6] and we tried to incorporate the Au NPs into CdTe and $CuInS_2$ thin films [12,13]. Au NPs were deposited onto CdTe layers by spray pyrolysis, spin coating and sputtering methods, each method resulting in different plasmonic effects for CdTe layers [12]. However, the spray pyrolysis forms on CdTe surface Au NPs with a size close to that suggested by the theoretical studies. In this paper we aim to prove the technological feasibility of placing chemically sprayed Au NPs between CdTe absorber and Te/Ni back contact and to achieve enhanced efficiencies of CdS/CdTe solar cells.

2. Materials and methods

CdS/CdTe solar cells were fabricated in a superstrate configuration [14,15] by close spaced sublimation (CSS) on Pilkington Tec 15 glass coated with a 200 nm thick fluorine doped tin oxide (FTO)

http://dx.doi.org/10.1016/j.apsusc.2015.04.065
0169-4332/© 2015 Elsevier B.V. All rights reserved.

layer. Films of CdS, 100–150 nm thick, were deposited at 400 °C from high-purity 5 N CdS powder. CdTe films with a thickness of 2–3 μm were deposited onto CdS layers from 99.999% purity CdTe powder. Source material was heated in the graphite boat by a tungsten coils connected to the main power supply through temperature controller with K-type thermocouple. The substrate was fixed at a distance of 7 mm from the source material, which also was heated by a similar system, while the type K thermocouple was placed above the substrate. The source and substrate temperatures were kept at 600 and 450 °C respectively. The residual pressure in the main chamber during deposition was below 2×10^{-6} torr. The deposition time of each film was 5 min, after which the source and substrate heaters were switched off. The chamber was opened after the temperature fell below 30 °C. After deposition the CdTe/CdS/FTO/glass samples were soaked in a saturated $CdCl_2$ methanol solution (2.15 g/100 mL methanol), followed by a 30 min heat treatment in air at 420 °C in a two-zone tube furnace. Anhydrous, 99.99% $CdCl_2$ was supplied from Alfa Aesar. The heat treated samples were rinsed in deionized water and etched in standard NP (H_3PO_4:HNO_3:H_2O) solution to remove chloride and oxide residues. After CdS/CdTe deposition and heat treatment in $CdCl_2$, Au NPs on the CdTe surface were formed by spray pyrolysis as described in [12]. After the coating no drying or annealing was applied for sprayed samples due to enough high temperature for decomposition of $AuCl_3$. Finally, Te/Ni bi-layer back contact by thermal evaporation was applied for CdS/CdTe cells. Tellurium prior to back contact formation, is a heavily (p^+) doped film at the back surface of CdTe which aim is to reduce the Schottky barrier or to moderate its width adjacent to the contact. The structure of the plasmonic devices was glass/FTO/CdS/CdTe/Au NPs/Te/Ni. Several plasmonic CdTe/CdS solar cells with sprayed Au NPs from different amounts of $HAuCl_4$ solution (2.5–15 ml) were compared with a similar devices without Au NPs.

The morphology of the CdTe film and CdS/CdTe cross-section was investigated by scanning electron microscopy (SEM) Zeiss EVO-MA15 at an operating voltage of 10 kV, while the elemental composition was analyzed by energy-dispersive X-ray spectroscopy (EDX) with the Röntec EDX XFlash 3001 detector and the Oxford Instruments INCA Energy system. The crystallographic structure of the films was studied by X-ray diffraction (XRD) with a Rigaku Ultima IV diffractometer (Cu Kα radiation, λ = 1.5406 Å, 40 kV at 40 mA) in the Bragg–Brentano (θ–2θ) geometry. The crystallite size and lattice parameters were calculated using the PDXL Version 1.4.0.3 software on the Rigaku system. Solar cells were characterized by current–voltage (*I*–*V*) and external quantum efficiency (EQE) measurements under AM1.5 simulated standard test conditions. The quantum efficiency of the solar cells was measured in the range of 300–1000 nm on a Newport Oriel kit that uses 300 W Xe-lamp. The dispersed light from the Xe lamp, incident on the solar cell as monochromatic light was optically chopped at 30 Hz.

3. Results and discussion

Au NPs with different shapes are randomly distributed and partly agglomerated directly on the CdTe surface (Figs. 1 and 2). A mean size of 30 nm for NPs was reached for the lowest quantity of sprayed $HAuCl_4$ solution, whereas increased amounts of solution led these crystallites to coagulate into grains with size from 80 nm to 100 nm. The size of these Au-containing grains corresponds to the optimal theoretical diameter of 90 nm, which should result in a 50% increase in absorption and a 36% increase in the efficiency of a CdTe solar cell [2]. The analysis of phase composition of the Au-sprayed CdTe surface indicated that an Au-containing grain consisted of Au and intermetallic compounds of AuCd and $AuTe_2$ as well as residuals of flux decomposition such as CdO, TeO_2 and non-volatilized $CdCl_2$ (Fig. 3). The XRD results were confirmed by EDX analysis (Table 1) which indicated to the 1:1 ratio of Cd and Te in the reference structure and to the increased contamination of the surface by oxides and chlorides with increasing amount of Au solution from 2.5 to 15 ml.

It should be mentioned that after $CdCl_2$ heat treatment and etching of CdTe/CdS structure the surface of CdTe film remained smooth without residuals (Fig. 2a), while in the case of $HAuCl_4$ sprayed films the CdTe surface has been coated with a tightly adherent thin layer

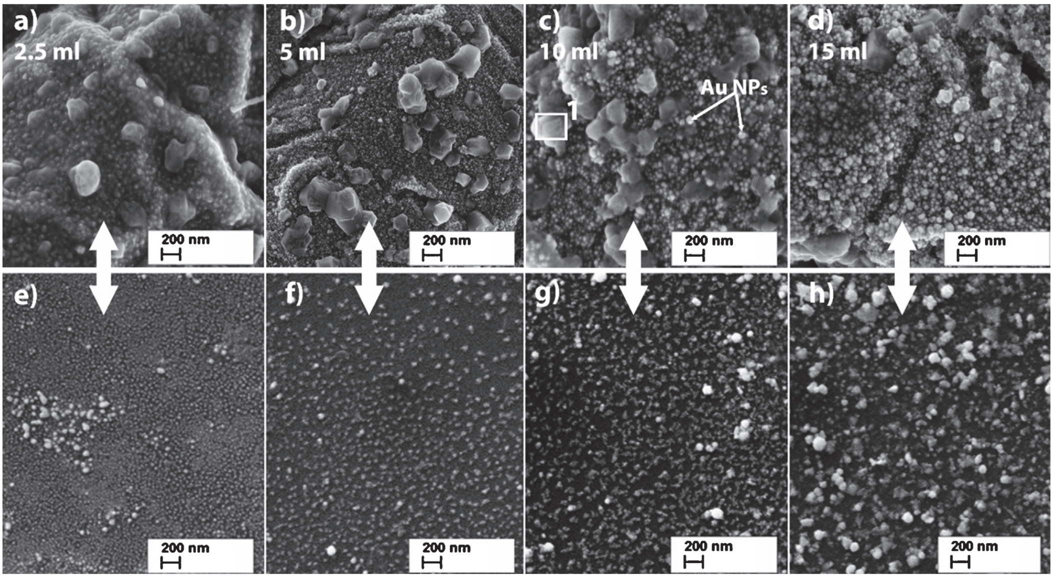

Fig. 1. SEM images of sprayed Au on CdTe/CdS thin films (a–d) and on reference glass (e–h) from various amounts of $HAuCl_4$ solution: 2.5, 5, 10 and 15 ml. Insert 1 on (c) represent a secondary particle grown in spray process and the area analyzed by EDX.

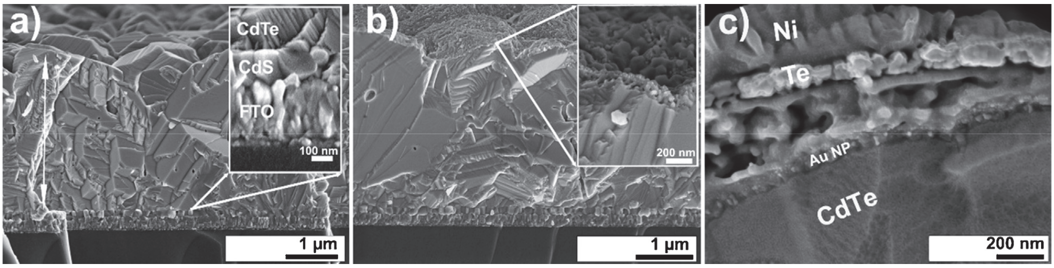

Fig. 2. Cross-sectional images of CdTe/CdS/FTO/glass reference sample (a), after spray-coating of 10 ml $HAuCl_4$ solution (b) and 15 ml, with back contact In/Te/Ni (c).

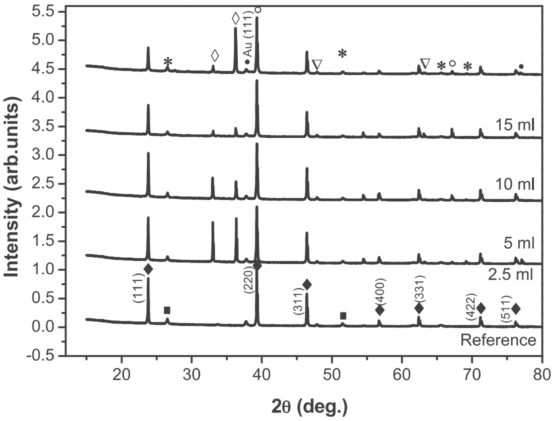

Fig. 3. XRD pattern of full solar cell structures In/Ni/Te/CdTe/CdS/FTO/glass before (reference) and after spray-coating with different amounts of Au solution (2.5, 5, 10 and 15 ml): ■, CdS (JCPDS 01-089-0440); ♦, CdTe (JCPDS 01-070-8043); •, Au (JCPDS 01-071-4614); *, AuCd (JCPDS 01-072-0833); *, $AuTe_2$ (JCPDS 03-065-2307); ◊, CdO (JCPDS 00-005-0640; □, TeO_2 (JCPDS 00-052-0795); $CdCl_2$ (JCPDS 01-089-1568); ○, Te (JCPDS 05-001-0207) Ni (JCPDS 01-071-4653); ◊, In (JCPDS 00-70-2888).

Table 1
Elemental composition of CdTe/CdS structures sprayed with different amounts of Au solution.

Sample	Scanned area	Elements, at.%				
		Cd	Te	Cl	Au	O
Reference	300 × 300 µm	50.46	49.48		–	–
AuNP-2.5 ml	300 × 300 µm	41.12	38.35	1.78	0.83	17.92
AuNP-5 ml	300 × 300 µm	31.55	31.00	4.84	1.70	30.92
AuNP-7.5 ml	300 × 300 µm	29.91	29.86	5.17	2.00	33.06
AuNP-10 ml	300 × 300 µm	27.27	26.77	8.22	2.48	35.25
AuNP-10 ml	Area 1 on Fig. 1c	60.94	–	39.06	–	–
AuNP-15 ml	300 × 300 µm	22.69	22.79	9.59	3.17	41.76

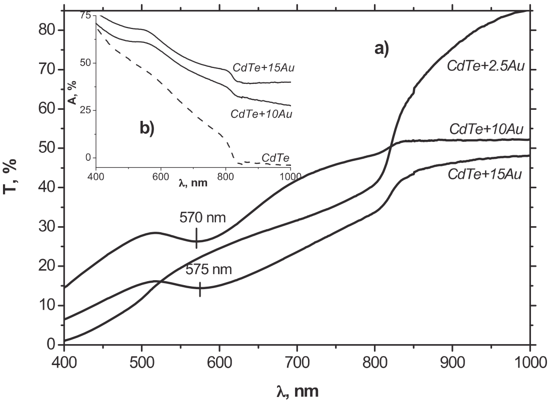

Fig. 4. Total transmittance (a) and absorption (b) spectra of CdTe films sprayed with different amounts of Au solution: 2.5 ml, 10 ml and 15 ml.

(Fig. 2b). This surface layer is composed of aggregated grains about 200 nm and their EDX analysis showed a significantly higher concentration of Cl compared to the large surface (Table 1 and Fig. 1c). However, at the maximum amount of $HAuCl_4$ solution (15 ml) this surface layer became porous, substantially reducing the contacting area of the back contact with CdTe (Fig. 2c).

In order to show the role of spray-deposited Au NPs onto CdTe surface, including the effect of NP size and solution concentration, we followed the plasmonic effect for the CdTe–Au layers from the spectral responces (Fig. 4). The absorption of the CdTe layer was enhanced over the 400–1000 nm wavelength range when Au NPs are sprayed on the top (Fig. 4b). The SPR peak at 570 nm was observed only for CdTe–Au samples sprayed with 10 ml and 15 ml of $HAuCl_4$ solution (Fig. 4a). For these amounts of $HAuCl_4$ solution the XRD patterns of CdTe–Au layers recorded greater intensity of AuCd peaks. The 570 nm peak (Fig. 4a) shifts slightly to the red due to the decreased separation of NPs [16] and to the increased size of agglomerated Au crystallites at 15 ml Au solution. In addition, the 570 nm peak became broader as the particle diameter increased to 100 nm with increasing amount of sprayed $HAuCl_4$ from 10 ml to 15 ml (Fig. 1). This broadening was attributed to the enhanced radiation damping by large particles [17].

When these CdTe–Au layers were used in a CdS/CdTe solar cell, the EQE is enhanced in the region of 600–840 nm (Fig. 5) due to the gain in optical absorptance induced by the SPR. A condition for this effect to occur is a lower refractive index of the scattering medium – Au (1.5–0.2 [18]) compared to the absorbing medium – CdTe (3–2.6 [19]) and Te (4.8). When larger volumes of the Au-containing solution are sprayed (up to 15 ml) onto the CdTe, a further relative increase in the EQE is evident due to the previously mentioned broadening of 570 nm peak of plasmonic resonance. Highest EQE was revealed by the CdS/CdTe structure with 10 ml sprayed solution. At this amount of solution an optimal balance between the size and distribution of Au NPs and additionally formed aggregate grains (Fig. 2) caused a wide absorption band and a corresponding EQE gain due to the overlapping plasmon resonances [20]. However the EQE spectra look similar for both 10 ml and 15 ml of Au-containing solution onto CdTe, indicating that higher amount of $HAuCl_4$ formed larger conglomerates with no change in the interparticle distance.

The representative photovoltaic *I*–*V* characteristics and parameters of the CdS/CdTe solar cell with and without Au NPs (Fig. 6 and

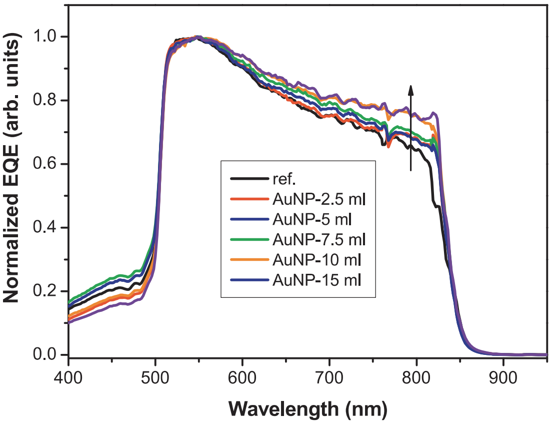

Fig. 5. Normalized EQE curves of CdTe/CdS solar cells sprayed with different amounts of Au solution.

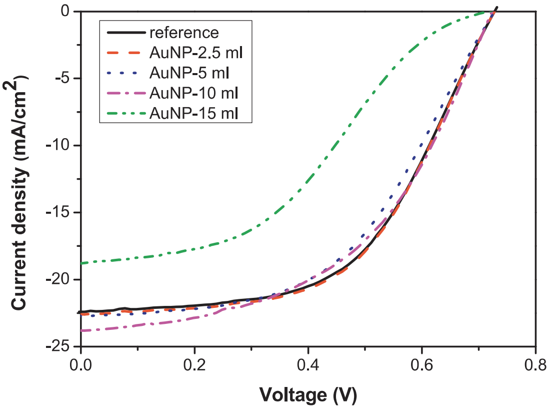

Fig. 6. *J*–*V* characteristics of CdTe/CdS solar cells with and without (reference) sprayed Au NPs.

Table 2
Device results.

Sample	V_{oc} (mV)	J_{sc} (mA/cm^2)	FF (%)	Eff (%)
Reference	740	22.4	50	8.3
AuNP-2.5 ml	740	22.5	50	8.3
AuNP-5 ml	740	22.7	49	8.3
AuNP-7.5 ml	740	23.8	49	8.6
AuNP-10 ml	740	24	50	8.9
AuNP-15 ml	720	18.5	39	5.2

Table 2) indicate to a variation in the photovoltaic parameters of plasmonic CdTe/CdS solar cell using different amounts of sprayed Au solution. The conversion efficiency was gradually improved from 8.3% to 9%, clearly determined by the enhancement of the J_{sc} value from 22.4 to 24 mA/cm^2 (Table 2). The highest conversion efficiency was reached for the CdS/CdTe solar cell with 10 ml HAuCl$_4$ solution. The same sample showed better absorption and EQE gain (Fig. 5) due to the optimal balance between the size (80 nm) and distribution of Au NPs.

When the amount of HAuCl$_4$ solution was higher than the optimal 10 ml, both J_{sc} and *FF* values degraded due to the porous surface layer that substantially reduced the contacting area of the back contact with CdTe (Fig. 2c). These results together with EQE improvement suggest that the conversion efficiency enhancement of plasmonic CdTe/CdS solar cell has been generated by the fundamental optical engineering via the incorporated Au NPs. We also admit that the charge transfer at the back contact region (Ni/Te/gold/CdTe) might be improved compared to the reference back contact (Ni/Te/CdTe), but the presence of the resonant absorption peaks in the red/infrared region (Fig. 4) bring clear arguments for the contribution by plasmon effect.

4. Conclusions

The chemical spray pyrolysis of HAuCl$_4$ ethanol solution was shown to be a feasible and flexible method to deposit Au NPs of 30–100 nm size onto CdTe surface. Also, the CdTe-Au layers were implemented in a CdS/CdTe solar cell. The EQE of the solar cell was enhanced in the range of 600–840 nm, highest EQE being revealed by the CdS/CdTe structure with 10 ml sprayed solution. The same amount of sprayed Au-containing solution onto CdTe has contributed to the increase of J_{sc} and efficiency of plasmonical CdS/CdTe solar cell from 22.4 to 24 mA/cm^2 and from 8.3% to 9%, respectively. This is attributed to the suitable size of Au NPs that cause a large absorption and a corresponding EQE enhancement due to the overlapping plasmon resonances. Higher amount of sprayed solution (15 ml) generates a porous surface layer onto CdTe and degrades the photovoltaic parameters of CdS/CdTe SC. Additional studies should be performed to better understand the influence of Au NPs parameters on the final characteristics of CdS/CdTe solar cells and to improve their efficiency.

Acknowledgements

This study was supported by European Regional Development Fund ("Efficient plasmonic absorbers for solar cells" (3.2.1101.12-0023) and TK114 "Mesosystems: Theory and Applications" (3.2.0101.11-0029)), by Estonian Ministry of Education and Research (IUT19-4), by European Union through 7th FP project FLEXSOLCELL (GA-2008-230861) and by Estonian Science Foundation grant ETF9142. The authors wish to thank Dr. Erki Kärber for valuable discussions.

References

[1] J. Poortmans, V. Arkhipov, Thin Film Solar Cells: Fabrication, Characterization and Applications, Wiley-VCH, New York, 2006.
[2] Q. Gu, Plasmonic metallic nanostructures for efficient absorption enhancement in ultrathin CdTe-based photovoltaic cells, J. Phys. D: Appl. Phys. 43 (2010) 465101.
[3] H.A. Atwater, A. Polman, Plasmonics for improved photovoltaic devices, Nat. Mater. 9 (3) (2010) 205–213.
[4] S. Pillai, M.A. Green, Plasmonics for photovoltaic applications, Sol. Energy Mater. Sol. Cells 94 (9) (2010) 1481–1486.
[5] D.M. Schaadt, B. Feng, E.T. Yu, Enhanced semiconductor optical absorption via surface plasmon excitation in metal nanoparticles, Appl. Phys. Lett. 86 (6) (2005) 063106.
[6] T. Repän, S. Pikker, L. Dolgov, A. Loot, J. Hiie, M. Krunks, I. Sildos, Increased efficiency inside the CdTe solar cell absorber caused by plasmonic metal nanoparticles, Energy Proc. 44 (2014) 229–233.
[7] V. Kumar, H. Wang, Plasmonic Au nanoparticles for enhanced broad band light absorption in inverted organic photovoltaic de-vices by plasma assisted physical vapour deposition, Org. Electron. 14 (2) (2013) 560–568.
[8] J. Schmitt, P. Machtle, D. Eck, H. Mohwald, C.A. Helm, Preparation and optical properties of colloidal gold monolayers, Langmuir 15 (1999) 3256–3266.
[9] L. Amelao, D. Barreca, G. Bottaro, A. Gasparotto, E. Tondello, M. Ferroni, S. Polizzi, Au/TiO$_2$ nanosystems: a combined RF-sputtering/sol–gel approach, Chem. Mater. 16 (2004) 3331–3338.
[10] M.D.L. Garza, I. Líopez, I. Gíomez, In situ synthesis and deposition of gold nanoparticles with different morphologies on glass and ITO substrate by ultrasonic spray pyrolysis, Adv. Mater. Sci. Eng. 2013 (2013) 1–5.
[11] N. Kumar, V.K. Komarala, V. Dutta, Deposition of gold nanoparticle films using spray pyrolysis technique: tunability of SPR band by electric field, Phys. Status Solidi RRL 6 (9–10) (2012) 406–408.

[12] N. Maticiuc, N. Spalatu, A. Katerski, J. Hiie, V. Mikli, M. Krunks, L. Dolgov, I. Sildos, Plasmonic modification of CdTe thin films by gold nanoparticles: methods, difficulties and solutions, Microelectron. Eng. 126 (2014) 173–178.

[13] E. Kärber, A. Katerski, I. Oja Acik, V. Mikli, A. Mere, I. Sildos, M. Krunks, Low-cost plasmonic solar cells by chemical spray pyrolysis method, Beilstein J. Nanotechnol. 5 (2014) 2398–2402.

[14] N. Spalatu, J. Hiie, V. Valdna, M. Caramana, N. Maticiuc, V. Mikli, T. Potlog, M. Krunks, V. Lughi, Properties of the $CdCl_2$ air-annealed CSS CdTe thin films, Energy Proc. 44 (2014) 85–95.

[15] N. Spalatu, J. Hiie, V. Mikli, M. Krunks, V. Valdna, N. Maticiuc, T. Raadik, M. Caraman, Effect of $CdCl_2$ annealing treatment on structural and optoelectronic properties of close spaced sublimation CdTe/CdS thin film solar cells vs deposition conditions, Nano Lett. 582 (2015) 128–133.

[16] J.B. Lassiter, J. Aizpurua, L.I. Hernandez, D.W. Brandl, I. Romero, S. Lal, J.H. Hafner, P. Nordlander, N.J. Halas, Close encounters between two nanoshells, Nano Lett. 8 (2008) 1212–1218.

[17] U. Kreibig, M. Vollmer, Optical Properties of Metal Clusters, Springer, Berlin, 1995.

[18] A.D. Rakić, A.B. Djurišić, J.M. Elazar, M.L. Majewski, Optical properties of metallic films for vertical-cavity optoelectronic devices, Appl. Opt. 37 (1998) 5271–5283.

[19] P. Hlıídek, J. Bok, J. Franc, R. Grill, Refractive index of CdTe: spectral and temperature dependence, J. Appl. Phys. 90 (2001) 1672–1674.

[20] T. Repan, L. Dolgov, A. Katerski, I. Oja Acik, E. Kärber, A. Mere, V. Mikli, M. Krunks, I. Sildos, $CuInS_2$ solar cell absorber plasmonically modified by gold nanoparticles, Appl. Phys. A 117 (2014) 455–458.

APPENDIX B

CURRICULUM VITAE

1. Personal data

Name: Nicolae Spalatu
Date and place of birth: 26.02.1986, Telenesti, Moldova
E-mail address: nicolae.spalatu@ttu.ee

2. Education

Educational institution	Graduation year	Education (field of study/degree)
“Anton Crihan” Gymnasium, Sîngerei, Moldova	2003	Secondary education
Faculty of Physics and Engineering, Moldova State University, Chişinău	2008	Semiconductor Physics/Bachelor degree
Faculty of Physics and Engineering, Moldova State University, Chişinău	2010	Theoretical Physics/Master degree
Faculty of Chemical and Materials Technology, Tallinn University of Technology	2013 - ...	Doctoral studies

3. Language competence/skills

Language	Level
Romanian	Native
English	Fluent
Russian	Fluent

4. Special courses

Period	Educational or other organisation
05.09-07.09.2016	FMTDK Autumn School “New Trends in Chemistry, Physics, Material Science and Environmental Technology” Pühajärve, Estonia

14 May 2015	Workshop of E-MRS 2015 Spring Meeting: “EUROPE IN MOTION EUROSUNMED symposium WA-Advanced materials and technologies for renewable energies”, Lille, France
15 September 2014	Workshop of Science and Applications of Thin Films, Conference & Exhibition (SATF 2014): “Thin Films in Photovoltaic Cells and Energy”, CESME, IZMIR, TURKEY
25 May 2014	Workshop of E-MRS 2014 Spring Meeting: “Young Scientist Tutorial on Characterization Techniques for Thin-Film Solar Cells”, Lille, France
2012-2014	Graduate school „Functional materials and technologies FMTDK“, Tallinn University of Technology, Estonia
26 May 2013	Workshop of E-MRS 2013 Spring Meeting: “Nanostructures for solar cells with optimized solar spectrum usage ”, Strasbourg, France

5. Professional employment

Period	Organisation	Position
2006 - 2011	Faculty of Physics and Engineering, Moldova State University, Chisinau, Moldova	Laboratory Assistant
2009 - 2013	Faculty of Physics and Engineering, Moldova State University, Chisinau, Moldova	Early stage researcher
2013 - …	Faculty of Chemical and Materials Technology, Tallinn University of Technology, Estonia	Junior Research Fellow

6. Research activity, including honors and thesis supervised

Projects

01.01.2008 – 31.12.2013	Thin film and nanostructured materials by chemical methods (SF 2008);
01.10.2009 – 30.09.2013	Development of flexible single and tandem II-VI based high efficiency thin film solar cells,

	FLEXCOLCELL (International agreement, FP7);
01.01.2012 – 31.12.2015	Absorber layers by chemical spray pyrolysis for nanostructured solar cells (ETF 2012);
01.01.2012 – 31.12.2015	Thin film solar cells on the basis of chalcogenide layers deposited from water solution (ETF 2012);
01.07.2012 – 31.12.2015	Efficient plasmonic absorbers for solar cells (National R&D program „Materials technology“);
01.01.2014 – 31.12.2019	Thin films and nanomaterials by wet-chemical methods for next-generation photovoltaics (IUT19-4, 2014);
01.01.2016 – 01.03.2023	Advanced materials and high-technology devices for sustainable energetics, sensorics and nanoelectronics (TK141, 2016).

Awards

2016	Gala of the students originally from Moldova, 28.12.2016, Chisinau, Moldova, Diploma;
2011	The 15th International Conference "Inventica", 08.06-10.06.201, Iasi, Romania, Diploma of Honor (co-author);
2011	European Exhibition of Creativity and Innovation, 14.05.2011, Iasi, Romania, Gold medal (co-author);
2010	33st International Semiconductor Conference CAS 2010, organized by IEEE, 13.10-15.10.2010, Sinaia, Romania, Best Student Paper;
2008	31st International Semiconductor Conference CAS 2008, organized by IEEE, 13.10-15.10.2008, Sinaia, Romania, Best Student Paper.

Supervision

01.09.2014 – 31.05.2016	Wangjun Yang, Master's Degree, “Influence of secondary thermal annealing on the properties of $CdS/CdTe:CdCl_2:O_2$ structure”, Tallinn University of Technology, Faculty of Chemical and Materials Technology, Department of Materials Science, Laboratory of Thin Film Chemical Technologies.

Defended dissertations

2010 Development and physical properties study of flexible $CdTe/CdS/ITO/Poly$ thin film solar cells, master's thesis (Moldova State University), supervisor: Associate Professor Tamara Potlog.

2008 $CdS/CdTe$-based thin film solar cells, bachelor's thesis (Moldova State University), supervisor: Associate Professor Tamara Potlog.

LIST OF PUBLICATIONS

1. **N. Spalatu**, M. Krunks, J. Hiie, Structural and optoelectronic properties of $CdCl_2$ activated CdTe thin films modified by multiple thermal annealing, *Thin Solid Films* (2016) *in press,* http://dx.doi.org/10.1016/j.tsf.2016.09.042.
2. I. Caraman, **N. Spalatu**, I. Evtodiev, D. Untila, L. Leontie, M. Caraman, Photoelectric and photoluminescence properties of CdTe–GaTe composite, *Physica Status Solidi B* 253 (2016) 2515-2522.
3. W. Yang, **N. Spalatu**, N. Maticiuc, M. Krunks, J. Hiie, Influence of the secondary thermal annealing on the properties of $CdTe/CdS:CdCl_2:O_2$ structure, *Proceedings of 13th International Conference of Young Scientists on Energy Issues*, May 26-27 (2016) Kaunas, Lithuanian Energy Institute, VII-220−VII-225.
4. **N. Spalatu**, J. Hiie, V. Mikli, M. Krunks, V. Valdna, N. Maticiuc, et al., Effect of $CdCl_2$ annealing treatment on structural and optoelectronic properties of close spaced sublimation CdTe/CdS thin film solar cells vs deposition conditions, *Thin Solid Films* 582 (2015) 128-133.
5. **N. Spalatu**, J. Hiie, N. Maticiuc, M. Krunks, A. Katerski, V. Mikli, I. Sildos, Plasmonic effect of spray-deposited Au nanoparticles on the performance of CSS CdS/CdTe solar cells, *Appl. Surf. Sci.* 350 (2015) 69-73.
6. N. Maticiuc, **N. Spalatu**, V. Mikli, J. Hiie, Impact of CdS annealing atmosphere on the performance of CdS-CdTe solar cell, *Appl. Surf. Sci.* 350 (2015) 14-18.
7. A. Graf, N. Maticiuc, **N. Spalatu**, V. Mikli, A. Mere, A. Gavrilov, J. Hiie, Electrical characterization of annealed chemical bath-deposited CdS films and their application in superstrate configuration CdTe/CdS solar cells, *Thin Solid Films* 582 (2015) 351-355.
8. **N. Spalatu**, J. Hiie, V. Valdna, M. Caraman, N. Maticiuc, V. Mikli, et al., Properties of the $CdCl_2$ air-annealed CSS CdTe thin films, *Energy Procedia* 44 (2014) 85-95.
9. N. Maticiuc, **N. Spalatu**, A. Katerski, J. Hiie, V. Mikli, M. Krunks, et al., Plasmonic modification of CdTe thin films by gold nanoparticles: Methods, difficulties and solutions, *Microelectron. Eng.* 126 (2014) 173-178.
10. N. Maticiuc, M. Kukk, **N. Spalatu**, T. Potlog, M. Krunks, V. Valdna, J. Hiie, Comparative study of CdS films annealed in neutral, oxidizing and reducing atmospheres, *Energy Procedia* 44 (2014) 77-84.
11. L. Leontie, I. Evtodiev, **N. Spalatu**, M. Caraman, S. Evtodiev, O. Racovet, M. Girtan, C. Focsa, Optical and photosensitive properties of lamellar nanocomposites obtained by Cd intercalation of GaTe, *Journal of Alloys and Compounds*, 584 (2014) 542 - 545.

12. T. Raadik, J. Krustok, R. Josepson, J. Hiie, T. Potlog, **N. Spalatu**, Temperature dependent electroreflectance study of CdTe solar cells, *Thin Solid Films*, 535 (2013) 279 - 282.
13. T. Potlog, **N. Spalatu**, N. Maticiuc, J. Hiie, V. Valdna, V. Mikli, A. Mere, Structural reproducibility of CdTe thin films deposited on different substrates by close space sublimation method, *Phys. Status Solidi A* 209 (2012) 272-276.
14. T. Potlog, **N. Spalatu**, A. Mere, J. Hiie, V. Mikli, A comparative study of the thin-film CdTe solar cells with ZnSe/TCO and CdS/TCO buffers layers. In: *Materials Research Society Symposium Proceedings*: San Francisco, CA; 25 - 29 April (2011) 51-56.
15. T. Potlog, **N. Spalatu**, V. Fedorov, N. Maticiuc, C. Antoniuc, J. Hiie, et al., The performance of thin film solar cells employing photovoltaic ZnSe/CdTe, CdS/CdTe and ZnTe/CdTe heterojunctions. In: *Proceedings of the 37th IEEE: Photovoltaic Specialists Conference (PVSC)*: 2011 Jun 19-24; Seattle, USA (001365-001370).
16. **N. Spalatu**, T. Potlog, D. Serban, ZnSe films prepared by close-spaced sublimation and their influence on ZnSe/CdTe solar cell performance. In: *Proceedings of the International semiconductor conference (CAS 2011)*: 2011 Oct 11-13; Sinaia, Romania. Bucharest: I.E.E.E. Press (2011) 451-454.
17. N. Maticiuc, V. Nicorici, **N. Spalatu**, D. Scortescu, T. Potlog, J. Hiie, et al., Electrical properties of thermally annealed CdS thin films obtained by chemical bath deposition. In: *Proceedings of the International semiconductor conference (CAS 2011)*: 2011 Oct 11-13; Sinaia, Romania. Bucharest: I.E.E.E. Press (2011) 455-458.
18. T. Potlog, **N. Spalatu**, V. Ciobanu, J. Hiie, A. Mere, V. Mikli, V. Valdna, Analysis of fill factor losses in thin film CdS/CdTe photovoltaic devices. *Moldavian Journal of the Physical Sciences*, 9(3-4), (2010) 363-367.
19. N. Maticiuc, T. Potlog, **N. Spalatu**, Optical properties of CdS thin films deposited by close space sublimation. In: *Proceedings of International Semiconductor Conference (CAS 2010)*: 2010 Oct 11-13; Sinaia, Romania. Bucharest: I.E.E.E. Press (2010) 537-540.
20. T. Potlog V. Botnariuc L. Gorceac **N. Spalatu**, N. Maticiuc, S. Raievschi, The characterization of the CdS-based solar cell heterojunctions. In: *Proceedings of International Semiconductor Conference (CAS 2010)*: 2010 Oct 11-13; Sinaia, Romania. Bucharest: I.E.E.E. Press (2010) 105-108.
21. T. Potlog, **N. Spalatu**, The fabrication of cadmium-telluride thin film solar cells. In: Proceedings of the International Conference (CAS 2009), 32nd Edition, October 12-14, Sinaia, Romania Bucharest: I.E.E.E. Press (2009) 177-180.
22. T. Potlog, N. Maticiuc, **N. Spalatu**, L. Ghimpu, The influence of interface states on the efficiency of CdTe photovoltaic devices. In: *ICPTTFN- XII Intern. Conference*, Ivano-Frankivsk, Ukraine. (2009) 310.

23. T. Potlog, **N. Spalatu**, N. Maticiuc, Flexible ITO/CdS/CdTe solar cells. In: *ICPTTFN- XII Intern. Conference*, Ivano-Frankivsk, Ukraine. (2009) 363.
24. **N. Spalatu**, T. Potlog, Influence of temperature and illumination on photovoltaic parameters of CdS/CdTe solar cells, *Abstracts of International Conference of Young researchers*, Chişinău, 5-6 november, Moldova, (2009) 39.
25. T. Potlog, N. Maticiuc, **N. Spalatu**, Capacitance-voltage characteristics of the CdS/CdTe/Te heterojunctions. In: *Proceedings of the International Conference (CAS 2008),* 31th Edition: October 13-15, 2008, Sinaia, Romania. IEEE, (2008) 317-320.
26. T. Potlog, **N. Spalatu**, Influence of the substrate temperature on photovoltaic parameters of CdS/CdTe solar cells fabricated by close space sublimation. In: *Proceedings of the International Conference (CAS 2008)*, 31th Edition, October 13-15, Sinaia, Romania, (2008) 117-120.
27. T. Potlog, **N. Spalatu**, Effect of the Ni/CdTe back contact on capacitance-voltage characteristics of Ni/CdTe/CdS/SnO2 Solar Cells, *Proceedings of the 4th Int. Conf. on Materials Science and Condensed Matter Physics*, September 23-26, (2008) 106.
28. T. Potlog, **N. Spalatu**, N. Maticiuc, Carrier transport mechanism in CdS/CdTe solar cells prepared by close space sublimation. In: *Proceedings of the 4th Int. Conf. on Materials Science and Condensed Matter Physics*, September 23-26, Chisinau, Moldova, (2008) 81.
29. T. Potlog, **N. Spalatu**, N. Maticiuc, V. Movila, Analysis of thin film CdTe solar cells fabricated by close space sublimation. In: *Proceedings of 23rd European Photovoltaic Solar Energy Conference and Exhibition*: Valencia, Spain, Sept 1-5 (2008) 105.
30. **N. Spalatu**, N. Maticiuc, T. Potlog, Flexible photovoltaic system based on CdTe. In: *Student Conferences, 14-18 april, CEP USM*, Chisinau, Moldova, (2008) 71.
31. T. Potlog, **N. Spalatu**, N. Capros, Development of the technology of fabrication ITO/CdS/CdTe solar cells on flexible substrates. *Scientific Journal Studia Universitas* USM, Chisinau, Moldova, (2007) 252.

ELULOOKIRJELDUS

1. Isikuandmed

Ees- ja perekonnanimi:	Nicolae Spalatu
Sünniaeg ja -koht:	26.02.1986, Telenesti, Moldova
Kodakondsus:	Moldova
E-posti aadress:	nicolae.spalatu@ttu.ee

2. Hariduskäik

Õppeasutus (nimetus lõpetamise ajal)	Lõpetamise aeg	Haridus (eriala/kraad)
"Anton Crihan" Gümnaasium, Sîngerei, Moldova	2003	Keskharidus
Füüsika ja Tehnika Teaduskonna, Moldova Riigi Ülikool	2008	Semiconductor Füüsika/Bakalaureusekraad
Füüsika ja Tehnika Teaduskonna, Moldova Riigi Ülikool	2010	Teoreetiline füüsika /Magistrikraad
Tallinna Tehnikaülikool, Keemia-ja materjalitehnoloogia õppekava	2013 - ...	Doktorantuur

3. Keelteoskus

Keel	Tase
Rumeenia	Emakeel
Inglise	Kõrgtase
Vene	Kõrgtase

4. Täiendusõpe

Õppimise aeg	Täiendusõppe korraldaja nimetus
05.09-07.09.2016	FMTDK Suvekool, Pühajärve, Eesti
14 May 2015	Workshop of E-MRS 2015 Spring Meeting: "EUROPE IN MOTION EUROSUNMED symposium WA- Advanced materials and technologies for renewable energies", Lille, Prantsusmaa
15 September 2014	Workshop of Science and Applications of Thin Films, Conference & Exhibition (SATF 2014): "Thin Films in Photovoltaic Cells and

	Energy”, CESME, IZMIR, TÜRGI
25 May 2014	Workshop of E-MRS 2014 Spring Meeting: “Young Scientist Tutorial on Characterization Techniques for Thin-Film Solar Cells”, Lille, Prantsusmaa
2012-2014	TÜ ja TTÜ doktorikool „Funktsionaalsed materjalid ja tehnoloogiad” (FMTDK), Eesti
26 May 2013	Workshop of E-MRS 2013 Spring Meeting: “Nanostructures for solar cells with optimized solar spectrum usage ”, Strasbourg, Prantsusmaa

5. Teenistuskäik

Töötamise aeg	Tööandja nimetus	Ametikoht
2006 - 2011	Moldova Riigi Ülikool	Labori assistant
2009 - 2013	Moldova Riigi Ülikool	nooremteadur
2013 - …	Tallinna Tehnikaülikool, Keemia ja materjaliteaduse instituut	nooremteadur

6. Teadustegevus, sh tunnustused ja juhendatud lõputööd

Projektid

01.01.2008 – 31.12.2013	Õhukesekilelised ja nanostruktuursed materjalid keemilistel meetoditel (SF 2008);
01.10.2009 – 30.09.2013	Kõrge kasuteguriga õhukesekileliste elastsete mono- ja tandem päikesepatareide arendamine II-VI pooljuhtühendite baasil, FLEXCOLCELL (Välisleping, VII raamprogramm);
01.01.2012 – 31.12.2015	Absorberkihid keemilise pihustuspürolüüsi meetodil nanostruktuursetele päikesepatareidele (ETF9081);
01.01.2012 – 31.12.2015	Õhukesekilelised päikesepatareid vesilahustest sadestatud kalkogeniidsete kilede baasil (ETF9142);
01.07.2012 – 31.12.2015	Efektiivsed plasmoonilised absorberid päikesepatareidele (Riiklik T&A programm "Materjalitehnoloogia");
01.01.2014 – 31.12.2019	Õhukesed kiled ja nanomaterjalid keemilistel vedeliksadestusmeetoditel uue põlvkonna fotovoltseadistele (IUT 2014).

01.01.2016 – 01.03.2023	Uudsed materjalid ja kõrgtehnoloogilised seadmed energia salvestamise ja muundamise süsteemidele (TK141, 2016).

Tunnustused

2016	Diplom, Moldovast pärit tudengite gala, Chisinau (Moldova), 27. detsember 2016;
2011	Austamise Diplom, XV rahvusvaheline konverents "Inventica", Iasi (Rumeenia) 8-10 juuni 2011 (kaasautor);
2011	Kuldmedal, Euroopa Näitus loovuse ja innovatsiooni, Iasi (Rumeenia), 14. mai 2011 (kaasautor);
2010	Parim õpilane raamatut CAS konverentsi 2010, korraldas IEEE, Sinaia (Rumeenia), 13-15 Oktoober 2010;
2008	Parim õpilane raamatut CAS konverentsi 2008, korraldas IEEE, Sinaia (Rumeenia), 13-15 Oktoober 2008.

Juhtimine

01.09.2014 – 31.05.2016 Wangjun Yang, magistritöö, “Sekundaarse termilise käsitluse toime $CdS/CdTe:CdCl_2:O_2$ struktuuri omadustele”, Tallinna Tehnikaülikool, Keemia ja materjalitehnoloogia teaduskond, Materjaliteaduse instituut, Keemiliste kiletehnoloogiate teaduslaboratoorium.

Kaitstud lõputööd

2010 Painduvate õhukesekileliste CdTe/CdS/ITO polükristalsete päikesepatareide arendamine ja füüsikaliste omaduste uurimine, magistritöö (Moldova Riiklik Ülikool), juhendajad: Dotsent Tamara Potlog;

2008 Õhukesekihilised päikesepatareid CdS/CdTe baasil, bakalaureusetöö (Moldova Riiklik Ülikool), juhendajad: Dotsent Tamara Potlog.

DISSERTATIONS DEFENDED AT TALLINN UNIVERSITY OF TECHNOLOGY ON *NATURAL AND EXACT SCIENCES*

1. **Olav Kongas**. Nonlinear Dynamics in Modeling Cardiac Arrhytmias. 1998.
2. **Kalju Vanatalu**. Optimization of Processes of Microbial Biosynthesis of Isotopically Labeled Biomolecules and Their Complexes. 1999.
3. **Ahto Buldas**. An Algebraic Approach to the Structure of Graphs. 1999.
4. **Monika Drews**. A Metabolic Study of Insect Cells in Batch and Continuous Culture: Application of Chemostat and Turbidostat to the Production of Recombinant Proteins. 1999.
5. **Eola Valdre**. Endothelial-Specific Regulation of Vessel Formation: Role of Receptor Tyrosine Kinases. 2000.
6. **Kalju Lott**. Doping and Defect Thermodynamic Equilibrium in ZnS. 2000.
7. **Reet Koljak**. Novel Fatty Acid Dioxygenases from the Corals *Plexaura homomalla* and *Gersemia fruticosa.* 2001.
8. **Anne Paju**. Asymmetric oxidation of Prochiral and Racemic Ketones by Using Sharpless Catalyst. 2001.
9. **Marko Vendelin**. Cardiac Mechanoenergetics *in silico*. 2001.
10. **Pearu Peterson**. Multi-Soliton Interactions and the Inverse Problem of Wave Crest. 2001.
11. **Anne Menert**. Microcalorimetry of Anaerobic Digestion. 2001.
12. **Toomas Tiivel**. The Role of the Mitochondrial Outer Membrane in *in vivo* Regulation of Respiration in Normal Heart and Skeletal Muscle Cell. 2002.
13. **Olle Hints**. Ordovician Scolecodonts of Estonia and Neighbouring Areas: Taxonomy, Distribution, Palaeoecology, and Application. 2002.
14. **Jaak Nõlvak**. Chitinozoan Biostratigrapy in the Ordovician of Baltoscandia. 2002.
15. **Liivi Kluge**. On Algebraic Structure of Pre-Operad. 2002.
16. **Jaanus Lass**. Biosignal Interpretation: Study of Cardiac Arrhytmias and Electromagnetic Field Effects on Human Nervous System. 2002.
17. **Janek Peterson**. Synthesis, Structural Characterization and Modification of PAMAM Dendrimers. 2002.
18. **Merike Vaher**. Room Temperature Ionic Liquids as Background Electrolyte Additives in Capillary Electrophoresis. 2002.
19. **Valdek Mikli**. Electron Microscopy and Image Analysis Study of Powdered Hardmetal Materials and Optoelectronic Thin Films. 2003.
20. **Mart Viljus**. The Microstructure and Properties of Fine-Grained Cermets. 2003.
21. **Signe Kask**. Identification and Characterization of Dairy-Related *Lactobacillus.* 2003.
22. **Tiiu-Mai Laht**. Influence of Microstructure of the Curd on Enzymatic and Microbiological Processes in Swiss-Type Cheese. 2003.
23. **Anne Kuusksalu**. 2–5A Synthetase in the Marine Sponge *Geodia cydonium*. 2003.
24. **Sergei Bereznev**. Solar Cells Based on Polycristalline Copper-Indium Chalcogenides and Conductive Polymers. 2003.

25. **Kadri Kriis**. Asymmetric Synthesis of C_2-Symmetric Bimorpholines and Their Application as Chiral Ligands in the Transfer Hydrogenation of Aromatic Ketones. 2004.
26. **Jekaterina Reut**. Polypyrrole Coatings on Conducting and Insulating Substracts. 2004.
27. **Sven Nõmm**. Realization and Identification of Discrete-Time Nonlinear Systems. 2004.
28. **Olga Kijatkina**. Deposition of Copper Indium Disulphide Films by Chemical Spray Pyrolysis. 2004.
29. **Gert Tamberg**. On Sampling Operators Defined by Rogosinski, Hann and Blackman Windows. 2004.
30. **Monika Übner**. Interaction of Humic Substances with Metal Cations. 2004.
31. **Kaarel Adamberg**. Growth Characteristics of Non-Starter Lactic Acid Bacteria from Cheese. 2004.
32. **Imre Vallikivi**. Lipase-Catalysed Reactions of Prostaglandins. 2004.
33. **Merike Peld**. Substituted Apatites as Sorbents for Heavy Metals. 2005.
34. **Vitali Syritski**. Study of Synthesis and Redox Switching of Polypyrrole and Poly(3,4-ethylenedioxythiophene) by Using *in-situ* Techniques. 2004.
35. **Lee Põllumaa**. Evaluation of Ecotoxicological Effects Related to Oil Shale Industry. 2004.
36. **Riina Aav**. Synthesis of 9,11-Secosterols Intermediates. 2005.
37. **Andres Braunbrück**. Wave Interaction in Weakly Inhomogeneous Materials. 2005.
38. **Robert Kitt**. Generalised Scale-Invariance in Financial Time Series. 2005.
39. **Juss Pavelson**. Mesoscale Physical Processes and the Related Impact on the Summer Nutrient Fields and Phytoplankton Blooms in the Western Gulf of Finland. 2005.
40. **Olari Ilison**. Solitons and Solitary Waves in Media with Higher Order Dispersive and Nonlinear Effects. 2005.
41. **Maksim Säkki**. Intermittency and Long-Range Structurization of Heart Rate. 2005.
42. **Enli Kiipli**. Modelling Seawater Chemistry of the East Baltic Basin in the Late Ordovician–Early Silurian. 2005.
43. **Igor Golovtsov**. Modification of Conductive Properties and Processability of Polyparaphenylene, Polypyrrole and polyaniline. 2005.
44. **Katrin Laos**. Interaction Between Furcellaran and the Globular Proteins (Bovine Serum Albumin β-Lactoglobulin). 2005.
45. **Arvo Mere**. Structural and Electrical Properties of Spray Deposited Copper Indium Disulphide Films for Solar Cells. 2006.
46. **Sille Ehala**. Development and Application of Various On- and Off-Line Analytical Methods for the Analysis of Bioactive Compounds. 2006.
47. **Maria Kulp**. Capillary Electrophoretic Monitoring of Biochemical Reaction Kinetics. 2006.
48. **Anu Aaspõllu.** Proteinases from *Vipera lebetina* Snake Venom Affecting Hemostasis. 2006.

49. **Lyudmila Chekulayeva**. Photosensitized Inactivation of Tumor Cells by Porphyrins and Chlorins. 2006.
50. **Merle Uudsemaa**. Quantum-Chemical Modeling of Solvated First Row Transition Metal Ions. 2006.
51. **Tagli Pitsi**. Nutrition Situation of Pre-School Children in Estonia from 1995 to 2004. 2006.
52. **Angela Ivask**. Luminescent Recombinant Sensor Bacteria for the Analysis of Bioavailable Heavy Metals. 2006.
53. **Tiina Lõugas**. Study on Physico-Chemical Properties and Some Bioactive Compounds of Sea Buckthorn (*Hippophae rhamnoides* L.). 2006.
54. **Kaja Kasemets**. Effect of Changing Environmental Conditions on the Fermentative Growth of *Saccharomyces cerevisae* S288C: Auxo-accelerostat Study. 2006.
55. **Ildar Nisamedtinov**. Application of ^{13}C and Fluorescence Labeling in Metabolic Studies of *Saccharomyces* spp. 2006.
56. **Alar Leibak**. On Additive Generalisation of Voronoï's Theory of Perfect Forms over Algebraic Number Fields. 2006.
57. **Andri Jagomägi**. Photoluminescence of Chalcopyrite Tellurides. 2006.
58. **Tõnu Martma**. Application of Carbon Isotopes to the Study of the Ordovician and Silurian of the Baltic. 2006.
59. **Marit Kauk**. Chemical Composition of $CuInSe_2$ Monograin Powders for Solar Cell Application. 2006.
60. **Julia Kois**. Electrochemical Deposition of $CuInSe_2$ Thin Films for Photovoltaic Applications. 2006.
61. **Ilona Oja Açik**. Sol-Gel Deposition of Titanium Dioxide Films. 2007.
62. **Tiia Anmann**. Integrated and Organized Cellular Bioenergetic Systems in Heart and Brain. 2007.
63. **Katrin Trummal**. Purification, Characterization and Specificity Studies of Metalloproteinases from *Vipera lebetina* Snake Venom. 2007.
64. **Gennadi Lessin**. Biochemical Definition of Coastal Zone Using Numerical Modeling and Measurement Data. 2007.
65. **Enno Pais**. Inverse problems to determine non-homogeneous degenerate memory kernels in heat flow. 2007.
66. **Maria Borissova**. Capillary Electrophoresis on Alkylimidazolium Salts. 2007.
67. **Karin Valmsen**. Prostaglandin Synthesis in the Coral *Plexaura homomalla*: Control of Prostaglandin Stereochemistry at Carbon 15 by Cyclooxygenases. 2007.
68. **Kristjan Piirimäe**. Long-Term Changes of Nutrient Fluxes in the Drainage Basin of the Gulf of Finland – Application of the PolFlow Model. 2007.
69. **Tatjana Dedova**. Chemical Spray Pyrolysis Deposition of Zinc Sulfide Thin Films and Zinc Oxide Nanostructured Layers. 2007.
70. **Katrin Tomson**. Production of Labelled Recombinant Proteins in Fed-Batch Systems in *Escherichia coli*. 2007.
71. **Cecilia Sarmiento**. Suppressors of RNA Silencing in Plants. 2008.
72. **Vilja Mardla**. Inhibition of Platelet Aggregation with Combination of Antiplatelet Agents. 2008.

73. **Maie Bachmann**. Effect of Modulated Microwave Radiation on Human Resting Electroencephalographic Signal. 2008.
74. **Dan Hüvonen**. Terahertz Spectroscopy of Low-Dimensional Spin Systems. 2008.
75. **Ly Villo**. Stereoselective Chemoenzymatic Synthesis of Deoxy Sugar Esters Involving *Candida antarctica* Lipase B. 2008.
76. **Johan Anton**. Technology of Integrated Photoelasticity for Residual Stress Measurement in Glass Articles of Axisymmetric Shape. 2008.
77. **Olga Volobujeva**. SEM Study of Selenization of Different Thin Metallic Films. 2008.
78. **Artur Jõgi**. Synthesis of 4'-Substituted 2,3'-dideoxynucleoside Analogues. 2008.
79. **Mario Kadastik**. Doubly Charged Higgs Boson Decays and Implications on Neutrino Physics. 2008.
80. **Fernando Pérez-Caballero**. Carbon Aerogels from 5-Methylresorcinol-Formaldehyde Gels. 2008.
81. **Sirje Vaask**. The Comparability, Reproducibility and Validity of Estonian Food Consumption Surveys. 2008.
82. **Anna Menaker**. Electrosynthesized Conducting Polymers, Polypyrrole and Poly(3,4-ethylenedioxythiophene), for Molecular Imprinting. 2009.
83. **Lauri Ilison**. Solitons and Solitary Waves in Hierarchical Korteweg-de Vries Type Systems. 2009.
84. **Kaia Ernits**. Study of In_2S_3 and ZnS Thin Films Deposited by Ultrasonic Spray Pyrolysis and Chemical Deposition. 2009.
85. **Veljo Sinivee**. Portable Spectrometer for Ionizing Radiation "Gammamapper". 2009.
86. **Jüri Virkepu**. On Lagrange Formalism for Lie Theory and Operadic Harmonic Oscillator in Low Dimensions. 2009.
87. **Marko Piirsoo**. Deciphering Molecular Basis of Schwann Cell Development. 2009.
88. **Kati Helmja**. Determination of Phenolic Compounds and Their Antioxidative Capability in Plant Extracts. 2010.
89. **Merike Sõmera**. Sobemoviruses: Genomic Organization, Potential for Recombination and Necessity of P1 in Systemic Infection. 2010.
90. **Kristjan Laes**. Preparation and Impedance Spectroscopy of Hybrid Structures Based on $CuIn_3Se_5$ Photoabsorber. 2010.
91. **Kristin Lippur**. Asymmetric Synthesis of 2,2'-Bimorpholine and its 5,5'-Substituted Derivatives. 2010.
92. **Merike Luman**. Dialysis Dose and Nutrition Assessment by an Optical Method. 2010.
93. **Mihhail Berezovski**. Numerical Simulation of Wave Propagation in Heterogeneous and Microstructured Materials. 2010.
94. **Tamara Aid-Pavlidis**. Structure and Regulation of BDNF Gene. 2010.
95. **Olga Bragina**. The Role of Sonic Hedgehog Pathway in Neuro- and Tumorigenesis. 2010.

96. **Merle Randrüüt**. Wave Propagation in Microstructured Solids: Solitary and Periodic Waves. 2010.
97. **Marju Laars**. Asymmetric Organocatalytic Michael and Aldol Reactions Mediated by Cyclic Amines. 2010.
98. **Maarja Grossberg**. Optical Properties of Multinary Semiconductor Compounds for Photovoltaic Applications. 2010.
99. **Alla Maloverjan**. Vertebrate Homologues of Drosophila Fused Kinase and Their Role in Sonic Hedgehog Signalling Pathway. 2010.
100. **Priit Pruunsild**. Neuronal Activity-Dependent Transcription Factors and Regulation of Human *BDNF* Gene. 2010.
101. **Tatjana Knjazeva**. New Approaches in Capillary Electrophoresis for Separation and Study of Proteins. 2011.
102. **Atanas Katerski**. Chemical Composition of Sprayed Copper Indium Disulfide Films for Nanostructured Solar Cells. 2011.
103. **Kristi Timmo.** Formation of Properties of $CuInSe_2$ and $Cu_2ZnSn(S,Se)_4$ Monograin Powders Synthesized in Molten KI. 2011.
104. **Kert Tamm**. Wave Propagation and Interaction in Mindlin-Type Microstructured Solids: Numerical Simulation. 2011.
105. **Adrian Popp**. Ordovician Proetid Trilobites in Baltoscandia and Germany. 2011.
106. **Ove Pärn**. Sea Ice Deformation Events in the Gulf of Finland and This Impact on Shipping. 2011.
107. **Germo Väli**. Numerical Experiments on Matter Transport in the Baltic Sea. 2011.
108. **Andrus Seiman**. Point-of-Care Analyser Based on Capillary Electrophoresis. 2011.
109. **Olga Katargina**. Tick-Borne Pathogens Circulating in Estonia (Tick-Borne Encephalitis Virus, *Anaplasma phagocytophilum*, *Babesia* Species): Their Prevalence and Genetic Characterization. 2011.
110. **Ingrid Sumeri**. The Study of Probiotic Bacteria in Human Gastrointestinal Tract Simulator. 2011.
111. **Kairit Zovo**. Functional Characterization of Cellular Copper Proteome. 2011.
112. **Natalja Makarytsheva**. Analysis of Organic Species in Sediments and Soil by High Performance Separation Methods. 2011.
113. **Monika Mortimer**. Evaluation of the Biological Effects of Engineered Nanoparticles on Unicellular Pro- and Eukaryotic Organisms. 2011.
114. **Kersti Tepp**. Molecular System Bioenergetics of Cardiac Cells: Quantitative Analysis of Structure-Function Relationship. 2011.
115. **Anna-Liisa Peikolainen**. Organic Aerogels Based on 5-Methylresorcinol. 2011.
116. **Leeli Amon**. Palaeoecological Reconstruction of Late-Glacial Vegetation Dynamics in Eastern Baltic Area: A View Based on Plant Macrofossil Analysis. 2011.
117. **Tanel Peets**. Dispersion Analysis of Wave Motion in Microstructured Solids. 2011.

118. **Liina Kaupmees**. Selenization of Molybdenum as Contact Material in Solar Cells. 2011.
119. **Allan Olspert**. Properties of VPg and Coat Protein of Sobemoviruses. 2011.
120. **Kadri Koppel**. Food Category Appraisal Using Sensory Methods. 2011.
121. **Jelena Gorbatšova**. Development of Methods for CE Analysis of Plant Phenolics and Vitamins. 2011.
122. **Karin Viipsi**. Impact of EDTA and Humic Substances on the Removal of Cd and Zn from Aqueous Solutions by Apatite. 2012.
123. **David Schryer**. Metabolic Flux Analysis of Compartmentalized Systems Using Dynamic Isotopologue Modeling. 2012.
124. **Ardo Illaste**. Analysis of Molecular Movements in Cardiac Myocytes. 2012.
125. **Indrek Reile**. 3-Alkylcyclopentane-1,2-Diones in Asymmetric Oxidation and Alkylation Reactions. 2012.
126. **Tatjana Tamberg**. Some Classes of Finite 2-Groups and Their Endomorphism Semigroups. 2012.
127. **Taavi Liblik**. Variability of Thermohaline Structure in the Gulf of Finland in Summer. 2012.
128. **Priidik Lagemaa**. Operational Forecasting in Estonian Marine Waters. 2012.
129. **Andrei Errapart**. Photoelastic Tomography in Linear and Non-linear Approximation. 2012.
130. **Külliki Krabbi**. Biochemical Diagnosis of Classical Galactosemia and Mucopolysaccharidoses in Estonia. 2012.
131. **Kristel Kaseleht**. Identification of Aroma Compounds in Food using SPME-GC/MS and GC-Olfactometry. 2012.
132. **Kristel Kodar**. Immunoglobulin G Glycosylation Profiling in Patients with Gastric Cancer. 2012.
133. **Kai Rosin**. Solar Radiation and Wind as Agents of the Formation of the Radiation Regime in Water Bodies. 2012.
134. **Ann Tiiman**. Interactions of Alzheimer's Amyloid-Beta Peptides with Zn(II) and Cu(II) Ions. 2012.
135. **Olga Gavrilova**. Application and Elaboration of Accounting Approaches for Sustainable Development. 2012.
136. **Olesja Bondarenko**. Development of Bacterial Biosensors and Human Stem Cell-Based *In Vitro* Assays for the Toxicological Profiling of Synthetic Nanoparticles. 2012.
137. **Katri Muska**. Study of Composition and Thermal Treatments of Quaternary Compounds for Monograin Layer Solar Cells. 2012.
138. **Ranno Nahku**. Validation of Critical Factors for the Quantitative Characterization of Bacterial Physiology in Accelerostat Cultures. 2012.
139. **Petri-Jaan Lahtvee**. Quantitative Omics-level Analysis of Growth Rate Dependent Energy Metabolism in *Lactococcus lactis*. 2012.
140. **Kerti Orumets**. Molecular Mechanisms Controlling Intracellular Glutathione Levels in Baker's Yeast *Saccharomyces cerevisiae* and its Random Mutagenized Glutathione Over-Accumulating Isolate. 2012.
141. **Loreida Timberg**. Spice-Cured Sprats Ripening, Sensory Parameters Development, and Quality Indicators. 2012.

142. **Anna Mihhalevski**. Rye Sourdough Fermentation and Bread Stability. 2012.
143. **Liisa Arike**. Quantitative Proteomics of *Escherichia coli*: From Relative to Absolute Scale. 2012.
144. **Kairi Otto**. Deposition of In_2S_3 Thin Films by Chemical Spray Pyrolysis. 2012.
145. **Mari Sepp**. Functions of the Basic Helix-Loop-Helix Transcription Factor TCF4 in Health and Disease. 2012.
146. **Anna Suhhova**. Detection of the Effect of Weak Stressors on Human Resting Electroencephalographic Signal. 2012.
147. **Aram Kazarjan**. Development and Production of Extruded Food and Feed Products Containing Probiotic Microorganisms. 2012.
148. **Rivo Uiboupin**. Application of Remote Sensing Methods for the Investigation of Spatio-Temporal Variability of Sea Surface Temperature and Chlorophyll Fields in the Gulf of Finland. 2013.
149. **Tiina Kriščiunaite**. A Study of Milk Coagulability. 2013.
150. **Tuuli Levandi**. Comparative Study of Cereal Varieties by Analytical Separation Methods and Chemometrics. 2013.
151. **Natalja Kabanova**. Development of a Microcalorimetric Method for the Study of Fermentation Processes. 2013.
152. **Himani Khanduri**. Magnetic Properties of Functional Oxides. 2013.
153. **Julia Smirnova**. Investigation of Properties and Reaction Mechanisms of Redox-Active Proteins by ESI MS. 2013.
154. **Mervi Sepp**. Estimation of Diffusion Restrictions in Cardiomyocytes Using Kinetic Measurements. 2013.
155. **Kersti Jääger**. Differentiation and Heterogeneity of Mesenchymal Stem Cells. 2013.
156. **Victor Alari**. Multi-Scale Wind Wave Modeling in the Baltic Sea. 2013.
157. **Taavi Päll**. Studies of CD44 Hyaluronan Binding Domain as Novel Angiogenesis Inhibitor. 2013.
158. **Allan Niidu**. Synthesis of Cyclopentane and Tetrahydrofuran Derivatives. 2013.
159. **Julia Geller**. Detection and Genetic Characterization of *Borrelia* Species Circulating in Tick Population in Estonia. 2013.
160. **Irina Stulova**. The Effects of Milk Composition and Treatment on the Growth of Lactic Acid Bacteria. 2013.
161. **Jana Holmar**. Optical Method for Uric Acid Removal Assessment During Dialysis. 2013.
162. **Kerti Ausmees**. Synthesis of Heterobicyclo[3.2.0]heptane Derivatives *via* Multicomponent Cascade Reaction. 2013.
163. **Minna Varikmaa**. Structural and Functional Studies of Mitochondrial Respiration Regulation in Muscle Cells. 2013.
164. **Indrek Koppel**. Transcriptional Mechanisms of BDNF Gene Regulation. 2014.
165. **Kristjan Pilt**. Optical Pulse Wave Signal Analysis for Determination of Early Arterial Ageing in Diabetic Patients. 2014.
166. **Andres Anier**. Estimation of the Complexity of the Electroencephalogram for Brain Monitoring in Intensive Care. 2014.

167. **Toivo Kallaste**. Pyroclastic Sanidine in the Lower Palaeozoic Bentonites – A Tool for Regional Geological Correlations. 2014.
168. **Erki Kärber**. Properties of ZnO-nanorod/In_2S_3/$CuInS_2$ Solar Cell and the Constituent Layers Deposited by Chemical Spray Method. 2014.
169. **Julia Lehner**. Formation of Cu_2ZnSnS_4 and $Cu_2ZnSnSe_4$ by Chalcogenisation of Electrochemically Deposited Precursor Layers. 2014.
170. **Peep Pitk**. Protein- and Lipid-rich Solid Slaughterhouse Waste Anaerobic Co-digestion: Resource Analysis and Process Optimization. 2014.
171. **Kaspar Valgepea**. Absolute Quantitative Multi-omics Characterization of Specific Growth Rate-dependent Metabolism of *Escherichia coli*. 2014.
172. **Artur Noole**. Asymmetric Organocatalytic Synthesis of 3,3'-Disubstituted Oxindoles. 2014.
173. **Robert Tsanev**. Identification and Structure-Functional Characterisation of the Gene Transcriptional Repressor Domain of Human Gli Proteins. 2014.
174. **Dmitri Kartofelev**. Nonlinear Sound Generation Mechanisms in Musical Acoustic. 2014.
175. **Sigrid Hade**. GIS Applications in the Studies of the Palaeozoic Graptolite Argillite and Landscape Change. 2014.
176. **Agne Velthut-Meikas**. Ovarian Follicle as the Environment of Oocyte Maturation: The Role of Granulosa Cells and Follicular Fluid at Pre-Ovulatory Development. 2014.
177. **Kristel Hälvin**. Determination of B-group Vitamins in Food Using an LC-MS Stable Isotope Dilution Assay. 2014.
178. **Mailis Päri**. Characterization of the Oligoadenylate Synthetase Subgroup from Phylum Porifera. 2014.
179. **Jekaterina Kazantseva**. Alternative Splicing of *TAF4*: A Dynamic Switch between Distinct Cell Functions. 2014.
180. **Jaanus Suurväli**. Regulator of G Protein Signalling 16 (RGS16): Functions in Immunity and Genomic Location in an Ancient MHC-Related Evolutionarily Conserved Synteny Group. 2014.
181. **Ene Viiard**. Diversity and Stability of Lactic Acid Bacteria During Rye Sourdough Propagation. 2014.
182. **Kristella Hansen**. Prostaglandin Synthesis in Marine Arthropods and Red Algae. 2014.
183. **Helike Lõhelaid**. Allene Oxide Synthase-lipoxygenase Pathway in Coral Stress Response. 2015.
184. **Normunds Stivrinš**. Postglacial Environmental Conditions, Vegetation Succession and Human Impact in Latvia. 2015.
185. **Mary-Liis Kütt**. Identification and Characterization of Bioactive Peptides with Antimicrobial and Immunoregulating Properties Derived from Bovine Colostrum and Milk. 2015.
186. **Kazbulat Šogenov**. Petrophysical Models of the CO_2 Plume at Prospective Storage Sites in the Baltic Basin. 2015.
187. **Taavi Raadik**. Application of Modulation Spectroscopy Methods in Photovoltaic Materials Research. 2015.

188. **Reio Põder**. Study of Oxygen Vacancy Dynamics in Sc-doped Ceria with NMR Techniques. 2015.
189. **Sven Siir**. Internal Geochemical Stratification of Bentonites (Altered Volcanic Ash Beds) and its Interpretation. 2015.
190. **Kaur Jaanson**. Novel Transgenic Models Based on Bacterial Artificial Chromosomes for Studying BDNF Gene Regulation. 2015.
191. **Niina Karro**. Analysis of ADP Compartmentation in Cardiomyocytes and Its Role in Protection Against Mitochondrial Permeability Transition Pore Opening. 2015.
192. **Piret Laht**. B-plexins Regulate the Maturation of Neurons Through Microtubule Dynamics. 2015.
193. **Sergei Žari**. Organocatalytic Asymmetric Addition to Unsaturated 1,4-Dicarbonyl Compounds. 2015.
194. **Natalja Buhhalko**. Processes Influencing the Spatio-temporal Dynamics of Nutrients and Phytoplankton in Summer in the Gulf of Finland, Baltic Sea. 2015.
195. **Natalia Maticiuc**. Mechanism of Changes in the Properties of Chemically Deposited CdS Thin Films Induced by Thermal Annealing. 2015.
196. **Mario Öeren**. Computational Study of Cyclohexylhemicucurbiturils. 2015.
197. **Mari Kalda**. Mechanoenergetics of a Single Cardiomyocyte. 2015.
198. **Ieva Grudzinska**. Diatom Stratigraphy and Relative Sea Level Changes of the Eastern Baltic Sea over the Holocene. 2015.
199. **Anna Kazantseva**. Alternative Splicing in Health and Disease. 2015.
200. **Jana Kazarjan**. Investigation of Endogenous Antioxidants and Their Synthetic Analogues by Capillary Electrophoresis. 2016.
201. **Maria Safonova**. SnS Thin Films Deposition by Chemical Solution Method and Characterization. 2016.
202. **Jekaterina Mazina**. Detection of Psycho- and Bioactive Drugs in Different Sample Matrices by Fluorescence Spectroscopy and Capillary Electrophoresis. 2016.
203. **Karin Rosenstein**. Genes Regulated by Estrogen and Progesterone in Human Endometrium. 2016.
204. **Aleksei Tretjakov**. A Macromolecular Imprinting Approach to Design Synthetic Receptors for Label-Free Biosensing Applications. 2016.
205. **Mati Danilson**. Temperature Dependent Electrical Properties of Kesterite Monograin Layer Solar Cells. 2016.
206. **Kaspar Kevvai**. Applications of ^{15}N-labeled Yeast Hydrolysates in Metabolic Studies of *Lactococcus lactis* and *Saccharomyces Cerevisiae*. 2016.
207. **Kadri Aller**. Development and Applications of Chemically Defined Media for Lactic Acid Bacteria. 2016.
208. **Gert Preegel**. Cyclopentane-1,2-dione and Cyclopent-2-en-1-one in Asymmetric Organocatalytic Reactions. 2016.
209. **Jekaterina Služenikina**. Applications of Marine Scatterometer Winds and Quality Aspects of their Assimilation into Numerical Weather Prediction Model HIRLAM. 2016.
210. **Erkki Kask**. Study of Kesterite Solar Cell Absorbers by Capacitance Spectroscopy Methods. 2016.

211. **Jürgen Arund**. Major Chromophores and Fluorophores in the Spent Dialysate as Cornerstones for Optical Monitoring of Kidney Replacement Therapy. 2016.
212. **Andrei Šamarin**. Hybrid PET/MR Imaging of Bone Metabolism and Morphology. 2016.
213. **Kairi Kasemets**. Inverse Problems for Parabolic Integro-Differential Equations with Instant and Integral Conditions. 2016.
214. **Edith Soosaar**. An Evolution of Freshwater Bulge in Laboratory Scale Experiments and Natural Conditions. 2016.
215. **Peeter Laas**. Spatiotemporal Niche-Partitioning of Bacterioplankton Community across Environmental Gradients in the Baltic Sea. 2016.
216. **Margus Voolma**. Geochemistry of Organic-Rich Metalliferous Oil Shale/Black Shale of Jordan and Estonia. 2016.
217. **Karin Ojamäe**. The Ecology and Photobiology of Mixotrophic Alveolates in the Baltic Sea. 2016.
218. **Anne Pink**. The Role of CD44 in the Control of Endothelial Cell Proliferation and Angiogenesis. 2016.
219. **Kristiina Kreek**. Metal-Doped Aerogels Based on Resorcinol Derivatives. 2016.
220. **Kaia Kukk**. Expression of Human Prostaglandin H Synthases in the Yeast Pichia pastoris. 2016.
221. **Martin Laasmaa**. Revealing Aspects of Cardiac Function from Fluorescence and Electrophysiological Recordings. 2016.
222. **Eeva-Gerda Kobrin**. Development of Point of Care Applications for Capillary Electrophoresis. 2016.
223. **Villu Kikas**. Physical Processes Controlling the Surface Layer Dynamics in the Stratified Gulf of Finland: An Application of Ferrybox Technology. 2016.
224. **Maris Skudra**. Features of Thermohaline Structure and Circulation in the Gulf of Riga. 2017.
225. **Sirje Sildever**. Influence of Physical-Chemical Factors on Community and Populations of the Baltic Sea Spring Bloom Microalgae. 2017.